JAAVSO

Volume 44
Number 2
2016

The Journal of the American Association of Variable Star Observers

Variable Stars with the *Kepler* Space Telescope

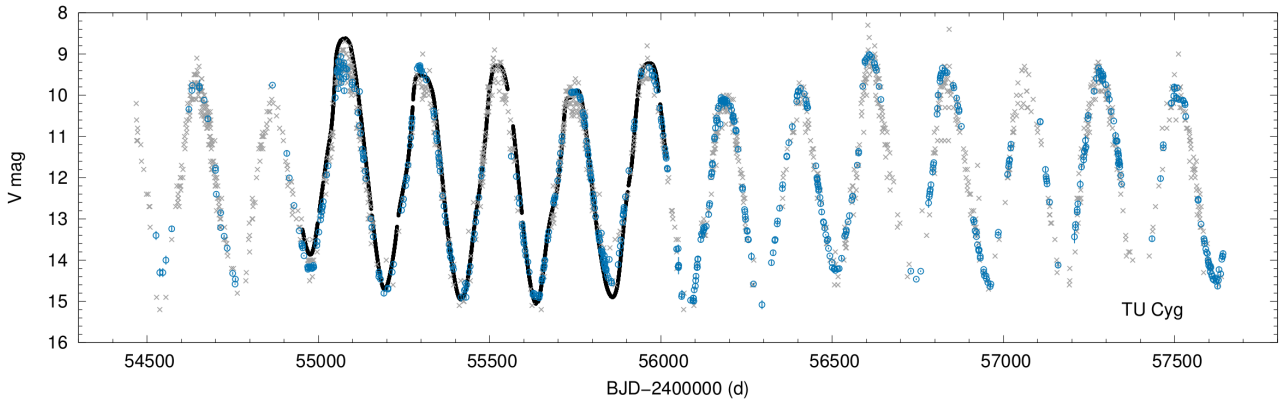

A comparison of the AAVSO visual (gray), digital V-band and green-filter (blue) observations, and the Kepler light curve (black) of the Mira star TU Cyg.

Also in this issue...

The American Association of Variable Star Observers
49 Bay State Road, Cambridge, MA 02138, USA

ISSN 0271-9053 (print)
ISSN 2380-3606 (online)

JAAVSO

The Journal of
The American Association
of Variable Star Observers

Volume 44
Number 2
2016

ISSN 0271-9053 (print)
ISSN 2380-3606 (online)

AAVSO
49 Bay State Road
Cambridge, MA 02138
USA

Publication Schedule

The Journal of the American Association of Variable Star Observers is published twice a year, June 15 (Number 1 of the volume) and December 15 (Number 2 of the volume). The submission window for inclusion in the next issue of JAAVSO closes six weeks before the publication date. A manuscript will be added to the table of contents for an issue when it has been fully accepted for publication upon successful completion of the referee process; these articles will be available online prior to the publication date. An author may not specify in which issue of JAAVSO a manuscript is to be published; accepted manuscripts will be published in the next available issue, except under extraordinary circumstances.

Page Charges

Page charges are waived for Members of the AAVSO. Publication of unsolicited manuscripts in JAAVSO requires a page charge of US $100/page for the final printed manuscript. Page charge waivers may be provided under certain circumstances.

Publication in *JAAVSO*

With the exception of abstracts of papers presented at AAVSO meetings, papers submitted to JAAVSO are peer-reviewed by individuals knowledgable about the topic being discussed. We cannot guarantee that all submissions to JAAVSO will be published, but we encourage authors of all experience levels and in all fields related to variable star astronomy and the AAVSO to submit manuscripts. We especially encourage students and other mentees of researchers affiliated with the AAVSO to submit results of their completed research.

Subscriptions

Institutions and Libraries may subscribe to JAAVSO as part of the Complete Publications Package or as an individual subscription. Individuals may purchase printed copies of recent JAAVSO issues via Createspace. Paper copies of JAAVSO issues prior to volume 36 are available in limited quantities directly from AAVSO Headquarters; please contact the AAVSO for available issues.

Instructions for Submissions

The *Journal of the AAVSO* welcomes papers from all persons concerned with the study of variable stars and topics specifically related to variability. All manuscripts should be written in a style designed to provide clear expositions of the topic. Contributors are encouraged to submit digitized text in MS WORD, LATEX+POSTSCRIPT, or plain-text format. Manuscripts may be mailed electronically to journal@aavso.org or submitted by postal mail to JAAVSO, 49 Bay State Road, Cambridge, MA 02138, USA.

Manuscripts must be submitted according to the following guidelines, or they will be returned to the author for correction:

Manuscripts must be:
1) original, unpublished material;
2) written in English;
3) accompanied by an abstract of no more than 100 words.
4) not more than 2,500–3,000 words in length (10–12 pages double-spaced).

Figures for publication must:
1) be camera-ready or in a high-contrast, high-resolution, standard digitized image format;
2) have all coordinates labeled with division marks on all four sides;
3) be accompanied by a caption that clearly explains all symbols and significance, so that the reader can understand the figure without reference to the text.

Maximum published figure space is 4.5″ by 7″. When submitting original figures, be sure to allow for reduction in size by making all symbols, letters, and division marks sufficiently large.

Photographs and halftone images will be considered for publication if they directly illustrate the text.

Tables should be:
1) provided separate from the main body of the text;
2) numbered sequentially and referred to by Arabic number in the text, e.g., Table 1.

References:
1) References should relate directly to the text.
2) References should be keyed into the text with the author's last name and the year of publication, e.g., (Smith 1974; Jones 1974) or Smith (1974) and Jones (1974).
3) In the case of three or more joint authors, the text reference should be written as follows: (Smith et al. 1976).
4) All references must be listed at the end of the text in alphabetical order by the author's last name and the year of publication, according to the following format: Brown, J., and Green, E. B. 1974, *Astrophys. J.*, **200**, 765.
Thomas, K. 1982, *Phys. Rep.*, **33**, 96.
5) Abbreviations used in references should be based on recent issues of the *Journal* or the listing provided at the beginning of *Astronomy and Astrophysics Abstracts* (Springer-Verlag).

Miscellaneous:
1) Equations should be written on a separate line and given a sequential Arabic number in parentheses near the right-hand margin. Equations should be referred to in the text as, e.g., equation (1).
2) Magnitude will be assumed to be visual unless otherwise specified.
3) Manuscripts may be submitted to referees for review without obligation of publication.

Online Access

Articles published in JAAVSO, and information for authors and referees may be found online at: https://www.aavso.org/apps/jaavso/

The Journal of the American Association of Variable Star Observers
Volume 44, Number 2, 2016

Editorial

Variable Star Research

Instruments, Methods, and Techniques

Variable Star Data

Table of Contents continued on following pages

Review Papers

Abstracts of Papers and Posters Presented at the 105th Spring Meeting of the AAVSO, Held in St. Louis, Missouri, May 5–7, 2016

Table of Contents continued on next page

Erratum

Editorial

The Publishing Landscape: It's the "Wild West" Out There

John R. Percy
Editor-in-Chief, *Journal of the AAVSO*

Department of Astronomy and Astrophysics, and Dunlap Institute for Astronomy and Astrophysics, University of Toronto, 50 St. George Street, Toronto, ON M5S 3H4, Canada; john.percy@utoronto.ca

Received November 8, 2016

A few weeks ago, AAVSO Director Dr. Stella Kafka sent me a link to "A Quick Tour Around the World of Scholarly Journal Publishing" (Crotty 2016). As Editor of *JAAVSO*, I found it interesting and timely. It touched on publishing issues which have been front-and-center in recent science media.

Scholarly Publishing

JAAVSO is a scholarly journal. There are thousands of them out there (28,100 according to a 2012 survey), some of them hundreds of times larger in content and circulation than *JAAVSO*. The volume is growing because of the information explosion, and the increasing participation of scholars in emerging nations. They are written and read mostly by professional scholars and researchers in academe and elsewhere. See *wikipedia* (https://en.wikipedia.org/wiki/Academic_journal) for a brief overview.

A good journal is one whose publishers facilitate and guard the editorial process, including the peer-reviewing or refereeing, to ensure that the journal content is of the highest quality—correct, appropriate, and original. It is one whose editors are committed to their work and whose editorial board members are genuinely interested in supporting and improving the quality and reach of the journal.

Cynics might say that many journal articles are read by only a handful of readers, or perhaps by no one. Authors use journals to disseminate their research and ideas and to critique others' research, but also to amass "Brownie points" for publications and citations. It's "publish or perish" for tenure and promotion. Ambitious authors aim for prestigious, peer-reviewed journals with high standards and high impact. The concept of journal impact or ranking is increasingly used, but controversial. Publication and citation data are also used for university ranking, which is a big thing for universities like mine (we rank somewhere between #4 and #23 in the world, and significantly higher among public universities).

The main astronomy journals (*Astrophysical Journal, Astronomical Journal, Astronomy and Astrophysics, Monthly Notices of the Royal Astronomical Society*) are published on behalf of non-profit scientific societies by specialized and experienced non-commercial publishers. Revenue can come from a combination of membership dues, society funding, library subscriptions, advertising, and page charges. There are also a few for-profit astronomical journals, of mixed quality.

Current Trends

Things are changing. Some of the changes serve the audience of authors and readers; some do not. Journals are increasingly electronic. Some no longer produce hard copies. In a sense, that's good and efficient, considering the increasing volume. Readers can purchase individual articles, rather than whole volumes. There's also a move towards open access, encouraged by governments and funding agencies who want the fruits of their largesse to be known. But who pays the cost? There is also a move to require publication of raw research data, partly so readers can verify that the results are correct and reproducible (see below). Again, who pays the cost? And this can be complicated if, for instance, the data are clinical and protected by a confidentiality agreement.

In some disciplines such as astronomy, there is widespread use of open-access preprint servers such as astro-ph (arxiv.org) to make unrefereed papers immediately available. How necessary is refereeing anyway, if the authors themselves are experts? And how effective is refereeing? It takes a great deal of time and effort to referee a long and complex paper. And referees are not paid or recognized. For some journals, refereeing is done on-line, by readers.

In many disciplines, notably medicine but also physical science, for-profit publishers are creating new journals. My wife and I (she is a biomedical scientist and co-editor of a non-profit journal much like *JAAVSO*) are constantly bombarded by messages from for-profit publishers to submit manuscripts—for a price. They especially want papers from established scientists, to give them credibility. The same publishers may organize conferences and invite speakers—again, for a price. It's "present or perish" as well as "publish or perish." And there's a trend to consolidation: large for-profit publishers engulf and devour (though consolidation does produce some economies of scale). They then "bundle" their journals and encourage university libraries to subscribe to the whole bundle. In an era of declining library budgets, this means that new journals, or small journals (such as *JAAVSO*) get cut. Not surprisingly, intrepid hackers are "stealing" papers from publishers' or universities' websites, and posting them where all can see. Their motives may be well-intentioned; scholars in less-developed countries may be unable to afford "astronomical" subscription costs.

For-profit publishers are also selling metadata, just as corporations like *Google* collect and sell information about

what users read online. *ResearchGate* (www.researchgate.net) is a searchable site where research papers are archived. My wife swears by it. But it is for-profit, and supported by the metadata that the publisher collects and sells. In a sense, the publishers themselves are becoming repositories, replacing libraries.

The Dark Side

There is enough hanky-panky in scholarly publishing to keep the tabloids busy. Papers are occasionally retracted from journals, voluntarily or otherwise, due to errors which may be accidental or deliberate. There are numerous cases of plagiarism, including self-plagiarism (or "recycling"), and of authors publishing several very similar papers, differing only in some "minimum publishable unit" of new data. Deserving authors may be omitted, or "honorary" authors added (perhaps for a price). Referees may steal ideas from the papers that they are reviewing. In medicine especially, there may be real or perceived conflicts of interest if the author and/or research is supported by "big pharma."

Positive results tend to be published, negative results not, even when negative results are as important as positive ones. A recent study (Open Science Collaboration 2015) showed that the results of over half of a sample of 100 prominent psychology studies were not reproducible. This is one reason for requiring that raw data, and details of analysis, should be made available on-line. Several other studies have suggested that authors grossly over-estimate the statistical significance of the results of their research. In a survey (Fanelli 2009), about 2 percent of authors admitted to data fabrication, and up to 34 percent admitted to other questionable practices.

Female authors, or authors from smaller institutions, are judged more harshly by referees than male authors from Harvard. That's one of the reasons for using "blind" refereeing, as *JAAVSO* does, though it's often impossible to hide the identity of the author.

There are predatory publishers of "refereed" journals who do little or no refereeing, but say that they do. Estimates of the number of predatory journals range from hundreds to thousands. There are cases of publishers "selling" authorship of papers to those who need it and can afford it. This often occurs in emerging nations; it is estimated (Stone 2016) that 10 percent of masters and Ph.D. theses in Iran are purchased. The U.S. Federal Trade Commission recently charged one large commercial publisher with misleading authors about the standards and impacts of their journals (Bohannon 2016). These are just a few examples, so it *is* the "wild west" out there. Fortunately, these examples are not representative of the majority of scholarly journals, especially the non-profit ones.

JAAVSO

As far as I know, *JAAVSO* does not have a dark side. We have an ethics statement on our website. We happily exist to serve the authors, AAVSO members, and observers, and other readers—both current and future. We are cheerfully supported (within fiscal reason) by the AAVSO, and depend upon the fine work by the staff—especially Mike Saladyga and Elizabeth Waagen. I and the Editorial Board and the referees are unpaid. I have never, in my half-century of refereeing and editing, been offered a bribe. We try to maintain high standards, while being sensitive to the needs and nature of our authors and our readers. We encourage existing and potential authors to publish in *JAAVSO*, and readers to read it! We encourage feedback; like anything, it can always be improved.

Acknowledgement: I thank Drs. Stella Kafka and Michael Saladyga for reading and commenting on a draft of this editorial.

References

Bohannon, J. 2016, *Science*, **354**, 23.
Crotty, D. 2016, web post 18 Aug. 2016 (https://scholarlykitchen.sspnet.org/2016/08/18/a-quick-tour-around-the-world-of-scholarly-journal/publishing/).
Fanelli, D. 2009, *Plos One* (http://journals.plos.org/plosone/article?id=10.1371/journal.pone.0005738).
Open Science Collaboration. 2015, *Science*, **349**, 943.
Stone, R. 2016, *Science*, **353**, 1197.

CCD Photometry and Roche Modeling of the Eclipsing Overcontact Binary Star System TYC 01963-0488-1

Kevin B. Alton
UnderOak Observatory, 70 Summit Avenue, Cedar Knolls, NJ 07927; kbalton@optonline.net

Received May 17, 2016; revised June 7, 2016; accepted June 8, 2016

Abstract TYC 01963-0488-1 (ASAS J094440+2632.1) is a W UMa binary system (P = 0.427036 d) which has been largely overlooked since first being detected nearly 15 years ago by the ROTSE-I telescope. Other than the monochromatic ROTSE-I survey data, no multi-colored light curves have been published. Photometric data collected in three bandpasses (B, V, and I_c) at UnderOak Observatory produced five new times-of-minimum for TYC 01963-0488-1 which were used to establish a linear ephemeris from the first Min I epoch (HJD_0). No published radial velocity data are available for this system; however, since this W UMa binary undergoes very obvious total eclipses, Roche modeling yielded a well-constrained photometric value for q (~0.25). There is a suggestion from the ROTSE-I data and new results herein that Max II is more variable than Max I. Therefore, Roche model fits for the TYC 01963-0488-1 light curves collected in 2015 were assessed with and without spots.

1. Introduction

The variable behavior of TYC 01963-0488-1 was first observed during the ROTSE-I CCD survey (Gettel *et al.* 2006); the system was later classified by Hoffman *et al.* (2009). Photometric data are accessible on the Northern Sky Variable Survey website (Wozniak *et al.* 2004). Other than the reduced on-line data (Gettel *et al.* 2006) at VizieR and an entry in the International Variable Star Index (VSX; Watson *et al.* 2014), no other reference to this binary system was found in the literature. The paper herein marks the first robust determination of orbital period and Roche model assessment of TYC 01963-0488-1 which has been published.

2. Observations and data reduction

2.1. Photometry

Equipment included a 0.28-m catadioptic telescope with an SBIG ST-8XME CCD camera mounted at primary focus. Automated imaging was performed with SBIG photometric B, V, and I_c filters manufactured to match the Bessell prescription. The computer clock was updated immediately prior to each session and exposure time for all images adjusted to 75 seconds. Image acquisition (lights, darks, and flats) was performed using CCDSOFT v5 (Software Bisque 2011) while calibration and registration were performed with AIP4WIN v2.4.0 (Berry and Burnell 2011). Images of TYC 01963-0488-1 were plate-solved using the standard star fields (MPOSC3) provided in MPO CANOPUS v10.7.1.3 (Minor Planet Observer 2015). MPO CANOPUS also provided the means for further photometric reduction to light curves using a fixed ensemble of five non-varying comparison stars in the same field-of-view (FOV). To minimize error due to differential refraction and color extinction, only data from images taken above 30° altitude (airmass < 2.0) were used. Instrumental readings were reduced to catalog-based magnitudes using the MPOSC3 reference star fields built into MPO CANOPUS. Stars in MPOSC3 with BVI_c magnitudes derived from 2MASS J-K magnitudes have an internal consistency of ±0.05 mag. for V, ±0.08 mag. for B, ±0.03 mag. for I_c, and ±0.05 mag. for B–V (Warner 2007).

2.2. Light curve analyses

Roche type modeling was performed with the assistance of BINARY MAKER 3 (BM3; Bradstreet and Steelman 2004), WDWINT5.6A (Nelson 2009), and PHOEBE 0.31a (Prša and Zwitter 2005), the latter two of which employ the Wilson-Devinney (WD) code (Wilson and Devinney 1971; Wilson 1979). Spatial renderings of TYC 01963-0488-1 were also produced by BM3 once model fits were finalized. Times-of-minimum were calculated using the method of Kwee and van Woerden (1956) as implemented in PERANSO v2.5 (Vannmunster 2006).

3. Results and discussion

3.1. Photometry and ephemerides

Five stars in the same FOV with TYC 01963-0488-1 which were used to derive catalog-based (MPOSC3) magnitudes (Table 1) showed no evidence of inherent variability over the period of image acquisition and stayed within ±0.03 magnitude for V and I_c filters and ±0.05 for B. Photometric values in B (n = 407), V (n = 407), and I_c (n = 410) were processed to generate three LCs that spanned 45 days between March 24 and May 8, 2015 (Figure 1). In total, four new secondary (s) and one primary (p) minima were captured during this investigation; data from all filters were averaged for each session (Table 2) since no color dependency on the timings was noted. A period determination (P = 0.427028 ± 0.000008) from unfiltered data (ROTSE-I) collected in 1999–2000 was made using PERANSO (Vanmunster 2006) by applying periodic orthogonals (Schwarzenberg-Czerny 1996) to fit observations and analysis of variance (ANOVA) to evaluate fit quality. After converting magnitude to flux, ROTSE-I and Underoak Observatory (UO) light curve data (V mag.) were then folded together; the best fit was found where the orbital period was 0.427036 ± 0.000004 day (Figure 2). The Fourier routine (FALC) in MPO CANOPUS provided a similar period solution (0.427036 ± 0.000006) using only the multicolor data from UO. The first epoch (HJD_0) for this eclipsing binary is therefore defined by the following linear ephemeris equation:

$$\text{Min. I hel.} = 2457150.63657\ (3) + 0.427036\ (4)\ E \quad (1)$$

Table 1. Astrometric coordinates (J2000) and MPOSC3 catalog magnitudes (B, V, and I_c) for TYC 01963-0488-1 and five comparison stars used in this photometric study.

Star Identification	*R. A. h m s*	*Dec. ° ′ ″*	*MPOSC3[a] B mag.*	*MPOSC3 V mag.*	*MPOSC3 I_c mag.*	*MPOSC3 (B–V)*
TYC 01963-0488-1	09 44 40.44	26 32 07.2	11.57–12.11[b]	11.17–11.63[b]	10.69–11.15[b]	0.399
TYC 01963-0389-1	09 44 44.82	26 39 33.5	12.574	11.830	11.017	0.744
GSC 01963-00146	09 44 52.06	26 42 27.5	13.288	12.685	12.000	0.603
TYC 01963-0461-1	09 44 07.14	26 36 36.9	12.272	11.418	10.508	0.854
GSC 01963-00102	09 44 46.83	26 33 28.5	14.237	13.722	13.120	0.515
GSC 01963-00586	09 44 44.41	26 34 30.3	14.501	13.971	13.355	0.530

a: MPOSC3 is a hybrid catalog which includes a large subset of the Carlsberg Meridian Catalog (CMC-14) as well as from the Sloan Digital Sky Survey (SDSS).
b: Range of observed magnitudes in UO light curves for TYC 01963-0488-1

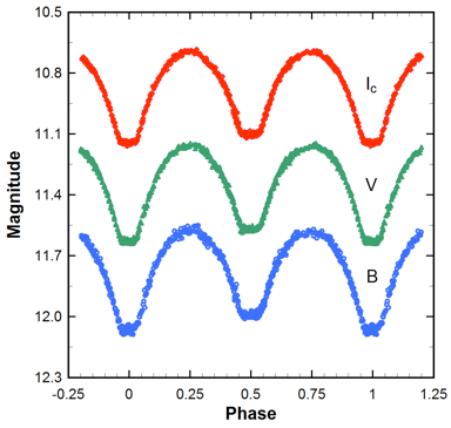

Figure 1. Folded CCD light curves for TYC 01963-0488-1 produced from photometric data obtained between March 24 and May 8, 2015. The top (I_c), middle (V), and bottom curve (B) shown above were reduced to MPOSC3-based catalog magnitudes using MPO CANOPUS.

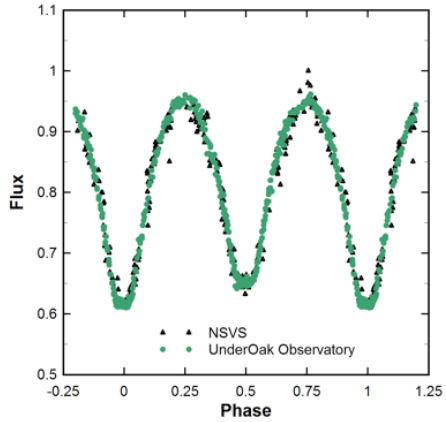

Figure 2. Survey data from the ROTSE-I telescope and photometric results (V mag.) collected at UnderOak Observatory were folded together using period analysis (P = 0.427036 ± 0.000004 d). Greater scatter at Min II (φ = 0.75) suggests the possibility of an active photosphere for TYC 01963-0488-1.

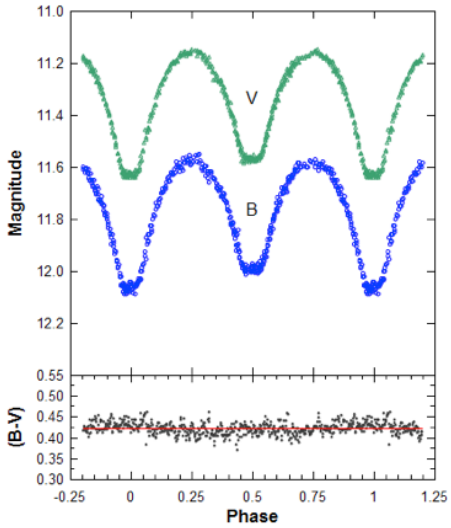

Figure 3. Color change (B–V) of TYC 01963-0488-1 during varying phases of eclipse was evaluated from binned data (φ = 0.002). Relatively minor deviations from the solid-line mean (0.423 ±0.014) suggest that the effective temperatures of both stars are not very different.

Table 2. New times-of-minimum for TYC 01963-0488-1 acquired at UnderOak Observatory.

Mean Observed Time-of-Minimum (HJD–2400000)	*± Error*	*UT Date of Observations*	*Type of Minimum[a]*
57114.5523	0.0002	02Apr2015	s
57117.5433	0.0001	05Apr2015	s
57134.6238	0.0002	22Apr2015	s
57137.6136	0.0001	25Apr2015	s
57150.6366	0.0002	08May2015	p

a: s = secondary; p = primary.

Table 3. Difference in light curve minima and maxima by bandpass.

Band	*Max II – Max I*	*Min I – Min II*	*Min I – Max I*	*Min II – Max II*
B	0.015	0.0739	0.5002	0.4113
V	0.005	0.0581	0.4766	0.4131
I_c	0.004	0.0405	0.4551	0.4110

No attempt was made to determine whether there are secular changes in eclipse timings over time since these data were only collected over 45 days.

3.2. Light curve behavior

As expected from a overcontact binary system, LCs (Figure 1) exhibit minima which are separated by 0.5 phase (φ) and consistent with a synchronous circular orbit. Flattened bottoms at Min I and Min II strongly suggest that this binary system undergoes total eclipses. Data from the ROTSE-I survey tend to exhibit greater variability around Max II compared to Max I (Figure 2). A slightly positive O'Connell effect (Max II fainter than Max I) is observed most notably with the B passband during the 2015 campaign whereas both V and I_c passbands exhibit vanishingly smaller differences (Table 3). In general this effect has been attributed to the presence of cool starspot(s), hot region(s), gas stream impact on either or both of the binary cohorts, and/or other unknown phenomena which produce surface inhomogeneities (Yakut and Eggleton 2005). The net result can be unequal heights during maximum light and is often simulated by the introduction of starspots during Roche-type modeling of the LC data.

3.3. Spectral classification

Data from folded LCs (V- and B-mag) were binned into equal phase intervals (0.002) to produce a difference (B–V) plot (Figure 3). It would appear that changes in color with phase are small (0.423 ± 0.014) suggesting relatively minor differences in effective temperature between stars. Color index (B–V) data from UO and three other surveys (Table 4) were corrected using the reddening value (E(B–V) = 0.0175 ± 0.0005) observed within a 5 arcmin radius of TYC 01963-0488-1 (Schlafly and Finkbeiner 2011; Schlegel *et al.* 1998). The mean result, $(B–V)_0$ = 0.393 ± 0.014, which was adopted for subsequent Roche modeling, indicates that the most luminous star in this system has an effective temperature of 6705 K, and ranges between spectral type F2V and F3V (Pecaut and Mamajek 2013) .

3.4. Roche modeling approach

In the absence of radial velocity (RV) data, it is not possible to unequivocally determine q, the mass ratio (m_2 / m_1), or whether TYC 01963-0488-1 is an A- or W-type overcontact binary system. According to Binnendijk (1970), the deepest minimum (Min I) of an A-type W UMa variable results from the eclipse of the hotter more massive star by the cooler less massive cohort. This is in contrast to W-types where the deepest minimum results from the hotter but less massive star being eclipsed by the more massive but cooler cohort. In general, A-type W UMa variables can be characterized by their total mass ($M_T > 1.8\ M_\odot$), spectral class (A–F), orbital period (P > 0.4 d), extent of thermal contact (*f*), propensity to exhibit a total eclipse due to large size differences, mass ratio (q < 0.3), and the temperature difference (ΔT < 100 K) between the hottest and coolest star (Skelton and Smits 2009). On balance, when all of these factors are considered, TYC 01963 0488-1 would appear to best fit those parameters which define an A-subtype. A reliable photometric value for mass ratio (q_{ph}) can be determined but only for those W UMa systems where a total eclipse is observed from our vantage point (Terrell and Wilson 2005). A recent paper published by Hambálek and Pribulla (2013) offered an approach to estimate mass ratio (q) and the orbital inclination (i) prior to Roche modeling. These investigators employed the code ROCHE (Pribulla 2012) to simulate a total of 11,895 LCs from overcontact binaries as defined by varying values for three parameters (q (0.05–1; Δ = 0.025), fill-out (*f* = 0, 0.25, 0.50, 0.75, 1), and i (30°–90°; Δ=1°)). A LC from an eclipsing binary can be represented by trigonometric polynomials such that the corresponding Fourier coefficients define the "informational contents" of the system. A partial eclipse can be adequately represented by a 10th order trigonometric polynomial, whereas a total eclipse is more difficult to model. In this case only the first 11 Fourier coefficients (a_0–a_{10}) were used to investigate the uniqueness of each solution (Table 5). The amplitude of the LC and the minima width are respectively constrained by the values for a_2 and a_4. The uniqueness (δq) for a photometric mass ratio (q_{ph}) solution is defined by the a_2–a_4 plane (Hambálek and Pribulla 2013) and varies according to the number and precision of the LC data points. The authors have conveniently provided an on-line link to UNIQUE (http://www.ta3.sk/~lhambalek/download/unique.zip), which can be used to calculate the geometric elements [q, *f*, and i] along with the corresponding Fourier coefficients.

In preparation for analysis by UNIQUE, monochromatic LC data (n = 407; V mag.) collected at UO were converted to normalized flux and then binned into constant phase intervals (0.002) to satisfy a requirement of the program. When third light (l_3) was assumed to be zero, the best match from the LC data library (coef.dat) used by UNIQUE corresponded to q = 0.225, *f* = 0.5, and i = 79°. Roche modeling of LC data

Table 4. Spectral classification of TYC 01963-0488-1 based upon dereddened[a] (B–V) data from various surveys and the present study.

Stellar Attribute	*MPOSC3*	*2MASS*	*SDSS-DR8*	*Present Study*
$(B–V)_0$	0.382 ±0.094	0.381 ±0.050	0.407 ±0.04	0.404 ±0.014
T_{eff1}[b] (K)	6765	6765	6656	6673
Spectral Class[c]	F2-F3V	F2-F3V	F3-F4V	F3-F4V

a: E(B–V) = 0.0175 ±0.0005. b: T_{eff1} interpolated and spectral class assigned from Pecaut and Mamajek (2013). c: Mean value for $(B–V)_0$ = 0.393 ± 0.014; T_{eff1} = 6705 K; Spectral type = F2 to F3V.

Table 5 Fourier coefficients derived from Vmag light curve using UNIQUE[a].

Coefficient	*Calculated Value*	*Library Value*
a_0	+0.848932	+0.850691
a_1	–0.008729	–0.006636
a_2	–0.165170	–0.166897
a_3	–0.006588	–0.008652
a_4	–0.030641	–0.024858
a_5	–0.001247	–0.000322
a_6	–0.005090	–0.006625
a_7	–0.001790	–0.001988
a_8	+0.002385	+0.001871
a_9	–0.002313	–0.001730
a_{10}	+0.003141	+0.002698

a: Fit difference = 0.007449 corresponds to q = 0.225, f = 0.5, i = 79°.

from TYC 01963-0488-1 was primarily accomplished using the program PHOEBE 0.31a (Prša and Zwitter 2005). The model selected was for an overcontact binary not in thermal contact (Mode 3) and each curve was weighted based upon observational scatter. Bolometric albedo ($A_{1,2}$ = 0.5) and gravity darkening coefficients ($g_{1,2}$ = 0.32) for cooler stars (< 7500 K) with convective envelopes were assigned by theory according to Ruciński (1969) and Lucy (1967), respectively. The effective temperature of the more massive primary star was fixed (T_{eff1} = 6705 K) according to the earlier designation as spectral type F2V to F3V. Following any change in the effective temperature for the secondary (T_{eff2}), new logarithmic limb darkening coefficients (x_1, x_2, y_1, y_2) were interpolated according to Van Hamme (1993). All parameters except for T_{eff1}, $A_{1,2}$, and $g_{1,2}$ were allowed to vary during DC iterations. Roche modeling was initially seeded with q = 0.225 and i = 79° from UNIQUE (Hambálek and Pribulla 2013) and a lower effective temperature for the secondary (T_{eff2} = 6600 K) in order to comply with the definition of an A-type system. This assessment included synthesis of light curves for TYC 01963-0488-1 with and without the incorporation of a cool spot to address the so-called O'Connell effect (Max I brighter than Max II). The possibility of hot spots which can also produce LC asymmetry cannot be discounted; however, the appearance of cold spot(s) can be persistent and could explain the same Max II asymmetry observed between 1999 and 2000 by the ROTSE-I survey (Akerlof *et al.* 2000).

3.5. Modeling results

3.5.1. Light curve analysis

The initial estimates for q, i, and T_{eff2} quickly converged to best fit Roche model solutions. In this case the values (q and i) derived from UNIQUE were reasonably close to the final values determined from Roche modeling (Table 6). Corresponding unspotted (Figure 4) and spotted (Figure 5) simulations reveal that the addition of a cool spot on the less massive secondary star resulted in a modestly improved fit (χ^2) of these multi-color data. A pictorial model rendered with BM3 using the physical and geometric elements from the system with a cool spot on the secondary star is shown in Figure 6. After a best model fit was found, values and errors for T_{eff2}, i, q, and $\Omega_{1,2}$ were further examined using the PHOEBE scripter in which the WD minimization program (DC) was programmatically executed 1,000 times (Bonanos 2009). During each heuristic scan, input parameter values were updated for the next iteration and the formal error derived from the standard deviations; a representative example (Figure 7) illustrates the probabilistic relationship between q, i, and $\Delta\chi^2$. The fairly steep boundary which defines the 99.99% confidence interval ($\Delta\chi^2$ = 15.1) is consistent with a well-constrained value for q (0.248 ± 0.002).

The fill-out parameter (f), which is a measure of the shared photospheric volume between each star, was calculated according to Bradstreet (2005) as:

$$f = \frac{(\Omega_{inner} - \Omega_{1,2})}{(\Omega_{inner} - \Omega_{outer})} \quad (2)$$

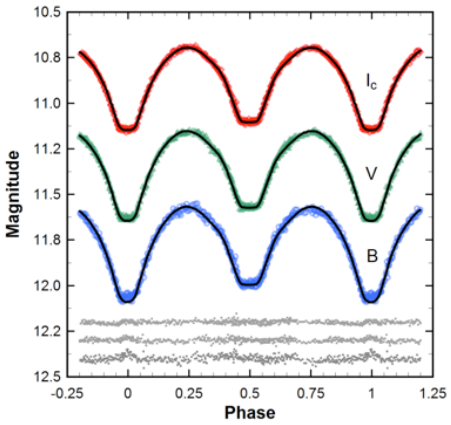

Figure 4. Synthetic fits (solid-line) of TYC 01963-0488-1 light curves (B-, V-, and I_c-mag.) produced from CCD data collected at UO during 2015. The Roche model assumed an A-subtype overcontact binary with no spots; residuals from the model fits are offset at the bottom of the plot to keep the values on scale.

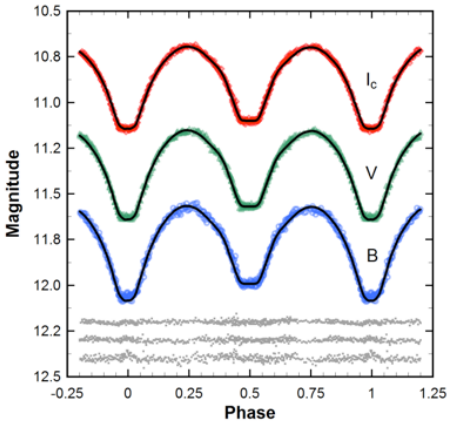

Figure 5. Synthetic fits (solid-line) of TYC 01963-0488-1 light curves (B-, V-, and I_c-mag.) produced from CCD data collected at UO during 2015. The Roche model assumed an A-subtype overcontact binary with a cool spot on the secondary; residuals from the model fits are offset at the bottom of the plot to keep the values on scale.

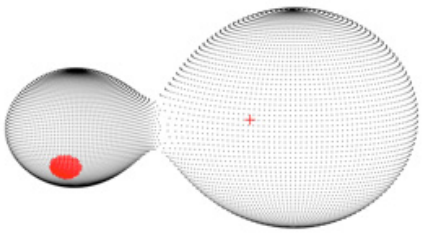

Figure 6. 3-D spatial model (φ = 0.79) of TYC 01963-0488-1 generated from 2015 photometric data showing the location of a cool spot on the secondary star.

where Ω_{outer} is the outer critical Roche equipotential, Ω_{inner} is the value for the inner critical Roche equipotential, and $\Omega = \Omega_{1,2}$ denotes the common envelope surface potential for the binary system. Since the fill-out value (~ 0.34) for TYC 01963-0488-1 lies between $0 < f < 1$, the system is defined as an overcontact binary. This is in contrast to semi-detached and detached systems where $f = 0$ and $f < 0$, respectively.

Table 6. Synthetic light curve parameters employed for Roche modeling and the geometric elements determined when assuming that TYC 01963-0488-1 is an A-type W UMa variable.

Parameter	*No Spot*	*Cool Spot (Secondary Star)*
T_{eff1} (K)[a]	6705	6705
T_{eff2} (K)[b]	6518 ± 18	6544 ± 13
q (m_2 / m_1)[b]	0.251 ± 0.003	0.248 ± 0.002
A[a]	0.5	0.5
g[a]	0.32	0.32
$\Omega_1 = \Omega_2$ [b]	2.302 ± 0.007	2.294 ± 0.004
i° [b]	81.61 ± 0.17	81.99 ± 0.57
$A_S = T_S / T$ [c]	—	0.86 ± 0.03[d]
Θ_S (spot co-latitude)[c]	—	122 ± 6[d]
φ_S (spot longitude)[c]	—	240 ± 5[d]
r_S (angular radius)[c]	—	14.0 ± 2[d]
$L_1 / (L_1 + L_2)_B$ [d,e]	0.8006 ± 0.0011	0.7980 ± 0.0005
$L_1 / (L_1 + L_2)_V$ [d,e]	0.7915 ± 0.0009	0.7903 ± 0.0004
$L_1 / (L_1 + L_2)_{Ic}$ [d,e]	0.7833 ± 0.0007	0.7833 ± 0.0004
r_1 (pole)[d]	0.4817 ± 0.0004	0.4829 ± 0.0005
r_1 (side)[d]	0.5242 ± 0.0006	0.5258 ± 0.0008
r_1 (back)[d]	0.5522 ± 0.0007	0.5538 ± 0.0010
r_2 (pole)[d]	0.2615 ± 0.0012	0.2609 ± 0.0011
r_2 (side)[d]	0.2740 ± 0.0015	0.2735 ± 0.0013
r_2 (back)[d]	0.3191 ± 0.0031	0.3190 ± 0.0029
Fill-out factor	33.67%	34.68%
χ^2 (B)[f]	0.003294	0.003094
χ^2 (V)[f]	0.002768	0.002782
χ^2 (I_c)[f]	0.005724	0.005574

a: Fixed during DC.
b: Error estimates for q, i, $\Omega_1 = \Omega_2$, and T_{eff2} from heuristic scanning .
c: Spot temperature, location, and size parameters in degrees.
d: Error estimates for spot parameters, $L_1 / (L_1 + L_2)$, r_1, and r_2 (pole, side and back) from WDWint v5.6a (Nelson 2009).
e: Bandpass dependent fractional luminosity; L_1 and L_2 refer to luminosities of the primary and secondary stars, respectively.
f: Monochromatic best Roche model fits ($\chi 2$) from PHOEBE 0.31a (Prša and Zwitter 2005).

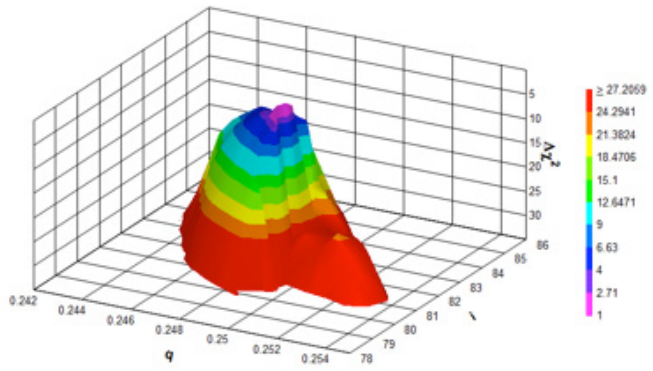

Figure 7. Probability contour illustrating the sharply defined surface boundaries for a best fit when mass ratio (q) and the orbital inclination (i) are iteratively adjusted during DC. Randomized q and i values (n=1000) were generated within ± 4% of the nominal input values for q (0.248) and i (81.99°). The parameter $\Delta\chi^2$ is a function of confidence level such that when $\Delta\chi^2$ =1 the probability in a paired comparison is 68.3% (1σ).

3.6. Absolute Parameter Estimates

Absolute parameters (Table 7) were derived for each star in this A-type W UMa binary system using results from the best fit simulation (spotted model) of the 2015 LC. In the absence of RV data ($v_{1r} + v_{2r}$), total mass can not be calculated directly. However, stellar mass and radii from binary systems have been tabulated over a wide range of spectral types (Harmanec 1988) where the primary star (T_{eff1} = 6705 K) in TYC 01963-0488-1 is estimated to have a mass of 1.48 ± 0.06 $M_\odot$. Alternatively, two different empirical period-mass relationships for W UMa-binaries have been reported by Gazeas and Stępień (2008) and Qian (2003). According to Gazeas and Stępień (2008) the mass of the primary star (M_1) can be determined from the expression (3):

Table 7. Absolute parameters for TYC 01963-0488-1 using results from the 2015 spotted Roche model.

Parameter	*Primary*	*Secondary*
Mass ($M_\odot$)	1.46 ± 0.07	0.36 ± 0.02
Radius ($R_\odot$)	1.46 ± 0.02	0.78 ± 0.01
a ($R_\odot$)	2.91 ± 0.04	—
Luminosity ($L_\odot$)	3.88 ± 0.09	1.00 ± 0.04
M_{bol}	3.28 ± 0.024	4.75 ± 0.024
Log (g)	4.27 ± 0.023	4.21 ± 0.024

$$\log M_1 = (0.755 \pm 0.059) \log P + (0.416 \pm 0.024), \quad (3)$$

while the mass of the secondary (M_2) can be similarly calculated from the orbital period (P) with the following relationship (4):

$$\log M_2 = (0.352 \pm 0.166) \log P - (0.262 \pm 0.067) \quad (4)$$

This leads to M_1 = 1.37 ± 0.1 $M_\odot$ for the primary and M_2 = 0.405 ± 0.086 $M_\odot$ for the secondary star. The value for the photometrically determined mass ratio (q_{ph} = 0.248 ± 0.002) from this study is contained within the mass ratio and error (q = 0.296 ± 0.066) calculated using equations 3 and 4. Another mass-period relationship (equation 5) was derived by Qian (2003) and largely corresponds to A-type W UMa systems where $M_1 > 1.35\ M_\odot$ and P > 0.41 d.

$$\log M_1 = 0.761\ (\pm 0.150) + 1.82\ (\pm 0.28) \times P \quad (5)$$

In this case the solution leads to a somewhat higher estimate for the primary star mass (M_1 = 1.54 ± 0.20). The average of all three values (M_1 = 1.46 ± 0.07) was used for subsequent determinations of M_2, semi-major axis (a), volume-radius (r_L), bolometric magnitude (M_{bol}), and distance (pc) to TYC 0163-0488-1. The semi-major axis, $a(R_\odot)$ = 2.91 ± 0.04, was calculated according to Kepler's third law where:

$$a_3 = \frac{(G \times P^2\ (M_1 + M_2))}{(4\pi^2)} \quad (6)$$

According to the expression (7) derived by Eggleton (1983), the effective radius of each Roche lobe (r_L) can be calculated to within an error of 1% over the entire range of mass ratios ($0 < q < \infty$):

$$r_L = \frac{0.49q^{2/3}}{0.6q^{2/3} + \ln(1 + q^{1/3})} \quad (7)$$

Volume-radius values were determined for the primary ($r_1 = 0.5021 \pm 0.0001$) and secondary ($r_2 = 0.2670 \pm 0.0001$) stars. The absolute radii for both binary constituents can then be calculated where $R_1 = a \times r_1 = 1.46 \pm 0.02\ R_\odot$ and $R_2 = a \times r_2 = 0.78 \pm 0.01\ R_\odot$. The bolometric magnitude (M_{bol}) and luminosity ($L_{1,2}$) in solar units ($L_\odot$) for the primary and secondary stars were calculated from well-established relationships where

$$M_{bol1,2} = 4.75 - 5 \log \left(\frac{R_{1,2}}{R_\odot} \right) - 10 \log \left(\frac{T_{1,2}}{T_\odot} \right) \quad (8)$$

and

$$L_{1,2} = \left(\frac{R_{1,2}}{R_\odot} \right)^2 \left(\frac{T_{1,2}}{T_\odot} \right)^4 \quad (9)$$

Assuming that $T_{eff1} = 6705$ K, $T_{eff2} = 6544$ K and $T_\odot = 5778$ K, the bolometric magnitudes are $M_{bol1} = 3.278 \pm 0.024$ and $M_{bol2} = 4.754 \pm 0.024$, while the solar luminosities for the primary and secondary are $L_1 = 3.88 \pm 0.09\ L_\odot$ and $L_2 = 1.00 \pm 0.04\ L_\odot$, respectively.

The distance to TYC 0163-0488-1 (438 ± 5 pc) was estimated using the distance modulus Equation (10) corrected for interstellar extinction. In this case V mag at Min II ($m = 11.57 \pm 0.01$) is defined when the primary totally eclipses the secondary, and M_V is the absolute magnitude derived using the bolometrically corrected magnitude ($M_{bol1} - BC$). The interstellar extinction ($A_V = 0.05425 \pm 0.00155$) was determined from E(B–V), the color excess previously described in section 3.3 where E = 3.1.

$$d(pc) = 10^{(((m - M_V) - A_V + 5) / 5)} \quad (10)$$

Another value for distance (399 ± 36 pc) was calculated according to the empirical expression (11)

$$\log D = 0.2 \times V_{max} - 0.18 \times \log P - 1.6\,(J–H) + 0.56 \quad (11)$$

derived by Gettel *et al.* (2006) from a ROTSE-I catalog of overcontact binary stars where D is distance in parsecs, P is the orbital period in days, $V_{max} = 11.17 \pm 0.01$, and (J–H) is the 2MASS color for TYC 01963-0488-1. The combined mean distance to this system is therefore estimated to be 419 ± 18 pc.

4. Conclusions

CCD-based photometric data captured in B, V, and I_c passbands produced five new times-of-minimum for the W UMa binary system TYC 01963 0488-1. A first epoch (HJD_0) linear ephemeris for TYC 01963-0488-1 was established for this system; many more years of data will likely be required to determine whether there are any secular changes in orbital period. The weight of evidence from this study and other surveys suggested that the effective temperature of the most luminous star is 6705 K and corresponds to F2V-F3V spectral class. The greatest challenge to definitive Roche modeling of the rapidly expanding catalog of newly discovered W UMa binaries is the absence of published RV data to unequivocally determine a mass ratio (q) and subtype (A or W). Fortuitously this system experiences clearly defined total eclipses which help constrain a photometrically determined mass ratio result ($q \sim 0.25$). Since maximum light at $\varphi = 0.25$ and 0.75 was not equal, a cool-spot solution was necessary to achieve the best Roche model fits for TYC 01963-0488-1. Similar LC behavior observed between 1999 and 2000 suggests that this system has an active photosphere. Until which time RV data become publically available, these Roche model fits and any absolute parameters derived for this W UMa binary are subject to some uncertainty. The sum total of all data collected thus far suggests that TYC 01963-0488-1 is most likely an A-type W UMa variable located over 400 pc from our home planet. Public access to any data associated with this research can be obtained by request (mail@underoakobservatory.com).

5. Acknowledgements

This research has made use of the SIMBAD database, operated at Centre de Données astronomiques de Strasbourg, France, the Northern Sky Variability Survey hosted by the Los Alamos National Laboratory, and the International Variable Star Index maintained by the AAVSO. The diligence and dedication shown by all associated with these organizations is very much appreciated. The author gratefully acknowledges the comments and helpful suggestions that the referee offered to improve the overall quality of this research paper.

References

Akerlof, C., *et al.* 2000, *Astron. J.*, **119**, 1901.

Berry, R., and Burnell, J. 2011, "Astronomical Image Processing for Windows," version 2.4.0, provided with *The Handbook of Astronomical Image Processing*, Willmann-Bell, Richmond, VA.

Binnendijk, L. 1970, *Vistas Astron.*, **12**, 217.

Bonanos, A. 2009, *Astron. J.*, **691**, 407.

Bradstreet, D. H. 2005, in *Society for Astronomical Sciences, 24th Annual Symposium*, Society for Astronomical Sciences, Rancho Cucamonga, CA, 23.

Bradstreet, D. H., and Steelman, D. P. 2004, BINARY MAKER 3, Contact Software (http://www.binarymaker.com).

Eggleton, P. P. 1983, *Astrophys. J.*, **268**, 368.

Gazeas, K., and Stępień, K. 2008, *Mon. Roy. Astron. Soc.*, **390**, 1577.

Gettel, S. J., Geske, M. T., and McKay, T. A. 2006, *Astron. J.*, **131**, 621.

Hambálek, L., and Pribulla, T. 2013, *Contrib. Astron. Obs. Skalnatè Pleso*, **43**, 27.

Harmanec, P. 1988, *Bull. Astron. Inst. Czechoslovakia*, **39**, 329.

Hoffman, D. J., Harrison, T. E., and McNamara, B. J. 2009, *Astron. J.*, **138**, 466.

Kwee, K. K., and van Woerden, H. 1956, *Bull. Astron. Inst. Netherlands*, **12**, 327.

Lucy, L. B. 1967, *Z. Astrophys.*, **65**, 89.

Minor Planet Observer. 2015, MPO Software Suite (http://www.minorplanetobserver.com), BDW Publishing, Colorado Springs.

Nelson, R. H. 2009, WDWINT5.6A, astronomy software by Bob Nelson (http://members.shaw.ca/bob.nelson/software1.htm).
Pecaut, M. J., and Mamajek, E. E. 2013, *Astrophys. J., Suppl. Ser.*, **208**, 1.
Pribulla, T. 2012, in *From Interacting Binaries to Exoplanets: Essential Modelling Tools*, IAU Symp. 282, eds. M. T. Richards, I. Hubeny, Cambridge Univ. Press, Cambridge, 279.
Prša, A., and Zwitter, T. 2005, *Astrophys. J.*, **628**, 426.
Qian, S. 2003, *Mon. Not. Roy. Astron. Soc.*, **342**, 1260.
Ruciński, S. M. 1969, *Acta Astron.*, **19**, 245.
Schlafly, E. F., and Finkbeiner, D. P. 2011, *Astrophys. J.*, **737**, 103.
Schlegel, D. J., Finkbeiner, D. P., and Davis, M. 1998, *Astrophys. J.*, **500**, 525.
Schwarzenberg-Czerny, A. 1996, *Astrophys. J., Lett. Ed.*, **460**, L107.
Skelton, P. L., and Smits, D. P. 2009, *South African J. Sci.*, **105**, 120.
Software Bisque. 2011, CCDSOFT CCD control software (http://www.bisque.com).
Terrell, D., and Wilson, R. E. 2005, *Astrophys. Space Sci.*, **296**, 221.
Van Hamme, W. 1993, *Astrophys. J.*, **106**, 2096.
Vanmunster, T. 2006, Light Curve and Period Analysis Software, PERANSO v.2.5 (http://www.peranso.com/), CBA Belgium Observatory.
Warner, B. D. 2007, *Minor Planet Bull.*, **34**, 113.
Watson, C., Henden, A. A., and Price, C. A. 2014, AAVSO International Variable Star Index VSX (Watson+, 2006–2014; http://www.aavso.org/vsx).
Wilson, R. E. 1979, *Astrophys. J.*, **234**, 1054.
Wilson, R. E. and Devinney, E. J. 1971, *Astrophys. J.*, **166**, 605.
Wozniak, P. R., *et al.* 2004, *Astron. J.*, **127**, 2436.
Yakut, K., and Eggleton, P. P. 2005, *Astrophys. J.*, **629**, 1055.

Studies of the Long Secondary Periods in Pulsating Red Giants

John R. Percy
Emily Deibert
Department of Astronomy and Astrophysics, and Dunlap Institute of Astronomy and Astrophysics, University of Toronto, Toronto ON M5S 3H4, Canada; john.percy@utoronto.ca

Received, May 17, 2016; revised September 28, 2016; accepted October 3, 2016

Abstract We have used systematic, sustained visual observations from the AAVSO International Database and the AAVSO time-series analysis package VSTAR to study the unexplained "long secondary periods" (LSPs) in 27 pulsating red giants. In our sample, the LSPs range from 479 to 2,967 days, and are on average 8.1 ± 1.3 times the excited pulsation period. There is no evidence for more than one LSP in each star. In stars with both the fundamental and first overtone radial period present, LSP is more often about 5 times the former and 10 times the latter. The visual amplitudes of the LSPs are typically 0.1 magnitude and do not correlate with the LSP. The phase curves tend to be sinusoidal, but at least two are sawtooth. The LSPs are stable, within their errors, over the timespan of our data, which is typically 25,000 days. The amplitudes, however, vary by up to a factor of two or more on a time scale of roughly 20–30 LSPs. There is no obvious difference between the behavior of the carbon (C) stars and the normal oxygen (M) stars. Previous multicolor photoelectric observations showed that the LSP color variations are similar to those of the pulsation period, and of the LSPs in the Magellanic Clouds, and not like those of eclipsing stars. Although our results are suggestive of rotational variability, there are several arguments against this. So the cause of the LSPs remains unknown.

1. Introduction

About a third of pulsating red giants show a long secondary period (LSP) an order of magnitude longer than the pulsation period (Wood 2000; Percy and Bakos 2003). LSPs have been known for many decades (O'Connell 1933; Payne-Gaposchkin 1954; Houk 1963) from visual or photographic observations. LSPs have also been discovered photoelectrically in many small-amplitude pulsating red giants (Percy *et al.* 1996, 2001; Percy and Bakos 2003). LSPs were rediscovered in 1999 by Peter Wood and colleagues (Wood *et al.* 1999; Wood 2000) from large-scale survey observations of pulsating red giants in the Large Magellanic Cloud (LMC). Since then, he and others have accumulated many more observations of this phenomenon, and have considered many possible explanations. None of them explains these LSPs satisfactorily. Wood considers this to be the most significant unsolved problem in stellar pulsation.

There are at least three possible mechanisms that are still of interest: the turnover of giant convective cells (Stothers 2010), oscillatory convective modes (Saio *et al.* 2015), or the presence of a dusty cloud, orbiting the red giant, together with a low-mass companion in a close, circular orbit (Soszyński and Udalski 2014), or some combination of these.

Nicholls *et al.* (2009) (hereinafter NWCS) discussed the problem of the LSPs in detail, and "are unable to find a suitable model for the LSPs," so they ended by listing "all the currently known properties of LSPs"—a list of 13 items. A few other properties have been added in the literature since then. The purpose of the present paper is to use the systematic, sustained visual data in the AAVSO International Database (Kafka 2016) to add further "knowns" to this list.

LSPs are not the only unsolved mystery in pulsating red giants. Percy and Abachi (2013) found that the pulsation amplitudes in these stars varied by factors of 2 to over 10 on median time scales of 44 pulsation periods. There are also random cycle-to-cycle period fluctuations in red giants (Eddington and Plakidis 1929; Percy and Colivas 1999) which may be related to large convection cells in these stars.

2. Data and analysis

We used visual observations from the AAVSO International Database (AID; Kafka 2016), and the AAVSO VSTAR time-series analysis package (Benn 2013), which includes both a Fourier analysis and a wavelet analysis routine. Stars (listed in Table 1) with sufficient observations in the AID were chosen for analysis from several sources, including Payne-Gaposhkin (1954), Houk (1963), and Kiss *et al.* (1999), among others. We have included three pulsating red supergiants (SG) for comparison. We have also included V Hya, which has unusually-deep and stable LSP minima and may be an eclipsing binary star (Knapp *et al.* 1999). The columns give the star name, the type (M, C, or SG), the starting JD (otherwise all the AID data were used), the pulsation period P, the LSP, the ratio of these, the mean, maximum, and minimum LSP amplitudes, and notes. The notes are as follows: pcs—sinusoidal phase curve; pcs:—possibly sinusoidal phase curve; pc?—phase curve uncertain, but possibly non-sinusoidal; pcst—phase curve sawtooth; dsp—data sparse; *—see section 3.12. The phase curve is a graph of magnitude versus phase, determined with VSTAR using the known period; it essentially folds all of the observations into one cycle. Note that the mean amplitude was determined by Fourier analysis, the maximum and minimum amplitude by wavelet analysis.

Figure 1 shows the long-term light curve of U Del. The visual observations have also been averaged in bins of 119 days (the pulsation period) to show the LSP more clearly.

3. Results

3.1. Lengths of LSPs

NWCS gave a range of 250 to 1400 days, primarily based on observations of stars in the Magellanic Clouds. Olivier and

Table 1. Pulsation periods and long secondary periods in red giants.

Star	*Type*	*JD(start)*	*P(d)*	*LSP*	*LSP/P*	*A/Amax/Amin*	*Notes*
TZ And	M	2440093	114.8	1355.1	11.8	0.078 0.096 0.049	pc?, dsp
RZ Ari	M	all	56.5	479.4	8.48	0.043 0.102 0.037	pc?
T Ari	M	2415000	320.6	2617.8	8.17	0.429 0.485 0.315	pc?, *
RX Boo	M	all	160.3	2205.1	13.76	0.108 0.136 0.091	pc?, *
RS Cam	M	2443500	90.5	999	11.04	0.157 0.255 0.082	pc:
U Cam	C	2425400	219.4	2967.4	13.53	0.147 0.151 0.147	pcs
IX Car	SG	2442500	371.5	4608.3	12.40	0.188 0.249 0.213	pcs:, dsp
AA Cas	M	2437500	80.1	866.8	10.82	0.041 0.066 0.022	pc?
SS Cep	M	2432500	101.1	955.2	9.45	0.083 0.137 0.064	pcs:
RT Cnc	M	all	89.3	691.7	7.75	0.067 0.116 0.035	pc?
FS Com	M	2440000	55.7	688.7	12.36	0.033 0.080 0.042	pc?
Y CVn	C	2430000	160	2008.9	6.88	0.071 0.096 0.049	pcs, *
AW Cyg	C	2431500	209:	2289:	6.40	0.084 0.091 0.081	pcs:, *
BC Cyg	SG	2437500	698.8	3459.6	4.95	0.128 0.171 0.010	pc?
U Del	M	all	119.0	1162.8	9.77	0.211 0.257 0.153	pcs
RY Dra	C	2432500	276.7:	1135.6:	4.10	0.108 0.137 0.064	pcs, *
TX Dra	M	2431702	77.5	711.8	9.18	0.080 0.193 0.101	pcs:, dsp
RW Eri	M	all	91.4	952.0	10.42	0.148 0.172 0.126	pcs:
Z Eri	M	2430000	78.5	692.4	8.82	0.065 0.197 0.080	pc?
TU Gem	C	all	214.6	2413.7	11.25	0.093 0.101 0.097	pcs:
g Her	M	2430000	87.6	878.7	10.03	0.164 0.222 0.132	pcs, *
X Her	M	2430240	176.6	1185.3	6.71	0.060 0.134 0.047	pc?
V Hya	C	all	531.4	6907.4	13.00	1.132 1.160 1.092	*
RV Lac	M	all	70.0	632.6	9.04	0.320 0.453 0.261	pcst
Y Lyn	M	all	134.7	1258.7	9.34	0.322 0.398 0.149	pcst
BQ Ori	M	2430000	246.6	2147.8	8.71	0.034 0.047 0.026	pc?
W Ori	C	2430000	210.7	2335.1	11.08	0.197 0.213 0.176	pc?
SU Per	SG	2432500	469.0	3355.7	7.16	0.115 0.122 0.111	pc?
UZ Per	M	all	186.3	893.4	4.80	0.293 0.357 0.236	pc?
τ4 Ser	M	all	111	1151.2	13.51	0.104 0.117 0.071	pcsa, *:
ST UMa	M	2430000	90.3	623.1	6.90	0.070 0.117 0.041	pc?
V UMi	M	2430644	72.9	757.3	18.7	0.078 0.103 0.031	pcs:, *

Wood (2003) analyzed 26 Galactic stars with LSPs between 500 and 3,735 days (excluding V Hya, which is peculiar and possibly a binary). Our study includes both short-period and longer-period stars in the Milky Way. The Galactic stars in Table 1 may have different properties than the low-metallicity stars in the Magellanic Clouds studied by Wood and others. Excluding supergiants, our range is 479 to 2,967 days (Table 1; Figure 2). There may be stars with shorter or longer LSPs, presumably with pulsation periods shorter or longer than those in Table 1.

3.2. LSPs in red supergiants

It is important to note that LSPs are also found in pulsating red *supergiants* (Kiss *et al.* 2006; Percy and Sato 2009); the LSP phenomenon seems to be continuous from class III to class II to class I stars. Kiss *et al.* (2006) used Fourier techniques to analyze visual measurements; Percy and Sato (2009) used self-correlation techniques to analyze similar datasets. There are about ten stars for which the above-mentioned papers obtained consistent pulsation periods and LSPs; for these, the median value of LSP/P is 6.0 and the median LSP visual amplitude is 0.10 magnitude, similar to those in red giants. For red supergiants in the Large Magellanic Cloud, the median LSP/P is about 4, and the median V amplitude is about 0.08 (Yang and Jiang 2012). Kiss *et al.* (2006) concluded, on the basis of the Lorentzian envelopes of the peaks in the Fourier spectra, and the strong 1/f noise, that large convection cells play an important role in the behavior of these red supergiant stars.

3.3. The amplitudes of the LSPs

The median LSP amplitude for the stars in Table 1 is 0.10 for both the M stars and the C stars. There is no evidence that it varies with LSP (and therefore with the size and/or temperature of the star), according to Figure 3, which shows the LSP amplitude as a function of LSP. Note that we find LSPs in short-period pulsators such as RZ Ari, whose variability is best studied photoelectrically (Percy *et al.* 2008). Nicholls *et al.* (2010) show that the LSP *velocity* amplitude is constant, at a few km/s, over a very wide range of LSPs.

It is said that Mira stars do not have LSPs, but low-amplitude LSPs may be hidden by the large-amplitude pulsation, and by

the complex Fourier spectra of these stars, which arise from the systematics in the time distribution of the observations, and from the stars' random changes in period and amplitude. For instance, the Fourier spectra of AAVSO visual data on Mira stars tend to have strong one-cycle-per-year aliases at periods of a few thousand days (the possible values of the LSPs), and the noise level in the spectra exceeds 0.1 magnitude.

3.4. The phase curves of the LSPs

For most of the stars in our sample, the LSP phase curves are indistinguishable from sine curves, with the exception of a very small number which have sawtooth or possibly sawtooth shapes. The clearest example is Y Lyn (Figure 4). This figure shows the long-term light curve of Y Lyn; the visual observations have also been averaged in bins of 134.7 days (the pulsation period) to show the sawtooth shape of the LSP light curve more clearly. The other star with a distinctly saw-tooth phase curve is RV Lac. We note that both these stars have higher-than-average LSP amplitudes. The model of Soszyński and Udalski (2014) predicts a different shape for the phase curve; see section 4.

3.5. Is the LSP always ten times the fundamental pulsation Period?

Some stars with LSPs pulsate in the fundamental mode, and others in the first overtone. Is the LSP always ten times the excited period, no matter which mode is excited?

Fuentes-Morales and Vogt (2014) used the ASAS database to study 72 pulsating red giants. Of the stars which they identified as triply periodic (their Table 2), eight appear to have an LSP and a fundamental (P0) and a first overtone (P1) radial period present. In three of these, LSP/P1 is closer to 8.1 than LSP/P0; in two of these, LSP/P0 is closer, and in three of them, both ratios are equidistant from 8.1. In Kiss *et al.* (1999)'s list of triply-periodic stars, there are nine with LSP, P0, and P1. In six cases, LSP/P1 is closer to 8.1, in two, LSP/P0 is closer, and in one case, they are equidistant from 8.1. In our sample, there are four stars (RX Boo, RS Cam, TX Dra, and X Her) which appear to have these three periods present. In three, LSP/P0 is closer to 8.1; in the other, LSP/P1 is closer to 8.1. We conclude that, although LSP is slightly more often about 8.1 times the first overtone radial period, this is not always the case. This may explain some of the scatter in Figure 2.

A different approach is to consider a plot (Figure 5) of LSP/P0 and LSP/P1 versus LSP. For stars with LSP less than about 1,500 days, LSP/P0 is about 5–6, LSP/P1 about 9–11. This suggests that the LSP is generally about 5–6 times the fundamental period. For stars with LSP greater than 1,500 days, the behavior is much less consistent.

3.6. Uniqueness of the LSP

Some theories of the LSP suggest that there may be two or more long timescales in a pulsating red giant, such as the turnover time of a bright or dark convective cell, and the rotation period of the star. There are already four timescales which we have identified in our sample: (1) the pulsation period; (2) the LSP; (3) the timescale for increase and decrease of the amplitude of the pulsation period; and (4) the timescale for increase and decrease of the amplitude of the LSP. As noted below, timescale (3) is not the same as the LSP.

We have used Fourier analysis to look for stars in our sample which might have more than one LSP, but there are none in which a second LSP is significantly above the noise level. For example, the LSP light curves in Figures 1 and 4 appear to be monoperiodic.

3.7. LSP Period stability

For most of the stars in Table 1—those for which the observations are both dense and sustained—the half-width at half-maximum errors in determining the LSP are 3 to 5 percent. Figure 6 shows the Fourier spectrum of TZ And, showing how the HWHM uncertainly of the LSP was determined. We adopt 3 percent as a reasonable intrinsic uncertainty caused by the finite length of the dataset and the scatter in the visual observations. We then used wavelet analysis to study changes in the LSP with time. We did not find any stars for which LSP varied by more than three times the error—that is, by 10 percent or more, over the timespan of the observations, which is typically 25,000 days. A possible exception may be Z Eri, for which the mean LSP is 722 days, the range is 695 to 740 days, and the formal error of the LSP is only 7 days. This error seems unreasonably low, however, being only 1 percent.

3.8. LSP amplitude stability

Percy and Abachi (2013) showed that, for a small sample of red giants with LSPs, the amplitudes of most of the LSPs varied by a factor of up to 2, on a time scale of typically 30 LSPs or greater. Figure 7 shows the amplitude of the LSP of RT Cnc as a function of time. The amplitude rises and falls on a time scale of about 20 LSPs. This is true of the other stars in Table 1, as it was for the LSPs of the stars studued by Percy and Abachi (2013). It is difficult to determine the time scale of the LSP amplitude variability because of its length, but one way of doing so is shown in Figure 8, which plots a measure of the *change* in LSP amplitude against the LSP. Stars with longer LSPs change less in amplitude, presumably because, for these stars, the time scale of amplitude variability, being tens of times greater than the LSP itself, is longer than the timespan of our observations. This interpretation of Figure 8 is therefore consistent with the results of Percy and Abachi (2013).

3.9. Correlation of pulsation amplitude with LSP Phase

NWCS note that the primary pulsation is visible in the light curve at all times throughout the LSP and the primary *period* does not significantly change with LSP phase. Because the cycles of increase and decrease of the primary pulsation period's *amplitude* vary on a median time scale of 44 periods (Percy and Abachi 2013), whereas the LSP is about 8.1 times the excited pulsation period, it follows that the pulsation period's *amplitude* is not correlated with the LSP phase. For instance: for W Ori, the cycles of pulsation amplitude increase and decrease are about 4,500 days, whereas the LSP is about half that.

3.10. Oxygen (M) stars versus carbon (C) stars

In our previous studies of red giants, Percy and Yook (2014) identified one possible difference in pulsational behavior between oxygen (M) stars and carbon (C) stars, namely that, in C stars, amplitude changes correlated with period changes,

whereas this was not true for M stars. We have therefore looked in our database to see whether there are any differences between M and C stars in the LSPs or their amplitudes. In doing this, we have been careful to compare stars with similar periods. Carbon stars have longer pulsation periods, on average, than oxygen stars, because the carbon-star phenomenon is associated with a more advanced stage of evolution, when the star is larger and cooler. Figures 2 and 8 show no obvious differences between the behavior of the two classes of star.

3.11. LSP color to light variations

Derekas *et al.* (2006) pointed out that, on the basis of their observations, the relative color amplitudes were similar, for the LSPs, to those for the pulsation period, but this was not true for stars with ellipsoidal variability. Percy *et al.* (2008) used merged AAVSO and robotic telescope photometry to show that the same was true for the LSPs of 12 small-amplitude pulsating red giants (EG And, RZ Ari, ψ Aur, BC CMi, TU CVn, FS Com, α Her, V642 Her, 30 Her, Y Lyn, UX Lyn, TV Psc), with the possible exception of EG And, which appears to be a genuine symbiotic spectroscopic binary (their Figures 7 and 8). Specifically, these stars had a visual LSP amplitude about twice the red amplitude which, in turn, was about twice the near-infrared amplitude; they are brighter when hotter. These relative amplitudes are slightly larger, on average, than the ΔV/ΔI ratios shown in Figure 4 of Soszyński and Udalski (2014), but are within the same range. Also, the metallicities of the Galactic and LMC stars are quite different.

3.12. Notes on individual stars

T Ari This star, because of its large amplitude, is classified as a Mira star.

RX Boo There may also be a 372.99-day period.

Y CVn The pulsation period is uncertain, but is most likely 160 days.

AW Cyg The pulsation period (most likely 358 days) and the LSP are uncertain.

RY Dra The 276.7-day pulsation period is consistent with the DIRBE photometry (Price *et al.* 2010), and the 1,135.6-day LSP in the AAVSO data seems secure. But the DIRBE data suggest that the LSP may be longer.

g Her There may also be a 61.21-day pulsation period.

V Hya This is a peculiar pulsating red giant with an LSP (6,907 days) which has a large amplitude (1.13 magnitudes), a V-shaped phase curve, and a stable LSP and LSP amplitude—very much like the RVB star U Mon. Knapp *et al.* (1999) suggest that this is a binary in which the secondary component is surrounded by dust.

τ4 Ser The pulsation period is uncertain, but is most likely 111 days.

V UMi There may also be a 125.45-day pulsation period.

4. Discussion

Numerous possible explanations for the LSPs have been proposed and examined but, as NWCS have described, most have not been successful. These include radial or non-radial pulsation—unless there is some non-standard pulsation mode yet to be discovered. Standard binary models fail to explain the highly non-random distribution of velocity-curve amplitudes, shapes, and orientations (but the situation is reminiscent of the "Barr effect" (Percy 2015) in which the velocity curves of spectroscopic binary stars were distorted by mass transfer).

Saio *et al.* (2015) have proposed that oscillatory convective modes are a possible explanation for the LSPs. The timescales are consistent with the LSPs, assuming that the modes are actually excited. The amplitudes, shapes, and color dependences of the phase curves are in reasonable agreement with observations. We would need some explanation for the variable amplitudes of the LSPs. Saio *et al.* (2015) state that there is a minimum luminosity for the presence of oscillatory convective modes. We find LSPs in many less-luminous stars, with amplitudes comparable to those in more luminous ones.

Another interesting and still-viable explanation is the rise and fall of giant convective cells, which are known to occur in cool stars (Stothers 2010). The time scales of rise and fall are similar to those of LSPs, but we must remember that these stars are also rotating, so this phenomenon would be modulated by the rotation period. We do not find evidence for two different LSPs in the same star (section 3.6). Also: we would need an explanation for the variable amplitude of the LSPs.

There are possible mechanisms which are based on rotational modulation. These include the effect of a dusty cloud, orbiting the red giant with a low-mass companion in a close, circular orbit (Soszyński and Udalski 2014); the period would be the orbital period but, since the authors suggest that the red giant would be co-rotating with the companion, the period would be essentially the rotation period. It may seem improbable that a third of red giants should have such configurations, but we should remember that the not-uncommon LSPs in RV Tauri stars (the so-called RVb stars) are thought to be due to the effects of a binary companion (Percy 1993; Waelkens and Waters 1993). Another rotation explanation would be the presence of a large, hot/bright or cool/dark convective cell with a lifetime of a few LSPs.

There are problems with any rotational explanation. Olivier and Wood (2003) carried out a careful spectroscopic study of 26 red giants with LSPs and 30 without. The power spectra of the flux spectra were analyzed for rotation and microturbulence according to the methods of Gray (1976). There was no significant difference between the two samples so, for instance, there was no evidence that the LSP stars were seen equator-on and the non-LSP stars were seen pole-on, or that high or low rotation was related to the cause. Olivier and Wood (2003) derived a general *upper limit* to the equatorial rotational velocity of 3 km/s. This would lead to LSPs in excess of about 3,000 days, whereas most LSPs are much less than this.

Furthermore: theoretical models of evolution, with rotation, predict very slow rotation in red giants, unless some process could transfer angular momentum to the outer layers (Privitera *et al.* 2016 and references therein). Rotation could be spun up by the engulfment of Jupiter-mass planets (for example, Privitera *et al.* 2016), but this would result in a distribution of rotation periods. In fact, the natural distribution of initial rotation rates in red giant progenitors should also produce a distribution of rotation periods in the red giants, whereas the LSPs are well

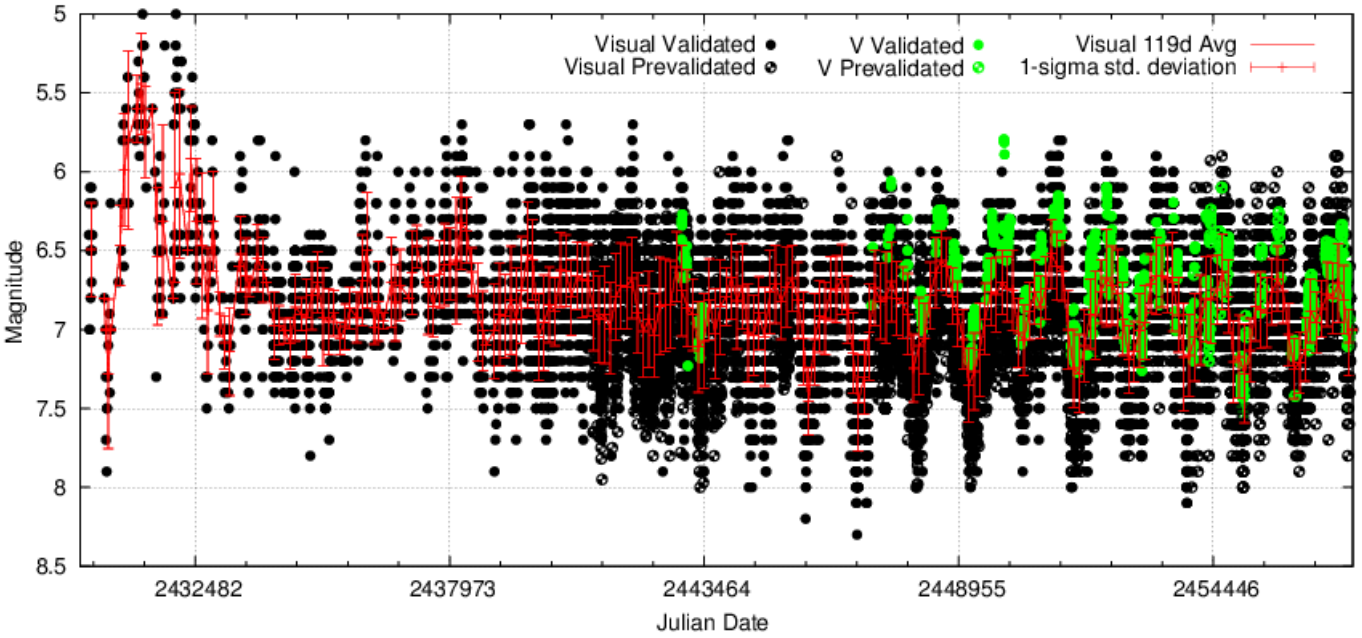

Figure 1. The long-term AAVSO light curve of U Del, also showing the data averaged in bins of 119 days (the pulsation period) to shown the LSP light curve (red curve, points with error bars) more clearly. The LSP, as determined by VSTAR, is 1,162.8 days, and this is consistent with the value which would be determined by counting cycles in this figure. We have plotted all the observations, to show how the density of observations and the clarity of the LSP increase after JD 2440000. The black points are visual; the green ones (lighter circles) are photoelectric V.

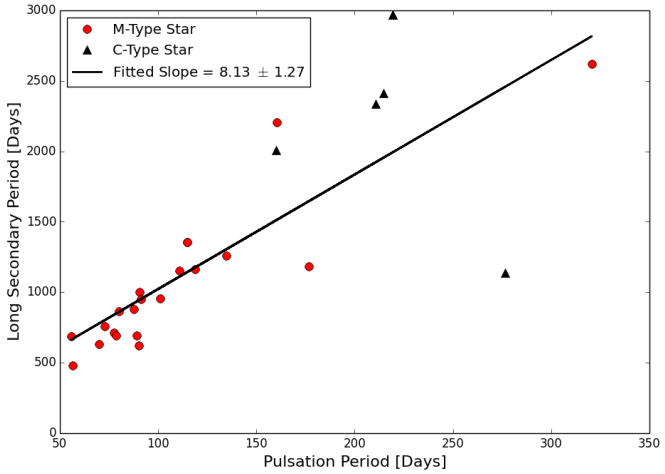

Figure 2. The LSP as a function of pulsation period. The slope of a linear fit is 8.1 ± 1.3.

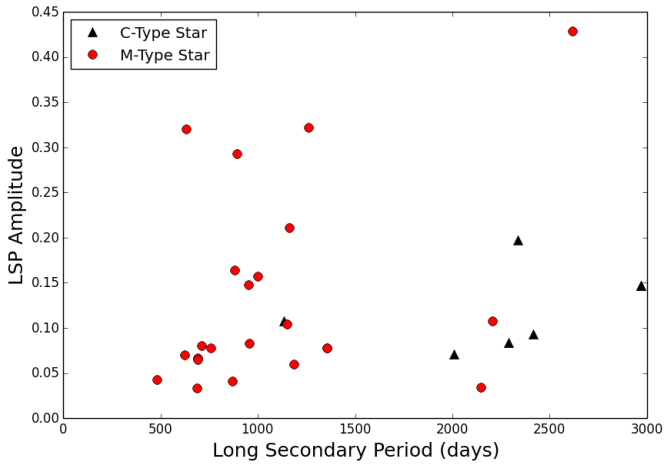

Figure 3. The LSP amplitude, in magnitudes, as a function of LSP. There is much scatter, but the median amplitude is about 0.10 magnitude, and there is no obvious correlation between the two.

correlated with the pulsation period and therefore with the radius of the star.

On the other hand, Zamanov *et al.* (2008) have measured the equatorial rotational velocities of 28 M-type red giants, and found rotational velocities closer to 5 km/s. These would result in shorter rotation periods. These authors used different methods of analysis—cross-correlation, and absorption-line width—to estimate the velocities. These methods may well under-estimate the contribution of convection and velocity gradients due to winds and pulsation on the spectral line profiles, because the calibration and cross-correlation were done against K-type (rather than M-type) comparisons, so their rotational velocities are upper limits. In summary: rotational mechanisms for the LSP phenomenon are problematic, but not entirely ruled out.

5. Conclusions

We have used systematic, sustained visual observations from the AAVSO International Database and the AAVSO time-series analysis software package VSTAR to study the LSPs in 27 red giants. The LSPs are, on average, 8.1 ± 1.3 times the excited pulsation period, and the median visual amplitude is 0.1, independent of the LSP. The LSPs are stable over many decades, but the amplitudes rise and fall on a time scale of a few tens of LSPs. The LSP phase curves are not well-defined, but at least two appear to have a sawtooth shape. The similarity between the LSP and the rotation period of the star suggests that the LSP phenomenon may be due to rotational variability, modulated by a large bright or dark convective cell, or by obscuring material near the photosphere, but there are also strong arguments against the rotational hypothesis, as explained above.

We also note that visual observations, despite their lower accuracy, are able to delineate the long-term behavior of these stars because they are sustained over up to a century. Whether

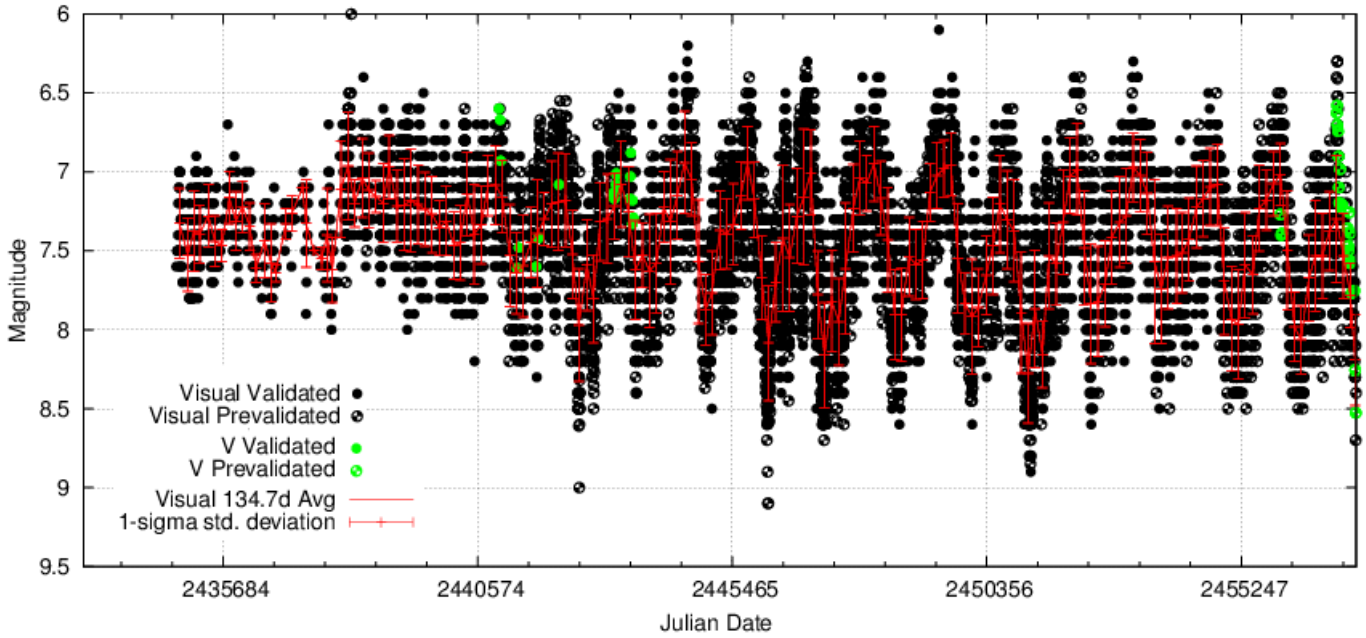

Figure 4. The long-term light curve of Y Lyn, also showing the data averaged in bins of 134.7 days (the pulsation period) to show the sawtoothed shape of the LSP light curve (red curve, with error bars) more clearly. The LSP, as determined from vstar, is 1,258.7 days, and this is consistent with the value which would be obtained by counting cycles in this figure. We have plotted all the observations, to show how the density of the observations and the clarity of the LSP increase after JD 2440000. The black points are visual; the green ones (lighter circles) are photoelectric V.

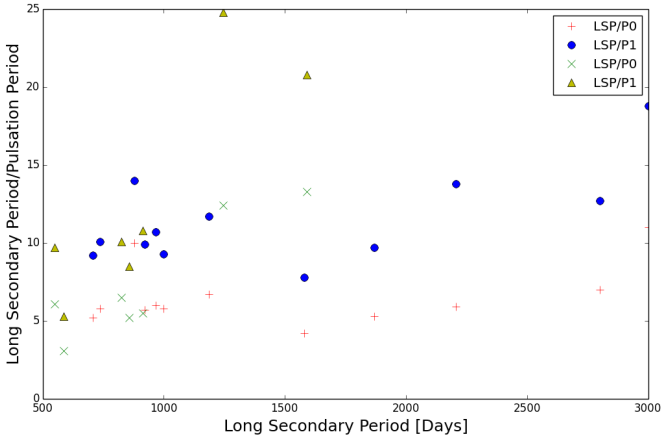

Figure 5. For stars with both P0 and P1 excited: the ratio of the LSP to P0 (plus signs and x's), and to P1 (filled circles and triangles). The plus signs and filled circles are from the visual data of Kiss *et al.* (1999) and from Percy and Huang (2015); the x's and filled triangles are from the ASAS data of Fuentes-Morales and Vogt (2014).

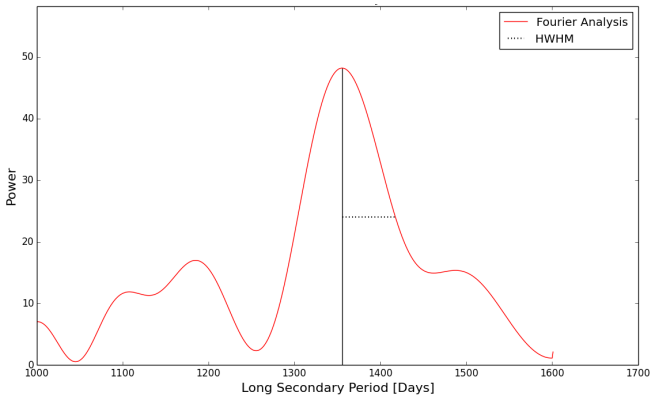

Figure 6. The Fourier spectrum of TZ And, showing how the uncertainty σ in the LSP is determined from the half-width at half-maximum of the LSP peak.

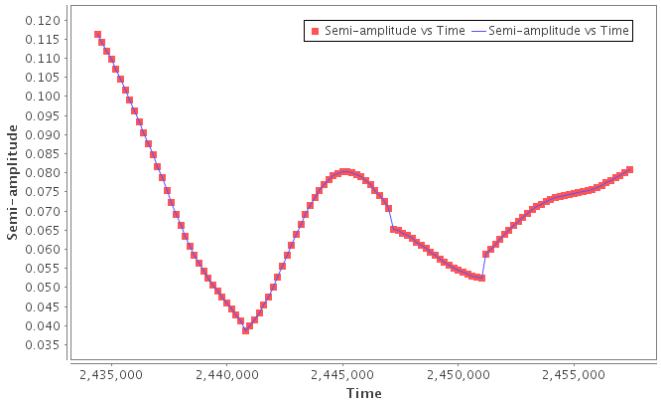

Figure 7. The LSP amplitude of RT Cnc as a function of time, determined by wavelet analysis. The amplitude rises and falls on a time scale of about 20 LSPs.

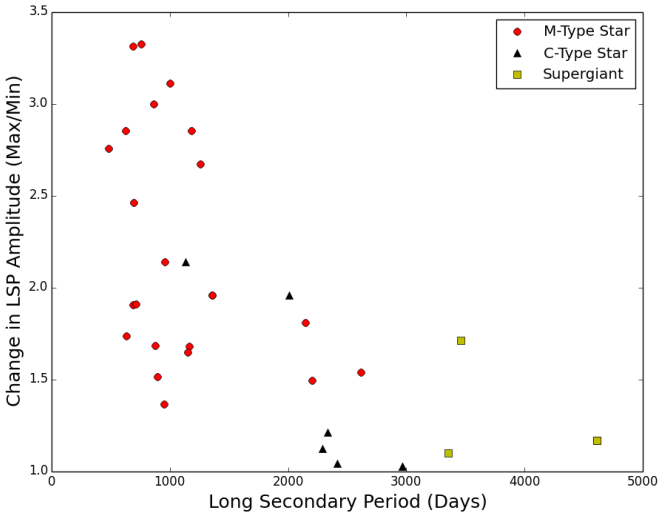

Figure 8. The relative change in LSP amplitude (max/min) over the timespan of the data, as a function of LSP. As explained in the text, this suggests that the LSP amplitude varies slowly, on a time scale of a few tens of LSPs.

or not the rotational hypothesis is still viable, we believe that we have added a few more "knowns" to the NWCS list, and have brought us a bit closer to solving this longstanding mystery.

6. Acknowledgements

We thank the AAVSO observers who made the observations on which this project is based, the AAVSO staff who archived them and made them publicly available, and the developers of the VSTAR package which we used for analysis. We are very grateful to Professor Peter Wood for reading and commenting on a draft of this paper, and to the referee for helpful suggestions. We acknowledge and thank the University of Toronto Work-Study Program for financial support. JRP thanks co-author ED, an astronomy and physics (and English) major, for carrying out this project so professionally. ED thanks co-author JRP for the opportunity to work on this project. This project made use of the SIMBAD database, maintained in Strasbourg, France.

References

Benn, D. 2013, VSTAR data analysis software (http://www.aavso.org/vstar-overview).

Derekas, A., Kiss, L. L., Bedding, T. R., Kjeldsen, H., Lah, P., and Szabó, Gy. M. 2006, *Astrophys. J. Lett.*, **650**, L55.

Eddington, A. S., and Plakidis, S. 1929, *Mon. Not. Roy. Astron. Soc.*, **90**, 65.

Fuentes-Morales, I., and Vogt, N. 2014, *Astron. Nachr.*, **335**, 1072.

Gray, D. F. 1976, *The Observation and Analysis of Stellar Photospheres*, Wiley, New York.

Houk, N. 1963, *Astron. J.*, **68**, 253.

Kafka, S. 2016, variable star observations from the AAVSO International Database (https://www.aavso.org/aavso-international-database).

Kiss, L. L., Szabó, G. Y., and Bedding, T. R. 2006, *Mon. Not. Roy. Astron. Soc.*, **372**, 1721.

Kiss, L. L., Szatmáry, K., Cadmus, R. R., Jr., and Mattei, J. A. 1999, *Astron. Astrophys.*, **346**, 542.

Knapp, G. R., Dobrovolsky, S. L., Ivesic, Z., Young, K., Crosas, M., Mattei, J. A., and Rupen, M. P. 1999, *Astron. Astrophys.*, **351**, 97.

Nicholls, C. P., Wood, P. R., and Cioni, M.-R. L. 2010, *Mon. Not. Roy. Astron. Soc.*, **405**, 1770.

Nicholls, C. P., Wood, P. R., Cioni, M.-R. L., and Soszyński, I. 2009, *Mon. Not. Roy. Astron. Soc.*, 399, 2063 (NWCS).

O'Connell, D. J. K. 1933, *Bull. Harvard Coll. Obs.*, No. 893, 19.

Olivier, E. A., and Wood, P. R. 2003, *Astrophys. J.*, **584**, 1035.

Payne-Gaposchkin, C. 1954, *Ann. Harvard Coll. Obs.*, **113**, 189.

Percy, J. R. 1993, in *Luminous High-Latitude Stars*, ed. D. D. Sasselov, ASP Conf. Ser. 45, Asronomical Society of the Pacific, San Francisco, 295.

Percy, J. R. 2015, *J. Roy. Astron. Soc. Canada*, **109**, 270.

Percy, J. R., and Abachi, R. 2013, *J. Amer. Assoc. Var. Star Obs.*, **41**, 193.

Percy, J. R., and Bakos, G. A. 2003, in *The Garrison Festschrift*, ed. R. O. Gray, C. Corbally, C., and A. G. D. Philip, L. Davis Press, Schenectady, NY, 49.

Percy, J. R., and Colivas, T. 1999, *Publ. Astron. Soc. Pacific*, **111**, 94.

Percy, J. R., Desjardins, A., Yu, L., and Landis, H. J. 1996, *Publ. Astron. Soc. Pacific*, **108**, 139.

Percy, J. R., and Huang, D. J. 2015, *J. Amer. Assoc. Var. Star Obs.*, **43**, 118.

Percy, J. R., Mashintsova, M., Nasui, C. O., Seneviratne, R., and Henry, G. W. 2008, *Publ. Astron. Soc. Pacific*, **120**, 523.

Percy, J. R., and Sato, H. 2009, *J. Roy. Astron. Soc. Canada*, **103**, 11.

Percy, J. R., Wilson, J. B., and Henry, G. W. 2001, *Publ. Astron. Soc. Pacific*, **113**, 983.

Percy, J. R., and Yook, J. Y. 2014, *J. Amer. Assoc. Var. Star Obs.*, **42**, 245.

Price, S. D., Smith, B. J., Kuchar, T. A., Mizuno, D. R., and Kraemer, K. E. 2010, *Astrophys. J., Suppl. Ser.*, **190**, 203.

Privitera, G., Meynet, G., Eggenberger, P., Vidotto, A. A., Villaver, E., and Bianda, M. 2016, arXiv: 1606.08027.

Saio, H., Wood, P. R., Takayama, M., and Ita, Y. 2015, *Mon. Not. Roy. Astron. Soc.*, **452**, 3863.

Soszyński, I., and Udalski, A. 2014, *Astrophys. J.*, **788**, 13.

Stothers, R. B. 2010, *Astrophys. J.*, **725**, 1170.

Waelkens, C. and Waters, L. B. F. M. 1993, in *Luminous High-Latitude Stars*, ed. D. D. Sasselov, ASP Conf. Ser. 45, Astronomical Society of the Pacific, San Francisco, 219.

Wood, P. R. 2000, *Publ. Astron. Soc. Australia*, **17**, 18.

Wood, P. R., *et al.* 1999, in *Asymptotic Giant Branch Stars*, ed. T. Le Bertre, A. Lebre, and C. Waelkens, IAU Symp. 191, Cambridge Univ. Press, Cambridge, 151.

Yang, M., and Jiang, B. W. 2012, *Astrophys. J.*, **754**, 35.

Zamanov, R. K., Bode, M. F., Melo, C. H. F., Stateva, I. K., Bachev, R., Gomboc, A., Konstantinova-Antova, R., and Stoyabov, K. A. 2008, *Mon. Not. Roy. Astron. Soc.*, **390**, 377.

First Photometric Analysis of the Solar-Type Binary, V428 Cep (NSV 395), in the field of NGC 188

Ronald G. Samec
Astronomy Group, Department of Natural Sciences, Emmanuel College, 181 Springs Street, Franklin Springs, GA 30639; ronaldsamec@gmail.com

Jeremy Clark
David Maloney
Astronomy Program, Department of Physics and Engineering, Bob Jones University, 1700 Wade Hampton Boulevard, Greenville, SC 29614; clarky1123@gmail.com; david.edward.maloney@gmail.com

Daniel B. Caton
Dark Sky Observatory, Physics and Astronomy Department, Appalachian State University, 525 Rivers Street, Boone, NC 28608-2106; catondb@appstate.edu

Danny R. Faulkner
Director, Johnson Observatory, 1414 Bur Oak Court, Hebron, KY 41048

Received June 25, 2016; revised September 13, October 4, 2016; accepted October 6, 2016

Abstract V428 Cep (or NSV 395) is a faint 15th magnitude binary observed in a study of the open cluster NGC 188. However, its distance from the core of the cluster might exclude its membership. Its light curve was classified as a short period EB type eclipsing binary with a period of 0.3079 d and an amplitude of ~0.7 magnitude in all curves. The difference in component temperatures is some $\Delta T = 180$ K and its fill-out is a hefty 35%. A brief, 2.5 year period study yields, as expected, a constant period, which is 0.3076789 d. More monitoring is needed to determine its true orbital evolution. The inclination, 80º is not quite enough to produce total eclipses, so a q-search was performed using the September 17, 2004 version of the Wilson-Devinney program. Our lowest residual solution gives a $q = 0.4$. A cool spot was modeled on the primary component to take care of the light curve asymmetries. V428 Cep is a K-type W UMa contact binary.

1. Introduction

This paper represents the first precision, four-color, BVRI photometric study of this interesting contact binary which is in the field of the open cluster NGC 188.

2. History and observations

The variable was originally listed as short period variable NSV 395 (S8282) from photographic data (Hoffmeister 1964). It was observed in a study of the very old open cluster (age 5–7 Gyr) NGC 188 (Popov *et al.* 2013). This cluster age is what we might expect for such a W UMa binary. This paper designated it as a β Lyr-type eclipsing binary with a period of 0.3077 day and an Rmag range of 14.392–15.675 and a secondary minimum of 15.552. They gave the first published ephemeris:

$$\text{JD Hel MinI} = 2455632.260 + 0.3077\ \text{d} \times \text{E}. \quad (1)$$

Popov *et al.*'s (2013) CCD light curves are given in Figure 1.

This system was observed as a part of our student/professional collaborative studies of interacting binaries from data taken from Dark Sky Observatory (DSO) observations. The observations were taken by Dr. Dan Caton, Dr. Ron Samec, and Jeremy Clark. Reduction and analyses were mostly done by Dr. Samec and David Maloney. Our 2013 BVRI light curves were taken with the DSO 0.81-meter reflector at Philips Gap, North Carolina, on 2, 3, and 4 November 2013 with a thermoelectrically cooled (–40ºC) 2KX2K Apogee Alta camera.

Individual observations included 128 in B and R, and 132 in V and I. The probable error of a single observation was 2% in B and V, and 1% in R and I. The relatively large errors are assumed due to the faintness of the binary. Figures 2a and 2b show sample observations of R, I, and R–I color curves on the night of 2 November, and of B, V, and B–V color curves on the night of 3 November 2013, respectively.

Our complete observations are given in Table 1, in delta magnitudes, ΔB, ΔV, ΔR_c and ΔI_c, in the sense of variable minus comparison star (V–C), phased with Equation 2.

3. Finding chart

The finding chart, given here for future observers, is shown in Figure 3. The coordinates and magnitudes of the variable star, comparison star, and check star are given in Table 2. The C–K values stayed fairly constant throughout the observing run, varying 1–2%.

4. Period study

Five times of minimum light were calculated, three primary and two secondary eclipses from our present observations:

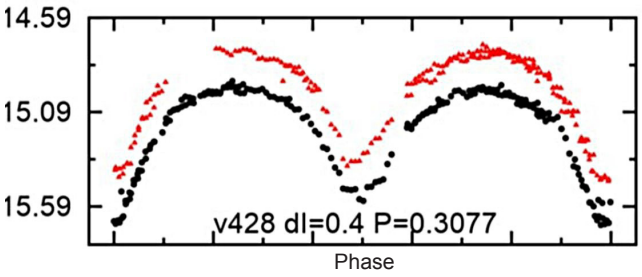

Figure 1. V428 Cep-NGC 188. R, I CCD light curves were taken by Popov *et al.* 2013.

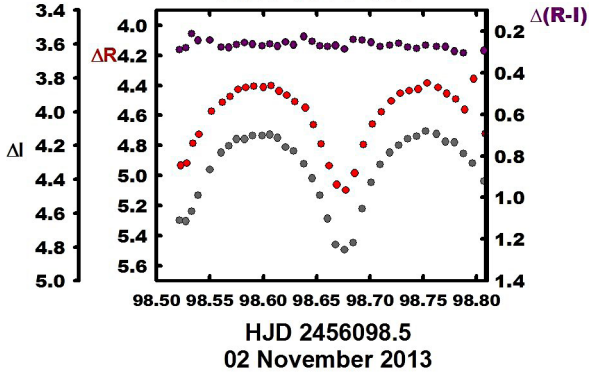

Figure 2a. V428 Cep-NGC 188. R (middle), I (bottom) delta magnitudes from sample observations and color curve (top) on 2 November 2013.

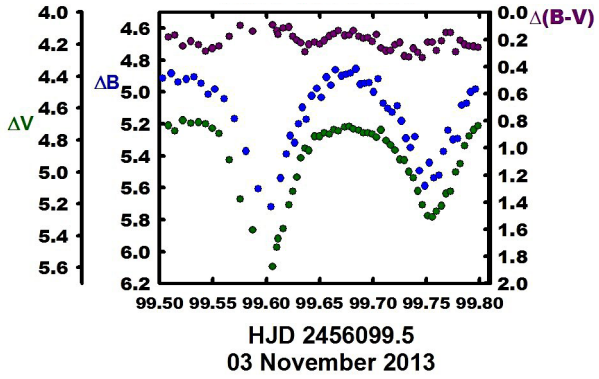

Figure 2b. V428 Cep-NGC 188. B (middle), V (bottom) delta magnitudes and color curve (top) on 3 November 2013.

HJD I = 2456598.6746 ± 0.0007
2456599.5990 ± 0.0014
2456600.8292 ±0.0013

HJD II = 2456598.8299 ± 0.0026
2456599.7549 ± 0.00025.

Six CCD times of minimum light were determined using previous observations of Popov *et al.* 2013. These were included in our determination of an improved linear ephemeris:

$$\text{HJD MinI} = 2456599.5990 + 0.30767914 \times E \qquad (2)$$
$$\pm 0.0010 \quad \pm 0.00000043$$

Since this study covers only 2.5 years of observations, at least 10 more years of patrolling are needed to determine if the period is changing. The times of minimum light and the linear residuals are given in Table 3. Figure 4 shows the linear residuals (O–C's) from this calculation.

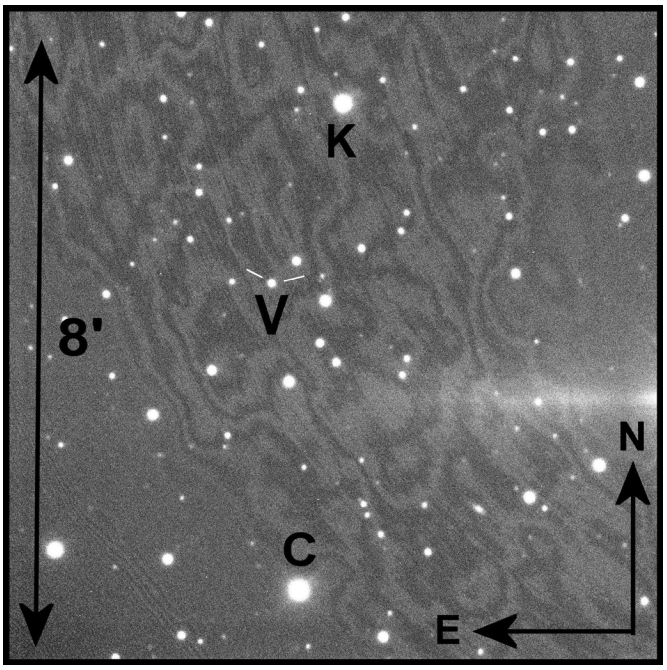

Figure 3. V428 Cep-NGC 188 finding chart. V428 Cep Variable (V), Comparison (C) and Check (K).

5. NGC 188

NGC 188 is an old open cluster of age 5–10 Gyr and has quite a few W UMa binaries (for example, six in Zhang *et al.* 2002), which fall in this age range. From his analysis of the precontact W UMa binary, V12, Meibom (2009) gives a cluster distance of 1,770 ± 75 pc and a main sequence age of 6.2 ± 0.2 Gyr. The position of V428 Cep on the color magnitude diagram is to the right of the main sequence branch before the turnoff, as expected for this cool-type binary system. We believe that the binary could well be a part of the cluster despite its position in the field (43' from the cluster center). W UMa binaries are noted for having high velocity dispersions, and it may be escaping the cluster (Guinan and Bradstreet 1988). The R, R–I color magnitude diagram is shown in Figure 5.

6. Light curve characteristics

The light curves were phased using Equation (2). These are given in Figures 6a and 6b. A table of light curve characteristics is given in Table 4. The curves are only of fair precision, averaging between 1 and 3%, probably due to the binary's faintness. The amplitude of the light curve varies from 0.76 to 0.65 magnitude in B to I, respectively. The O'Connell effect (the difference in maxima), which is classically an indication of spot activity, is slightly larger than the scatter/ averaging 4%. The difference between the two minima is substantial for a W UMa binary, some 0.1–0.2 magnitude, and is undoubtedly the reason it was designated a β Lyr type EB by Popov *et al.* (2013). However, the light curve characteristics point to a

Table 1. V428 Cep-NGC 188 observations, ΔB, ΔV, ΔR, and ΔI, variable star minus comparison star.

ΔB	HJD 2455800+	ΔB	HJD 2455800+	ΔB	HJD 2455800+	ΔB	HJD 2455800+	ΔB	HJD 2455800+
5.486	98.5258	5.029	98.7333	5.187	99.4821	5.024	99.6427	5.538	99.7570
5.404	98.5315	4.986	98.7417	5.075	99.4844	4.977	99.6475	5.523	99.7618
5.367	98.5372	4.947	98.7501	5.082	99.4906	5.036	99.6516	5.372	99.7659
5.236	98.548	4.957	98.7602	5.033	99.4929	4.908	99.6565	5.241	99.7701
5.055	98.5584	4.975	98.7686	4.905	99.4951	4.957	99.6606	5.298	99.7750
5.028	98.5658	5.044	98.777	4.913	99.4974	4.861	99.6648	5.292	99.7792
4.983	98.5731	5.055	98.7854	4.915	99.5029	4.900	99.6707	5.083	99.7833
4.928	98.5804	5.156	98.7938	4.884	99.511	4.888	99.6749	5.071	99.7876
4.941	98.5878	5.252	98.8044	4.937	99.5175	4.882	99.679	5.000	99.7917
4.901	98.5968	5.378	98.8128	4.920	99.525	4.855	99.684	4.983	99.7961
4.910	98.6041	5.527	98.8212	4.906	99.5323	4.952	99.6882	5.026	100.7737
4.922	98.6115	5.524	98.8296	4.945	99.5391	4.946	99.6924	5.011	100.7807
4.996	98.6188	5.440	98.838	5.016	99.5455	4.942	99.6965	5.050	100.7877
5.040	98.6262	5.302	98.8475	4.983	99.5519	5.000	99.7007	5.128	100.7948
5.115	98.6362	5.133	98.8559	5.043	99.5604	4.919	99.7048	5.196	100.8026
5.202	98.6436	5.025	98.8644	5.169	99.5702	5.070	99.7097	5.351	100.8097
5.279	98.6509	4.904	98.8727	5.371	99.581	5.102	99.7139	5.516	100.8171
5.335	98.6584	5.004	98.8811	5.606	99.5923	5.126	99.718	5.615	100.8241
5.518	98.6657	4.941	98.9113	5.718	99.6043	5.086	99.7227	5.673	100.8311
5.564	98.6738	4.999	98.9221	5.540	99.6136	5.182	99.7268	5.600	100.8382
5.539	98.6822	5.019	98.9302	5.390	99.6188	5.290	99.731	5.397	100.8456
5.366	98.6906	5.115	98.941	5.274	99.6226	5.350	99.7352	5.288	100.8534
5.205	98.699	5.263	98.9519	5.319	99.6265	5.281	99.7393	5.100	100.8608
5.099	98.7074	5.655	98.9599	5.201	99.6301	5.494	99.7435	5.018	100.8678
5.001	98.7165	4.989	99.4776	5.097	99.6339	5.588	99.7487		
5.064	98.7249	5.084	99.4799	5.171	99.6375	5.443	99.7528		
ΔV	HJD 2455800+	ΔV	HJD 2455800+	ΔV	HJD 2455800+	ΔV	HJD 2455800+	ΔV	HJD 2455800+
5.227	98.524	4.702	98.7388	4.946	99.479	4.778	99.650	5.137	99.769
5.173	98.530	4.679	98.7472	4.959	99.481	4.756	99.654	5.122	99.773
5.071	98.535	4.661	98.7556	4.881	99.484	4.763	99.659	5.001	99.778
5.009	98.541	4.696	98.7657	4.900	99.486	4.736	99.663	4.951	99.782
4.841	98.553	4.727	98.7741	4.790	99.492	4.744	99.668	4.838	99.786
4.790	98.563	4.764	98.7825	4.821	99.494	4.721	99.673	4.776	99.790
4.734	98.571	4.838	98.7909	4.784	99.497	4.715	99.678	4.738	99.794
4.684	98.578	4.912	98.7993	4.785	99.499	4.732	99.682	4.712	99.799
4.677	98.585	5.029	98.8099	4.710	99.509	4.740	99.687	4.708	100.759
4.653	98.593	5.149	98.8183	4.743	99.514	4.756	99.691	4.690	100.768
4.653	98.602	5.300	98.8267	4.677	99.522	4.757	99.695	4.713	100.778
4.674	98.609	5.270	98.8351	4.697	99.530	4.764	99.699	4.749	100.785
4.702	98.616	5.103	98.8435	4.690	99.536	4.784	99.703	4.826	100.792
4.760	98.624	4.972	98.853	4.701	99.543	4.738	99.708	4.906	100.799
4.759	98.631	4.864	98.8615	4.729	99.550	4.805	99.712	5.042	100.807
4.883	98.641	4.815	98.8698	4.760	99.556	4.833	99.717	5.177	100.814
4.951	98.649	4.780	98.8782	4.927	99.565	4.864	99.721	5.337	100.821
5.093	98.656	4.732	98.8866	5.172	99.576	4.924	99.725	5.362	100.828
5.247	98.663	4.683	98.8953	5.364	99.587	4.928	99.730	5.355	100.835
5.344	98.671	4.675	98.9019	5.357	99.616	5.000	99.734	5.199	100.843
5.360	98.679	4.677	98.9069	5.208	99.621	5.039	99.738	5.043	100.850
5.206	98.688	4.696	98.9164	5.124	99.625	5.121	99.742	4.894	100.858
5.028	98.696	4.749	98.9272	5.033	99.629	5.206	99.746	4.784	100.865
4.902	98.705	4.766	98.9353	4.912	99.632	5.275	99.751	4.752	100.872
4.813	98.713	4.859	98.9462	4.853	99.636	5.283	99.756		
4.739	98.722	5.062	98.957	4.867	99.640	5.248	99.760		
4.740	98.7304	5.087	98.965	4.778	99.645	5.214	99.765		

Table continued on next page

Table 1. V428 Cep-NGC 188 observations, ΔB, ΔV, ΔR, and ΔI, variable star minus comparison star, cont.

Δ*R*	*HJD 2455800+*	Δ*R*	*HJD 2455800+*	Δ*R*	*HJD 2455800+*	Δ*R*	*HJD 2455800+*	Δ*R*	*HJD 2455800+*
4.933	98.523	4.425	98.745	4.544	99.481	4.502	99.644	4.817	99.763
4.918	98.528	4.385	98.754	4.512	99.483	4.453	99.649	4.814	99.767
4.574	98.551	4.414	98.764	4.504	99.485	4.441	99.653	4.738	99.772
4.513	98.562	4.455	98.772	4.477	99.492	4.392	99.658	4.639	99.777
4.475	98.569	4.490	98.781	4.471	99.494	4.418	99.662	4.631	99.781
4.429	98.577	4.562	98.789	4.447	99.496	4.389	99.666	4.614	99.785
4.415	98.584	4.723	98.808	4.467	99.498	4.367	99.672	4.542	99.789
4.406	98.591	4.843	98.816	4.417	99.507	4.379	99.676	4.514	99.793
4.413	98.600	4.979	98.825	4.399	99.513	4.383	99.681	4.518	99.798
4.401	98.608	5.004	98.833	4.409	99.520	4.397	99.686	4.389	100.759
4.438	98.615	4.868	98.842	4.415	99.528	4.396	99.690	4.399	100.767
4.467	98.622	4.765	98.851	4.402	99.535	4.429	99.698	4.449	100.777
4.510	98.630	4.658	98.860	4.442	99.542	4.472	99.702	4.475	100.784
4.550	98.640	4.548	98.868	4.484	99.548	4.502	99.706	4.552	100.791
4.662	98.647	4.517	98.876	4.505	99.555	4.490	99.711	4.622	100.798
4.791	98.654	4.464	98.885	4.580	99.564	4.528	99.715	4.752	100.806
4.935	98.662	4.406	98.892	4.720	99.574	4.585	99.720	4.879	100.813
5.061	98.669	4.394	98.900	4.945	99.585	4.612	99.724	5.055	100.820
5.097	98.677	4.410	98.905	4.950	99.605	4.685	99.728	5.081	100.827
4.985	98.686	4.430	98.915	4.867	99.615	4.738	99.733	5.045	100.834
4.795	98.694	4.440	98.925	4.774	99.620	4.804	99.737	4.820	100.841
4.657	98.703	4.496	98.933	4.688	99.624	4.835	99.741	4.774	100.849
4.578	98.711	4.557	98.944	4.644	99.628	4.951	99.745	4.670	100.856
4.505	98.720	4.697	98.955	4.557	99.632	4.966	99.750	4.560	100.864
4.453	98.729	4.809	98.963	4.561	99.635	4.990	99.754		
4.436	98.737	4.535	99.479	4.520	99.639	4.930	99.759		

Δ*I*	*HJD 2455800+*	Δ*I*	*HJD 2455800+*	Δ*I*	*HJD 2455800+*	Δ*I*	*HJD 2455800+*	Δ*I*	*HJD 2455800+*
4.642	98.522	4.702	98.739	4.946	99.479	4.778	99.650	5.137	99.769
4.648	98.527	4.679	98.747	4.959	99.481	4.756	99.654	5.122	99.773
4.590	98.533	4.661	98.756	4.881	99.484	4.763	99.659	5.001	99.778
4.496	98.539	4.696	98.766	4.900	99.486	4.736	99.663	4.951	99.782
4.343	98.550	4.727	98.774	4.790	99.492	4.744	99.668	4.838	99.786
4.243	98.561	4.764	98.783	4.821	99.494	4.721	99.673	4.776	99.790
4.203	98.568	4.838	98.791	4.784	99.497	4.715	99.678	4.738	99.794
4.163	98.575	4.912	98.799	4.785	99.499	4.732	99.682	4.712	99.799
4.163	98.583	5.029	98.810	4.710	99.509	4.740	99.687	4.708	100.759
4.142	98.590	5.149	98.818	4.743	99.514	4.756	99.691	4.690	100.768
4.143	98.599	5.300	98.827	4.677	99.522	4.757	99.695	4.713	100.778
4.136	98.606	5.270	98.835	4.697	99.530	4.764	99.699	4.749	100.785
4.155	98.614	5.103	98.844	4.690	99.536	4.784	99.703	4.826	100.792
4.211	98.621	4.972	98.853	4.701	99.543	4.738	99.708	4.906	100.799
4.234	98.628	4.864	98.862	4.729	99.550	4.805	99.712	5.042	100.807
4.308	98.638	4.815	98.870	4.760	99.556	4.833	99.717	5.177	100.814
4.394	98.646	4.780	98.878	4.927	99.565	4.864	99.721	5.337	100.821
4.496	98.653	4.732	98.887	5.172	99.576	4.924	99.725	5.362	100.828
4.633	98.661	4.683	98.895	5.364	99.587	4.928	99.730	5.355	100.835
4.786	98.668	4.675	98.902	5.357	99.616	5.000	99.734	5.199	100.843
4.816	98.676	4.677	98.907	5.208	99.621	5.039	99.738	5.043	100.850
4.776	98.685	4.696	98.916	5.124	99.625	5.121	99.742	4.894	100.858
4.574	98.693	4.749	98.927	5.033	99.629	5.206	99.746	4.784	100.865
4.418	98.701	4.766	98.935	4.912	99.632	5.275	99.751	4.752	100.872
4.314	98.710	4.859	98.946	4.853	99.636	5.283	99.756		
4.242	98.719	5.062	98.957	4.867	99.640	5.248	99.760		
4.199	98.727	5.087	98.965	4.778	99.645	5.214	99.765		

Table 2. Information on the stars used in this study.

Star	*Name*	*R.A. (2000) h m s*	*Dec. (2000) ° ′ ″*	*V*	*B–V*	*J–K*
V	3UC350-001392[1]	01 08 12.900	+84 38 06.00	15.51	—	0.581
C	TYC 4619 738	01 07 54.577	+84 33 30.58[2]	10.917	0.535	
K (Check)	TYC 4619 618	01 07 29.1344	+84 40 41.871[2]	12.029	0.813	

[1] *USNO CCD Astrograph Catalog (Zacharias et al. 2012).* [2] *TYCHO (Perryman et al. 1997).*

Table 3. V428 Cep-NGC 188 times of minimum light and linear residuals.

No.	*Epoch HJD 2400000+*	*Cycle*	*Weight*	*O–C*	*Reference*
1	55632.2584	–3144.0	1.0	0.0026	Popov *et al.* 2012
2	55635.3352	–3134.0	1.0	0.0026	Popov *et al.* 2012
3	55638.2565	–3124.5	0.5	0.0009	Popov *et al.* 2012
4	55638.2593	–3124.5	0.5	0.0037	Popov *et al.* 2012
5	55639.3325	–3121.0	1.0	0.0000	Popov *et al.* 2012
6	55640.2480	–3118.0	1.0	–0.0075	Popov *et al.* 2012
7	56598.6746	–3.0	1.0	–0.0014	Present Observations
8	56598.8299	–2.5	1.0	0.0001	Present Observations
9	56599.5990	0.0	1.0	0.0000	Present Observations
10	56599.7549	0.5	1.0	0.0020	Present Observations
11	56600.8292	4.0	1.0	–0.0006	Present Observations

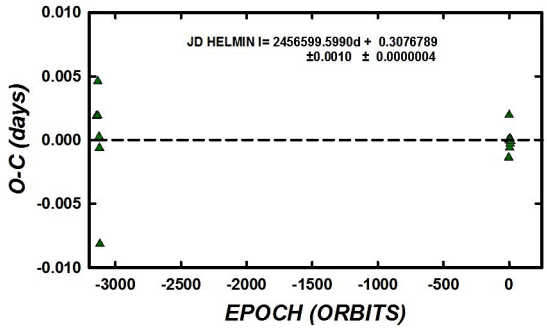

Figure 4. V428 Cep-NGC 188. Linear O–C residuals from the period study.

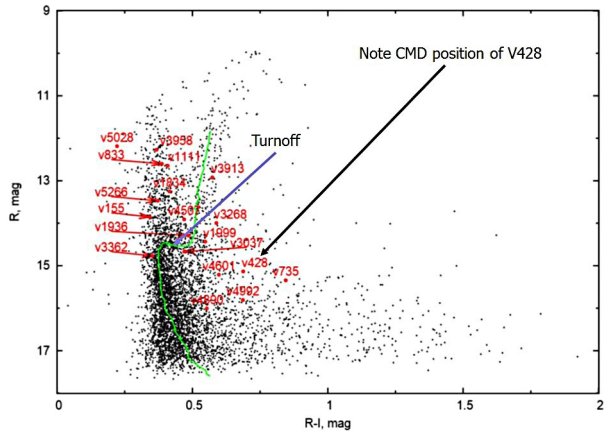

Figure 5. V428 Cep-NGC 188. R, R–I color magnitude diagram of NGC 188 with the turnoff and the position of V428 Cep identified.

contact binary—the B–V color curves dip downward at phase 0.0 and at phase 0.5, which point to each component filling its Roche Lobe. At each quadrature, beginning at phase 0.0, the Δ(B–V) values are 0.31, 0.20, 0.24, and 0.23, respectively. Thus, the curves indicate a contact, classical EW-type binary.

7. Temperature

Table 4 of Popov *et al.* (2013) gives the color indices of the newly discovered variable stars. The V428 Cep spectral type is given as K1. Its period tells us it is of class V. So we have assigned the temperature 5000 K (spectral type, K2V) to the primary component. These results closely match those of 2MASS photometry. Although its faintness is of the right magnitude and its placement is to the right of the main sequence of the CMD (Bettis 1975), its spatial position is rather far from the center of the cluster. It is assumed to be a field star (see section 4). It is of interest that K-type contact binaries, with periods shorter than 0.3 day, and the period of V428 Cep is on the borderline, are important objects for explaining the period cutoff phenomenon (Liu *et al.* 2014).

8. Synthetic light curve solution

The B, V, R, and I curves were pre-modeled with BINARY MAKER 3.0 (Bradstreet and Steelman 2002) and fits were determined in all filter bands. The resulting parameters were then averaged and input into a four-color simultaneous light curve calculation using the Wilson-Devinney Program (WD; Wilson and Devinney 1971; Wilson 1990, 1994; van Hamme and Wilson 1998). The solution was computed in Mode 3 (contact mode). Convective parameters g = 0.32, A = 0.5 were used.

Since eclipses did not appear to be quite total, a q (m_2 / m_1)-search was performed over the range q = 0.27 to 4.0 (see Figure 7). The sum of square residuals minimized at approximately q = 0.4. Beginning at this value, q was included with the rest of the adjustable parameters to obtain a final solution. The solution is given in Table 5. The normalized curves overlain by our light curve solutions are shown as Figures 8a and 8b. The geometrical (Roche-Lobe) representation of the system is given in Figures 9a, b, c, and d at the light curve quadratures so that the reader may see the placement of the spot and the relative size of the stars as compared to the orbit.

9. Discussion

V428 Cep in the field of NGC 188 is a W UMa binary in a classic contact configuration. Its spectral type, K1V, indicates

Table 4. V428 Cep-NGC 188 light curve characteristics.

Filter	*Phase*	*Magnitude Max. I*	*Phase*	*Magnitude Max. II*
	0.25		0.75	
B		4.91 ± 0.04		4.92 ± 0.03
V		4.71 ± 0.03		4.68 ± 0.03
R		4.38 ± 0.01		4.40 ± 0.01
I		4.12 ± 0.01		4.17 ± 0.02
Filter	*Phase*	*Magnitude Min. II*	*Phase*	*Magnitude Min. I*
	0.50		0.00	
B		5.51 ± 0.05		5.66 ± 0.06
V		5.27 ± 0.02		5.35 ± 0.01
R		4.96 ± 0.03		5.07 ± 0.01
I		4.67 ± 0.01		4.82 ± 0.02
Filter	*Min. I – Max. I*	*Max. I – Max. II*	*Phase*	*Min. I – Min. II*
B	0.76	0.10 ± -0.01	0.06	0.16 ± 0.11
V	0.65	0.04 ± 0.02	0.06	0.09 ± 0.03
R	0.69	0.02 ± -0.02	0.01	0.11 ± 0.04
I	0.70	0.04 ± -0.04	0.03	0.15 ± 0.03

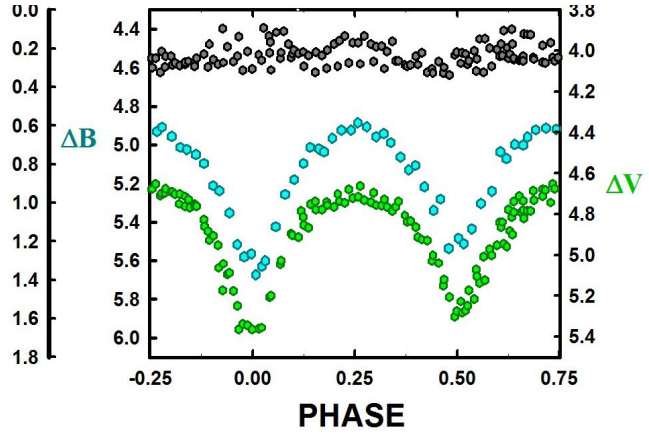

Figure 6a. V428 Cep-NGC 188. B (middle), V (bottom) delta magnitude and color magnitudes vs. phase plots in the sense of V–C (top).

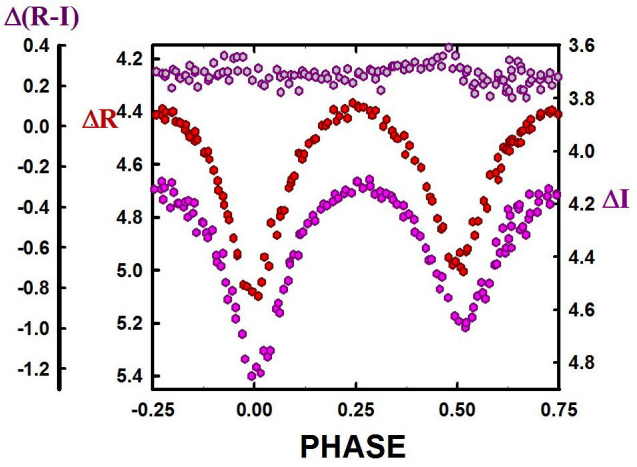

Figure 6b. V428 Cep-NGC 188. R (middle), I (bottom) delta magnitude and color magnitudes vs. phase plots in the sense of V–C (top).

Table 5. V428 Cep-NGC 188 light curve solution.

Parameters	*Values*
$\lambda_B, \lambda_V, \lambda_R, \lambda_I$ (nm)	440, 550, 640, 790
$x_{bol1,2}$, $y_{bol1,2}$	0.643, 0. 643, 0.160, 0.160
$x_{1I,2I}$, $y_{1I,2I}$	0. 647, 0.647, 0. 183, 0. 183
$x_{1R,2R}$, $y_{1R,2R}$	0. 735, 0.735, 0. 165 0.165
$x_{1V,2V}$, $y_{1V,2V}$	0.797, 0.797, 0. 108, 0. 108
$x_{1B,2B}$, $y_{1B,2B}$	0. 852, 0.852, –0.018, –0.018
g_1 , g_2	0.32
A_1 , A_2	0.5
Inclination (°)	80.9 ± 0.1
T_1, T_2 (K)	5000, 4822 ± 6
$\Omega_1 = \Omega_2$	2. 634 ± 0.003
$q(m_2 / m_1)$	0.4228 ± 0.0009
Fill–outs: $F_1 = F_2$	34.5 ± 1.5 %
$L_1 / (L_1 + L_2)_I$	0.710 ± 0.002
$L_1 / (L_1 + L_2)_R$	0715 ± 0.002
$L_1 / (L_1 + L_2)_V$	0.724 ± 0.003
$L_1 / (L_1 + L_2)_B$	0.734 ± 0.005
JD_0 (days)	2456599.6001 ± 0.0002
Period (days)	0. 30790 ± 0.00007
r_1, r_2 (pole)	0.445 ± 0.007, 0.30 ± 0.01
r_1, r_2 (side)	0.48 ± 0.01, 0.32 ± 0.01
r_1, r_2 (back)	0.51 ± 0.01, 0.37 ± 0.03
SPOT Parameters	
Spot 1 On STAR 1	*Cool Spot*
Colatitude (°)	75.0 ± 2
Longitude (°)	39 ± 1
Spot radius (°)	16.6 ± 0.5
Spot T–factor	0.89 ± 0.01
Sum(res)^2	0.125

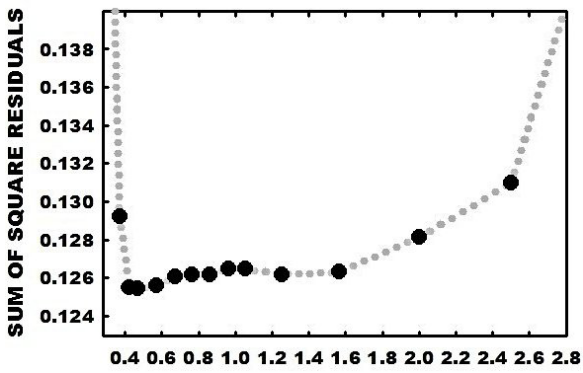

Figure 7. V428 Cep-NGC 188. Chart of solution residuals of mass ratios extending from 0.35 to 3 minimizes near 0.4.

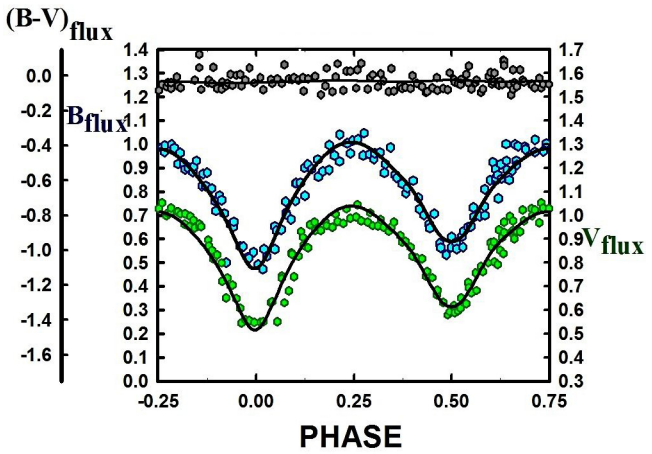

Figure 8a. V428 Cep-NGC 188. B (middle), V (bottom) synthetic light curve solutions overlaying the normalized flux curves.

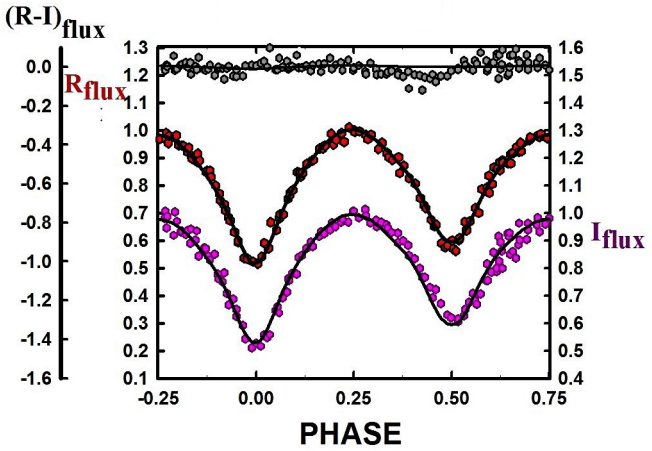

Figure 8b. V428 Cep-NGC 188. R (middle), I (bottom) synthetic light curve solutions overlaying the normalized flux curves.

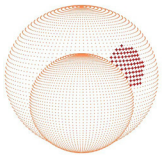

Figure 9a. V428 Cep-NGC 188. Roche Lobe surfaces from our BVRI simultaneous solution, phase 0.00 (the primary eclipse).

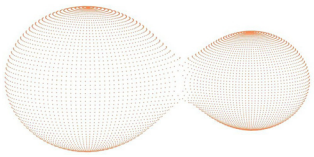

Figure 9b. V428 Cep-NGC 188. Roche Lobe surfaces from our BVRI simultaneous solution, phase 0.25.

Figure 9c. V428 Cep-NGC 188. Roche Lobe surfaces from our BVRI simultaneous solution, phase 0.50.

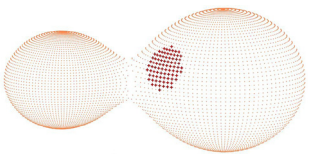

Figure 9d. V428 Cep-NGC 188. Roche Lobe surfaces from our BVRI simultaneous solution, phase 0.75.

a surface temperature of 5000 K for the primary component. The q-search indicates the mass ratio is 0.4, with a light curve amplitude of 0.76–0.65 magnitude in B to I, respectively. The secondary component has a temperature of ~4822 K (K3), which means the secondary is over luminous for its main sequence mass. The fill-out is 35%. The high inclination of 80° results in a near total eclipse with less than 1% of the light due to the secondary component at phase 0.5. It is an A-type W UMa binary that has not quite reached thermal equilibrium. The primary component was modeled with a moderately sized cool spot region of 16° radius and a mean T-factor of ~0.89 (T~4300K) -- not unusual in solar-type binaries.

10. Conclusion

Our 2.5-year period study yields little information about the orbital evolution of the binary. However, since the system has strong magnetic activity, over time, the system should slowly coalesce due to magnetic braking as it loses angular momentum due to ion winds moving outward on stiff magnetic field lines rotating with the binary (out to the Alfvén radius). If the mass ratio becomes more extreme and the fill-out increases, than we would predict the binary will coalesce, producing a rather fast rotating, single A-type main sequence field star (Guinan and Bradstreet 1988). Radial velocity curves are needed to obtain absolute (not relative) system parameters.

11. Acknowledgements

We wish to thank Bob Jones University for their coverage of travel expenses and their support of Dark Sky Observatory.

References

Bettis, C. 1975, *Publ. Astron. Soc. Pacific*, **87**, 707.

Bradstreet, D. H., and Steelman, D. P. 2002, *Bull. Amer. Astron. Soc.*, **34**, 1224.

Guinan, E. F., and Bradstreet, D. H. 1988, in *Formation and Evolution of Low Mass Stars*, ed. M. T. V. T. Lago, NATO Advanced Sci. Inst. (ASI) Ser. C, 241, Kluwer, Dordrecht, 345.

Hoffmeister, C. 1964, *Astron. Nachr.*, **288**, 49.

Liu, N.-P., Qian, S.-B., Soonthornthum, B., Leung, K.-C., Liao, W.-P., Zhu, L.-Y., He, J.-J., Liu, L., and Zhao, E.-G. 2014, *Astron. J.*, **147**, 41.

Meibom, S., *et al.* 2009, *Astron. J.*, **137**, 5086.

Perryman, M. A. C., European Space Agency Space Science Department, and the Hipparcos Science Team. 1997, *The Hipparcos and Tycho Catalogues*, ESA SP-1200 (VizieR On-line Data Catalog: I/239), ESA Publications Division, Noordwijk, The Netherlands.

Popov, A. A., Krushinsky, V. V., Avvakumova, E. A., Burdanov, A. Y., Punanova, A. F., and Zalozhnih, I. S. 2013, *Open Eur. J. Var. Stars*, **157**, 1.

van Hamme, W. V., and Wilson, R. E. 1998, *Bull. Amer. Astron. Soc.*, **30**, 1402.

Wilson, R. E. 1990, *Astrophys. J.*, **356**, 613.

Wilson, R. E. 1994, *Publ. Astron. Soc. Pacific*, **106**, 921

Wilson, R. E., and Devinney, E. J. 1971, *Astrophys. J.*, **166**, 605.

Zacharias, N., Finch, C. T., Girard, T. M., Henden, A., Bartlett, J. L., Monet, D. G., and Zacharias, M. I. 2012, *The Fourth U.S. Naval Observatory CCD Astrograph Catalog* (UCAC4), VizieR On-line Data Catalog (http://cdsarc.u-strasbg.fr/viz-bin/Cat?I/322).

Zhang, X. B., Deng, L., Tian, B., and Zhou, X. 2002, *Astron. J.*, **123**, 1548.

New Observations of V530 Andromedae: a Critical Contact Binary?

Ronald G. Samec
Astronomy Group, Department of Natural Sciences, Emmanuel College, 181 Springs Street, Franklin Springs, GA 30639; ronaldsamec@gmail.com

Heather Chamberlain
American Public University System, 111 W. Congress Street, Charles Town, WV 25414; 4hcham@gmail.com

Daniel B. Caton
Dark Sky Observatory, Physics and Astronomy Department, Appalachian State University, 525 Rivers Street, Boone, NC 28608-2106; dbcaton@apstate.edu

Danny R. Faulkner
Johnson Observatory, 1414 Bur Oak Court, Hebron, KY 41048; drfaulkn@mailbox.sc.edu

Jeremy D. Clark
Bob Jones University, 1700 Wade Hampton Boulevard, Greenville, SC 29614;jclar904@students.bju.edu

Travis Shebs
University of South Carolina, Department of Physics and Astronomy, Jones PSC Room 404, Columbia, SC 29208; shebs@email.sc.edu

Received July 1, 2016; revised August 28, 2016; accepted October 17, 2016

Abstract We follow up on single coverage UBVR$_c$I$_c$ light curves taken in 2011 and analyses. Our present BVR$_c$I$_c$ light curves with ample coverage were taken October and November 2013 and January 2014 with the Dark Sky Observatory 0.81-meter reflector of Appalachian State University. They reveal the early-type V530 And as a totally eclipsing shallow or critical contact solar-type binary rather than semidetached near-contact one. In our extended period study, over a 14.25-year interval, we find a continuously decreasing period. This fits the scenario of magnetic braking for solar-type binaries. The temperatures of the primary and secondary components are estimated at 6750 and 6030 K. The component temperature difference is large for a contact binary. The fill-out, however, is a mere 5% so it is near critical contact. The mass ratio, M_2/M_1, was found to be 0.386. Two star spots, probably magnetic in origin, were determined. We suspect that the binary has recently achieved physical contact for the first time.

1. Introduction

This paper represents follow-up observations on single coverage UBVR$_c$I$_c$ light curves (Samec *et al.* 2013) and analyses, adding needed orbital period coverage to ascertain a period change in the system.

2. History and observations

V530 And was discovered by Khruslov (2008). It was designated as EB with a 12.6–13.3 R-magnitude range (MinII = 13.0). Its ephemeris was given as

$$\text{JD Hel Min I} = 2451479.632\ \text{d} + 0.57723 \bullet \text{E}. \quad (1)$$

It appeared in Hoffman *et al.* (2009) with period P = 0.57721 and mean ROTSE unfiltered magnitude = 12.769. An amplitude of 0.633 magnitude was given. The variable was found to be in the Fourier region where β Lyrae types are expected. V530 And is also known as 2MASS J01274106+3351552, NSVS 6447718, TYC 2300-116-1, and GSC 2300 0116. Its position is R.A. (2000) = 01^h 27^m 41.050^s, Dec. (2000) = +33° 51' 55.47" (ICRS). V530 And appeared in the 80th Name-List of Variable Stars (Kazarovets *et al.* 2011). It was designated as EB type. Our earlier, somewhat sparse observations were taken 27 and 29 September 2011. This earlier solution gave a near contact, semidetached configuration with a fill-out of 99 and 100% (Samec *et al.* 2013). But the coverage was scant and only two precision minima and some times of low light were used in the period determination. A follow-up was needed to complete the initial study and to make a more definitive determination of its configuration.

Consequently, we (RGS, DBC, JDC, TS) undertook additional BVR$_c$I$_c$ observations in 2013 on October 1, 2, 9, November 4, 5, and January 4, 2014, at Dark Sky Observatory's 0.81-meter reflector in Philips Gap, North Carolina, with the (–40° C) 2KX2K Apogee Alta CCD. The same check and comp stars were used from the earlier paper. The precision of the R$_c$ and I$_c$ curves were less than 1% while the B and V curves had nightly values of less than this value, but nightly variations took the overall curves to 2% in V and 3% in B. We believe this was due to magnetic activity on the binary since we normally attain mmag precision on stars of this magnitude. Figure 1a and b show B,V typical nightly curves on 1 October 2013 and

4 January 2014. Our complete observations are given in Table 1, in delta magnitudes, ΔB, ΔV, ΔR_c, and ΔI_c in the sense of variable minus comparison star (V–C).

3. Period study

The previous eclipse timings were (Samec *et al.* 2013) HJD Min I = 2455832.74595 (±0.0004) d, and HJD Min II = 2455830.72806 (±0.00045) d. In addition, four more timings were added with our present observations, HJD Min I = 2456566.84275 (± 0.00007), 2456601.76665 (±0.00046), 2456598.8820 (± 0.0005), and HJD Min II= 2456600.6111 (± 0.0002). These produced enough minima to calculate a linear ephemeris, improving on the last estimate:

$$\text{JD Hel Min I} = 2456566.8487 + 0.5771241 \cdot E. \quad (2)$$
$$\pm 0.0012 \quad \pm 0.0000016$$

While producing this updated ephemeris we discovered a way to extend our O–C orbital diagram. NSVS data from 1999–2000 on this binary (Wozniak *et al.* 2004) were phased into a light curve with the current period. The curves were then shifted so that the eclipses were easily seen and worked with. The eclipses were fit with parabolas and the HJD data within 0.005 phase of the primary and secondary eclipses were used as times of minimum light in our O–C analysis. These were weighted at only 0.1 of a regular eclipse timing, while precision timings were weighted 1.0. The complete set of timings revealed that the period has been decreasing over the past 9,000 orbits! This method could be used with any set of nearly complete light curves (which include the minima) even if the observations are taken with only a few sets of observations per night (as most surveys) so no normal minima determinations could be done. This also improves on the conventional "times of low light" method. The following quadratic ephemeris resulted.

$$\text{JD Hel Min I} = 2456566.8496 + 0.5771072 \cdot E - 0.0000000140 \cdot E^2 \quad (3)$$
$$\pm 0.0012 \pm 0.0000019 \quad \pm 0.0000000002$$

The plotted residuals overlaid by the quadratic term of Equation 3 are given in Figure 2. The times of minimum light and the linear residuals are given as Table 2.

4. Light curves

The light curves were phased using Equation 2. These are given as Figures 3a and 3b. A table of light curve characteristics are given in Table 3. The primary amplitudes of this EB system averaged 0.7–0.6 magnitude in the primary from B to I, respectively, and ~0.4 magnitude in the secondary eclipse. The O'Connell effect (difference of magnitudes Max I and Max II, O'Connell 1951) was small, but consistently positive at 0.3–1.4%. These values were mostly within the errors. Thus, we expect the binary is undergoing some magnetic activity. The secondary eclipse showed a time of constant light of 41.5 minutes. This means that the eclipses are total and that the more massive, larger star is the hotter component. This is to be expected in normal stellar evolution.

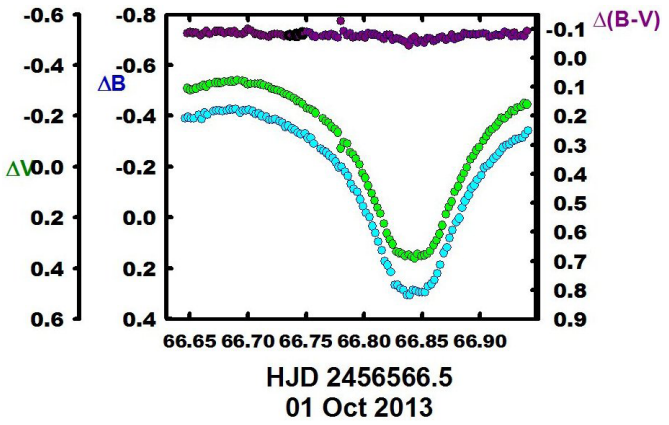

Figure 1a. B, V delta magnitudes from sample observations and color curves on October 1, 2013.

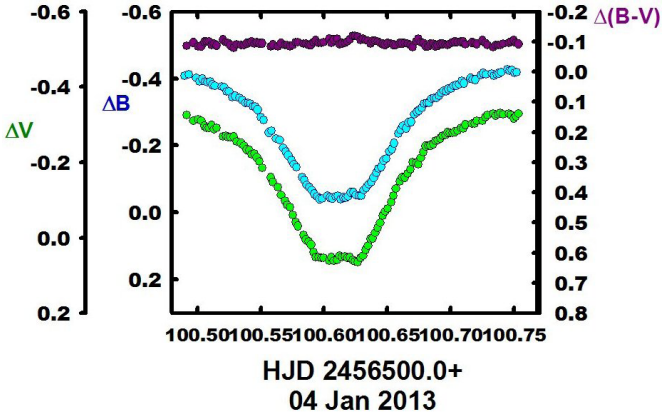

Figure 1b. B, V delta magnitudes and color curves on May 11, 2012.

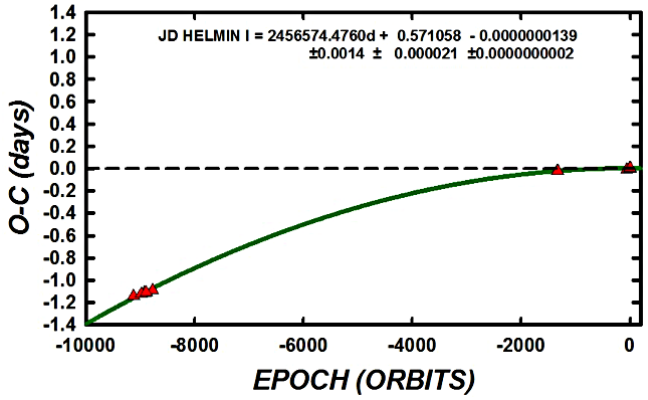

Figure 2. Linear and Quadratic O–C residuals from the period study.

5. Synthetic light curve solution

As before, we used the 2MASS Photometry J–K value of 0.258 to determine the temperature of the binary. From this we found that the primary component was an F4V type, thus we assigned the primary component a surface temperature of ~6750 K in our light curve solution. The system was pre-modeled with BINARY MAKER 3.0 (Bradstreet and Steelman 2002). We used these results as starting values for the Wilson-

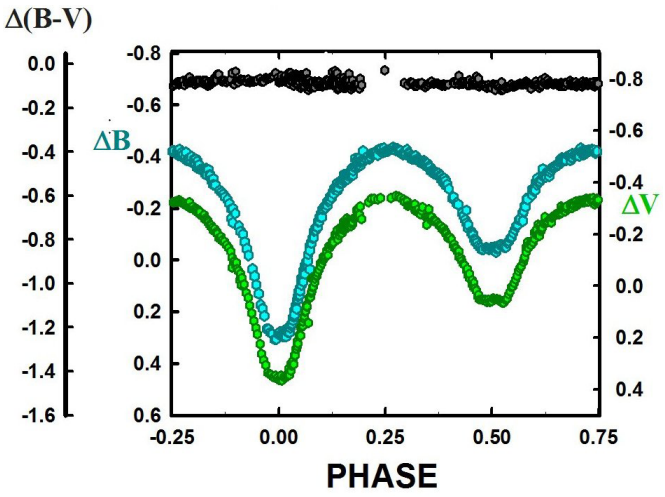

Figure 3a. B, V delta magnitude and color magnitudes vs. phase plots in the sense of V–C.

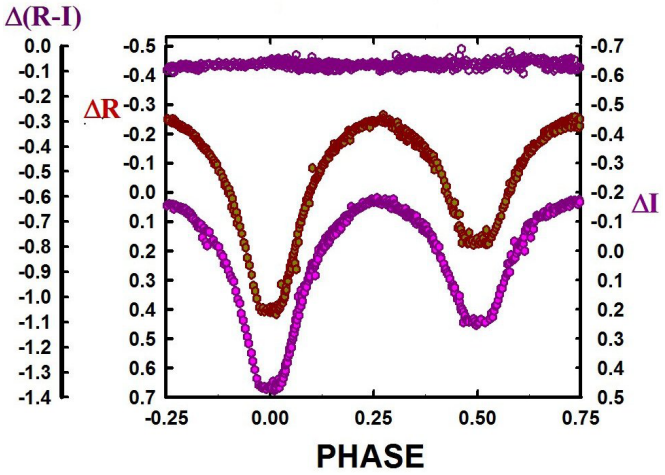

Figure 3b. R_c, I_c delta magnitude and color magnitudes vs. phase plots in the sense of V–C.

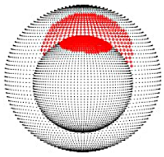

Figure 4a. Roche Lobe surfaces from our BVRI solution, phase 0.00 (the primary eclipse).

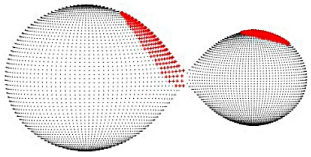

Figure 4b. Roche Lobe surfaces from our BVRI solution, phase 0.25.

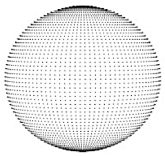

Figure 4c. Roche Lobe surfaces from our BVRI solution, phase 0.50.

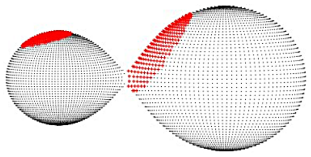

Figure 4d. Roche Lobe surfaces from our BVRI solution, phase 0.75.

Devinney program. A simultaneous four-color synthetic light curve solution was obtained with the Wilson-Devinney program (Wilson and Devinney 1971; Wilson 1990, 1994, 2001, 2004; Van Hamme and Wilson 1998, 2003). We note that one surface spot stayed remarkably stable throughout the iterations and is near the L_1 position of the primary component. Third light

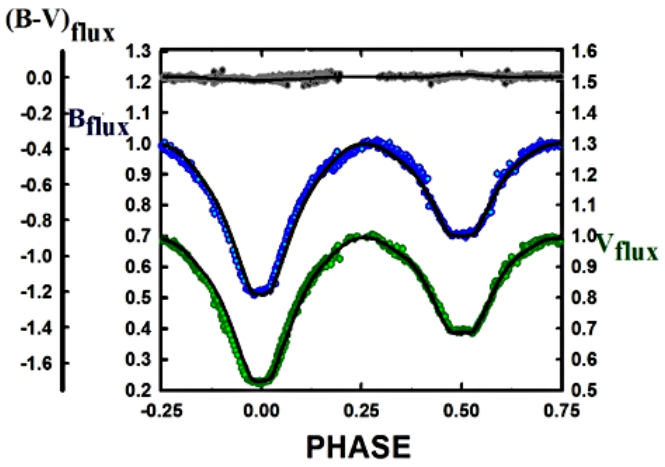

Figure 5a. B, V synthetic light curve solutions overlaying the normalized flux curves.

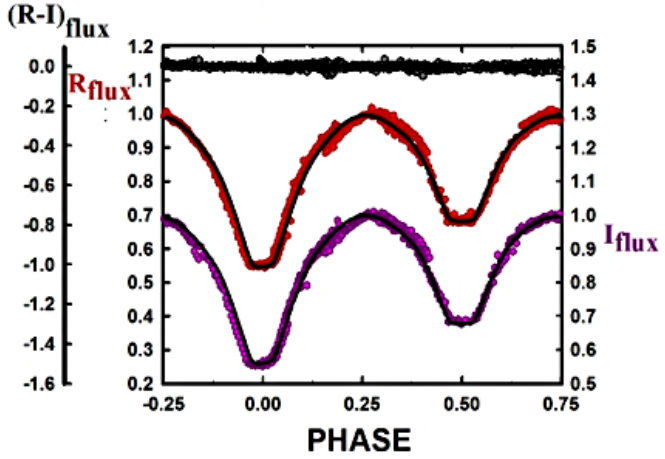

Figure 5b. R_c, I_c synthetic light curve solutions overlaying the normalized flux curves.

was small but still persisted. No q-search was needed since the curves display total eclipses. Mode 4 was used in our initial iterations as before, but the iterations took the solution into contact. We switched to mode 3 and the program proceeded in this configuration with no problems. The solution converged in contact. Since the binary is in contact and undergoes total eclipses, the mass ratio is well determined (Terrell and Wilson 2005). The synthetic light curve solution is given in Table 4. A geometrical representation of the system is given in Figures 4a, b, c, d, so that the reader may visualize the placement of the spots and the relative size of the stars as compared to the orbit. The normalized curves overlain by our light curve solutions are shown as Figures 5a and 5b.

6. Conclusion

Our present curves reveal the early-type V530 And system as a totally eclipsing, marginal contact, magnetically active binary. This is opposed to the semidetached, near-contact configuration that our earlier sparse but complete curves gave. In our new, extended period study over a 14.25 year interval, we find a continuously decreasing period. This fits the scenario

of magnetic braking for solar-type binaries. The temperatures of the primary and secondary components are estimated at 6750 and 6030 K, respectively, which is arguably hot for solar-type binaries. However, our earlier studies show that spots persist into early F-type and even late A-type binaries (Samec 2015). Our third light model gave a fill-out of only 5% (the no-third-light solution gave 4%). The mass ratio, M_2/M_1, was found to be 0.386. Two star spots, probably magnetic in origin, were determined. There is a large temperature difference in components showing that the binary has not yet achieved thermal contact. This suggests that the system has just recently come into contact. It is possible that the binary came into contact in the last two years. However, no "red novae" are on record in this vicinity (Tylenda *et al.* 2011). But with our present curves with their night-to-night variations, we are unable to make such a definite determination. It may also be true that our early observations covering only two observing days may have allowed a better "picture" of the binary without the variability to better constrain the solution. The third light may indicate a third body is present, which may lead us to believe that the period changes may be a part of a sinusoidal variation. Further eclipse timings are needed over the next decade or so to give a firm handle on the orbital period evolution. Also, radial velocity curves are needed to affirm or disaffirm our solution and to obtain absolute (not relative) system parameters. Spectroscopy or standard star photometry will yield a precision temperature of the binary.

7. Acknowledgements

We wish to thank Dr. Caton for joining our research team of observers and we appreciate him scheduling us in for regular observations at Dark Sky Observatory on his 32- and 18-inch research grade instruments.

References

Bradstreet, D. H., and Steelman, D. P. 2002, *Bull. Amer. Astron. Soc.*, **34**, 1224.

Hoffman, D. I., Harrison, T. E., and McNamara, B. J. 2009, *Astron. J.*, **138**, 466.

Kazarovets, E. V., Samus, N. N., Durlevich, O. V., Kireeva, N. N., and Pastukhova, E. N. 2011, *Inf. Bull. Var. Stars*, No. 5969, 1.

Khruslov, A. V. 2008, *Perem. Zvezdy, Prilozh.*, **8**, 40.

O'Connell, D. J. K. 1951, *Publ. Riverview Coll. Obs.*, **2**, 85.

Samec, R. G. 2015, in *IAU General Assembly*, Meeting No. 29, id.2226853.

Samec, R. G., Flaaten, D., Kring, J., and Faulkner, D. R. 2013, *ISRN Astronomy and Astrophysics*, **2013**, 35, article ID 201235 (https://www.hindawi.com/journals/isrn/contents/astronomy.astrophysics/).

Terrell, D., and Wilson, R. E. 2005, *Astrophys. Space Sci.,* **296**, 221.

Tylenda, R., *et al.* 2011*, Astron. Astrophys.*, **528A**, 114.

Van Hamme, W. V., and Wilson, R. E. 1998, *Bull. Amer. Astron. Soc.*, **30**, 1402.

Van Hamme, W. V., and Wilson, R. E. 2003, in *GAIA Spectroscopy: Science and Technology*, ed. U. Munari, ASP Conf. Ser. 298, Astronomy Society of the Pacific, San Francisco, 323.

Wilson, R. E. 1990, *Astrophys. J.*, **356**, 613.

Wilson, R. E. 1994, *Publ. Astron. Soc. Pacific*, **106**, 921.

Wilson, R. E. 2001, *Inf. Bull. Var. Stars*, No. 5076, 1.

Wilson, R. E. 2004, *New Astr. Rev.*, **48**, 695.

Wilson, R. E., and Devinney, E. J. 1971, *Astrophys. J.*, **166**, 605.

Wozniak, P. R., *et al.* 2004, *Astron. J.*, **127**, 2436.

Table 1. V530 And Observations ΔB, ΔV, ΔRc, and ΔIc, variable minus comparison star.

Δ*B*	*HJD 2456500+*	Δ*B*	*HJD 2456500+*	Δ*B*	*HJD 2456500+*	Δ*B*	*HJD 2456500+*	Δ*B*	*HJD 2456500+*
–0.389	66.6460	–0.350	67.9021	–0.306	100.5477	0.096	101.5074	–0.413	161.6834
–0.326	100.6829	–0.375	100.5193	–0.426	100.7446	–0.431	161.6619	–0.070	66.7969
–0.381	75.0359	–0.392	100.7086	–0.415	161.6404	–0.270	66.7627	–0.112	74.9715
–0.327	100.6810	–0.378	161.6190	–0.386	66.7236	0.195	74.9448	–0.039	100.6130
–0.305	161.5976	–0.424	66.6868	0.050	67.9472	–0.096	100.5846	–0.396	101.5847
–0.394	66.6486	–0.327	67.9043	–0.284	100.5501	0.084	101.5096	–0.410	161.6851
–0.087	66.8901	–0.373	100.5212	–0.423	100.7465	–0.436	161.6636	–0.044	66.7994
–0.306	161.5959	–0.385	100.7105	–0.406	161.6421	–0.262	66.7652	–0.123	74.9734
–0.340	100.6848	–0.386	161.6207	–0.378	66.7272	0.176	74.9468	–0.044	100.6153
–0.326	161.5992	–0.427	66.6893	0.162	67.9495	–0.081	100.5865	–0.366	101.5870
–0.389	66.6510	–0.306	67.9066	–0.275	100.5523	0.055	101.5119	–0.397	161.6867
–0.116	66.8926	–0.361	100.5232	–0.424	100.7484	–0.429	161.6653	–0.018	66.8019
–0.421	75.0379	–0.400	100.7157	–0.428	161.6438	–0.255	66.7677	–0.128	74.9754
–0.342	100.6867	–0.389	161.6223	–0.372	66.7297	0.155	74.9487	–0.043	100.6172
–0.326	161.6009	–0.414	66.6935	0.286	74.9233	–0.075	100.5885	–0.136	101.6145
–0.390	66.6535	–0.292	67.9088	–0.238	100.5566	0.016	101.5151	–0.399	161.6884
–0.127	66.8951	–0.361	100.5251	–0.416	100.7503	–0.423	161.6669	0.035	66.8073
–0.408	100.4902	–0.397	100.7175	–0.422	161.6454	–0.244	66.7702	–0.148	74.9773
–0.341	100.6887	–0.384	161.6240	–0.357	66.7322	0.122	74.9507	–0.047	100.6191
–0.332	161.6025	–0.421	66.6960	0.278	74.9252	–0.067	100.5904	–0.192	101.7304
–0.403	66.6577	–0.257	67.9122	–0.244	100.5585	0.036	101.5184	–0.400	161.6900
–0.399	67.8793	–0.344	100.5277	–0.418	100.7522	–0.431	161.6685	0.062	66.8098
–0.412	100.4935	–0.396	100.7195	–0.429	161.6471	–0.234	66.7734	–0.165	74.9793
–0.348	100.6906	–0.392	161.6256	–0.360	66.7347	0.108	74.9526	–0.059	100.6214
–0.340	161.6042	–0.421	66.6985	0.290	74.9272	–0.055	100.5923	–0.124	101.7327
–0.386	66.6602	–0.245	67.9145	–0.220	100.5623	–0.310	101.5626	–0.390	161.6917
–0.390	67.8826	–0.347	100.5300	0.278	101.4882	–0.426	161.6702	0.095	66.8123
–0.401	100.4994	–0.410	100.7239	–0.417	161.6487	–0.218	66.7759	–0.178	74.9812
–0.357	100.6925	–0.393	161.6273	–0.349	66.7382	0.070	74.9548	–0.059	100.6233
–0.337	161.6058	–0.423	66.7010	0.283	74.9291	–0.048	100.5947	–0.110	101.7368
–0.411	66.6627	–0.229	67.9167	–0.215	100.5650	–0.313	101.5651	–0.402	161.6933
–0.390	67.8849	–0.341	100.5335	0.280	101.4911	–0.423	161.6719	0.130	66.8156
–0.390	100.5020	–0.415	100.7258	–0.432	161.6504	–0.198	66.7784	–0.195	74.9832
–0.362	100.6944	–0.401	161.6289	–0.345	66.7407	0.042	74.9567	–0.052	100.6252
–0.346	161.6075	–0.417	66.7044	0.273	74.9311	–0.040	100.5966	–0.099	101.7390
–0.405	66.6652	–0.190	67.9189	–0.192	100.5680	–0.324	101.5673	–0.390	161.6950
–0.382	67.8871	–0.335	100.5356	0.252	101.4933	–0.423	161.6735	0.173	66.8181
–0.398	100.5043	–0.412	100.7277	–0.419	161.6520	–0.199	66.7808	–0.205	74.9851
–0.361	100.6963	–0.391	161.6306	–0.333	66.7432	0.021	74.9587	–0.049	100.6277
–0.346	161.6091	–0.406	66.7069	0.276	74.9331	–0.041	100.5985	–0.069	101.7426
–0.418	66.6706	–0.161	67.9327	–0.182	100.5699	–0.333	101.5696	–0.390	161.6966
–0.368	67.8893	–0.326	100.5381	0.233	101.4957	–0.411	161.6752	0.188	66.8206
–0.391	100.5062	–0.414	100.7323	–0.423	161.6537	–0.180	66.7838	–0.206	74.9871
–0.368	100.6982	–0.399	161.6322	–0.328	66.7457	0.007	74.9606	–0.050	100.6296
–0.359	161.6108	–0.409	66.7094	0.266	74.9350	–0.049	100.6028	–0.023	101.7449
–0.422	66.6731	–0.145	67.9349	–0.170	100.5718	–0.288	101.5719	–0.384	161.6983
–0.352	67.8924	–0.327	100.5400	0.211	101.4980	–0.412	161.6768	0.216	66.8231
–0.388	100.5082	–0.407	100.7342	–0.421	161.6553	–0.162	66.7863	–0.225	74.9890
–0.369	100.7003	–0.412	161.6339	–0.331	66.7493	–0.022	74.9637	–0.067	100.6315
–0.362	161.6124	–0.400	66.7119	0.264	74.9370	–0.044	100.6047	–0.048	101.7495
–0.421	66.6756	–0.120	67.9371	–0.156	100.5745	–0.282	101.5746	–0.384	161.6999
–0.354	67.8946	–0.324	100.5419	0.189	101.5004	–0.418	161.6785	0.266	66.8264
–0.391	100.5101	–0.412	100.7361	–0.425	161.6570	–0.131	66.7888	–0.227	74.9910
–0.377	100.7022	–0.407	161.6355	–0.312	66.7518	–0.055	74.9656	–0.074	100.6335
–0.370	161.6141	–0.394	66.7161	0.254	74.9390	–0.042	100.6066	–0.044	101.7587
–0.419	66.6781	–0.110	67.9394	–0.144	100.5764	–0.329	101.5768	–0.375	161.7016
–0.349	67.8969	–0.316	100.5439	0.152	101.5026	–0.414	161.6801	0.268	66.8289
–0.381	100.5121	–0.415	100.7380	–0.428	161.6586	–0.111	66.7913	–0.243	74.9929
–0.379	100.7041	–0.413	161.6371	–0.314	66.7543	–0.069	74.9676	–0.084	100.6354
–0.365	161.6157	–0.385	66.7186	0.248	74.9409	–0.047	100.6092	–0.050	101.7682
–0.421	66.6818	–0.063	67.9427	–0.135	100.5783	–0.393	101.5799	–0.377	161.7032
–0.354	67.8991	–0.316	100.5458	0.136	101.5048	–0.427	161.6818	0.280	66.8314
–0.378	100.5140	–0.418	100.7399	–0.430	161.6603	–0.100	66.7944	–0.249	74.9948
–0.382	100.7067	–0.410	161.6388	–0.290	66.7568	–0.084	74.9695	–0.090	100.6373
–0.375	161.6174	–0.385	66.7211	0.223	74.9429	–0.049	100.6111	–0.031	101.7705
–0.425	66.6843	–0.016	67.9450	–0.105	100.5827	–0.385	101.5822	–0.383	161.7049

Table continued on following pages

Table 1. V530 And Observations ΔB, ΔV, ΔRc, and ΔIc, variable minus comparison star, cont.

ΔB	HJD 2456500+	ΔB	HJD 2456500+	ΔB	HJD 2456500+	ΔB	HJD 2456500+	ΔB	HJD 2456500+
0.286	66.8339	–0.294	75.0046	–0.206	100.6555	–0.321	101.8379	–0.295	161.7331
–0.263	74.9968	–0.155	100.6471	–0.316	101.8261	–0.322	161.7265	0.019	66.8796
–0.104	100.6393	–0.237	101.8115	–0.336	161.7199	0.140	66.8689	–0.367	75.0301
0.066	101.7765	–0.357	161.7132	0.262	66.8582	–0.354	75.0223	–0.304	100.6751
–0.371	161.7066	0.295	66.8476	–0.330	75.0143	–0.268	100.6669	–0.295	161.5910
0.307	66.8370	–0.312	75.0065	–0.235	100.6586	–0.324	101.8422	–0.287	161.7348
–0.276	74.9987	–0.160	100.6490	–0.243	101.8285	–0.312	161.7282	0.004	66.8821
–0.118	100.6412	–0.313	101.8155	–0.332	161.7215	0.119	66.8715	–0.361	75.0320
–0.014	101.7788	–0.345	161.7149	0.247	66.8607	–0.353	75.0242	–0.312	100.6772
–0.365	161.7083	0.294	66.8501	–0.329	75.0163	–0.270	100.6688	–0.294	161.5926
0.305	66.8395	–0.296	75.0085	–0.245	100.6605	–0.015	101.8462	–0.293	161.7365
–0.281	75.0007	–0.181	100.6517	–0.239	101.8307	–0.314	161.7298	–0.037	66.8846
–0.130	100.6431	–0.273	101.8195	–0.331	161.7232	0.081	66.8739	–0.395	75.0340
–0.151	101.8068	–0.342	161.7166	0.220	66.8632	–0.358	75.0262	–0.325	100.6791
–0.372	161.7099	0.295	66.8526	–0.326	75.0182	–0.292	100.6713	–0.309	161.5943
0.286	66.8420	–0.311	75.0104	–0.258	100.6624	–0.269	161.5877	–0.179	161.7381
–0.296	75.0026	–0.189	100.6536	–0.352	101.8339	–0.300	161.7315	–0.065	66.8871
–0.136	100.6451	–0.302	101.8238	–0.335	161.7248	0.051	66.8764		
–0.210	101.8093	–0.335	161.7182	0.186	66.8657	–0.358	75.0281		
–0.362	161.7116	0.271	66.8551	–0.334	75.0203	–0.300	100.6732		
0.289	66.8445	–0.330	75.0124	–0.251	100.6650	–0.279	161.5893		

ΔV	HJD 2456500+	ΔV	HJD 2456500+	ΔV	HJD 2456500+	ΔV	HJD 2456500+	ΔV	HJD 2456500+
–0.308	66.6478	–0.042	66.8943	–0.124	74.9885	–0.058	100.6465	–0.111	101.6199
0.159	66.8732	–0.015	74.9729	0.048	100.6309	–0.401	101.5905	–0.259	66.7424
0.153	74.9562	0.052	100.6142	–0.262	101.5689	–0.306	66.7203	–0.336	67.8407
0.052	100.5959	–0.125	101.5410	–0.333	66.6977	–0.245	66.9404	–0.232	75.0217
0.115	101.5112	–0.330	66.6749	–0.193	66.9186	–0.197	75.0060	–0.169	100.6662
–0.302	66.6503	–0.063	66.8968	–0.119	74.9904	–0.069	100.6484	–0.205	101.6224
0.138	66.8757	–0.039	74.9748	0.033	100.6328	–0.361	101.5952	–0.255	66.7449
0.127	74.9581	0.051	100.6166	–0.257	101.5712	–0.303	66.7228	–0.332	67.8620
0.054	100.5978	–0.153	101.5442	–0.324	66.7002	–0.315	67.8232	–0.247	75.0237
0.076	101.5134	–0.329	66.6773	–0.190	66.9211	–0.204	75.0079	–0.181	100.6681
–0.304	66.6528	–0.076	66.8993	–0.146	74.9924	–0.076	100.6503	–0.339	101.6281
0.099	66.8782	–0.052	74.9768	0.022	100.6348	–0.323	101.5982	–0.246	66.7474
0.096	74.9601	0.054	100.6185	–0.240	101.5761	–0.301	66.7253	–0.328	67.8645
0.054	100.5997	–0.164	101.5485	–0.326	66.7027	–0.318	67.8254	–0.260	75.0256
0.143	101.5167	–0.335	66.6798	–0.203	66.9244	–0.204	75.0099	–0.200	100.6700
–0.308	66.6553	–0.101	66.9027	–0.155	74.9943	–0.093	100.6529	–0.372	101.6310
0.079	66.8813	–0.062	74.9787	0.004	100.6367	–0.337	101.6023	–0.229	66.7510
0.081	74.9620	0.053	100.6204	–0.261	101.5784	–0.295	66.7289	–0.324	67.8670
0.062	100.6040	–0.198	101.5523	–0.326	66.7061	–0.330	67.8276	–0.264	75.0276
–0.029	101.5207	–0.335	66.6835	–0.220	66.9269	–0.217	75.0118	–0.198	100.6726
–0.315	66.6594	–0.118	66.9053	–0.172	74.9962	–0.111	100.6548	–0.348	101.6350
0.047	66.8838	–0.077	74.9807	0.002	100.6386	–0.337	101.6059	–0.226	66.7535
0.044	74.9651	0.060	100.6227	–0.293	101.5815	–0.287	66.7314	–0.316	67.8695
0.053	100.6059	–0.216	101.5559	–0.326	66.7086	–0.324	67.8299	–0.268	75.0295
–0.027	101.5236	–0.336	66.6860	–0.218	66.9294	–0.221	75.0138	–0.194	100.6745
–0.319	66.6619	–0.137	66.9077	–0.168	74.9982	–0.130	100.6567	–0.346	101.6384
0.027	66.8863	–0.088	74.9826	–0.012	100.6405	–0.334	101.6101	–0.222	66.7560
0.042	74.9670	0.064	100.6246	–0.288	101.5837	–0.283	66.7339	–0.311	67.8736
0.061	100.6078	–0.223	101.5595	–0.325	66.7111	–0.325	67.8332	–0.274	75.0315
–0.038	101.5276	–0.335	66.6885	–0.233	66.9319	–0.226	75.0157	–0.211	100.6764
–0.316	66.6644	–0.147	66.9102	–0.196	75.0001	–0.148	100.6598	–0.339	101.6417
0.004	66.8888	–0.106	74.9846	–0.026	100.6424	–0.341	101.6138	–0.211	66.7585
0.018	74.9690	0.065	100.6265	–0.308	101.5863	–0.278	66.7364	–0.325	67.8761
0.060	100.6104	–0.248	101.5641	–0.321	66.7136	–0.336	67.8357	–0.275	75.0334
–0.089	101.5324	–0.340	66.6910	–0.236	66.9354	–0.232	75.0177	–0.226	100.6784
–0.327	66.6669	–0.160	66.9137	–0.187	75.0021	–0.160	100.6617	–0.335	101.6455
–0.028	66.8919	–0.111	74.9865	–0.039	100.6443	–0.243	101.6170	–0.190	66.7644
0.002	74.9709	0.054	100.6290	–0.259	101.5885	–0.269	66.7399	–0.314	67.8785
0.048	100.6123	–0.248	101.5666	–0.315	66.7178	–0.327	67.8382	–0.325	100.4919
–0.111	101.5368	–0.337	66.6953	–0.248	66.9379	–0.234	75.0196	–0.242	100.6803
–0.330	66.6724	–0.176	66.9162	–0.180	75.0040	–0.159	100.6636	–0.327	101.6504

Table continued on following pages

Table 1. V530 And Observations ΔB, ΔV, ΔRc, and ΔIc, variable minus comparison star, cont.

Δ*V*	*HJD 2456500+*	Δ*V*	*HJD 2456500+*	Δ*V*	*HJD 2456500+*	Δ*V*	*HJD 2456500+*	Δ*V*	*HJD 2456500+*
–0.178	66.7669	–0.253	67.9006	–0.243	100.5369	–0.326	100.7374	–0.232	101.8300
–0.308	67.8808	–0.291	100.5152	–0.302	100.7169	0.019	101.7803	0.344	66.8544
–0.309	100.4971	–0.278	100.6976	–0.023	101.7383	0.344	66.8331	0.327	74.9404
–0.243	100.6822	–0.191	101.7055	0.162	66.8116	0.362	74.9247	–0.041	100.5776
–0.314	101.6541	–0.048	66.7906	–0.109	67.9342	–0.159	100.5579	0.301	101.4926
–0.172	66.7694	–0.237	67.9036	–0.233	100.5393	–0.330	100.7393	–0.220	101.8322
–0.299	67.8842	–0.268	100.5206	–0.302	100.7188	–0.103	101.8083	0.332	66.8569
–0.313	100.5006	–0.277	100.6995	–0.013	101.7406	0.352	66.8356	0.306	74.9423
–0.244	100.6842	–0.181	101.7103	0.186	66.8141	0.363	74.9266	–0.030	100.5795
–0.315	101.6608	–0.031	66.7930	–0.093	67.9365	–0.147	100.5598	0.294	101.4949
–0.157	66.7719	–0.234	67.9059	–0.231	100.5412	–0.327	100.7412	–0.267	101.8366
–0.297	67.8864	–0.269	100.5225	–0.309	100.7207	–0.150	101.8108	0.309	66.8599
–0.310	100.5033	–0.277	100.7015	0.018	101.7442	0.347	66.8387	0.303	74.9443
–0.248	100.6861	–0.162	101.7136	0.225	66.8173	0.365	74.9286	–0.007	100.5840
–0.276	101.6681	–0.007	66.7962	–0.080	67.9387	–0.134	100.5635	0.267	101.4973
–0.147	66.7751	–0.215	67.9081	–0.221	100.5431	–0.329	100.7458	–0.249	101.8406
–0.290	67.8886	–0.266	100.5245	–0.310	100.7252	–0.170	101.8131	0.290	66.8624
–0.295	100.5056	–0.280	100.7034	0.034	101.7464	0.355	66.8412	0.267	74.9462
–0.257	100.6880	–0.144	101.7169	0.263	66.8198	0.353	74.9305	0.006	100.5859
–0.304	101.6713	0.027	66.7987	–0.065	67.9409	–0.112	100.5662	0.243	101.4995
–0.134	66.7776	–0.212	67.9103	–0.223	100.5452	–0.324	100.7477	–0.245	101.8449
–0.285	67.8909	–0.266	100.5264	–0.319	100.7271	–0.173	101.8182	0.266	66.8649
–0.290	100.5075	–0.283	100.7053	0.052	101.7557	0.360	66.8437	0.244	74.9482
–0.259	100.6900	–0.134	101.7202	0.287	66.8223	0.354	74.9325	0.010	100.5878
–0.236	101.6763	0.045	66.8012	–0.022	67.9443	–0.097	100.5693	0.213	101.5019
–0.072	66.7801	–0.201	67.9138	–0.212	100.5471	–0.316	100.7496	0.362	161.6298
–0.268	67.8939	–0.267	100.5290	–0.324	100.7290	–0.206	101.8222	0.232	66.8674
–0.290	100.5094	–0.290	100.7080	0.082	101.7698	0.345	66.8462	0.223	74.9501
–0.263	100.6919	–0.107	101.7235	0.306	66.8248	0.348	74.9345	0.019	100.5898
–0.297	101.6796	0.076	66.8036	–0.003	67.9465	–0.086	100.5712	0.194	101.5041
–0.096	66.7826	–0.186	67.9160	–0.201	100.5490	–0.322	100.7515	0.363	161.6735
–0.274	67.8962	–0.254	100.5313	–0.329	100.7336	–0.218	101.8254	0.189	66.8707
–0.297	100.5113	–0.289	100.7098	0.030	101.7720	0.353	66.8494	0.190	74.9521
–0.269	100.6937	–0.065	101.7320	0.335	66.8281	0.339	74.9364	0.039	100.5917
–0.252	101.6829	0.105	66.8066	0.034	67.9488	–0.081	100.5731	0.160	101.5064
–0.090	66.7856	–0.185	67.9182	–0.185	100.5513	–0.328	100.7534	0.365	161.7171
–0.261	67.8984	–0.250	100.5347	–0.323	100.7355	–0.238	101.8276	0.159	66.8732
–0.287	100.5133	–0.299	100.7117	0.092	101.7781	0.348	66.8519	0.192	74.9540
–0.271	100.6957	–0.047	101.7342	0.340	66.8306	0.345	74.9384	0.052	100.5936
–0.208	101.7023	0.134	66.8091	0.053	67.9510	–0.060	100.5757	0.139	101.5089
–0.057	66.7880	–0.175	67.9205	–0.189	100.5535	0.319	101.4898	0.353	161.7607

ΔR_c	*HJD 2456500+*	ΔR_c	*HJD 2456500+*	ΔR_c	*HJD 2456500+*	ΔR_c	*HJD 2456500+*	ΔR_c	*HJD 2456500+*
–0.208	66.6472	–0.193	67.890	–0.192	100.511	–0.222	100.725	–0.209	161.6217
–0.214	67.880	–0.192	100.503	–0.199	100.711	–0.188	161.6151	–0.252	66.6972
–0.224	100.491	–0.178	100.703	–0.178	161.6085	–0.247	66.6854	–0.038	67.934
–0.167	100.695	–0.160	161.602	–0.243	66.6743	–0.128	67.913	–0.150	100.534
–0.139	161.595	–0.227	66.6613	–0.158	67.903	–0.172	100.524	–0.237	100.737
–0.211	66.6497	–0.194	67.893	–0.176	100.513	–0.213	100.727	–0.207	161.6233
–0.209	67.884	–0.194	100.505	–0.207	100.717	–0.192	161.6167	–0.251	66.6997
–0.218	100.497	–0.193	100.705	–0.177	161.6101	–0.254	66.6879	–0.022	67.936
–0.170	100.697	–0.162	161.6035	–0.243	66.6768	–0.122	67.916	–0.131	100.537
–0.142	161.597	–0.230	66.6638	–0.149	67.905	–0.160	100.526	–0.225	100.739
–0.215	66.6522	–0.180	67.896	–0.178	100.515	–0.231	100.729	–0.211	161.6250
–0.206	67.886	–0.193	100.507	–0.204	100.718	–0.204	161.6184	–0.246	66.7022
–0.207	100.500	–0.190	100.708	–0.188	161.6118	–0.260	66.6904	–0.003	67.938
–0.180	100.699	–0.172	161.6052	–0.244	66.6793	–0.110	67.918	–0.132	100.539
–0.143	161.599	–0.230	66.6663	–0.144	67.908	–0.158	100.529	–0.224	100.741
–0.215	66.6547	–0.175	67.898	–0.191	100.520	–0.221	100.733	–0.222	161.6266
–0.202	67.888	–0.196	100.509	–0.209	100.720	–0.197	161.6200	–0.240	66.7056
–0.207	100.500	–0.199	100.710	–0.190	161.6134	–0.250	66.6947	0.005	67.940
–0.181	100.701	–0.165	161.6068	–0.250	66.6829	–0.097	67.920	–0.122	100.541
–0.152	161.600	–0.242	66.6718	–0.139	67.910	–0.157	100.531	–0.226	100.745
–0.224	66.6588	–0.167	67.900	–0.183	100.522	–0.233	100.735	–0.223	161.6283

Table continued on following pages

Table 1. V530 And Observations ΔB, ΔV, ΔRc, and ΔIc, variable minus comparison star, cont.

ΔR_c	*HJD 2456500+*	ΔR_c	*HJD 2456500+*	ΔR_c	*HJD 2456500+*	ΔR_c	*HJD 2456500+*	ΔR_c	*HJD 2456500+*
–0.239	66.7081	0.361	74.942	0.167	100.614	–0.083	101.712	–0.176	161.7159
0.049	67.944	0.114	100.586	–0.180	101.588	–0.214	161.6943	0.401	66.8538
–0.122	100.543	0.241	101.511	–0.244	161.6729	0.318	66.8193	–0.176	75.021
–0.237	100.747	–0.245	161.6514	–0.012	66.7850	–0.094	74.996	–0.086	100.670
–0.220	161.6299	–0.159	66.7468	0.064	74.971	0.083	100.642	–0.013	101.813
–0.241	66.7105	0.341	74.944	0.172	100.616	–0.063	101.716	–0.176	161.7176
0.061	67.946	0.124	100.587	–0.224	101.616	–0.216	161.6960	0.392	66.8563
–0.114	100.545	0.262	101.513	–0.249	161.6745	0.337	66.8218	–0.175	75.023
–0.225	100.749	–0.244	161.6530	0.005	66.7875	–0.100	74.998	–0.090	100.672
–0.219	161.6316	–0.156	66.7505	0.049	74.972	0.080	100.644	–0.067	101.817
–0.238	66.7130	0.322	74.946	0.157	100.618	–0.040	101.719	–0.166	161.7192
0.075	67.948	0.142	100.589	–0.265	101.634	–0.214	161.6976	0.372	66.8594
–0.114	100.547	0.169	101.516	–0.242	161.6762	0.362	66.8243	–0.183	75.025
–0.222	100.751	–0.239	161.6547	0.021	66.7900	–0.104	75.000	–0.098	100.674
–0.228	161.6332	–0.151	66.7529	0.024	74.974	0.053	100.646	–0.082	101.821
–0.230	66.7173	0.292	74.948	0.172	100.620	–0.022	101.722	–0.164	161.7209
0.105	67.951	0.147	100.591	–0.239	101.637	–0.210	161.6993	0.363	66.8619
–0.101	100.549	0.004	101.520	–0.237	161.6779	0.392	66.8276	–0.173	75.027
–0.229	100.753	–0.241	161.6563	0.043	66.7925	–0.111	75.002	–0.110	100.676
–0.223	161.6349	–0.139	66.7554	0.026	74.976	0.043	100.648	–0.106	101.825
–0.228	66.7197	0.279	74.950	0.177	100.622	0.057	101.732	–0.159	161.7225
0.392	74.924	0.154	100.593	–0.242	101.641	–0.197	161.7010	0.337	66.8644
–0.078	100.551	0.036	101.531	–0.237	161.6795	0.405	66.8300	–0.194	75.029
0.397	101.489	–0.246	161.6580	0.066	66.7956	–0.116	75.004	–0.124	100.678
–0.223	161.6365	–0.133	66.7579	0.003	74.978	0.030	100.650	–0.108	101.827
–0.223	66.7222	0.253	74.952	0.177	100.624	0.034	101.734	–0.157	161.7242
0.404	74.926	0.170	100.596	–0.242	101.644	–0.204	161.7026	0.300	66.8669
–0.007	100.566	–0.084	101.535	–0.235	161.6812	0.394	66.8325	–0.189	75.031
0.313	101.492	–0.248	161.6597	0.091	66.7981	–0.133	75.006	–0.129	100.680
–0.235	161.6382	–0.111	66.7639	–0.012	74.980	0.010	100.653	–0.105	101.830
–0.218	66.7247	0.239	74.954	0.175	100.626	0.077	101.738	–0.144	161.7259
0.393	74.928	0.174	100.597	–0.209	101.664	–0.194	161.7043	0.270	66.8701
0.007	100.569	–0.140	101.564	–0.238	161.6828	0.406	66.8350	–0.212	75.033
0.376	101.494	–0.249	161.6613	0.116	66.8006	–0.137	75.008	–0.142	100.682
–0.232	161.6398	–0.102	66.7663	–0.018	74.982	–0.001	100.655	–0.119	101.832
–0.216	66.7284	0.215	74.956	0.155	100.629	0.073	101.740	–0.139	161.7275
0.397	74.930	0.171	100.599	–0.202	101.667	–0.199	161.7059	0.236	66.8726
0.022	100.571	–0.142	101.566	–0.234	161.6844	0.399	66.8382	–0.208	75.035
0.356	101.497	–0.248	161.6629	0.140	66.8031	–0.136	75.009	–0.134	100.684
–0.240	161.6414	–0.095	66.7688	–0.027	74.984	–0.006	100.656	–0.148	101.836
–0.206	66.7309	0.197	74.958	0.152	100.631	0.172	101.744	–0.137	161.7292
0.394	74.932	0.165	100.604	–0.186	101.670	–0.193	161.7076	0.210	66.8751
0.029	100.573	–0.150	101.568	–0.241	161.6861	0.407	66.8406	–0.224	100.491
0.333	101.499	–0.242	161.6646	0.171	66.8060	–0.149	75.011	–0.140	100.686
–0.241	161.6431	–0.075	66.7713	–0.048	74.986	–0.028	100.659	–0.153	101.840
–0.204	66.7334	0.171	74.960	0.140	100.632	0.137	101.754	–0.130	161.7309
0.384	74.934	0.178	100.606	–0.161	101.678	–0.190	161.7093	0.184	66.8776
0.049	100.575	–0.161	101.571	–0.226	161.6878	0.408	66.8431	–0.218	100.497
0.303	101.501	–0.254	161.6663	0.188	66.8085	–0.167	75.013	–0.150	100.688
–0.241	161.6448	–0.067	66.7745	–0.048	74.988	–0.042	100.661	–0.167	101.844
–0.197	66.7359	0.141	74.962	0.133	100.634	0.149	101.772	–0.112	161.7325
0.391	74.936	0.168	100.607	–0.132	101.701	–0.183	161.7109	–0.220	67.873
0.064	100.577	–0.132	101.578	–0.214	161.6894	0.400	66.8456	–0.189	75.031
0.276	101.504	–0.248	161.6679	0.223	66.8110	–0.156	75.015	–0.154	100.690
–0.242	161.6464	–0.051	66.7770	–0.053	74.990	–0.056	100.663	–0.112	161.587
–0.183	66.7394	0.108	74.965	0.121	100.636	0.128	101.778	–0.117	161.7342
0.384	74.938	0.158	100.610	–0.127	101.704	–0.183	161.7126	–0.223	67.876
0.072	100.579	–0.194	101.583	–0.215	161.6910	0.396	66.8488	–0.212	75.033
0.260	101.506	–0.247	161.6696	0.249	66.8135	–0.163	75.017	–0.164	100.692
–0.243	161.6481	–0.026	66.7795	–0.068	74.992	–0.050	100.666	–0.118	161.590
–0.179	66.7419	0.097	74.967	0.111	100.638	–0.003	101.808	–0.115	161.7358
0.377	74.940	0.175	100.612	–0.102	101.709	–0.176	161.7142	–0.217	67.878
0.120	100.584	–0.203	101.586	–0.212	161.6927	0.415	66.8513	–0.208	75.035
0.232	101.508	–0.248	161.6712	0.281	66.8168	–0.165	75.019	–0.164	100.693
–0.244	161.6497	–0.027	66.7820	–0.070	74.994	–0.068	100.668	–0.136	161.594
–0.171	66.7443	0.083	74.969	0.097	100.640	–0.032	101.810	–0.110	161.7375

Table continued on following pages

Table 1. V530 And Observations ΔB, ΔV, ΔRc, and ΔIc, variable minus comparison star, cont.

ΔI_c	*HJD 2456500+*	ΔI_c	*HJD 2456500+*	ΔI_c	*HJD 2456500+*	ΔI_c	*HJD 2456500+*	ΔI_c	*HJD 2456500+*
–0.133	66.647	–0.059	66.9344	–0.072	100.5340	0.134	101.5192	–0.156	161.6824
0.087	66.8983	–0.144	100.5026	–0.172	100.7509	–0.170	161.6609	0.164	66.798
–0.094	75.0188	–0.147	100.7181	–0.157	161.6395	–0.037	66.763	0.420	74.9415
–0.098	100.6893	–0.120	161.6180	–0.145	66.724	–0.080	67.8997	0.242	100.6033
–0.073	161.5966	–0.170	66.687	–0.156	67.8660	0.094	100.5724	–0.158	101.6435
–0.120	66.649	–0.077	66.9369	–0.079	100.5362	0.092	101.5305	–0.157	161.6841
0.064	66.9017	–0.136	100.5049	–0.175	100.7527	–0.169	161.6626	0.178	66.800
–0.091	75.0209	–0.141	100.7200	–0.159	161.6411	–0.025	66.766	0.412	74.9434
–0.104	100.6912	–0.127	161.6197	–0.128	66.728	–0.048	67.9027	0.232	100.6052
–0.073	161.5982	–0.167	66.690	–0.151	67.8685	0.121	100.5750	–0.177	101.6484
–0.121	66.652	–0.073	66.9394	–0.069	100.5387	0.083	101.5394	–0.147	161.6857
0.052	66.9042	–0.133	100.5068	0.454	101.4889	–0.160	161.6642	0.214	66.803
–0.094	75.0228	–0.149	100.7245	–0.162	161.6427	–0.020	66.768	0.390	74.9453
–0.122	100.6931	–0.129	161.6213	–0.133	66.730	–0.031	67.9072	0.240	100.6071
–0.080	161.5999	–0.161	66.694	–0.149	67.8725	0.123	100.5769	–0.147	101.6521
–0.128	66.654	–0.080	66.9419	–0.073	100.5406	–0.071	101.5632	–0.144	161.6874
0.040	66.9067	–0.132	100.5087	0.430	101.4939	–0.171	161.6659	0.237	66.806
–0.102	75.0248	–0.153	100.7264	–0.169	161.6444	–0.014	66.771	0.379	74.9473
–0.117	100.6950	–0.131	161.6230	–0.124	66.733	–0.019	67.9094	0.253	100.6097
–0.088	161.6015	–0.168	66.697	–0.147	67.8750	0.142	100.5788	–0.136	101.6588
–0.144	66.658	–0.143	67.8223	–0.067	100.5424	–0.069	101.5657	–0.148	161.6890
0.028	66.9092	–0.145	100.5106	0.419	101.4963	–0.173	161.6675	0.265	66.808
–0.096	75.0267	–0.162	100.7283	–0.164	161.6460	0.008	66.774	0.361	74.9493
–0.117	100.6969	–0.132	161.6246	–0.117	66.735	0.460	74.9238	0.246	100.6116
–0.094	161.6032	–0.156	66.699	–0.137	67.8775	0.164	100.5833	–0.136	101.6628
–0.130	66.661	–0.148	67.8245	–0.059	100.5445	–0.083	101.5680	–0.143	161.6907
0.007	66.9126	–0.127	100.5126	0.385	101.4986	–0.177	161.6692	0.292	66.811
–0.119	75.0287	–0.160	100.7329	–0.170	161.6477	0.018	66.777	0.334	74.9512
–0.121	100.6988	–0.141	161.6263	–0.106	66.739	0.457	74.9258	0.243	100.6135
–0.090	161.6048	–0.162	66.702	–0.142	67.8799	0.173	100.5852	–0.119	101.6660
–0.140	66.663	–0.150	67.8267	–0.039	100.5464	–0.082	101.5703	–0.142	161.6923
–0.001	66.9151	–0.132	100.5145	0.363	101.5010	–0.167	161.6709	0.315	66.813
–0.101	75.0306	–0.163	100.7348	–0.178	161.6494	0.043	66.779	0.309	74.9532
–0.119	100.7008	–0.141	161.6279	–0.099	66.741	0.446	74.9277	0.233	100.6159
–0.087	161.6065	–0.159	66.705	–0.135	67.8833	0.193	100.5871	–0.120	101.6693
–0.151	66.666	–0.149	67.8290	–0.034	100.5483	–0.096	101.5725	–0.131	161.6940
–0.013	66.9176	–0.126	100.5199	0.347	101.5032	–0.161	161.6725	0.348	66.816
–0.114	75.0345	–0.165	100.7367	–0.172	161.6510	0.040	66.782	0.284	74.9553
–0.128	100.7027	–0.142	161.6296	–0.093	66.744	0.469	74.9297	0.243	100.6220
–0.103	161.6081	–0.159	66.708	–0.132	67.8855	0.200	100.5891	–0.057	101.7003
–0.155	66.671	–0.157	67.8321	–0.022	100.5507	–0.118	101.5805	–0.137	161.6956
–0.016	66.9201	–0.119	100.5218	0.320	101.5055	–0.173	161.6742	0.376	66.819
–0.153	75.0365	–0.168	100.7386	–0.168	161.6527	0.065	66.785	0.263	74.9573
–0.122	100.7046	–0.149	161.6312	–0.092	66.746	0.452	74.9317	0.231	100.6283
–0.099	161.6098	–0.156	66.710	–0.115	67.8877	0.209	100.5910	–0.043	101.7035
–0.157	66.674	–0.160	67.8346	–0.006	100.5528	–0.112	101.5828	–0.129	161.6973
–0.026	66.9234	–0.118	100.5238	0.300	101.5080	–0.163	161.6758	0.405	66.821
–0.141	75.0384	–0.173	100.7405	–0.169	161.6543	0.084	66.787	0.234	74.9592
–0.139	100.7073	–0.152	161.6329	–0.080	66.750	0.454	74.9336	0.212	100.6302
–0.106	161.6114	–0.151	66.713	–0.109	67.8900	0.221	100.5929	–0.023	101.7083
–0.160	66.676	–0.154	67.8371	0.018	100.5591	–0.125	101.5854	–0.131	161.6989
–0.040	66.9258	–0.093	100.5257	0.280	101.5102	–0.161	161.6775	0.435	66.824
–0.147	100.4910	–0.172	100.7452	–0.173	161.6560	0.095	66.790	0.210	74.9612
–0.134	100.7092	–0.149	161.6345	–0.069	66.753	0.438	74.9356	0.226	100.6321
–0.119	161.6131	–0.144	66.717	–0.101	67.8930	0.235	100.5952	–0.015	101.7116
–0.165	66.679	–0.164	67.8396	0.063	100.5655	–0.171	101.6330	–0.134	161.7006
–0.054	66.9283	–0.100	100.5283	0.253	101.5125	–0.165	161.6791	0.457	66.827
–0.144	100.4965	–0.172	100.7471	–0.181	161.6576	0.104	66.792	0.198	74.9642
–0.150	100.7111	–0.152	161.6362	–0.069	66.755	0.448	74.9375	0.205	100.6341
–0.121	161.6147	–0.143	66.719	–0.091	67.8952	0.236	100.5971	0.025	101.7148
–0.162	66.683	–0.155	67.8610	0.074	100.5686	–0.163	101.6364	–0.125	161.7022
–0.053	66.9308	–0.094	100.5306	0.155	101.5158	–0.161	161.6808	0.461	66.830
–0.143	100.4999	–0.170	100.7490	–0.165	161.6593	0.136	66.795	0.179	74.9662
–0.139	100.7162	–0.165	161.6378	–0.065	66.757	0.446	74.9395	0.188	100.6360
–0.119	161.6164	–0.142	66.722	–0.082	67.8975	0.241	100.5990	0.043	101.7182
–0.163	66.685	–0.144	67.8635	0.081	100.5705	–0.159	101.6397	–0.124	161.7039

Table continued on next page

Table 1. V530 And Observations ΔB, ΔV, ΔRc, and ΔIc, variable minus comparison star, cont.

ΔI_c	*HJD 2456500+*	ΔI_c	*HJD 2456500+*	ΔI_c	*HJD 2456500+*	ΔI_c	*HJD 2456500+*	ΔI_c	*HJD 2456500+*
0.467	66.832	0.467	66.845	0.450	66.859	0.330	66.872	0.188	66.885
0.154	74.9681	0.080	74.9779	0.040	74.9876	–0.031	74.9993	–0.063	75.0090
0.184	100.6379	0.106	100.6477	0.032	100.6591	–0.022	100.6693	–0.078	100.6797
0.061	101.7215	0.201	101.7433	0.013	101.8122	–0.025	101.8291	–0.042	161.5867
–0.120	161.7056	–0.100	161.7139	–0.086	161.7222	–0.056	161.7305	–0.024	161.7387
0.465	66.835	0.475	66.848	0.435	66.861	0.290	66.875	0.171	66.888
0.141	74.9701	0.062	74.9798	0.018	74.9895	–0.045	75.0012	–0.072	75.0110
0.168	100.6398	0.089	100.6496	0.027	100.6610	–0.032	100.6719	–0.079	100.6816
0.113	101.7311	0.243	101.7455	–0.034	101.8166	–0.001	101.8313	–0.042	161.5883
–0.119	161.7072	–0.100	161.7155	–0.076	161.7238	–0.055	161.7321	–0.133	161.7387
0.471	66.838	0.464	66.851	0.408	66.864	0.265	66.877	0.141	66.891
0.117	74.9720	0.044	74.9818	–0.005	74.9915	–0.045	75.0032	–0.076	75.0129
0.148	100.6417	0.077	100.6523	0.023	100.6629	–0.039	100.6738	–0.093	100.6835
0.125	101.7333	0.234	101.7521	–0.015	101.8206	–0.089	101.8350	–0.057	161.5900
–0.107	161.7089	–0.098	161.7172	–0.087	161.7255	–0.052	161.7338	0.122	66.893
0.465	66.840	0.455	66.853	0.381	66.866	0.235	66.880	–0.075	75.0149
0.115	74.9740	0.048	74.9837	–0.014	74.9954	–0.036	75.0051	–0.095	100.6854
0.127	100.6436	0.074	100.6542	0.007	100.6655	–0.048	100.6757	–0.059	161.5916
0.163	101.7374	0.043	101.8074	–0.023	101.8244	–0.046	101.8390	0.103	66.896
–0.100	161.7105	–0.089	161.7188	–0.061	161.7272	–0.043	161.7355	–0.090	75.0168
0.466	66.843	0.466	66.856	0.350	66.870	0.220	66.883	–0.095	100.6873
0.098	74.9759	0.045	74.9857	–0.023	74.9973	–0.035	75.0071	–0.049	161.5933
0.128	100.6457	0.040	100.6561	–0.002	100.6674	–0.071	100.6778		
0.153	101.7397	0.071	101.8099	–0.014	101.8267	–0.075	101.8433		
–0.120	161.7122	–0.097	161.7205	–0.071	161.7288	–0.024	161.7371		

Table 2. V530 And times of minimum light and linear residuals.

No.	*Epochs JD 2400000+*	*Cycles*	*Initial Residuals*	*Linear Residuals**	*Quadratic Residuals*	*Weight*	*Notes*
1	51454.308	–8857.0	–0.0086	—	–0.0048	0.1	Fits to NSVS 6447718 Data
2	51335.399	–9063.0	–0.0083	—	0.0219	0.1	Fits to NSVS 6447718 Data
3	51454.309	–8857.0	–0.0075	—	–0.0037	0.1	Fits to NSVS 6447718 Data
4	51453.159	–8859.0	–0.0036	—	0.0005	0.1	Fits to NSVS 6447718 Data
5	51535.126	–8717.0	–0.0024	—	–0.0159	0.1	Fits to NSVS 6447718 Data
6	51414.193	–8926.5	–0.0064	—	0.0062	0.1	Fits to NSVS 6447718 Data
7	51467.300	–8834.5	–0.0045	—	–0.0035	0.1	Fits to NSVS 6447718 Data
8	51467.301	–8834.5	–0.0035	—	–0.0025	0.1	Fits to NSVS 6447718 Data
9	55830.7281	–1275.5	0.1422	0.0011	0.0016	1.0	Samec *et al.* 2012
10	55832.7460	–1272.0	0.1398	–0.0009	–0.0006	1.0	Samec *et al.* 2012
11	56566.8428	0.0	0.0000	–0.0059	–0.0068	1.0	Present Observations
12	56598.8820	55.5	0.0030	0.0030	0.0030	1.0	Present Observations
13	56600.6111	58.5	0.0004	0.0007	0.0008	1.0	Present Observations
14	56601.7667	60.5	0.0015	0.0020	0.0022	1.0	Present Observations

**The Linear Ephemeris is calculated from CCD determinations only.*

Table 3. V530 And light curve characteristics.

Filter	*Phase*	*Magnitude Min. I*	*Phase*	*Magnitude Max. I*
	0.00		0.25	
B		0.288 ± 0.005		–0.424 ± 0.008
V		0.356 ± 0.007		–0.343 ± 0.005
R		0.399 ± 0.008		–0.245 ± 0.007
I		0.466 ± 0.005		–0.170 ± 0.006
Filter	*Phase*	*Magnitude Min. II*	*Phase*	*Magnitude Max. II*
	0.50		0.75	
B		–0.045 ± 0.007		–0.420 ± 0.006
V		0.055 ± 0.005		–0.330 ± 0.006
R		0.167 ± 0.010		–0.240 ± 0.011
I		0.241 ± 0.007		–0.167 ± 0.007

Filter	*Min. I – Max. I*	*Max. II – Max. I*	*Min. I – Min. II*
B	0.712 ± 0.012	0.005 ± 0.013	0.332 ± 0.012
V	0.699 ± 0.012	0.014 ± 0.011	0.301 ± 0.012
R	0.645 ± 0.015	0.005 ± 0.017	0.233 ± 0.018
I	0.636 ± 0.010	0.003 ± 0.012	0.224 ± 0.012

Table 4. V530 And light curve solution.

Parameters	*Values*
$\lambda_B, \lambda_V, \lambda_R, \lambda_I$ (nm)	440, 550, 640, 790
$x_{bol1,2}$, $y_{bol1,2}$	0.638, 0.638, 0.248, 0.248
$x_{1I,2I}$, $y_{1I,2I}$	0.539, 0.539, 0.281, 0.281
$x_{1R,2R}$, $y_{1R,2R}$	0.624, 0.624, 0.291, 0.291
$x_{1V,2V}$, $y_{1V,2V}$	0.698, 0.698, 0.282, 0.282
$x_{1B,2B}$, $y_{1B,2B}$	0.796, 0.796, 0.255, 0.255
g_1 , g_2	0.32
A_1 , A_2	0.5
Inclination (°)	86.7±0.2
T_1, T_2 (K)	6750, 6030±30
Ω	2.637±0.004
$q(m_2 / m_1)$	0.386±0.004
Fill–outs: $F_1 = F_2$ (%)	5±1
$L_1 / (L_1 + L_2 + L_3)_I$	0.767±0.008
$L_1 / (L_1 + L_2 + L_3)_R$	0.779±0.009
$L_1 / (L_1 + L_2 + L_3)_V$	0.792±0.010
$L_1 / (L_1 + L_2 + L_3)_B$	0.816±0.012
$L_3 / (L_1 + L_2 + L_3)_I$	0.0026± 0.0004
$L_3 / (L_1 + L_2 + L_3)_R$	0.0045±0.0004
$L_3 / (L_1 + L_2 + L_3)_V$	0.0016±0.0004
$L_3 / (L_1 + L_2 + L_3)_B$	0.0072±0.0004
JD_o (days)	2456566.8434±0.0001
Period (days)	0.577233±0.000002
r_1, r_2 (pole)	0.438±0.001, 0.282±0.002
r_1, r_2 (side)	0.468±0.001, 0.294±0.003
r_1, r_2 (back)	0.495±0.002, 0.328±0.005
Spot Parameters	
Spot 1 On STAR 1	*Cool Spot*
Colatitude (°)	57.2±0.3
Longitude (°)	5.3±0.1
Spot radius (°)	36.7±0.1
Spot T-factor	0.844±0.001
Spot 2 On STAR 1	*Hot Spot*
Colatitude (°)	16.7±0.3
Longitude (°)	193±1
Spot radius (°)	31.9±0.1
Spot T-factor	1.397±0.002

The High Amplitude δ Scuti Star AD Canis Minoris

Roy Andrew Axelsen
P. O. Box 706, Kenmore, Queensland 4069, Australia; reaxelsen@gmail.com

Tim Napier-Munn
49 Limosa Street, Bellbowrie, Queensland 4070, Australia

Received July 26, 2016; revised September 13, 2016 and October 14, 2016; accepted October 14, 2016

Abstract The high amplitude δ Scuti star AD Canis Minoris was studied by photoelectric photometry (PEP) during one night in February 2011 and by digital single lens reflex (DSLR) photometry during seven nights in January and February 2016. Nine light curve peaks were captured, eight of them by DSLR photometry. A review of the literature enabled us to tabulate 109 times of maximum since 1959, to which we added 9 times of maximum from our data, thus creating the largest dataset to date for this star. Assuming a linear ephemeris, the period of AD CMi was calculated to be 0.122974511 (± 0.000000004) d, almost identical to that quoted in earlier literature. We constructed an observed minus computed (O–C) diagram which exhibited a quasi-sinusoidal shape, and fitted a weighted model characterized by combined quadratic and trigonometric functions. The fit indicates that the shape of the O–C diagram is attributable to the effects of a slow increase in the pulsation period of AD CMi at a constant rate, modulated by the light time effect of a binary system. These results confirm those of previous authors, and update most of the coefficients of the equation for the fitted model. The values of all of the coefficients in the function are statistically significant. The rate of increase in the pulsation period of AD CMi was calculated from the entire dataset to be $dP/dt = 6.17 (\pm 0.75) \times 10^{-9}$ d yr^{-1} or $dP/Pdt = 5.01 (\pm 0.61) \times 10^{-8}$ yr^{-1}.

1. Introduction

The variability of AD Canis Minoris was first reported by Hoffmeister in 1934 (quoted by Abhyankar 1959). The period of the star is approximately 0.12297 d (Abhyankar 1959; Anderson and McNamara 1960; Epstein and Abraham de Epstein 1973; Breger 1975), with the most precise period of 0.12297443 d reported up to that time by Breger (1975). O–C (observed minus computed) diagrams constructed from observations obtained from 1959 to 1992 revealed that the data were best described by a quadratic function, which indicated that the period was increasing at a slow constant rate (Jiang 1987 quoted by Rodríguez *et al.* 1988, 1990; Yang *et al.* 1992; Burchi *et al.* 1993). Subsequent O–C diagrams which included more recent observations revealed that the data were best fitted by combined quadratic and trigonometric functions, attributed to a slow constant increase in the period, modulated by the light time effect of a binary system (Fu and Jiang 1996; Fu 2000; Hurta *et al.* 2007; Khokhuntod *et al.* 2007). The period of the orbit of the binary system was variously calculated to be 30 yr (Fu and Jiang 1996), 30.44 yr (Fu 2000), 42.8 yr (Hurta *et al.* 2007), and 27.2 yr (Khokhuntod *et al.* 2007).

Since more than 9 years have elapsed since the last time of maximum (March 2006) published in the table of data for the most recent O–C diagram (Khokhuntod *et al.* 2007), it was decided to perform DSLR photometry of AD CMi, and undertake a detailed review of the literature. These efforts have resulted in an expanded listing of times of maximum from the literature, and the addition of nine new times of maximum from our own observations, one from photoelectric photometry in February 2011, and eight from digital single lens reflex (DSLR) photometry in January and February 2016. In all, this paper analyzes 118 times of maximum, a substantial increase on 81 times of maximum reported by Hurta *et al.* (2007) and 73 reported by Khokhuntod *et al.* (2007).

2. Data and analysis

2.1. Photoelectric photometry

Photoelectric photometry (PEP) was taken with an SSP-5 single channel instrument fitted with a Hamamatsu R6358 multialkali photomultiplier tube, from Optec Inc., Lowell, Michigan. Readings were taken through a Celestron C9.25 Schmidt-Cassegrain telescope on a Losmandy GM8 mount. Three 10-second integrations through a V photometric filter from Optec Inc. were averaged to obtain each observation, with the sequence of targets for each set of observations being: sky, comparison star, variable star, comparison star, sky. The comparison star was TYC 0181 00632 1, with the V magnitude taken to be 8.25. Non-transformed magnitudes in V were calculated since the B–V color indices of the variable and comparison stars (approximately 0.25 and 0.30, respectively) did not differ greatly. Data were collected during several nights, but only on one night in February 2011 were observations from a peak of the light curve obtained.

2.2. DSLR photometry

DSLR photometry was taken with a Canon EOS 500D camera during eight nights in January and February 2016. On two nights, images were obtained through a Celestron C9.25 Schmidt-Cassegrain telescope, and during the other six nights through an Orion ED80mm refracting telescope. A Losmandy GM8 mount was used for both telescopes. Images through the Celestron instrument were taken at 800 ISO with exposures of 120 seconds, and a 15- or 20-second gap between exposures. Images through the Orion instrument were taken at either 400

Table 1. Comparison and check stars for DSLR photometry.

Telescope	*Star*	*Star ID*	*V (V Error)*	*B (B Error)*	*B–V*
80-mm refractor	Comparison	HD 64561	8.25		0.30
	Check	HD 64632	8.52		0.26
235-mm SCT	Comparison	TYC 0181 00560 1	10.072 (0.027)	10.563 (0.039)	0.491
	Check	TYC 0181 00708 1	10.388 (0.021)	10.841 (0.028)	0.453

Notes: V and B–V for the comparison and check stars observed through the 235-mm SCT (Schmidt-Cassegrain telescope) were obtained from APASS (American Association of Variable Star Observers Photometric All Sky Survey (Henden et al. *2015)).*

or 800 ISO, and exposures of 120 or 225 seconds, with a gap of 15 or 30 seconds between exposures. Dark frames were taken during the meridian flip, or at the end of the night's observing run if no meridian flip was made. Flat fields were taken near sunrise the morning after the observations, through a sheet of white acrylic acting as a diffuser placed over the front of the telescope, which was aimed at the zenith.

Comparison and check stars (listed in Table 1) were chosen with B–V color indices as close as possible to those of the variable star. The B and V magnitudes of the comparison and check stars for the images through the Schmidt-Cassegrain instrument were obtained from the AAVSO Photometric All-Sky Survey (APASS; Henden *et al.* 2015), and the color indices calculated from those magnitudes.

Aperture photometry was performed on images from the green and blue channels of the DSLR sensor using the software AIP4WIN (Berry and Burnell 2011), and instrumental magnitudes were calculated. Transformed magnitudes in B and V were determined using transformation coefficients from images of standard stars in the E regions (Menzies *et al.* 1989). The time in JD of each magnitude calculation was taken to be the mid point of each DSLR exposure. The heliocentric correction for each night's data was calculated for the mid point in time of the observing run for the night, and the correction applied to all data points for that night.

2.3. Determination of the times of maximum of the light curves

For PEP, the time of maximum was taken as the time in heliocentric Julian days of the peak value of a fifth-order polynomial function fitted to the data in MICROSOFT EXCEL. The time of maximum was obtained by interpolation after zooming in to the peak of the fitted curve in the spreadsheet. For DSLR photometry the time of maximum for each peak in the light curve was taken as the time of the maximum value of a 10th order polynomial function fitted to the peak, with the polynomial functions calculated by the software PERANSO (Vanmunster 2013).

3. Results

Figures 1 and 2 show light curves of AD CMi from photoelectric photometry and DSLR photometry, respectively, each taken during one night. Photoelectric photometry yielded only one light curve peak. From DSLR photometry, usable light curves were obtained during seven nights of observation, from which eight peaks were captured. The times of maximum of the light curves from DSLR photometry and the errors of the estimates, determined using the software PERANSO, are listed in Table 2. Table 3 lists 118 times of maximum, epochs, and O–C values from the literature and from the observations reported by the present authors. The initial epoch and the initial period used to calculate the epochs and the O–C values were those used by Hurta *et al.* (2007), namely, HJD 2436601.82736 and 0.122974510 d, respectively.

A linear ephemeris calculated from the times of maximum and the epochs listed in Table 3 yielded a period of 0.122974511 (± 0.000000004) d.

We apply to the O–C diagram a model comprising combined quadratic and trigonometric functions, as published by Fu and Jiang (1996), Fu (2000), Hurta *et al.* (2007) and Khokhuntod

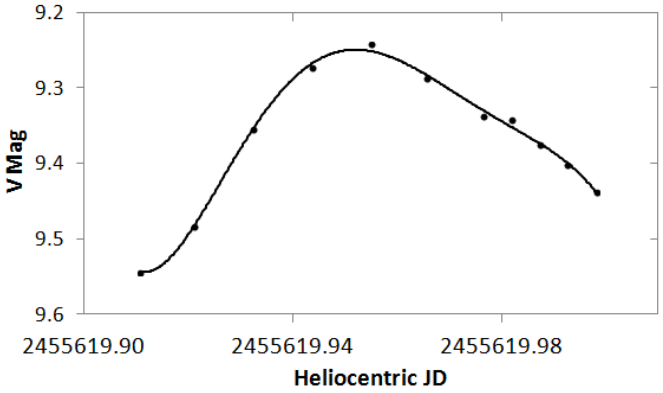

Figure 1. Light curve of AD CMi by photoelectric photometry taken during one night with observations over 2 hours 6 minutes. The solid line is a fifth-order polynomial function, fitted in MICROSOFT EXCEL.

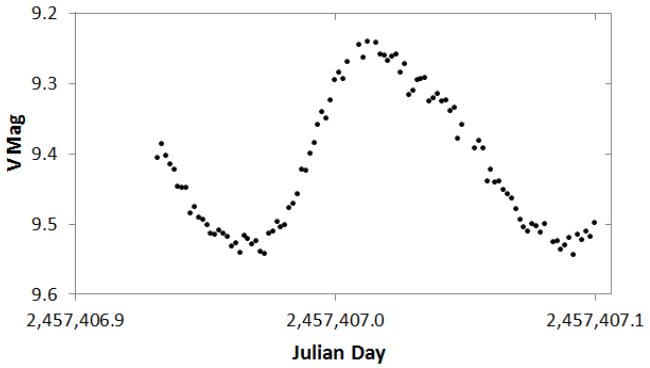

Figure 2. Light curve of AD CMi by DSLR photometry taken during one night with observations over 4 hours 2 minutes.

Table 2. Times of maximum (TOM) in heliocentric Julian days (HJD) of the light curves from DSLR photometry, and the errors of the estimates. The listed values are those output by PERANSO (Vanmunster 2013) , and are not rounded to the last significant digit.

Date	*TOM (HJD)*	*Error*
8-Jan-16	2457396.07261	0.00240
8-Jan-16	2457396.19553	0.00213
11-Jan-16	2457399.02654	0.00171
19-Jan-16	2457407.01750	0.00175
14-Feb-16	2457433.08808	0.00153
15-Feb-16	2457433.95010	0.00182
25-Feb-16	2457444.03359	0.00182
26-Feb-16	2457445.01557	0.00237

et al. (2007). The model implies that the shape of the O–C diagram is attributable to the combined effects of a slow constant rate of increase in the pulsation period of AD CMi, and the light time effect of a stellar pair in mutual orbit.

The model to be fitted is in essence similar to those quoted in the four papers in the previous paragraph, and is represented here in the form:

$$O - C = a + bE + cE^2 + A \sin \phi + B \cos \phi \qquad (1)$$

where E is the epoch (commencing at zero), a, b, c, A, and B are parameters to be estimated from data, and ϕ is the eccentric anomaly, which is the solution to Kepler's equation:

$$\phi - e \sin \phi = 2\pi (1 / P_{orb}) (P_{pul} E - T) \qquad (2)$$

where P_{orb} = orbital period of the pair, P_{pul} = pulsation period of the δ Scuti variable star, T is the time of periastron of the assumed elliptical orbit, and e is the eccentricity of the ellipse. The right-hand side of Equation 2 is the mean anomaly at a given time for a two-body system, M:

$$M = 2\pi (1 / P_{orb}) (P_{pul} E - T) \qquad (3)$$

Kepler's equation (Equation 2) cannot be solved analytically for ϕ and must be solved iteratively. There are several convenient algorithms in the literature. We have used a simple VB macro routine for EXCEL provided by Burnett (1998). This requires three arguments: the mean anomaly, M, the eccentricity, e, and a convergence criterion.

M is easily calculated, given P_{orb}, P_{pul}, and T, for a given epoch, E. Here the values of P_{orb} and T were taken from Hurta et al. (2007) as P_{orb} = 15660 and T = 13870. P_{pul} was assumed to be 0.12297451 day.

For each O–C, E, and ϕ data point, the model of Equation 1 was then fitted by non-linear regression using the MINITAB 16 statistical software package (Minitab 2016). This uses the Gauss-Newton least squares minimization algorithm to estimate the parameters. We did not find the method sensitive to parameter starting values.

Table 4 shows the fitted parameter values, their standard errors, the standard error of the fit, and the P-values for the parameters. The P-values were all statistically significant.

Figure 3 shows the O–C diagram with the predictions of the fitted model and the 95% confidence limits of the model

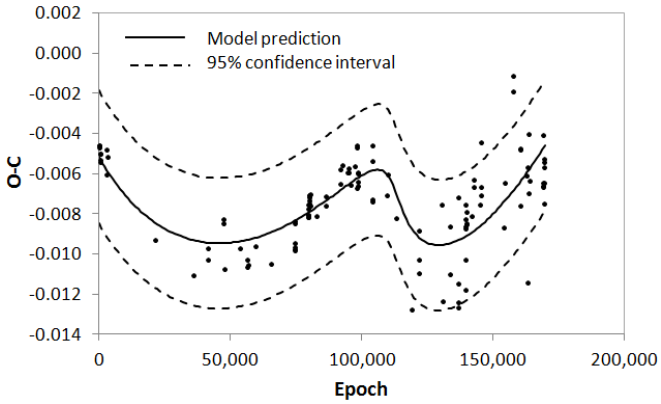

Figure 3. O–C diagram of AD CMi with fitted model prediction (Equation 1) and 95% prediction confidence limits.

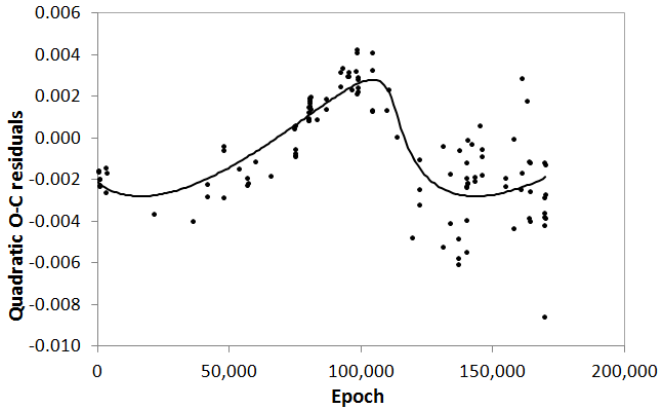

Figure 4. Quadratic residuals for the O–C data of AD CMi, fitted with a function that represents the trigonometric part of Equation 1. The shape of this function reflects the light time effect of the orbital motion of a binary pair.

predictions. The relatively wide confidence intervals reflect the uncertainty in the data and thus the model parameters.

Following Hurta *et al.* (2007), we can show that if the quadratic component of the fitted Equation 1 is subtracted from the original O–C data, the resultant residuals plot has a skewed sinusoidal shape which can then be directly fitted to the sinusoidal component of Equation 1. Thus if we compute $a + bE + cE^2$, where a, b, and c take the values given in Table 3, and subtract these values from the original O–C data, we get the plot shown in Figure 4.

The fitted line in Figure 4 is the function:

$$\text{Residual} = A \sin \phi + B \cos \phi \qquad (4)$$

for the prevailing values of ϕ (and M in Equation 3), fitted by non-linear regression, as before. Equation 4 is the sinusoidal part of Equation 1, and the fitted parameters A and B are identical to those in Table 4. Figure 4 effectively isolates the light time effect of the binary system, and is similar to Figure 2 of Hurta *et al.* (2007), but now extended to include the more recent data. It is worth noting the considerable scatter in the latter part of the plot, which suggests that the model is less well determined for this part of the series (see discussion of weighted regression below).

We can also show that if the trigonometric part of Equation 1 ($A \sin \phi + B \cos \phi$) is subtracted from the original O–C data, the resultant residuals plot has a parabolic shape which can then

Table 3. Data for the O–C diagrams and the key to the references from which the times of maximum (TOM) in heliocentric Julian days (HJD) were taken.

Max	*TOM (HJD)*	*Epoch*	*O–C*	*Reference Key*	*Max*	*TOM (HJD)*	*Epoch*	*O–C*	*Reference Key*
1	2436602.80660	8	–0.0046	1	60	2448714.07240	98494	–0.0063	15
2	2436602.92960	9	–0.0045	1	61	2448717.02420	98518	–0.0059	15
3	2436604.89710	25	–0.0046	1	62	2449399.16250	104065	–0.0072	16
4	2436627.77000	211	–0.0050	1	63	2449399.28820	104066	–0.0045	17
5	2436628.75380	219	–0.0050	1	64	2449400.14620	104073	–0.0073	16
6	2436629.73730	227	–0.0053	1	65	2449401.13200	104081	–0.0053	16
7	2436629.86020	228	–0.0053	1	66	2450071.21840	109530	–0.0070	18
8	2436931.76200	2683	–0.0060	2	67	2450153.36640	110198	–0.0060	19
9	2436932.74700	2691	–0.0048	2	68	2450517.36880	113158	–0.0082	20
10	2436969.76200	2992	–0.0051	2	69	2451268.36960	119265	–0.0127	21
11	2439202.72900	21150	–0.0092	3	70	2451567.07860	121694	–0.0088	5
12	2441010.69850	35852	–0.0110	4	71	2451577.53000	121779	–0.0102	22
13	2441681.52580	41307	–0.0096	5	72	2451598.31200	121948	–0.0109	23
14	2441682.50900	41315	–0.0102	5	73	2452667.57880	130643	–0.0075	5
15	2442429.45800	47389	–0.0084	6	74	2452695.36620	130869	–0.0123	23
16	2442429.45820	47389	–0.0082	7	75	2453028.50550	133578	–0.0110	24
17	2442461.42910	47649	–0.0107	5	76	2453039.57560	133668	–0.0086	5
18	2443182.42970	53512	–0.0096	8	77	2453409.23320	136674	–0.0123	25
19	2443536.34940	56390	–0.0106	8	78	2453411.20050	136690	–0.0126	25
20	2443536.47270	56391	–0.0103	8	79	2453412.18550	136698	–0.0114	25
21	2443572.38100	56683	–0.0105	5	80	2453452.27950	137024	–0.0071	5
22	2443936.26350	59642	–0.0096	5	81	2453776.19280	139658	–0.0087	25
23	2444645.08770	65406	–0.0105	9	82	2453777.05370	139665	–0.0086	25
24	2445766.37130	74524	–0.0084	10	83	2453777.17780	139666	–0.0075	25
25	2445768.33770	74540	–0.0096	10	84	2453781.10870	139698	–0.0118	25
26	2445768.46060	74541	–0.0097	10	85	2453785.04540	139730	–0.0102	25
27	2445771.41340	74565	–0.0083	10	86	2453785.17040	139731	–0.0082	25
28	2445772.39610	74573	–0.0094	10	87	2453810.62589	139938	–0.0085	DKS
29	2445772.51870	74574	–0.0098	10	88	2453810.62591	139938	–0.0084	26
30	2446392.43550	79615	–0.0075	11	89	2453822.55500	140035	–0.0079	5
31	2446417.39910	79818	–0.0077	9	90	2454044.89270	141843	–0.0081	DKS
32	2446418.25960	79825	–0.0080	9	91	2454165.28620	142822	–0.0066	5
33	2446418.38250	79826	–0.0081	9	92	2454172.29610	142879	–0.0063	5
34	2446419.24340	79833	–0.0080	9	93	2454425.86834	144941	–0.0075	DKS
35	2446419.36630	79834	–0.0081	9	94	2454479.36270	145376	–0.0070	27
36	2446443.10100	80027	–0.0075	9	95	2454479.48610	145377	–0.0066	27
37	2446443.22430	80028	–0.0071	9	96	2454515.27390	145668	–0.0044	28
38	2446443.34700	80029	–0.0074	9	97	2455584.53300	154363	–0.0086	29
39	2446444.08500	80035	–0.0073	9	98	2455619.95188	154651	–0.0064	30
40	2446444.20820	80036	–0.0070	9	99	2455997.36600	157720	–0.0011	6
41	2446444.33120	80037	–0.0070	9	100	2455998.34900	157728	–0.0019	6
42	2446493.76700	80439	–0.0070	12	101	2456333.82060	160456	–0.0047	31
43	2446495.73400	80455	–0.0076	12	102	2456346.73010	160561	–0.0076	31
44	2446775.62350	82731	–0.0080	5	103	2456349.68434	160585	–0.0047	HMB
45	2447219.43950	86340	–0.0071	13	104	2456614.93900	162742	–0.0061	31
46	2447220.42280	86348	–0.0075	13	105	2456685.76700	163318	–0.0114	31
47	2447912.27850	91974	–0.0064	11	106	2456699.66888	163431	–0.0056	HMB
48	2447912.40220	91975	–0.0057	11	107	2456726.35600	163648	–0.0040	32
49	2448001.19000	92697	–0.0055	11	108	2456726.47600	163649	–0.0069	32
50	2448254.51710	94757	–0.0059	5	109	2456753.65400	163870	–0.0063	31
51	2448275.29980	94926	–0.0059	11	110	2457396.07261	169094	–0.0065	30
52	2448276.28380	94934	–0.0057	11	111	2457396.19553	169095	–0.0066	30
53	2448406.39000	95992	–0.0065	14	112	2457399.02654	169118	–0.0040	30
54	2448601.42850	97578	–0.0056	11	113	2457407.01750	169183	–0.0064	30
55	2448653.20170	97999	–0.0047	15	114	2457433.08808	169395	–0.0064	30
56	2448656.15110	98023	–0.0067	15	115	2457433.95010	169402	–0.0052	30
57	2448656.27620	98024	–0.0045	15	116	2457444.03359	169484	–0.0056	30
58	2448708.17010	98446	–0.0059	11	117	2457445.01557	169492	–0.0074	30
59	2448713.08840	98486	–0.0066	15	118	2457473.54771	169724	–0.0054	HMB

Notes: The data in the above table were obtained from sources published between 1959 and 2016. The original references are: 1. Abhyankar 1959 (quoted by Rodríguez et al. *1988), 2. Anderson and McNamara 1960, 3. Langford 1976, 4. Epstein and Abraham de Epstein 1973, 5. Hurta* et al. *2007, 6. Paschke 2012b, 7. Breger 1975, 8. Balona and Stobie 1983, 9. Jiang 1987 (quoted by Rodríguez* et al. *1990), 10. Rodríguez* et al. *1988, 11. Kilambi and Rahman 1993 (quoted by Hurta* et al. *2007), 12. Kim and Joner 1994 (quoted by Hurta* et al. *2007), 13. Rodríguez* et al. *1990, 14. Perryman* et al. *1997 (quoted by Hurta al al. 2007), 15. Yang* et al. *1992, 16. Fu* et al. *1996, 17. Hübscher* et al. *1994, 18. Fu 2000, 19. Agerer and Hübscher 1997, 20. Agerer and Hübscher 1998, 21. Agerer and Hübscher 2000, 22. Agerer* et al. *2001, 23. Agerer and Hübscher 2003, 24. Hübscher 2005, 25. Khokhuntod* et al. *2007, 26. Klingenberg* et al. *2006, 27. Hübscher* et al. *2009a, 28. Hübscher* et al. *2009b, 29. Paschke 2012a, 30. Present paper, 31. Pena* et al. *2015, 32. Hübscher and Lehmann 2015. DKS, AAVSO Observer Shawn Dvorak, AAVSO International Database. HMB, AAVSO Observer Franz-Josef Hambsch, AAVSO International Database.*

Table 4. Details of model fit for Equation 1 (unweighted).

Parameter	*Values*	*Standard Errors*	*P-value*
a	-3.02087×10^{-3}	5.62187×10^{-4}	4.20×10^{-7}
b	-1.42480×10^{-7}	1.45067×10^{-8}	7.85×10^{-17}
c	8.49520×10^{-13}	8.24045×10^{-14}	5.76×10^{-18}
A	-2.38332×10^{-3}	2.76352×10^{-4}	4.57×10^{-14}
B	1.47535×10^{-3}	3.15462×10^{-4}	8.13×10^{-6}
Regression std.error	1.60030×10^{-3}		

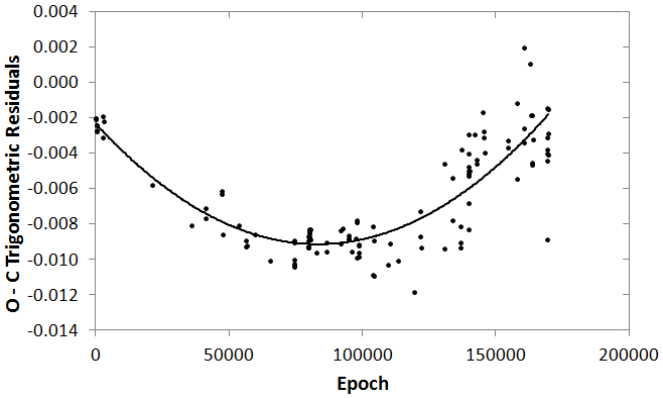

Figure 5. Trigonometric residuals for the O–C data of AD CMi, fitted with a function that represents the quadratic part of Equation 1. The shape of this function indicates the presence of a slow, constant increase in the pulsation period of AD CMi.

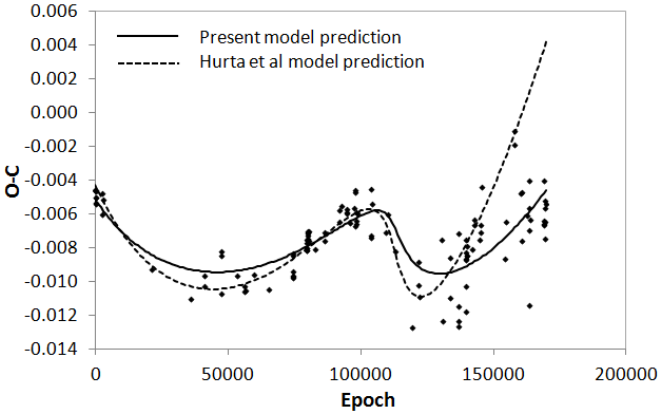

Figure 6. O–C diagram of AD CMi with the model prediction for the present dataset and the earlier dataset from Hurta *et al.* (2007).

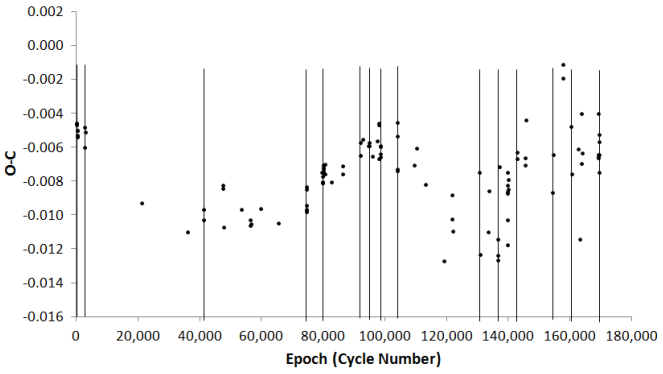

Figure 7. O–C diagram of AD CMi. The vertical lines delineate the groups of O–C values selected for the determination of variance.

be directly fitted to the quadratic component of Equation 1, as shown in Figure 5. This plot effectively isolates the O–C values determined by the pulsation properties of AD CMi. The shape of the O-C diagram and the fitted line (parabolic with concave up) indicates that the period of the star is increasing at a slow steady rate, the value of which is represented by the first differential (equal to 2c) of the second order term (cE^2) of Equation 1.

Figure 6 shows the full dataset again with our model prediction together with that of Hurta *et al.* (2007) as seen in the earlier, less extensive dataset of those authors. It is clear that the two model predictions depart significantly from one another at the later epochs when the new data were collected. The model of Hurta *et al.* is therefore unable to correctly account for the new data.

It is again apparent that the scatter of the data is larger in the later epochs than in the earlier ones. Scatter within a narrow range of epochs reflects experimental error, and is probably mostly due to differences in observers, equipment, and observing conditions. As the scatter varies over the dataset, it would seem sensible to weight the model fitting to reflect this. An appropriate weighting is the inverse of error variance, which can also be described as inverse variance weighting.

An estimate of error variance at a given epoch can be obtained by considering observations taken within any narrow range of epochs as "repeats," and calculating the variance of these to represent the experimental error at the mean epoch of these "repeats." The idea is illustrated in Figure 7, which shows some groupings, comprising the data points on the vertical lines, used to calculate variance.

The range chosen to define "repeats" must be small enough to be able to assume that variations in observational values within this range can be attributed mostly to experimental error and not to true changes in the star's behavior. After careful trial and inspection, 26 groupings of O–C values were found with epoch ranges not exceeding 16 days (the mean was about 9 days), with sample sizes in the range 2–6. We believe the variances of these groups to be attributable principally to observational (experimental) error which can then be used to weight the model fit appropriately.

The variances of the O–C values in these groups are plotted as a function of epoch in Figure 8.

There is a good deal of scatter, probably due to the small sample sizes used to estimate the variance (in the range 2–6), but the linear trend shown is statistically significant (P = 0.00047). Several other models were tried including a quadratic but none gave significantly better fits. Another grouping of data for the calculation of variance was also tried, with a larger number of observations per group, but again the fit was inferior. The equation of the line, which was constrained to pass through the origin, was:

$$\text{Variance} = 6.64 \times 10^{-12}\ \text{Epoch} \qquad (5)$$

This model was used to calculate the variance for each epoch in the original dataset, and the quadratic + sinusoidal model of Equation 1 was then refitted, with weights = 1 / variance. Table 5 shows the new parameters and associated statistics (compare with Table 1 for the unweighted equivalents). Again the P-values

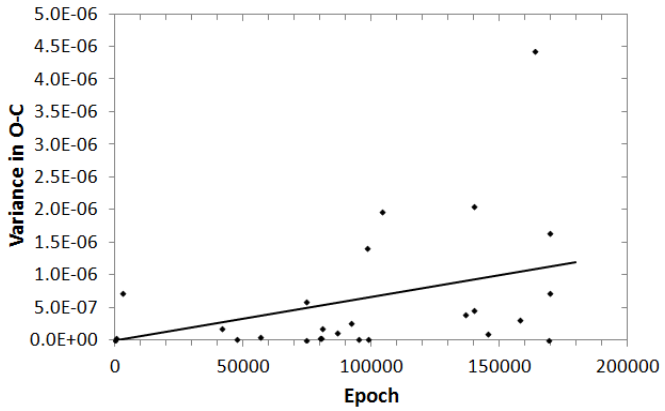

Figure 8. The variances of selected groups of O–C values vs mean epoch data.

Table 5. Details of model fit for Equation (1) (weighted).

Parameter	*Values*	*Standard Errors*	*P-value*
a	-1.98893×10^{-3}	4.84217×10^{-4}	7.60×10^{-5}
b	-1.73831×10^{-7}	2.03459×10^{-8}	6.98×10^{-14}
c	1.03832×10^{-12}	1.26469×10^{-13}	4.01×10^{-13}
A	-2.93094×10^{-3}	4.81185×10^{-4}	1.59×10^{-8}
B	2.01833×10^{-3}	4.32098×10^{-4}	8.32×10^{-6}
Regression std.error	1.64734×10^{-3}		

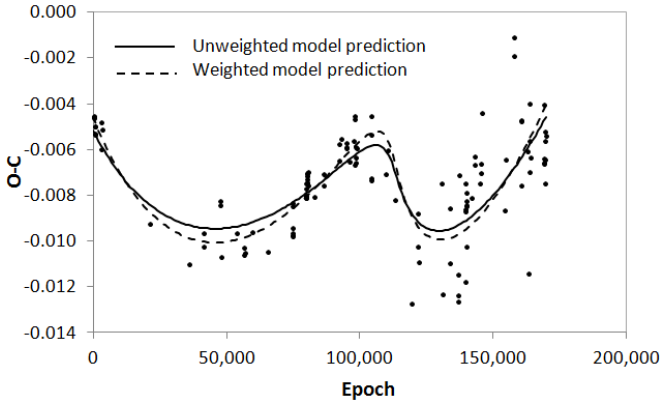

Figure 9. O–C diagram of AD CMi with model predictions for unweighted and weighted data.

show all the parameters to be statistically significant. Figure 9 shows the raw data with the two sets of model predictions, unweighted and weighted.

The two lines are similar but the weighted predictions exhibit higher amplitudes in the cycles. The regression standard errors (controlling prediction uncertainty) are similar (compare Tables 4 and 5).

The rates of change of the pulsation period of AD CMi from the literature and from the observations in the present paper (from the weighted model) are listed in Table 6. Results are included only for those papers which fit a combined quadratic and trigonometric function to the O–C diagram, and are listed in such a manner as to allow easy comparison of the values from the various published sources. It is apparent that there is substantial variation in the values.

4. Discussion

4.1. Issues concerning published times of maximum

Many authors have published data on AD CMi, and several have published tables of epochs and O–C values as well as O–C diagrams (Rodríguez *et al.* 1988, 1990; Yang *et al.* 1992; Fu and Jiang 1996; Hurta *et al.* 2007; Khokhuntod *et al.* 2007). When the literature was reviewed for this paper, a list was made of all published times of maximum, and a comparison of each time of maximum with all other published instances of that time, whether in tables of epochs and O–C values, or as isolated observations. In some cases, the original authors published time series photometry, listing magnitude determinations and the times in heliocentric Julian days or UT of those magnitudes, but did not publish times of maximum of the light curves (Abhyankar 1959; Anderson and McNamara 1960; Epstein and Abraham de Epstein 1973; Balona and Stobie 1983; Kilambi and Rahman 1993). Subsequent papers using those results calculated times of maximum. The present authors chose not to recalculate those times of maximum, instead using the results published by others.

The review of the literature revealed several issues. The first of these relates to the manner in which results published by Anderson and McNamara (1960) are reported by susbsequent authors. Anderson and McNamara reported 38 differential photoelectric observations (delta Y) secured with a yellow filter

Table 6. Rates of change (increase) in the pulsation period of AD CMi.

Reference	*Rate of Period Change* (Error) d cycle^{-13}	*Rate of Period Change* (Error) d yr^{-1}	*Rate of Periot Change* (Error) yr^{-1}
Fu and Jiang 1996	***4.6 × 10^{-13}**	0.14×10^{-8}	1.1×10^{-8}
Fu 2000		***0.10 × 10^{-8}**	*0.81×10^{-8}
Hurta *et al.* 2007		1.15×10^{-8} (0.01×10^{-8})	**9.32×10^{-8} (0.11×10^{-8})**
Khokhuntod *et al.* 2007	**8.6×10^{-13} (0.6×10^{-13})**	0.26×10^{-8} (0.02×10^{-8})	***2.1 × 10^{-8}**
This paper		**0.61×10^{-8} (0.07×10^{-8})**	**5.01×10^{-8} (0.61×10^{-8})**

Notes: These results are only from those papers where combined quadratic and trigonometric functions are fitted to the O–C diagrams. The results for this paper, in the last line of the table, are calculated from the weighted model. Different units were used in various publications, and these are noted at the head of the table. The decimal points are placed in such a way that the numbers in each column can be compared easily. The numbers in bold font represent the coefficients as reported in the original publications, listed in the first column. The numbers not in bold font were calculated by the first author of the present paper, with the aim of presenting all results as d yr^{-1} and yr^{-1} for comparison of the various published values.

** The original authors of these results did not quote estimates of errors.*

relative to the comparison star HD 64275, and listed the UT for each of those observations. The observations captured three peaks of the light curve, as shown in Figure 1 of those authors. However, Rodríguez *et al.* (1990) quote four (not three) times of maximum attributed to Anderson and McNamara, with the first two and the last being identical to the times of maximum listed in Rodríguez *et al.* (1988). It is a mystery why a fourth time of maximum is listed. In addition, the Anderson and McNamara reference is quoted to be *Publ. Astron. Soc. Pacific*, 1961, Vol. 94, p. 289. The year of publication is incorrect (it should be 1960), the volume number for 1961 is actually 72 (not 94), and there is no article beginning on page 289 of the 1961 edition of the journal (according to SAO/NASA ADS). The fourth time of maximum (HJD 2436934.836) attributed to Anderson and McNamara by Rodríguez *et al.* 1990 cannot be confirmed anywhere in the literature by the present authors. It has therefore been omitted from the present paper, although it was reproduced in the tables of times of maximum, epochs, and O–C values by Yang *et al.* (1992), Fu *et al.* (1996), and Khokhuntod *et al.* (2007).

The time of maximum in row 12 of Table 3 above (HJD 2441010.6985 published by Epstein and Abraham de Epstein 1973) is wrongly attributed by Fu *et al.* (1996) to Langford (1976). The time of maximum in row 16 of Table 3 above (HJD 2442429.4582 published by Breger (1975) is wrongly attributed by Fu *et al.* (1996) to Epstein and Abraham de Epstein (1973).

There are two times of maximum in the literature which are times from ephemerides, not directly-observed times of maximum of the peaks of light curves. They are HJD 2436601.8228 (Abhyankar 1959) and HJD 2447506.5815 (Burchi *et al.* 1993). These have therefore been omitted from the O-C table and diagrams in the present paper, although the Abhyankar (1959) time was used by several authors (Rodríguez *et al.* 1988, 1990; Yang *et al.* 1992; Fu *et al.* 1996; Hurta *et al.* 2007; Khokhuntod *et al.* 2007). The Burchi *et al.* (1993) time was used by Hurta *et al.* (2007) and Khokhuntod *et al.* (2007) but both quote it incorrectly as HJD 2447506.5825 (the second last decimal place is incorrect).

The times of maximum in rows 18 to 20 of Table 3 above (i.e., 2443182.4297, 2443536.3494, and 2443536.4727) were calculated from the observations of Balona and Stobie (1983) by Rodríguez *et al.* (1988). The times of maximum corresponding to these and listed by Yang *et al.* (1992), Fu *et al.* (1996), and Khokhuntod *et al.* (2007) are earlier by 0.0004 to 0.0013 HJD.

Kilambi and Rahman (1993) published extensive tables of photometric data on AD CMi, but did not publish times of maximum calculated from those data. Hurta *et al.* (2007) and Khokhuntod *et al.* (2007) calculated and published times of maximum from Kilambi and Rahman's data, and the times of maximum listed by Hurta *et al.* are used in the present paper. The times of maximum in the paper by Khokhuntod *et al.* vary from 0.0054 HJD earlier to 0.0002 HJD later than those of Hurta *et al.* The difference of 0.0054 HJD accounts for one point in the area of wider scatter in O–C values in the O–C diagram of Khokhuntod *et al.* (2007) in comparison with the O–C diagram in the present paper.

Khokhuntod *et al.* (2007) attribute many of the data in their Table 4 to Fu (2000), but that paper does not list any times of maximum for AD CMi. Khokhuntod *et al.* presumably meant to attribute the data to Fu *et al.* 1996. In addition, times of maximum 56 to 58 in Khokhuntod's Table 4 are also attributed to Fu 2000, but were actually first published, respectively, by Agerer and Hübscher (1997, 1998), and Hurta *et al.* (2007).

4.2. Analysis of the O–C diagram

Fu and Jiang (1996), Fu (2000), Hurta *et al.* (2007), and Khokhuntod *et al.* (2007) have indicated that the analysis of the O–C diagram yields a fitted model which can be represented by Equation 1 (repeated from section 3), although the form of the function used by those previous authors differs slightly from that used here:

$$O - C = a + bE + cE^2 + A \sin \phi + B \cos \phi \qquad (1)$$

where ϕ is the solution to Kepler's equation (Equation 2, repeated from section 3):

$$\phi - e \sin \phi = 2\pi \, (1 / P_{orb}) \, (P_{pul} \, E - T) \qquad (2)$$

The function in Equation 1 indicates that the behavior of the O–C diagram is attributable to the combined effects of a slow continuous change (increase) in the pulsation period of AD CMi modulated by the light time effect of a binary pair.

Fu and Jiang (1996), Fu (2000), and Hurta *et al.* (2007) tabulated the coefficients which are the equivalent of a, b, c, A, and B in Equation 1, but Khokhuntod *et al.* (2007) did not. Fu and Jiang (1996), Hurta *et al.* (2007), and Khokhuntod *et al.* (2007) do not describe what method or software was used to derive the fitted model. Fu (2000) indicates that the fit was derived using the software "OMC", referring the reader to a previous publication (Fu *et al.* 1998). We have identified the relevant issue of the journal for that publication, but have not been able to find a copy of the article itself.

We were not able to source software which would analyze the raw O–C data, presumably employing an iterative process or processes, to yield the coefficients a, b, c, A, and B in Equation 1 and simultaneously P_{orb} and T in Equation 2. Therefore, we used the approach outlined above, taking the values of P_{orb} and T (in Equation 2) from Hurta *et al.* (2007) as P_{orb} = 15,660 and T = 13,870. P_{pul} was assumed to be 0.12297451 day. The results from this approach, listed in Table 4, show that the values of the coefficients a, b, c, A, and B are all statistically significant. The model from these coefficients is plotted on the O–C diagram in Figure 3, together with the 95% confidence limits of the model. The quasi-sinusoidal shape of the function is in general similar to those previously published by Hurta *et al.* (2007) and Khokhuntod *et al.* (2007), and supports the modulation of the O–C diagram by the light time effects of a binary system.

The question now arises: does the inclusion of the more recent data in the O–C diagram alter the model? Figure 6 in the present paper indicates that it does. The solid line represents the model from the present paper extending to epoch 169,492, and the dashed line the model of Hurta *et al.* (2007), based on data to epoch 142,879. It can be seen that the model of Hurta *et al.*, when projected into recent epochs, does not predict the more recent data.

It can be seen from the O–C diagrams and Table 3 that the variance of O–C values from epoch 119,265 onwards is greater than the variance of the earlier data. Inspection of the O–C diagram and review of the sources of the more recent data reveal that interobserver variation is the more frequent source of greatest variance, with intraobserver variation contributing, but less frequently. Some observers published only one or two data points near particular epochs, thus preventing an optimal assessment of intraobserver variation in those cases. Given the fact of greater variance in more recent data, it was considered appropriate to weight the model fitting to reflect this. Figure 9 reveals the result. The weighted and unweighted model fitting differ only slightly from one another, the main difference being a greater amplitude of the fitted line as it follows its quasi-sinusoidal course through the data.

The rate of change of the pulsation period of AD CMi is represented by the coefficient (c) of the second order term (cE^2) in the quadratic component of Equation 1, which has the value 1.04 (± 0.13) × 10^{-12} d $cycle^{-1}$. The actual rate is the first derivative of this term, 2c, which has the value 2.08 (± 0.25) ×10^{-12} d $cycle^{-1}$ in the weighted model (Table 5). Converting to the usual units, this value becomes dP / dt = 6.17 (± 0.75) × 10-9 d yr^{-1} or dP / Pdt = 5.01 (± 0.61) × 10^{-8} yr^{-1}. On comparison of these results with previously published rates of increase in the pulsation period of AD CMi, it can be seen (Table 6) that there is substantial variation, with the results from the present paper occupying an intermediate position.

5. Conclusions

We have expanded the O–C diagram of the high amplitude δ Scuti star AD CMi from recent data in the literature and from our own PEP and DSLR photometric observations. Analysis of the O–C diagram has confirmed the work of others that there is a slow constant increase in the pulsational period of the star, modulated by the light time effect of a binary system. We fitted a new, weighted combined quadratic and trigonometric function to the O–C data, based on an orbital period of 42.8 years (Hurta *et al.* 2007), and recalculated the rate of increase in the pulsational period of the δ Scuti star. We note significant variation, in the literature, for the rate of increase in the pulsational period of AD CMi, and for the orbital period of the binary system. Given that the published values for the orbital period vary from 27.2 y (Khokhuntod *et al.* 2007) to 42.8 y (Hurta *et al.* 2007), it may be decades before accurate determinations can be made of the orbital period of the system and the pulsational period of the δ Scuti star.

6. Acknowledgements

We are grateful to AAVSO observers Shawn Dvorak and Franz-Josef Hambsch for their valuable observations from the AAVSO International Database.

The photoelectric photometer used in this study was purchased with a grant from the Edward Corbould Research Fund of the Astronomical Association of Queensland, Brisbane, Australia.

This work utilized data from the AAVSO Photometric All Sky Survey (APASS; Henden *et al.* 2015), funded by the Robert Martin Ayers Sciences Fund.

References

Abhyankar, K. D. 1959, *Astrophys. J.*, **130**, 834.

Agerer, F., Dahm, M., and Hübscher, J. 2001, *Inf. Bull. Var. Stars*, No. 5017, 1.

Agerer, F., and Hübscher, J. 1997, *Inf. Bull. Var. Stars*, No. 4472, 1.

Agerer, F., and Hübscher, J. 1998, *Inf. Bull. Var. Stars*, No. 4562, 1.

Agerer, F., and Hübscher, J. 2000, *Inf. Bull. Var. Stars*, No. 4912, 1.

Agerer, F., and Hübscher, J. 2003, *Inf. Bull. Var. Stars*, No. 5485, 1.

Anderson, L. R., and McNamara, D. H. 1960, *Publ. Astron. Soc. Pacific*, **72**, 506.

Balona, L. A., and Stobie, R. S. 1983, *S. Afr. Astron. Obs. Circ.*, No. 7, 19.

Breger, M. 1975, *Astrophys. J.*, **201**, 653.

Berry, R., and Burnell, J. 2011, "Astronomical Image Processing for Windows," version 2.4.0, provided with *The Handbook of Astronomical Image Processing,* Willmann-Bell, Richmond, VA.

Burchi, R., De Santis, R., Di Paolantonio, A., and Piersimoni, A. M. 1993, *Astron. Astrophys., Suppl. Ser.*, **97**, 827.

Burnett, K. 1998, "Kepler's equation and the Equation of Centre," (http://www.stargazing.net/kepler/kepler.html).

Epstein, I., and Abraham de Epstein, A. E. 1973, *Astron. J.*, **78**, 83.

Fu, J.-N. 2000, in *The Impact of Large-Scale Surveys on Pulsating Star Research*, ed. L. Szabados and D. Kurtz, ASP Conf. Ser. 203, 475.

Fu, J.-N., and Jiang, S.-Y. 1996, *Inf. Bull. Var. Stars*, No. 4325, 1.

Fu, J.-N., Jiang, S.-Y., and Zhou, A.-Y. 1998, *Astrophys. Rep., Publ. Beijing Astron. Obs.*, **32**, 35.

Henden, A. A., *et al.* 2015, AAVSO Photometric All-Sky Survey, data release 9 (http://www.aavso.org/apass).

Hoffmeister, C. 1934, *Astron. Nachr.*, **253**, 195 (quoted by Abhyankar 1959).

Hübscher, J. 2005, *Inf. Bull. Var. Stars*, No. 5643, 1.

Hübscher, J., Agerer, F., Frank, P., and Wunder. E. 1994, *BAV Mitt.*, **68**, 1.

Hübscher, J., and Lehmann, P. B. 2015, *Inf. Bull. Var. Stars*, No. 6149, 1.

Hübscher, J., Steinbach, H.-M., and Walter, F. 2009a, *Inf. Bull. Var. Stars*, No. 5874, 1.

Hübscher, J., Steinbach, H.-M., and Walter, F. 2009b, *Inf. Bull. Var. Stars*, No. 5889, 1.

Hurta, Z., Pócs, M. D., and Szeidl, B. 2007, *Inf. Bull. Var. Stars*, No. 5774, 1.

Jiang, S.-Y. 1987, *Chin. Astron. Astrophys.*, **11**, 343 (quoted by Rodríguez *et al.* 1990).

Khokhuntod, P., Fu, J.-N., Boonyarak, C., Marak, K., Chen, L., and Jiang, S.-Y. 2007, *Chin. J. Astron. Astrophys.*, **7**, 421.

Kilambi, G. C., and Rahman, A. 1993, *Bull. Astron. Soc. India*, **21**, 47.

Kim, C., and Joner, M. D. 1994, *Astrophys. Space Sci.*, **218**, 113 (quoted by Hurta *et al.* 2007).

Klingenberg, G., Dvorak, S. W., and Robertson, C. W. 2006, *Inf. Bull. Var. Stars*, No. 5701, 1.

Langford, W. R. 1976, Ph. thesis, Brigham University (quoted by Rodríguez *et al.* 1990).

Menzies, J. W., Cousins, A. W. J., Banfield, R. M., and Laing, J. D. 1989, *S. Afr. Astron. Obs. Circ.*, No. 13, 1.

Minitab. 2016, MINITAB statistical software (https://www.minitab.com/en-us/).

Paschke, A. 2012a, *Open Eur. J. Var. Stars*, **142**, 1 (http://var.astro.cz/oejv).

Paschke, A. 2012b, *Open Eur. J. Var. Stars*, **147**, 1 (http://var.astro.cz/oejv).

Pena, J. H., *et al.* 2015, *Inf. Bull. Var. Stars*, No. 6154, 1.

Perryman, M. A. C., European Space Agency Space Science Department, and the Hipparcos Science Team. 1997, *The Hipparcos and Tycho Catalogues*, ESA SP-1200 (VizieR On-line Data Catalog: I/239), ESA Publications Division, Noordwijk, The Netherlands (quoted by Hurta *et al.* 2007).

Rodríguez, E., Rolland, A., and López de Coca, P. 1988, *Rev. Mex. Astron. Astrofis.*, **16**, 7.

Rodríguez, E., Rolland, A., and López de Coca, P. 1990, *Inf. Bull. Var. Stars*, No. 3427, 1.

Vanmnuster, T. 2013, light curve and period analysis software PERANSO V.2.50 (http://www.peranso.com/).

Yang, D., Tang, Q., and Jiang, S. 1992, *Inf. Bull. Var. Stars*, No. 3770, 1.

UY Puppis—A New Anomalous Z Cam Type Dwarf Nova

Rod Stubbings
Tetoora Road Observatory, 2643 Warragul-Korumburra Road, Tetoora Road 3821, Victoria, Australia; stubbo@sympac.com.au

Mike Simonsen
AAVSO Headquarters, 49 Bay State Road, Cambridge, MA 02138; mikesimonsen@aavso.org

Received August 23, 2016; revised October 3, 2016; accepted October 3, 2016

Abstract The defining characteristic of Z Cam stars are "standstills" in their light curves. Some Z Cams exhibit atypical behavior by going into outburst from a standstill. It has previously been suggested that UY Pup had been a Z Cam star, but it was ruled out due to its long-term light curve. However, in December 2015 UY Pup went into outburst and unexpectedly entered into a short standstill instead of returning to quiescence. Furthermore, UY Pup exhibited additional unusual behavior with two outbursts detected during its standstill. After this standstill UY Pup made a brief excursion to a quiescent state and slowly rose to a longer and well-defined standstill, where it again went into another outburst. Through comparative analysis, research, and observational data of UY Pup, it is evident and thus concluded that it is indeed a Z Cam star, which renders it one of only four known "anomalous Z Cam stars."

1. Introduction

Dwarf novae are cataclysmic variable stars consisting of close binary systems in which a cool secondary star fills its Roche lobe and transfers mass to a white dwarf primary (Warner 1995). These systems experience recurring outbursts that last several days or more and range in brightness from 2 to 6 magnitudes in V with intervals that can vary from days to decades.

Dwarf novae can be classified into three subtypes: U Gem-type stars that have repeated outburst cycles, SU UMa-type stars that show both short and very long outbursts (superoutbursts), and Z Cam stars. The Z Cam subtype, a rare class of dwarf novae, is characterized by standstills at an intermediate brightness level below the outburst maximum and above the quiescent state. Currently there are only 22 known Z Cam stars (Stubbings and Simonsen 2014).

A standstill typically starts at the end of an outburst and remains at a relatively constant brightness of 1 to 1.5 magnitudes below maximum light. These standstills have been known to last from several days to several months. To date the orbital periods of Z Cam stars range from 3 hours to over 8.4 hours (Simonsen 2014). The observational data imply that a bona fide standstill will last up to the length of the mean outburst cycle or longer.

Simonsen (2009) coordinated an observing campaign, the Z CamPaign, to monitor their long-term light curves and correctly classify Z Cam systems. Another aim of the campaign was to determine if any Z Cam stars enter into outburst from a standstill (Simonsen 2010). The results thus far have shown that nine Z Cam stars go back into outburst from a standstill: Z Cam, HX Peg, AH Her, HL CMa, UZ Ser, AT Cnc, Leo5, V513 Cas, and IW And (Simonsen *et al.* 2014).

Two systems, V513 Cas and IW And, displayed unusual behaviors in their light curves by having brief excursions to quiescence in addition to going into outburst after a standstill (Simonsen 2011). The light curve of V513 Cas is shown in Figure 1.

The two anomalous Z Cam stars V513 Cas and IW And were studied further by Szkody (*et al.* 2013) to understand the reason why outbursts occur after standstills. The data revealed no explanation as to why outbursts occur from standstills instead of returning to the quiescent state, which is typical behavior for Z Cam systems (Szkody *et al.* 2013). This phenomenon in V513 Cas and IW And was further investigated by Hameury and Lasota (2014), who concluded that it is possibly due to magnetic activity of the secondary star which might be considerably stronger than in other systems. As shown in Figure 2, the recently classified anomalous Z Cam star ST Cha displays the same remarkable behavior as V513 Cas (Simonsen *et al.* 2014). ST Cha spends most of the time in standstills followed by outbursts, brief excursions to quiescence, and in standstills emerging from quiescence.

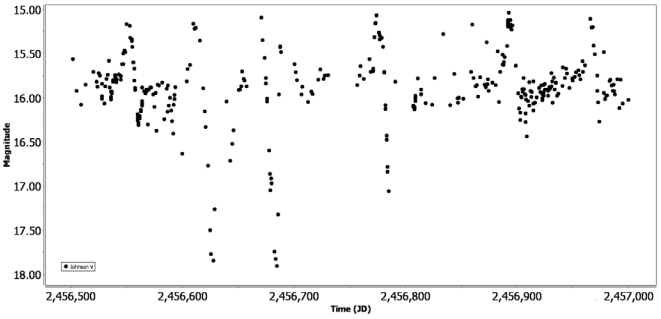

Figure 1. The AAVSO light curve of V513 Cas, JD 2456500–2457500 (July 2013–December 2016). The observed pattern of standstills and outbursts can be clearly seen as well as brief excursions to quiescence. Black dots are Johnson V.

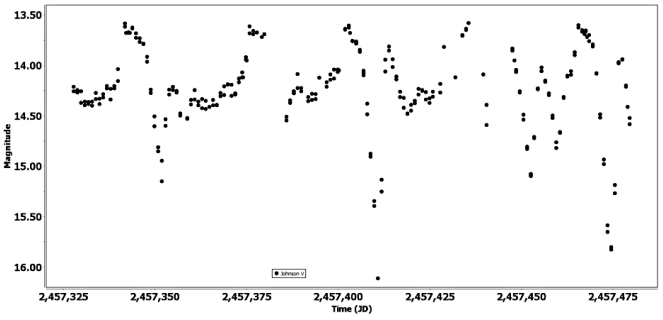

Figure 2. The AAVSO light curve of ST Cha, JD 2456500–2457000 (July 2013–December 2014), featuring standstills followed by outbursts and brief minima. Black dots are Johnson V.

UY Pup has shown numerous shared features in its light curve with anomalous Z Cam stars, in particular ST Cha. The commonalities between these stars and UY Pup include frequent outbursts, followed by a number of short duration standstills for an extended period of time, brief excursions to quiescence, and standstills starting from quiescence.

2. History

A spectroscopic study of UY Pup in outburst showed it to be a low inclination dwarf nova with an estimated orbital period of 10.20 hours (Lockley *et al.* 1999). John R. Thorstensen *et al.* (2004) found a more accurate period of 11.50 hours. Bateson (1991) analyzed the first 90 outbursts of UY Pup and found the mean cycle to be ~34.93 days. Long and short outbursts occurred, with the long outbursts being more frequent and both types of outbursts showing little difference in the mean brightness (Bateson 1991). There was no mention of UY Pup as a possible Z Cam star from the data collected by Bateson. UY Pup was measured in outburst at V = 14.1 with B–V = 0.09 and U–B = –0.78 (Bruch and Engel 1994), who classified UY Pup as a possible Z Cam type star.

3. Observations

UY Pup has an observing window from October through June and consequently has large gaps in the recorded observations. UY Pup has been monitored by the Royal Astronomical Society of New Zealand (RASNZ) and the AAVSO in which the brightness varies from magnitude ~13.0 V in outburst to ~16.1 V in quiescence. Furthermore, UY Pup has been monitored continually by one of the authors of this paper (RS) from the year 1995 to present. The outburst and quiescence pattern had become familiar over this time frame, especially in the later years due to closer monitoring. To determine the mean cycle of UY Pup during this period, consecutive outbursts with intervals of less than 60 days were selected. The conclusion from this analysis was that there were 67 outbursts which were considered consecutive and led to a mean cycle of ~31.86 days.

The increased monitoring of UY Pup on its rise and decline detected an interesting result that revealed that some of the short outbursts were in fact part of the long outbursts. The first evidence of this was noticed in December 2015 around JD 2457365 when UY Pup was near minimum at a visual magnitude of 15.6 (Figure 3). Five days later it rose to 14.4 and varied by ~0.2 magnitude for 11 days, then went into outburst on JD 2467386, reaching a visual magnitude of 13.8. The fall from this outburst lasted about 7 days, and then UY Pup stalled near magnitude 14.5 for 2 weeks, before going back into outburst on JD 2457417, where it attained a visual magnitude of 13.7. UY Pup declined from this outburst for about 4 days before stalling once again near visual magnitude 14.5 for a further 30 days, and then fading to quiescence and varying in magnitude between ~15.6 and ~15.9 in V.

This small standstill started on JD 2457370 and lasted for around 66 days; two outbursts were observed in this time frame. After the brief excursion to quiescence at ~15.9 V

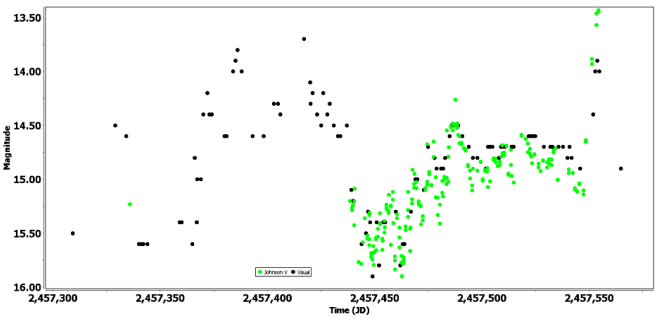

Figure 3. AAVSO light curve showing the first well-defined standstill of UY Pup, JD 2457474–2457545 (March 26, 2016–June 5, 2016), and lasting 71 days before going in outburst. Black dots are visual data, green dots are Johnson V.

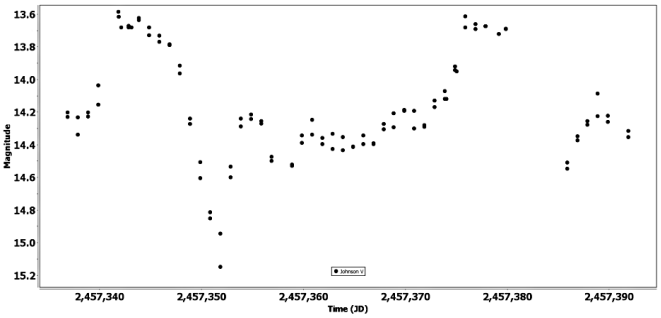

Figure 4. AAVSO light curve of ST Cha, JD 2457336–2457392 (November 2015–January 2016), showing a standstill starting from the quiescent state. Black dots are Johnson V.

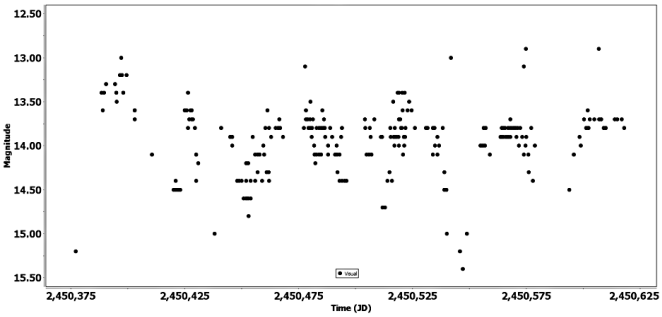

Figure 5. Hidden in the long-term AAVSO light curve, the almost continuous standstill of UY Pup followed by outbursts can be seen. Beginning on JD 2450389 (October 1996) the system shows a pattern of standstills in the mid-range of ~13.7 to ~14.3 and outbursts lasting for 228 days to June 1997 (JD 2450617). Black dots are visual data.

UY Pup started to slowly rise to a longer and well-defined standstill, evolving from the quiescent state on JD 2457474 and continuing for about 71 days. The magnitude varied ~0.5 during this period before going into an outburst at V = 13.4 (Figure 3).

A comparative analysis of the light curve of ST Cha from JD 2457336 to 2457392 was undertaken, in which showed a very similar light curve. Furthermore, the anomalous features in light curves of both UY Pup and ST Cha are also evident in the standstills that have emerged from quiescence in ST Cha (Figure 4).

Outbursts from standstills are quite rare in Z Cam stars, so it was decided that previous data on UY Pup should be examined. As a result of further research another well-defined anomalous standstill in October 1996 (starting on JD 2450389) was found (Figure 5). The total duration of this standstill was around 228 days and included two brief fades. The visual magnitudes of

the fades observed were 15.0 and 15.4, which lasted a few days before going straight back into outburst on each occasion. In this time frame, UY Pup went into outburst five times from standstills in the low to mid 14th magnitude range.

4. Conclusion

UY Pup has been subject to more thorough monitoring since 1995 and as a result several features and new findings that are atypical behaviors in this particular star have been highlighted. It is now evident that part of the long outbursts are associated with the short outbursts and on some occasions the short outbursts fail to decline to quiescence and enter into small standstills.

UY Pup shows definite signs of being one of the anomalous Z Cams stars like IW And, V513 Cas, and ST Cha. Standstills occur on the decline from outburst as seen in typical Z Cam systems, as well as brief fades to quiescence. The data also show that standstills can occur in the rising branch from the quiescent state and the emergence of outbursts following these standstills, as seen the light curve of ST Cha in Figure 2. UY Pup has one of the longest orbital periods for a Z Cam star at 11.5 hours, which makes it an interesting object for further study.

Past observations have presumed that all typical Z Cam standstills were terminated by the decline to quiescence. Since the introduction of the Z CamPaign and closer monitoring of these systems it is evident that some Z Cam stars have more complex behaviors in their light curves. In addition to the outbursts from standstills the light curves show brief fades to quiescence and standstills starting from the quiescent state. As a result of the research and data it has been concluded that there are now four anomalous Z Cam stars: IW And, V513 Cas, ST Cha, and UY Pup.

5. Acknowledgements

We acknowledge with thanks the variable star observations from the AAVSO International Database (Kafka 2016) contributed by observers worldwide and used in this research. This research has made use of the International Variable Star Index (VSX) database (Watson *et al.* 2015), operated at AAVSO, Cambridge, Massachusetts, USA. We would also like to thank the anonymous referee whose comments and suggestions were helpful.

References

Bateson, F. M. 1991, *Publ. Var. Star Sect. Roy. Astron. Soc. New Zealand*, **16**, 80.

Bruch, A., and Engel, A. 1994, *Astron. Astrophys., Suppl. Ser.*, **104**, 79.

Hameury, J. M., and Lasota, J. P. 2014, *Astron. Astrophys.*, **569**, A48.

Kafka, S. 2016, variable star observations from the AAVSO International Database (https://www.aavso.org/aavso-international-database).

Lockley, J. J., Wood, J. H., Jones, D. H. P., and Mineshige, S. 1999, *Astrophys. Space Sci.*, **266**, 453.

Simonsen, M. 2009, The Z Cam List (https://sites.google.com/site/thezcamlist/the-list).

Simonsen, M. 2010, in *The Society for Astronomical Sciences 29th Annual Symposium on Telescope Science*, Society for Astronomical Sciences, Rancho Cucamonga, CA, 87.

Simonsen, M. 2011, *J. Amer. Assoc. Var. Star Obs.*, **39**, 66.

Simonsen, M. 2014, in *The Society for Astronomical Sciences 33rd Annual Symposium on Telescope Science*, Society for Astronomical Sciences, Rancho Cucamonga, CA, 143.

Simonsen, M., Bohlsen, T., Hambsch, J., and Stubbings, R. 2014, *J. Amer. Assoc. Var. Star Obs.*, **42**, 199.

Simonsen, M., *et al*. 2014, *J. Amer. Assoc. Var. Star Obs.*, **42**, 177.

Stubbings, R., and Simonsen, M. 2014, *J. Amer. Assoc. Var. Star Obs.*, **42**, 204.

Szkody, P., *et al.* 2013, *Publ. Astron. Soc. Pacific*, **125**, 1421.

Thorstensen, J. R., Fenton, W. H., and Taylor, C. J. 2004, *Publ. Astron. Soc. Pacific*, **116**, 300.

Warner, B. 1995, *Cataclysmic Variable Stars*, Cambridge Univ. Press., Cambridge.

Watson, C., Henden, A. A., and Price, C. A. 2015, AAVSO International Variable Star Index VSX (Watson+, 2006–2015; http://www.aavso.org/vsx).

Discovery and Photometric Analysis of the δ Scuti Variable TYC 2168-132-1

Michael D. Joner
Eric G. Hintz
Department of Physics and Astronomy, Brigham Young University, N283 ESC, Provo, UT 84602; joner@byu.edu; hintz@byu.edu

Giorgio Corfini
Società Astronomica Lunae, Via Montefrancio, 77-1, Castelnuovo Magra, I-19030, Italy

Received August 23, 2016; revised November 7, 2016; accepted November 15, 2016

Abstract We detail the discovery of the short-period variable star presently known as TYC 2168-132-1. We have examined four nights of photometric observations of this star secured in 2015 and find it to be a δ Scuti variable with a primary period of 0.0737523 day. The star is multiperiodic with three dominant frequencies at 13.556, 7.047, and 11.757 cycles/day. Evidence from light curve morphology supports the δ Scuti classification. We estimate intrinsic values for color and luminosity that place TYC 2168-132-1 within the lower part of the instability strip.

1. Introduction

The Kilodegree Extremely Little Telescope (KELT) project (Pepper *et al.* 2007) is designed to find planetary transits of bright stars. During the KELT survey process, many variable objects are found and likely transit candidates are assigned an identifier and priority for follow-up observations. Of course, many variable objects are found in the survey that are not transit candidates. With the transit candidates, it is not uncommon for follow-up observers to find additional faint variable stars in the fields that are examined. These variable stars are generally found either during an examination of stars close to the KELT candidate in order to rule out a false positive from a blended source, or while selecting stars to serve as primary comparison sources within a field. In the case of TYC 2168-132-1, variation was detected during the observation of a KELT planetary transit candidate in survey Field 11 while selecting comparison stars. Giorgio Corfini (died December 2014) reported to the KELT Follow-Up Network (KFUN) on 7 August 2014 that he found variability in an object marked T10 on his finder image. He noted that he had checked the International Variable Star Index (VSX; Watson *et al.* 2014) maintained by the American Association of Variable Star Observers and did not find this star listed as a variable. Shortly after this report, it was realized that TYC 2168-132-1 had been noticed in the KELT survey but did not pass through the selection process for identification as a transit candidate. The newly reported depth estimate was promising enough that a decision was made to take another look at this target, which was then designated as KC11C050626 and assigned a rather low priority for follow-up observations.

There were two sets of data submitted for this target within a couple of days that clearly showed that the predicted planetary transit was unlikely. In one case, the observations were for a period of time that was shorter than the suspected transit window and the resulting light curve was reported as a saw tooth plot. In the other case, the shape of the light curve was such that the event was reported to be a deeper eclipse with a curious step just after the predicted egress. On UT 2014 August 16, the target was observed with the Brigham Young University West Mountain Observatory (WMO) 0.9-meter telescope for about four hours in the R filter. It was noted in the follow-up report to the KFUN that the resulting light curve appeared to be low amplitude pulsations from a multiperiodic δ Scuti variable star. These data are displayed in Figure 1.

After these observations the target was considered expired, but it remained on the candidate list at the lowest priority level until 21 September 2015 when the BVI data set given later in this paper was reported to the KFUN. The star was expired from the transit candidate list as the new BVI light curve varied amplitude with color, as would be expected from a δ Scuti variable star. At this point, it was absolutely certain that the observed variability was not due to a transit.

2. Observations

2.1. New observations

The new BVRI photometric data reported in this investigation were secured at WMO with the 0.9-meter telescope. The detector used for these observations is a Fairchild 3041-UV CCD mounted in a FLI ProLine camera. The CCD is a 2048 × 2048 array with 15-micron pixels. The plate scale

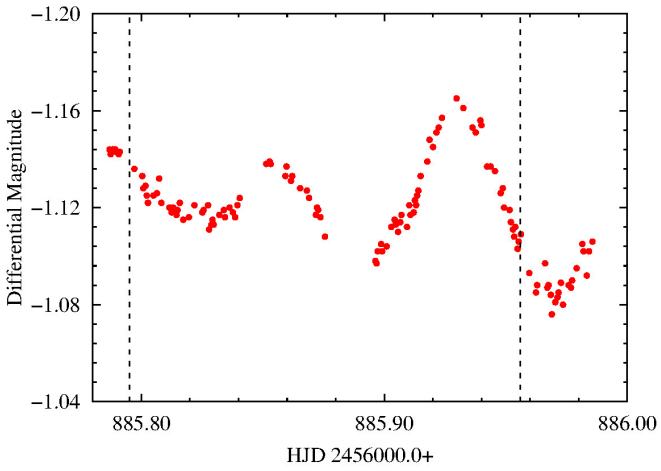

Figure 1. Light curve for TCY 2168-132-1 on UT 2014 August 16 that clearly showed that the observed variability was not due to a suspected planetary transit. The predicted times of ingress and egress for the previously suspected transit are shown as vertical dashed lines.

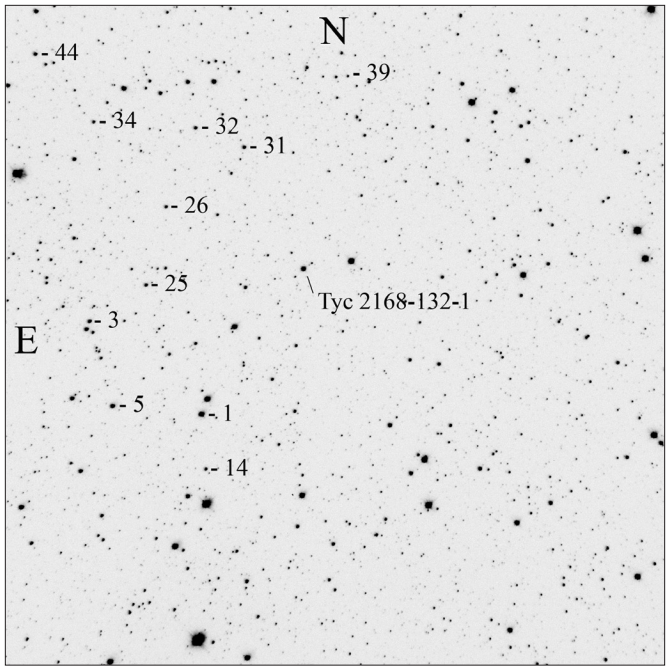

Figure 2. Finder chart for TYC 2168-132-1 from the 0.9-meter telescope at WMO. The field of view is a square 20.5'. Comparison stars and suspected longer period variable stars are marked as described in the text.

at the f/5.5 Cassegrain focus is 0.61"/pixel. During final processing, the frames are trimmed to 2000 × 2000 pixels, giving a square field of view that is 20.5' on a side. Standard BVRI Johnson/Cousins filters from Astrodon Photometrics were used for all observations. Each of the raw images was processed using standard IRAF routines to make overscan, trim, zero, dark, and flat field corrections before doing any analysis of the image data.

The WMO time series data for TYC 2168-132-1 was first obtained in the R filter on UT 2014 August 16. Four additional nights of observations were made between 2015 September 21 and October 14 in B, V, R, and I filters. A frame of the field examined is shown in Figure 2 with the primary target, a number of suspected variable stars with longer periods, comparison stars, and check stars marked. This field is 20.5' square and was taken using a standard V filter. Photometric values were determined using comparison stars 1, 3, 14, 26, 31, and 32. Along with these comparison stars, we also used stars 5 and 25 as check stars. In addition to the variations seen in our target star, we found that stars 34, 39, and 44 showed longer term variability of 0.05 magnitude or greater and are possibly eclipsing binaries with periods of several days to a week or more.

All the check and comparison stars had errors per observation of 0.011 or less in the combined four-night solution in V. A few of the reference stars had values listed in APASS (Henden *et al.* 2015), and these stars were used to establish a zero point for the B and V differential light curves. Multiple solutions were done in VPHOT using the comparison and check star sample given above. An iterative approach was used to improve the magnitude values in each filter for each star until the solutions converged to the final values used in the analysis.

2.2. Archive data

A search of the NASA/IPAC archive shows data for TYC

Table 1. Archive photometric measurements of TYC 2168-132-1. Magnitudes and Fv.

Filter	*TYC 2168-132-1 mag.*	*TYC 2168-132-1 mJy.*
B	12.418 ± 0.027	46.0
V	11.921 ± 0.019	65.4
J	10.760 ± 0.019	79.2
H	10.520 ± 0.020	63.4
K	10.432 ± 0.016	44.8
W1	10.366 ± 0.023	21.6
W2	10.389 ± 0.020	12.0
W3	10.470 ± 0.100	2.1
W4	9.130 ± 0.463	1.9

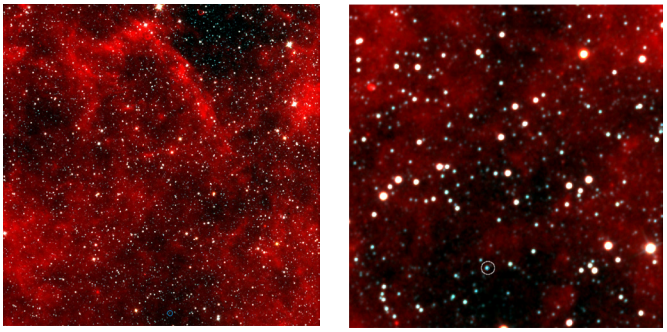

Figure 3. WISE Multi-Color Image from all four filters. The left image shows the full field which includes TYC 1268-132-1. A circle near the bottom of the frame marks the target. The right image is a 20' region zoomed in around the target.

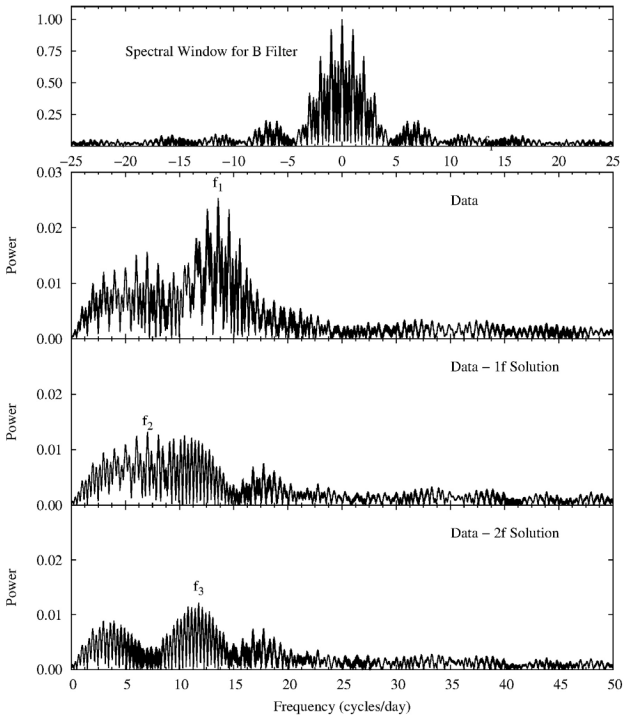

Figure 4. The power spectrum from the B filter for the first three frequencies.

2168-132-1 from the 2MASS Point Source Catalog (Skrutskie *et al.* 2006) and a number of listings from the WISE satellite mission (Wright *et al.* 2010; Mainzer *et al.* 2011). We have collected the measured magnitudes and examined a number of the published images from these sources to supplement the data used in this analysis. In Table 1 we display the average magnitude and flux for each filter. In addition, we collected individual measurements from the WISE W1 and W2 filters from the WISE All-Sky Single Exposure Source Table, the WISE Post-Cryo Single Exposure Source Table, and the NEOWISE-R Single Exposure Source Table. We were also able to examine a number of individual frames from the WISE AllWISE Release Atlas Image. This included the multicolor image shown in Figure 3 with the target marked with a circle near the bottom of the field. The field on the right is 20' on a side so that it matches the dimensions from Figure 2.

The WISE data came in four distinct observing groups; May 2010, November 2010, May 2014, and November 2014. Each group consisted of 16 or 17 observations taken over about a 1.25-day time frame, with an image secured about every two hours. This provided a total of 63 observations in the W1 and W2 filters. Clearly, these data would not be useful in the determination of times of maximum light given that the cadence is similar to the pulsation period as discussed later.

3. Analysis

3.1. Fourier decomposition

To begin our analysis, we examined the four nights of new data obtained in 2015 using PERIOD04 (Lenz and Breger 2005) to find the detectable pulsation frequencies in our target. The analysis proceeded for each of the four filters: B, V, R, and I. The B, V, and I observations are included in all four nights of new data, while the R observations were made on only the last three of those nights. For the B, V, and I nights the initial three frequencies were consistently 13.556 ± 0.001, 7.047 ± 0.002, and 11.757 ± 0.002 cycles / day. The primary frequency corresponds to a period of 0.07376 ± 0.00001 day. In Figure 4 and Figure 5 we show the spectral window and power spectrum for the first three frequencies in the B and V filters, respectively. It is interesting to note that the second and third frequencies reverse order between the two filters. For each filter we found additional frequencies that would be considered within the detection limit of Breger *et al.* (1993). However, given the lack of consistency across the four filters we have chosen to only report the first three frequencies that repeat across all four filters. The amplitudes for each frequency are gathered in Table 2, along with the S/N level for each.

We have a high level of confidence in the primary frequency detailed above. It is in excellent agreement with period determined from a times of maximum light analysis detailed below. An examination of the power spectra for the second and third frequencies doesn't make as strong a case; however, we feel that the consistency across filters argues strongly for these two additional frequencies. It is of note that the amplitude at each frequency decreases as we go from the B filter to the I filter, as would be expected for a pulsating variable such as a δ Scuti star. The data for all four nights of multi-filter photometry,

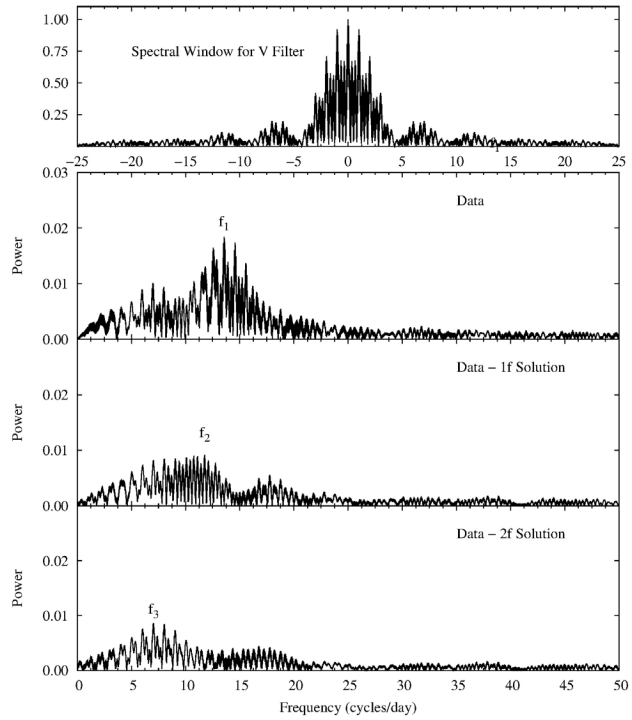

Figure 5. The power spectrum from the V filter for the first three frequencies.

Table 2. Fourier frequencies by filter.

Frequency	*B Ampl.*	*B S/N*	*V Ampl.*	*V S/N*	*R Ampl.*	*R S/N*	*I Ampl.*	*I S/N*
13.556 ± 0.001	0.025	15.8	0.019	20.7	0.012	13.2	0.011	11.9
7.047 ± 0.002	0.016	6.5	0.009	8.9	0.006	17.3	0.004	2.4
11.757 ± 0.002	0.013	8.6	0.008	10.3	0.008	9.9	0.005	4.4

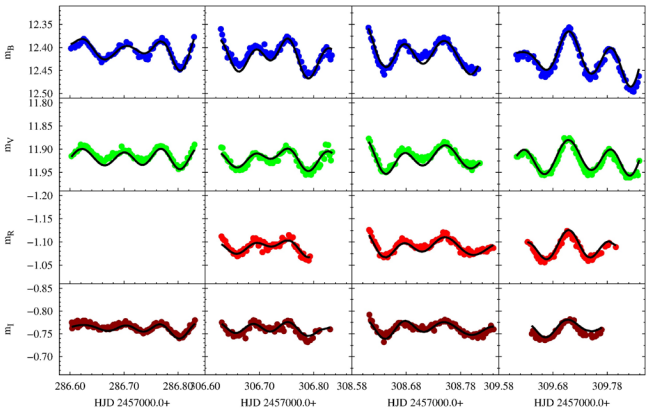

Figure 6. Four nights of multi-filter photometry along with the best Fourier fit for each filter.

along with the best Fourier fit for each filter from the frequency analysis described above, are displayed in Figure 6. We note that the two additional frequencies improve the curve that is fit to the observed data in the light curves displayed for each filter in Figure 6.

Using the Fourier fits to the B and V data, we determined a B–V curve for TYC 2168-132-1. In the upper panel of Figure 7 we show the B data and the Fourier fit to the B data for the four nights from 2015. In the lower panel of the figure we show the B–V curve from the two Fourier fits. The frequencies found,

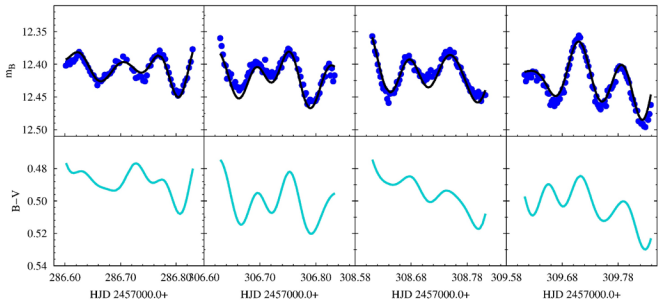

Figure 7. B–V curves from Fourier fits for TYC 2168-132-1 compared to the B-filter observations.

Table 3. Times of maximun light 2450000.0+.

Cycle Number	*B Time*	*V Time*	*R Time*	*I Time*
–5434	—	—	6885.85275	—
–5433	—	—	6885.93004	—
0	7286.62607	7286.62533	—	7286.62381
1	7286.70416	7286.70052	—	7286.69546
2	7286.76948	7286.76823	—	7286.76726
272	7306.69315	7306.69308	7306.69394	7306.69095
273	7306.75302	7306.75070	7306.75494	7306.75332
299	7308.67316	7308.67306	7308.67425	7308.67000
300	7308.74799	7308.74879	7308.75103	7308.75053
313	7309.70924	7309.70818	7309.70857	7309.70873
314	7309.78528	7309.78345	—	—

and the shape of the B–V curve, lead us to the conclusion that this star is a pulsating variable of the δ Scuti type.

Finally, we examined the data from the WISE satellite for TYC 2168-132-1. The reported error per observation for the various WISE data sets is on the order of 0.02 magnitude, which makes it unlikely that we would see the variations in such a low amplitude variable star. However, we gathered the data from the WISE All-sky Single Exposure Source Table and the NEOWISE-R Single Exposure data tables. The data from the Post-Cryo series were found to have larger errors and were not included in this analysis. In the WISE database the times of observation were given as Modified Julian Days (MJD). To match our other observations we converted those MJD values to Heliocentric Julian Days (HJD). Again, we used PERIOD04 to examine the WISE data. Given the poor spectral window from the sparse data we used the frequency at 13.556 cycles / day to phase the data and estimate the amplitude. For both the W1 and W2 filters the error on the amplitude is comparable to the amplitude, but is clearly less than 0.01.

This is reasonable when compared with the decreasing amplitudes with wavelength we reported earlier for the BVRI filters.

3.2. Times of maximum light

The next stage of our analysis was to examine the times of maximum light. To do this we used the PERANSO software (Paunzen and Vanmunster 2016) in order to apply two different methods to each maximum in our data set. We first used the Kwee and van Woerden (1956) method within PERANSO. We then applied a polynomial fit to each maximum to get a second estimate of each time of maximum light. For the B and V filters we found nine times of maximum light from the four nights of data. For the I filter we found eight times of maximum light, missing the last time on the last night. The determination of times of maximum light was most difficult for the R filter, where we have five times of maximum light that correspond to the nights that were also observed in B, V, and I. In addition, there are two additional times of maximum light from the 2014 R light curve. We report these times of maximum light in Table 3, where the reported time is the average of the two methods discussed above. In most cases, both methods provided reasonable estimates of the time of maximum light with only small differences.

To provide the longest range in time, we averaged the observed times of maximum light over the four filters. Using the period determined from the Fourier fits, we determined the cycle number of each observation. Fitting a linear regression to this set of data, we find an ephemeris as given in Equation 1.

$$HJD = 2457286.6242(9) + 0.0737523(4)E \quad (1)$$

Using this ephemeris, we determined O–C values for each average time of maximum light. The resulting values scatter evenly about a zero line. The period determined here closely matches the period associated with the f1 value from the Fourier fits. The O–C curve is shown in Figure 8. With such a short baseline, it is not surprising that the resulting curve is flat. We also note that there is a fairly wide range in values of O–C for a given epoch. We believe this is expected for a strongly modulated light curve in a multiperiodic star like TYC 2168-132-1.

3.3. Reddening and B–V color

As detailed in the observing section, our B filter and V filter observations were calibrated with nearby comparison stars. We measure B–V for the variable star in the range of 0.48 to 0.53. Even though it is slightly beyond the red edge of the instability strip, that range is reasonable to expect for a lightly reddened δ Scuti star in the instability strip close to the main sequence. Furthermore, from the image shown in Figure 3 it is clear from the visible material that our target could be significantly reddened. This is not surprising given the galactic coordinates for longitude and latitude of TYC 2168-132-1 of 68.772° and −5.13°, respectively. Using the maps of Schlafly and Finkbeiner (2011) we find an E(B–V) of 0.645 in the direction of our target. This reddening would be the maximum reddening that our star could experience. The actual reddening for a nearby star would likely be significantly less, but this upper limit is clearly sufficient to show the plausibility of the values estimated in the next section.

Given that δ Scuti variables normally lie in the spectral type range from about A5 to F5, we can estimate an approximate reddening range for our target. To keep the star within the instability strip, the E(B–V) needs to be in the range of 0.08 to 0.32. Using these E(B–V) values, we determined absorption values for each of our filters based on the methods detailed in Schlafly and Finkbeiner (2011). Using these values, we deredden our data and the archival data to generate SEDs for our object, which are shown in Figure 9. The lowest curve in Figure 9 is the observed curve with no reddening correction

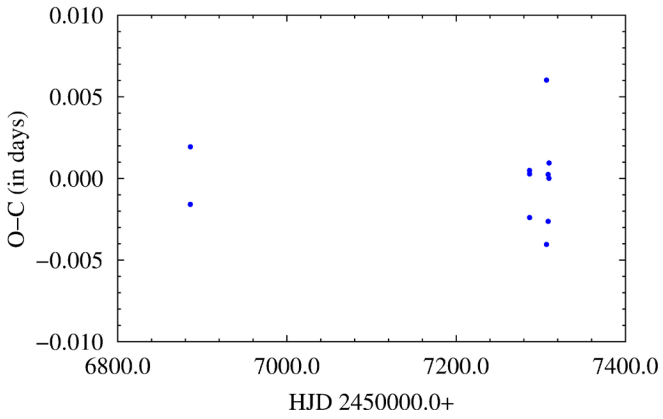

Figure 8. O–C diagram for TYC 2168-132-1.

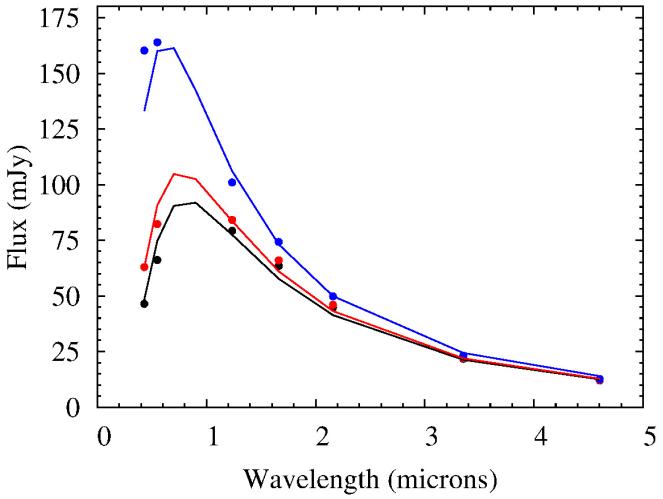

Figure 9. The spectral energy distribution plots for TYC 2168-132-1. Observed curve shown in black (bottom), the curve with a reddening correction for the red edge of instability strip shown in red (middle), and the curve with a reddening adjustment for the blue edge of the instability strip shown in blue (top).

applied. The middle curve was generated using values from Schlafly and Finkbeiner (2011) for E(B–V) = 0.08, for a star at the red edge of the instability strip. Finally, the top curve in Figure 9 is the curve based on values for E(B–V) = 0.32, corresponding to a star at the blue edge of the instability strip. Starting with the (B–V) for each curve, we used the relations in Flower (1996) and Torres (2010) to estimate the temperature for each SED. We then used a scaled Planck function to fit a blackbody curve to each data set. The blackbody fits are overlaid on the corresponding SED in Figure 9.

The scale factor used to bring the observed values in line with blackbody values is 5.7×10^{-21}. The square root of this value is the ratio of the radius of the target to the distance to the target. Therefore, we find a value of $r/R = 7.5 \times 10^{-11}$. Since the previous evidence presented in this paper points to this object being a δ Scuti variable, we can estimate the radius of our object. Given a target inside the instability strip, in the luminosity class range of IV–V, we calculate a radius of about 2.3 $R_\odot$. This estimate leads to a distance of approximately 700 parsecs.

4. Conclusion

We have summarized the discovery of variability for the former KELT target star TYC 2168-132-1. We present and analyze new data for the recently discovered variable star. Analysis of the data is done and provides evidence in support of the δ Scuti hypothesis. We show that the observed variations can be fit using Fourier decomposition techniques. The star is found to be periodic with three dominant frequencies at 13.556, 7.047, and 11.757 cycles / day. The results are similar to other pulsating variables in the δ Scuti class with the new data showing a primary period of 0.0737523 day. Evidence from light curve morphology also supports the suggested δ Scuti classification. We estimate intrinsic values for color and luminosity that place TYC 2168-132-1 within the lower region of the instability strip. With an estimated radius of 2.3 $R_\odot$ we find a distance of about 700 parsecs.

5. Acknowledgements

We thank Joao Gregorio and Eric L. N. Jensen for initial observations of KC11C050626 in the KELT Follow-up Network that helped first confirm the variable nature of this star. We thank all the KELT team members for their efforts in organizing and managing a project of this complexity. We also thank Roberto Zambelli and Josh Pepper for comments and direction given during the early stages of writing this paper. We acknowledge the Brigham Young University Department of Physics and Astronomy for its continued support of our research efforts. This research has made use of the APASS database, located at the AAVSO web site. Funding for APASS has been provided by the Robert Martin Ayers Sciences Fund. This publication makes use of data products from the Wide-field Infrared Survey Explorer, which is a joint project of the University of California, Los Angeles, and the Jet Propulsion Laboratory/California Institute of Technology, funded by the National Aeronautics and Space Administration. This publication also makes use of data products from NEOWISE, which is a project of the Jet Propulsion Laboratory / California Institute of Technology, funded by the Planetary Science Division of the National Aeronautics and Space Administration. This publication makes use of data products from the Two Micron All Sky Survey, which is a joint project of the University of Massachusetts and the Infrared Processing and Analysis Center / California Institute of Technology, funded by the National Aeronautics and Space Administration and the National Science Foundation.

Facility: BYU:0.9m, WISE, FLWO:2MASS, AAVSO
Software: IRAF, VPHOT, ASTROIMAGEJ

References

Breger, M., *et al.* 1993, *Astron. Astrophys.*, **271**, 482.
Flower, P. J. 1996, *Astrophys. J.*, **469**, 355.
Henden, A. A., *et al.* 2015, AAVSO Photometric All-Sky Survey, data release 9 (http://www.aavso.org/apass).
Kwee, K., and van Woerden, H. 1956, *Bull. Astron. Inst. Netherlands*, **12**, 327.
Lenz, P., and Breger, M. 2005, *Commun. Asteroseismology*, **146**, 53.
Mainzer, A., *et al.* 2011, *Astrophys. J.*, **731**, 53.

Paunzen, E., and Vanmunster, T. 2016, *Astron. Nachr.*, **337**, 239.
Pepper, J., *et al.* 2007, *Publ. Astron. Soc. Pacific*, **119**, 923.
Schlafly, E. F., and Finkbeiner, D. P. 2011, *Astrophys. J.*, **737**, 103.
Skrutskie, M. F., *et al.* 2006, *Astron. J.*, **131**, 1163.
Torres, G. 2010, *Astron. J.*, **140**, 1158,
Watson, C., Henden, A. A., and Price, C. A. 2014, AAVSO International Variable Star Index VSX (Watson+, 2006–2014; http://www.aavso.org/vsx).
Wright, E. L., *et al.* 2010, *Astron. J.*, **140**, 1868.

A Photometric Study of the Eclipsing Binary Star PY Boötis

Edward J. Michaels
Stephen F. Austin State University, Department of Physics and Astronomy, P.O. Box 13044, Nacogdoches, TX 75962; emichaels@sfasu.edu

Received August 27, 2016; revised October 3, 2016; accepted October 3, 2016

Abstract Presented here are the first precision multi-band CCD photometry of the eclipsing binary star PY Boötis. Best-fit stellar models were determined by analyzing the light curves with the Wilson-Devinney program. Asymmetries in the light curves were interpreted as resulting from magnetic activity which required spots to be included in the model. The resulting model is consistent with a W-type contact eclipsing binary having total eclipses.

1. Introduction

PY Boötis (GSC 3488-0585) was first identified as a contact binary from the sky patrol data taken by the ROTSE-I telescope (Gettel *et al.* 2006). The orbital period was given as 0.278045 day, a maximum and minimum visual magnitude of 12.09 and 12.67, and an estimated distance of 182 pc. This star was also identified by Hoffman *et al.* (2009) in the Northern Sky Variability Survey (NSVS; Wozniak *et al.* 2004). The Large Sky Area Multi-Object Fiber Spectroscopic Telescope (LAMOST) survey gives a spectral type of K3, a metallicity of [Fe/H] = –0.185, a heliocentric radial velocity of V_r = –68.81 km/sec, and surface gravity of log g = 4.1351 (cgs) (Luo *et al.* 2015). Several observers have reported times of minima for primary and secondary eclipses (see section 3).

In this paper, the first photometric study of PY Boo is presented. The paper is organized as follows. The observations and data reduction methods are presented in section 2. New times of minima and period analysis are presented in section 3. Analysis of the light curves using Binary Maker 3.0 (BM3; Bradstreet and Steelman 2002) and the Wilson-Devinney (WD; 1971) model is presented in section 4. Discussion of the results and conclusions are presented in section 5.

2. Observations

Photometric data for PY Boo were acquired with the 0.31-m Ritchey-Chretien robotic telescope at the Waffelow Creek Observatory (http://obs.ejmj.net/index.php). The imaging camera was a SBIG-STXL model equipped with a cooled KAF-6303E CCD (–30°C). Images were acquired on the following nights in 2016: March 13, 14, and 28, April 2, 3, 4, and 6. A total of 1,736 filtered images were taken in three Sloan passbands, 395 in g', 816 in r', and 525 in i'. This set of images was used in the light curve analysis of section 4. Additional images were acquired on April 21, 25, and 29, May 1, 3, and 31, June 3, 4,

Table 1. Stars used in this study.

Star	*R.A. (2000) h m s*	*Dec. (2000) ° ′ ″*	*g′*	*r′*	*i′*	*B–V*
PY Boo	15 28 22	+51 32 22				
GSC 3488-0933 (C1)	15 27 43	+51 22 51	11.756 ± 0.100	11.098 ± 0.073	10.838 ± 0.105	0.885 ± 0.108
GSC 3488-0648 (C2)	15 29 15	+51 30 27	12.212 ± 0.062	11.425 ± 0.040	11.047 ± 0.056	1.062 ± 0.072
GSC 3488-0033 (C3)	15 29 29	+51 41 59	12.894 ± 0.057	12.214 ± 0.045	11.889 ± 0.059	0.956 ± 0.059
GSC 3488-0559 (C4)	15 29 08	+51 33 27	13.346 ± 0.061	12.583 ± 0.040	12.194 ± 0.057	1.016 ± 0.075
GSC 3488-0473 (C5)	15 28 14	+51 36 30	13.512 ± 0.117	12.896 ± 0.073	12.618 ± 0.099	0.842 ± 0.111
GSC 3488-0014 (K)	15 28 10	+51 40 31	12.195 ± 0.103	11.761 ± 0.039	11.610 ± 0.080	0.664 ± 0.078
Observed check star magnitudes (K)			12.136 ± 0.037	11.753 ± 0.025	11.597 ± 0.035	
Standard Deviation of check star magnitudes (K)			± 0.006	± 0.005	± 0.006	

APASS comparison stars (C1–C5) and check (K) star magnitudes.

Table 2. Available times of minima and O–C residuals from Equation (2).

Epoch HJD 2400000+	*Error*	*Cycle*	*O–C Linear*	*References*
56029.86060	0.00050	0.0	0.00000	Diethelm 2012
56060.44490	0.00020	110.0	–0.00109	Hübscher 2013a
56400.49990	0.00480	1333.0	–0.00002	Hübscher 2013b
56407.45179	0.00006	1358.0	0.00065	Hoňková *et al.* 2014
56745.55690	0.00140	2574.0	–0.00183	Hübscher 2015a
57066.70370	0.00010	3729.0	–0.00162	Hübscher 2015b
57123.42540	0.00010	3933.0	–0.00192	Hübscher 2016
57134.82516	0.00003	3974.0	–0.00217	this paper
57142.88823	0.00006	4003.0	–0.00252	this paper
57146.78135	0.00006	4017.0	–0.00208	this paper
57174.86354	0.00007	4118.0	–0.00284	this paper
57179.86843	0.00003	4136.0	–0.00283	this paper
57180.70279	0.00002	4139.0	–0.00262	this paper
57185.70745	0.00005	4157.0	–0.00284	this paper
57461.80761	0.00005	5150.0	–0.00534	this paper
57481.82709	0.00005	5222.0	–0.00539	this paper
57483.77344	0.00006	5229.0	–0.00538	this paper
57485.71973	0.00004	5236.0	–0.00543	this paper
57513.80272	0.00009	5337.0	–0.00539	this paper
57514.63659	0.00008	5340.0	–0.00567	this paper

5, and 6, and July 12, 13, 14, and 15 in 2015 and May 4 and 5 in 2016. These additional images were used primarily for new times of minima but also proved useful in monitoring changes in the light curves over the course of one year. All light images were calibrated with bias, dark, and flat field frames. The calibration and ensemble differential aperture photometry was accomplished using MIRA software (Mirametrics 2015). Table 1 lists the comparison and check stars used in this study with a finder chart shown in Figure 1. The instrumental magnitudes of PY Boo were converted to standard magnitudes using the comparison star magnitudes from the AAVSO Photometric All-Sky Survey (APASS; Henden *et al.* 2014). The Heliocentric Julian Date (HJD) of each observation was converted to orbital phase using an epoch of T_0 = 2457514.6366 and an orbital period of P = 0.27804651. All light curves in this paper were plotted from phase –0.6 to 0.6 with negative phase defined by φ – 1. The folded light curves of the observations are shown in Figure 2 with the r' passband check star observations shown in the bottom panel. The check star magnitudes were inspected each night and no significant variability was found. The observations in this study are accessible from the AAVSO International Database (Kafka 2015).

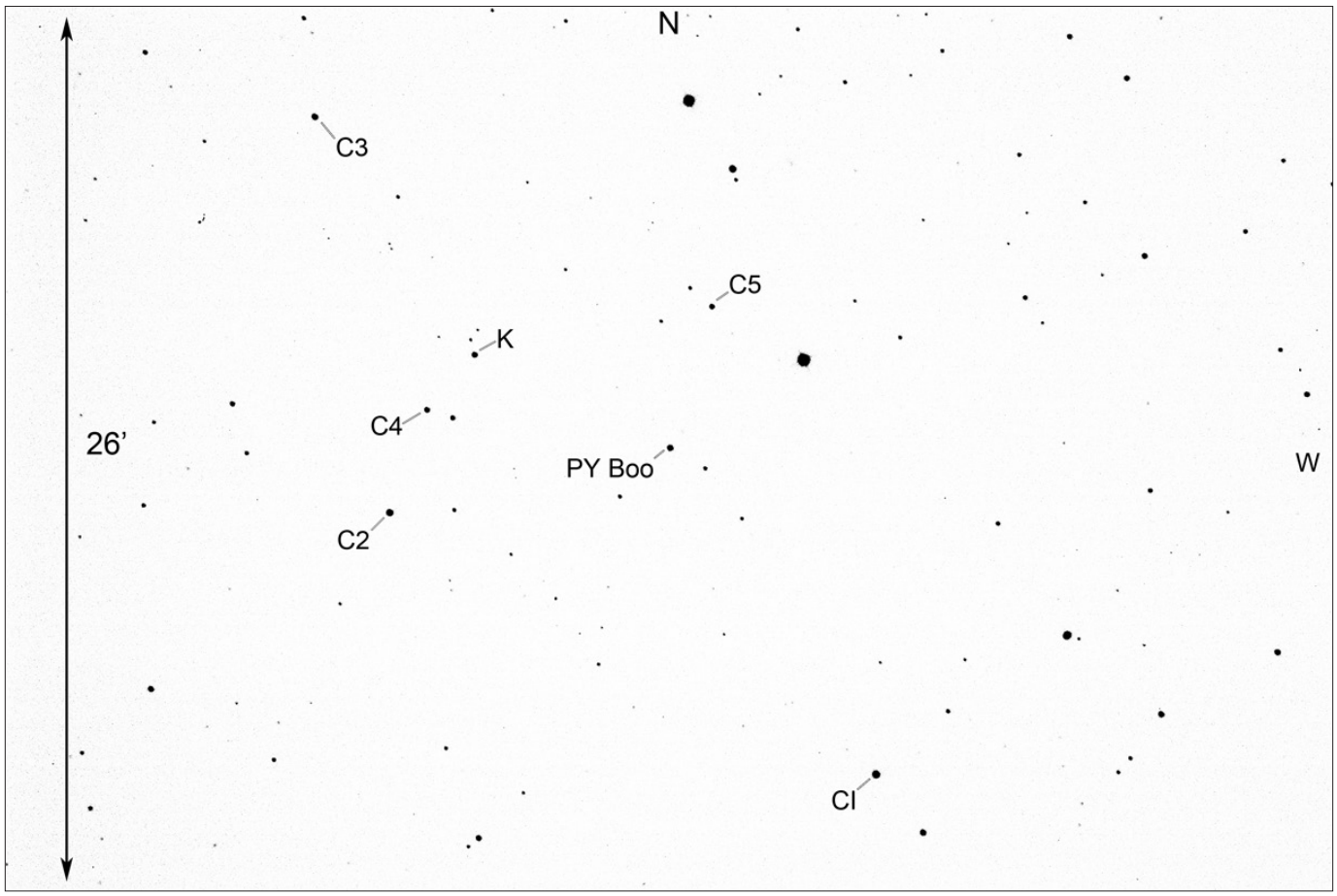

Figure 1. Finder chart for PY Boo, comparison stars (C1–C7), and the check (K) star.

3. Period study and ephemerides

From the observations the HJD for 13 new times of primary minima were determined. These new minima times along with all others found in the literature are collected in Table 2. The initial linear ephemeris for this study (Equation 1 below) contains the period from Paschke (2014) and the epoch from a primary minima reported by Deithelm (2012).

$$\text{HJD Min I} = 2456029.8606 + 0.278049\ E. \quad (1)$$

The residuals from Equation 1 were used to calculate a new linear ephemeris by least squares solution and is given by

$$\text{HJD Min I} = 2457514.6377\ (6) + 0.27804797\ (14)\ E. \quad (2)$$

The residuals from Equation 1 and the best-fit linear line of Equation 2 are shown in the Figure 3 ephemeris diagram. The general trend of the O–C residuals indicates the orbital period is continuously decreasing. A second least-squares solution of the residuals from Equation 2 yields the following quadratic ephemeris:

$$\text{HJD Min I} = 2457514.6416\ (3) + 0.27804620\ (24)\ E - 2.50\ (30) \times 10^{-9}\ E2. \quad (3)$$

Figure 4 shows the quadratic ephemeris (solid line) is an improved fit to the residuals compared to the linear solution. The rate of period change from this solution gives a value of $dP / dt = -9.13\ (1.08) \times 10^{-7}$ d yr^{-1}. Compared to other binaries of this type, this period change is quite rapid and will be discussed further in section 5.

4. Analysis

4.1. Temperature, spectral type

The effective temperature and spectral type were estimated from the observed (g'-r') color index and Jester's (2005) transformation equation,

$$(B–V) = \frac{(g' – r') + 0.23}{1.09}. \quad (4)$$

The phase and magnitude of the g' and r' observations were binned with a phase width of 0.01. The phases and magnitudes in each bin interval were averaged. The binned r' magnitudes were subtracted from the linearly interpolated g' magnitudes at primary eclipse ($\varphi = \pm 0.035$) which gives a (g' – r') value of 0.791 ± 0.018. Figure 5 shows the binned r' magnitude light curve with the bottom panel showing the (g' – r') color index. Using Equation 4 gives a (B–V) color of 0.937 ± 0.040. To correct for interstellar reddening, the Willingale *et al.* (2013) method based on the galactic column density of hydrogen was used. The galactic coordinates for this star gave a color excess of E(B–V) = 0.017 and a corrected color of (B–V) = 0.920. Using Table 5 of Pecaut and Mamajek (2013) gives an effective temperature of 4984 ± 82 K and a spectral type of K3. This

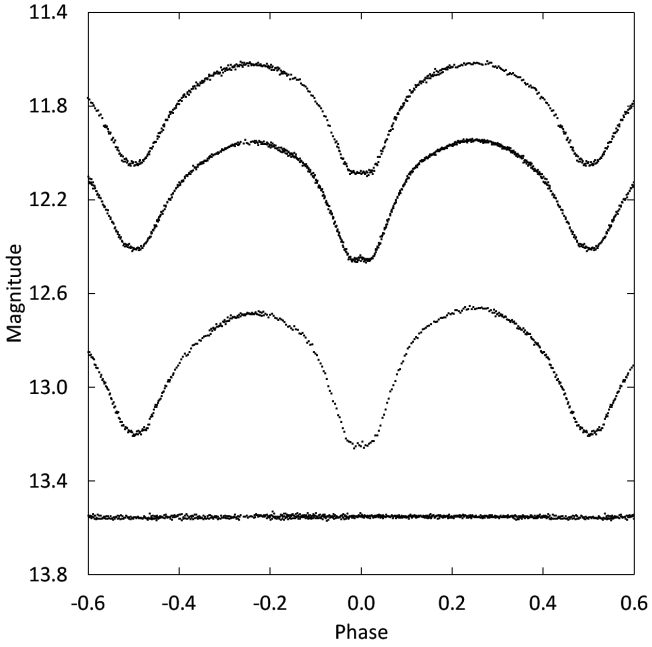

Figure 2. Folded light curves for each observed passband. The differential magnitudes of the variable were converted to standard magnitudes using the calibrated magnitudes of the comparison stars. From top to bottom the light curve passbands are Sloan i', Sloan r', Sloan g'. The bottom curve shows the Sloan r' magnitudes of the check star (offset +1.8 magnitudes). The standard deviations of check star magnitudes (all nights) are shown in Table 1. Error bars are not shown for clarity.

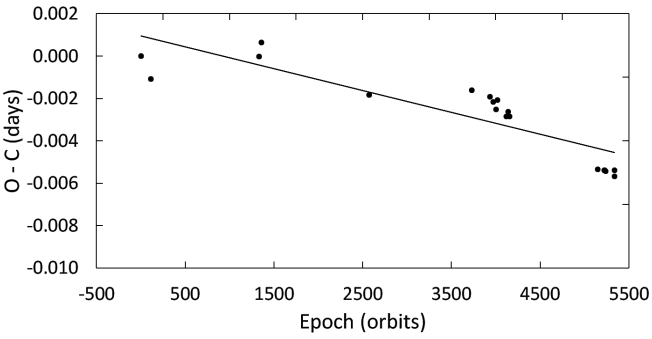

Figure 3. O–C residuals from Equation (1) with the solid line the linear ephemeris fit of Equation (2).

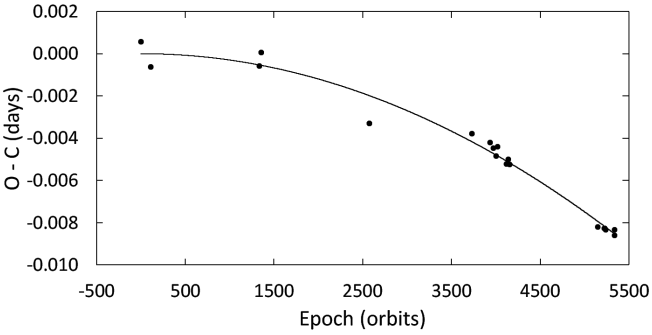

Figure 4. O–C residuals from Equation (2) with the solid line the quadratic ephemeris fit of Equation (3).

temperature was determined from the color at primary eclipse. Since the eclipse is total, only light from the larger secondary star was measured. This effective temperature will be assigned to the secondary star in the light curve analysis of section 4.2.

4.2. Synthetic light curve modeling

The Sloan g', r', and i' observations from March 13 to April 6, 2016, were used for the light curve modeling. The observations were binned in both phase and magnitude with a phase interval of 0.01. The average number of observations per bin was 6. The binned magnitudes were converted to relative flux for modeling. BINARY MAKER 3.0 (BM3) (Bradstreet and Steelman 2002) was used to make preliminary fits to each light curve. Standard convective parameters and limb darkening coefficients from Van Hamme's (1993) tabular values were utilized in the model. Obtaining a reasonably good fit required a third light contribution in all three passbands. There was also a noticeable asymmetry in the secondary eclipse of each light curve. The fit between the observed flux and the synthetic light curve showed a loss of light from phase φ = 0.51 to φ = 0.83, possibly caused by a dark spot on the secondary star. Since the initial BM3 light curve fits and the first WD solution attempt would not incorporate spots in the model, it was decided not to use observations from this phase range. With the observations for this phase range removed the synthetic BM3 light curve for each color fit well and was consistent. The resulting stellar parameter values from each light curve fit were averaged and used as the initial input parameters for computation of a simultaneous three-color light curve solution with the WD program (Wilson and Devinney 1971; Van Hamme and Wilson 1998). The light curve morphology is characteristic of a W-type eclipsing binary, therefore a common convective envelope was assumed and Mode 3 was set in the program. The weight assigned to each input data point was set to the number of observations that formed that point. To minimize strong correlations of the parameters, the Method of Multiple Subsets (MMS) (Wilson and Biermann 1976) was employed. The Kurucz stellar atmosphere model was applied and the fixed inputs included standard convective parameters: gravity darkening, $g_1 = g_2 = 0.32$ (Lucy 1968) and albedo value $A_1 = A_2 = 0.5$ (Ruciński 1969). The temperature of the cooler secondary star, T_2, was fixed at the value determined in section 4.1, 4984 K. Linear limb darkening coefficients were calculated by the program from tabulated values using the method of Van Hamme (1993). The solution's adjustable parameters include the inclination (i), mass ratio ($q = M_2 / M_1$), potential ($\Omega_1 = \Omega_2$), temperature of the primary star (T_1), the normalized flux for each wavelength (L), and third light (ℓ). The best-fit solution parameters with errors are shown in column 2 of Table 3 (Solution 1). The fill-out was computed using a modification of the parameter defined by Lucy and Wilson (1979) and is given by

$$f = \frac{(\Omega_{inner} - \Omega)}{(\Omega_{inner} - \Omega_{outer})}, \quad (5)$$

where Ω_{inner} and Ω_{outer} are the inner and outer critical equipotential surfaces that pass through the Lagrangian points L_1 and L_2

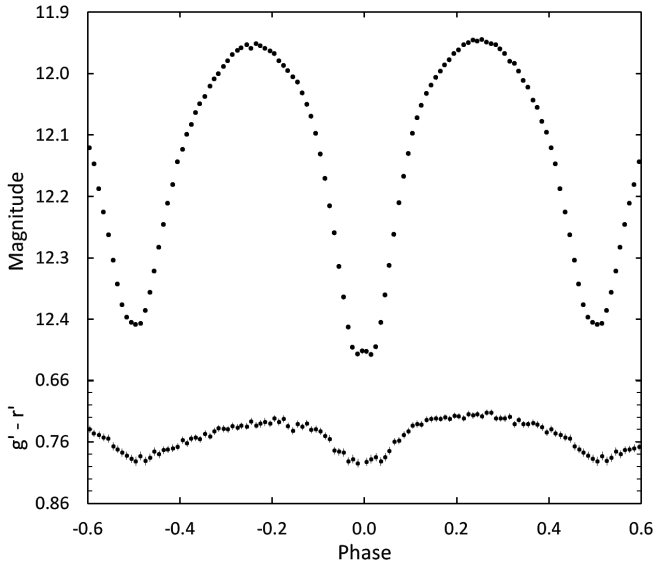

Figure 5. Light curve of all r'-band observations are in standard magnitudes (top panel). The observations were binned with a phase width of 0.01. The errors for each binned point are about the size of the plotted points. The g'–r' colors were calculated by subtracting the binned Sloan g' magnitudes from the linearly interpolated binned Sloan r' magnitudes.

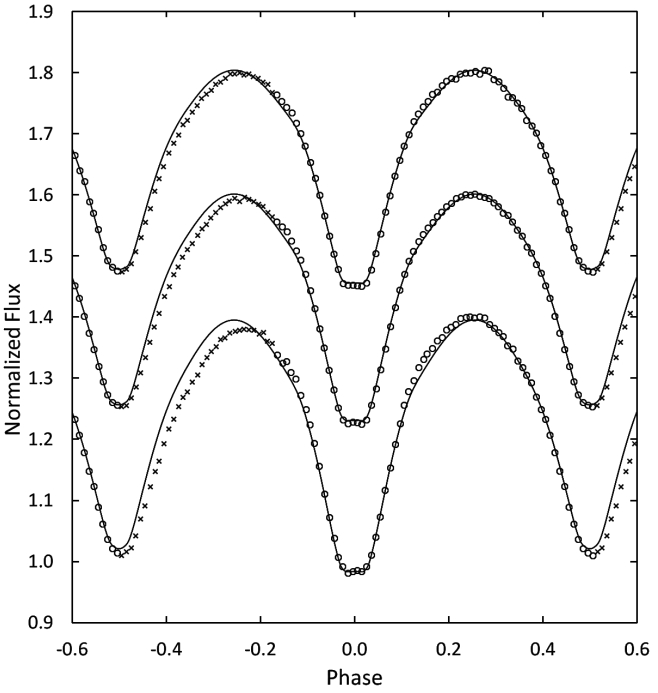

Figure 6. The WD model fit without spots (solid curve) to the observed normalized flux curves for each passband. For the data points plotted, the circles are the observations that were used in this solution and the crosses are the observations (phase 0.51–0.83) not used. From top to bottom the passbands are Sloan i', Sloan r', and Sloan g'. Each curve is offset by 0.2 for this combined plot. The best-fit parameters are given in column 2 of Table 3. Error bars are omitted from the points for clarity.

Table 3. PY Boo synthetic light curve solutions.

Parameter	*Solution 1 (no spots)*	*Solution 2 (with spots)*	*Solution 3 (g′ light curve only)*
phase shift	–0.0005 ± 0.0001	0.0000 ± 0.0001	[3] 0.0000 ± 0.0002
i (°)	89 ± 2	90 ± 3	[3] 90 ± 4
T_1 (K)	5248 ± 5	5254 ± 27	[3] 5254 ± 31
T_2 (K)	[1]4984	[1]4984	[1] 4984
$\Omega_1 = \Omega_2$	5.45 ± 0.02	5.46 ± 0.02	[3] 5.46 ± 0.02
$q(M_2 / M_1)$	2.22 ± 0.02	2.20 ± 0.01	[3] 2.20 ± 0.02
filling factor	17%	12%	[3] 12%
$L_1 / (L_1 + L_2)$ (g')	0.406 ± 0.001	0.409 ± 0.003	0.409 ± 0.002
$L_1 / (L_1 + L_2)$ (r')	0.385 ± 0.001	0.387 ± 0.002	—
$L_1 / (L_1 + L_2)$ (i')	0.376 ± 0.001	0.378 ± 0.001	—
[2]ℓ_3 (g')	0.210 ± 0.004	0.211 ± 0.010	0.210 ± 0.017
[2]ℓ_3 *(r')*	0.247 ± 0.004	0.248 ± 0.008	—
[2]ℓ_3 *(i')*	0.272 ± 0.004	0.273 ± 0.007	—
r_1 side	0.316 ± 0.001	0.311 ± 0.001	0.314 ± 0.001
r_2 side	0.436 ± 0.003	0.466 ± 0.002	0.468 ± 0.003
pot parameters		*Star 1 – Hot Spot*	*Star 1 – Hot Spot*
colatitude (°)	—	81 ± 9	85 ± 7
longitude (°)	—	0.0 ± 0.3	359.0 ± 0.6
spot radius (°)	—	15 ± 3	15 ± 3
temp.– factor	—	1.3 ± 0.1	1.3 ± 0.1
		Star 2 – Cool Spot	*Star 2 – Cool Spot*
colatitude (°)	—	62 ± 8	60 ± 11
longitude (°)	—	346 ± 3	337 ± 6
spot radius (°)	—	22 ± 6	26 ± 6
temp.– factor	—	0.89 ± 0.04	0.89 ± 0.04

[1] *Assumed.*
[2] *Third lights are the percent of light contributed at orbital phase 0.25.*
[3] *These parameters were fixed at the spotted Solution 2 values.*

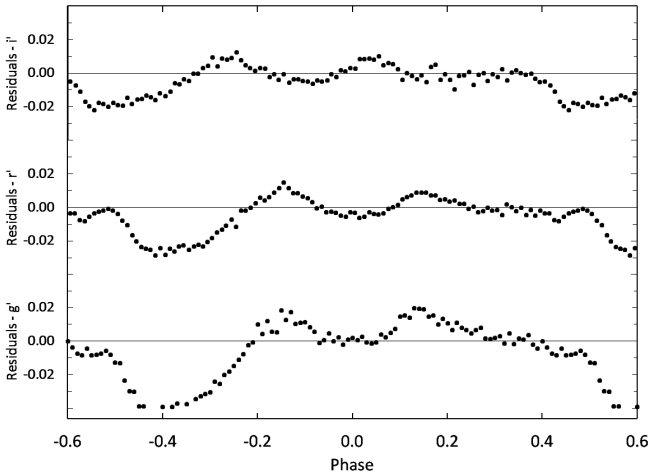

Figure 7. The residuals for the best-fit WD model without spots. Error bars are omitted from the points for clarity.

and Ω is the equipotential surface which describes the stellar surface. For this solution $\Omega_{inner} = 5.55$, $\Omega_{outer} = 4.95$, and $\Omega = 5.45$, which gives a fill-out value of f = 0.17 which indicates a contact system. The normalized light curves for each passband, overlaid by the synthetic solution curves, are shown in Figure 6 with the residuals shown in Figure 7.

4.3. Spot model

Low mass short period contact binaries are often magnetically active and therefore spotted. The asymmetries in the light curves seen in Figure 6 are most likely due to cool spots and hot regions such as faculae on the star surfaces. A new spot model was attempted but this time the entire phase range of observations was used for modeling in both BM3 and the WD program. As noted earlier, compared to the synthetic light curves, the observations show a light loss between phase φ = 0.51 and φ = 0.83 (see Figure 6). This indicates a possible under-luminous region (cool spot) on the larger secondary star. The residuals of Figure 7 also indicate excess light symmetrically located on either side of primary eclipse. The location of this excess light could be explained by an over-luminous region (hot spot) on the smaller primary star close to the line of centers between the two stars. It is important to note with an inclination close to i = 90°, the spots could be located either above or below the contact point and give essentially the same results. Two spots were therefore modeled

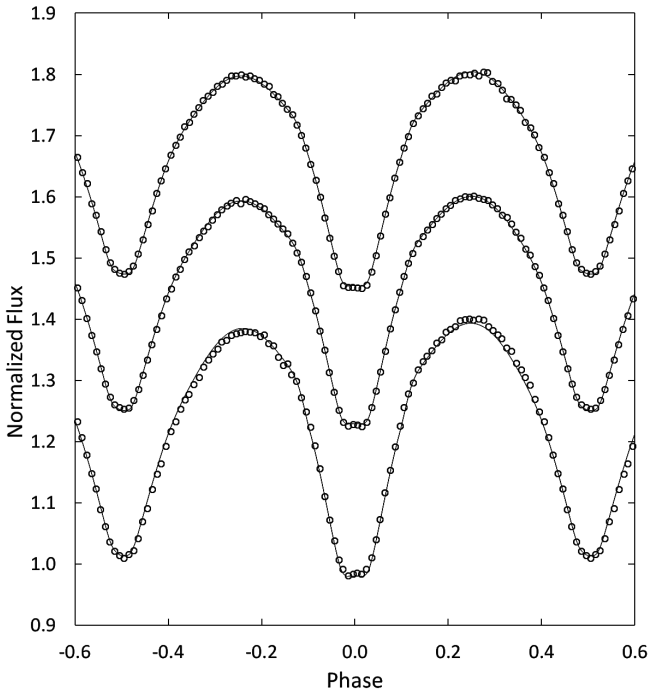

Figure 8. The WD model fit with spots (solid curve) to the observed normalized flux curves for each passband. From top to bottom the passbands are Sloan i', Sloan r', and Sloan g'. Each curve is offset by 0.2 for this combined plot. The best-fit parameters are given in column 3 of Table 3. Error bars are omitted from the points for clarity.

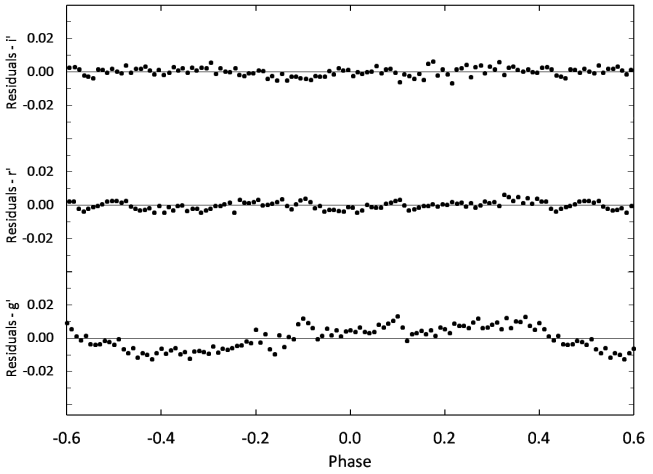

Figure 9. The residuals for the spotted WD model in each passband. Error bars are omitted from the points for clarity.

with BM3. Each spot's parameters (latitude, longitude, spot size, and temperature) were adjusted until a good fit resulted between the synthetic and observed light curves. The best-fit spot parameters from BM3 were then incorporated into a new WD solution attempt. Initially the stellar parameters were held fixed with only the light and spot parameters adjusted until the solution converged. At this point the spot parameters were held fixed and the stellar parameters adjusted until the solution converged again. This process was repeated until the model converged to a final solution. The best-fit WD spotted solution model is shown in column 3 of Table 3 (Solution 2). Figure 8 shows the final spotted model fit (solid line) to the observed light curves and Figure 9 the residuals. A graphical representation of the spotted model is shown in Figure 10.

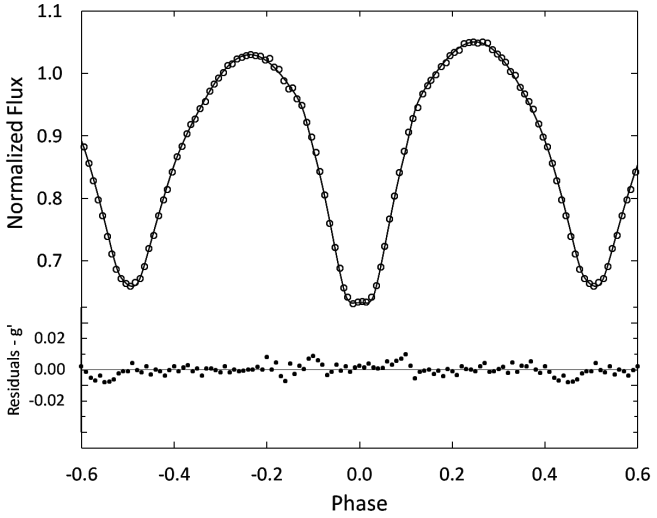

Figure 10. The WD model fit with spots (solid curve) to the observed normalized flux curves for Sloan g' passband. The residuals are shown in the bottom panel. The best-fit parameters are given in column 4 of Table 3. Error bars are omitted from the points for clarity.

5. Discussion and conclusions

PY Boo is a member of the W-type subclass of eclipsing binaries. Its more massive and cooler secondary star has a lower surface brightness than its companion and primary minimum is an occultation. The best-fit WD spotted solution with a fill-out value of 12% is consistent with a contact binary. The total eclipses provide the necessary constraints to calculate provisional absolute stellar parameters for the stars (Wilson 1978; Terrell and Wilson 2005). The secondary star's mass can be estimated from the orbital period using an empirical relationship derived by Qian's (2003) statistical study of contact systems. Using the orbital period in this relationship,

$$M_2 = 0.391\ (\pm 0.059) + 1.96\ (\pm 0.17)\ P, \qquad (6)$$

gives a mass for the secondary star of $M_2 = 0.94 \pm 0.06\ M_\odot$. Using the mass ratio from the WD spotted solution gives a primary star mass of $M_1 = 0.43 \pm 0.06\ M_\odot$. Kepler's Third law gives a distance between the mass centers of the stars of $1.99 \pm 0.01\ R_\odot$. The mean stellar densities were computed from Mochnacki's (1981) empirical relationship

$$\bar{\rho}_1 = \frac{0.0189}{(r_1^3\ (1 + q)\ P^2)} \text{ and } \bar{\rho}_2 = \frac{0.0189q}{(r_2^3\ (1 + q)\ P^2)}, \qquad (7)$$

where the stellar radius is normalized to the semi-major axis and P is in days. The computed values are $\bar{\rho}_1 = 2.30$ g cm^{-3} and $\bar{\rho}_2 = 1.74$ g cm^{-3}. The stellar radii, surface gravities, and bolometric magnitudes were calculated by the WD light curve program (LC). The visual luminosities of each star were calculated using the bolometric magnitudes from the LC output and the bolometric corrections from Pecaut and Mamajek (2013). The values for all the stellar parameters are reported in Table 4. The radii and masses are in good agreement with the mass and radius distribution of 112 contact binaries in a study by Gazeas and

Table 4. Provisional stellar parameters for PY Boo.

Parameter	*Symbol*	*Value*
Stellar masses	M_1 ($M_\odot$)	0.43 ± 0.06
	M_2 ($M_\odot$)	0.94 ± 0.06
Semi-major axis	a ($R_\odot$)	1.99 ± 0.01
Stellar radii	R_1 ($R_\odot$)	0.64 ± 0.01
	R_2 ($R_\odot$)	0.91 ± 0.02
Surface gravity	log g_1 (cgs)	4.46 ± 0.03
	log g_2 (cgs)	4.49 ± 0.06
Mean density	$\overline{\rho}_1$ (g cm^{-3})	2.30 ± 0.13
	$\overline{\rho}_2$ (g cm^{-3})	1.74 ± 0.09
Stellar luminosity	L_{1V} ($L_\odot$)	0.25 ± 0.02
	L_{2V} ($L_\odot$)	0.38 ± 0.04
Bolometric magnitude	$M_{bol,1}$	6.13 ± 0.09
	$M_{bol,2}$	5.59 ± 0.13

Values in this table are provisional (calculated). Radial velocity observations are necessary for direct determination of M_1, M_2, and a.

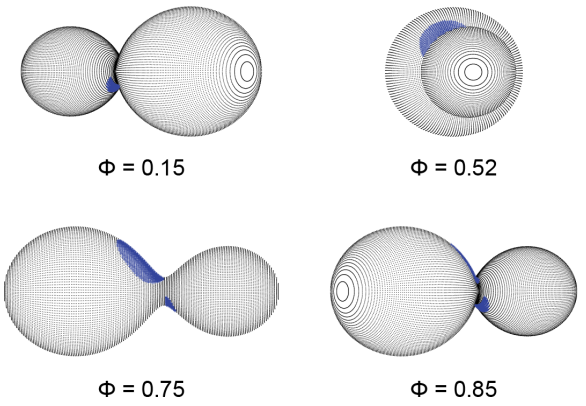

Figure 11. Roche Lobe surfaces of the best-fit WD spot model with orbital phase shown below each diagram.

Stępień (2008) (see their Figures 1–3). The geometrical and physical properties for those 112 stars were well determined. Two of their plots were reproduced in Figures 12 and 13 that also include the primary and secondary stars of PY Boo.

The third light contribution to the system light could possibly be another star orbiting the contact pair or an unresolved field star. The closest observed field star to PY Boo is located 35 arc seconds to the northwest. This star was well outside the annulus used in the photometric processing of the images, therefore it did not contribute to the third light measured. Assuming the third light source is a main-sequence star, its color can be estimated from the WD solution's g' and r' third light values. Converting the third light values to magnitudes gives a color of (g' – r') = 0.180 ± 0.008. Transforming this value using Equation 4 and correcting for color excess gives a color index of (B–V) = 0.378 ± 0.008. A main-sequence star of this color has an effective temperature of 6784 ± 46 K, a spectral type of F3V and a visual luminosity of L_{V3} = 4.9 ± 0.2 $L_\odot$ (Pecaut and Mamajek 2013). A star of this luminosity located in the PY Boo system would contribute 89% percent of the total system light (computed using L_{V1}, L_{V2} from Table 4 and L_{V3} above). This is much higher than the third light contribution found in the spotted WD solution whose values range from 21% – 27% for the g', r', and i' Sloan

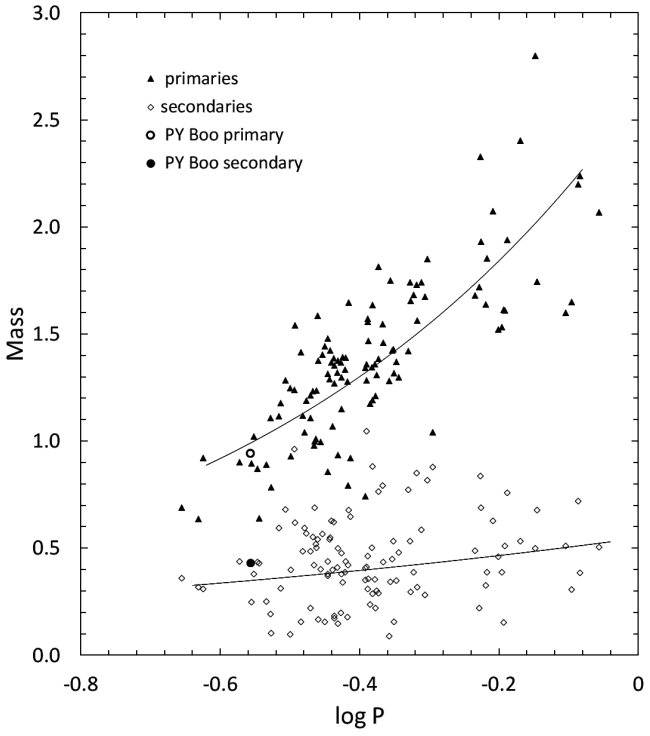

Figure 12. The mass distributions of 112 contact binaries with well determined geometrical and physical properties. The triangles are the primary star masses and the diamonds the secondary masses with PY Boo stars marked with the open and closed circles. The solid lines are the least-square fits from the analysis of Gazeas and Stępień (2008).

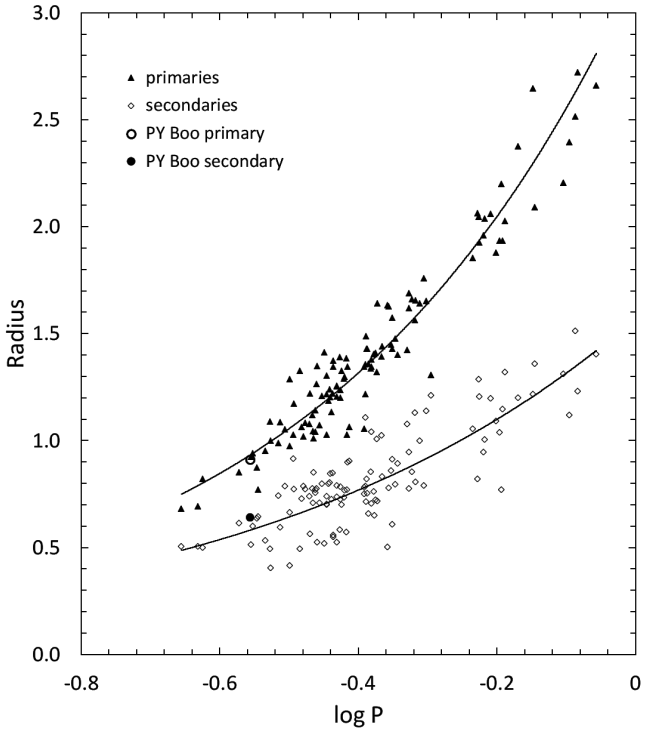

Figure 13. The radius distributions of 112 contact binaries with well determined geometrical and physical properties. The triangles are the primary star masses and the diamonds the secondary masses with PY Boo stars marked with the open and closed circles. The solid lines are the least-square fits from the analysis of Gazeas and Stępień (2008).

passbands (see Table 3). This result indicates the third light source is not in the PY Boo system but comes from a more distant unresolved field star.

The distance to PY Boo can be estimated from Ruciński and Duerbeck's (1997) luminosity calibration for contact binaries, which is based on HIPPARCOS parallaxes. This empirical relationship for absolute magnitude is given by

$$M_v = -4.44 \log_{10}(P) + 3.02 (B-V)_o + 0.12. \quad (8)$$

Substituting the orbital period and the (B–V) color index gives a value of $M_v = 5.37 \pm 0.22$ for the absolute magnitude. The apparent V-band magnitude at orbital phase $\varphi = 0.25$ was determined from the g' and r' magnitudes using Jordi *et al.*'s (2006) transformation equation which is given by

$$V = (-0.565 \pm 0.001)(g' - r') - (0.016 \pm 0.001) + g'. \quad (9)$$

The third light contribution was removed from the g' and r' magnitudes before substitution into Equation 9. This gives an apparent magnitude of $m_v = 12.53 \pm 0.01$. Correcting for extinction ($A_v = 0.05$) gives a distance modulus of $(m - M)_V = 7.11 \pm 0.22$ and a distance of 264 ± 27 pc.

As with many short period low mass contact binaries, PY Boo appears to be magnetically active. In this study, a number of light curves were obtained from different nights over a time span of 1 year. Noticeable changes were seen in the light curves over this time interval. At times Max I was brighter than Max II while at other times this reversed with Max II brighter than Max I (O'Connell effect). The observations used for the WD spotted solution had about equal maxima. In that solution the synthetic light curve did not fit the g' passband observations as well as the r' and i' passbands (see Figure 8). The g' band residuals in Figure 9 show a sinusoidal distribution. Since the g' observations were taken two weeks before the r' and i' observations it was suspected the spot configurations had changed over that two-week interval. To test this idea a new WD solution was attempted using only the g'-band observations with all stellar parameters held fixed at the spotted solution values (Solution 2). Only the light and spot parameters were allowed to vary. The initial spot parameter values were also taken from Solution 2. The resulting best-fit WD model for the g'-band observations is shown in column 4 of Table 3 (Solution 3). Figure 10 shows the improved model fit (solid line) with the bottom panel showing the residuals with the sinusoidal distribution no longer apparent. The most significant change in the spot configuration over the two-week interval was that the cool spot on the secondary star appears to have moved 9° in longitude and decreased in radius by 15%.

The decreasing orbital period reported in section 3 should be considered preliminary since the available set of minima times is small. A decreasing orbital period could be explained by magnetic braking. The rapidly changing spot configuration observed is a clear indication of magnetic activity in this binary. Angular momentum loss by magnetic braking was likely an important factor in bringing the stars into their current contact configuration (Stępień and Gazeas 2012). This process may be continuing at present time but may not be the only cause of the observed period change. With the stars in a contact configuration, conservative mass exchange from the larger more massive secondary star to the smaller hotter primary star could also be the cause of or contribute to the decreasing period. In this case the rate of mass transfer (Reed 2011) is given by

$$\frac{dM}{dt} = \frac{(\dot{P} M_1 M_2)}{3P(M_1 - M_2)}. \quad (10)$$

Substituting the rate of period change ($\dot{P}$) and the stellar masses gives a mass transfer rate of 2.3 (0.2) × 10^{-9} $M_\odot$ / day. It is also possible that the quadratic curve fit to the O–C data (Figure 4) is a small part of a sinusoidally varying ephemeris. This type of ephemeris would result from a third body in the system but the limited number of minima times does not support that supposition at this time.

PY Boo is a short period (P < 0.3 d) low mass contact binary. Model calculations by Stępień and Gazeas (2012) suggest it will remain in the contact phase for about 0.8 Gyr before eventually coalescing into single rapidly rotating star. A spectroscopic radial velocity study of this system combined with the photometric solution presented here would be invaluable in determining the absolute stellar parameters and providing insight into its current evolutionary state. New times of minima light with observations spread over several years would also be invaluable in confirming the decreasing orbital period and provide evidence for a third star if one exists.

6. Acknowledgements

This research was made possible through the use of the AAVSO Photometric All-Sky Survey (APASS), funded by the Robert Martin Ayers Sciences Fund. This research has made use of the SIMBAD database, operated at CDS, Strasbourg, France.

References

Bradstreet, D. H., and Steelman, D. P. 2002, *Bull. Amer. Astron. Soc.*, **34**, 1224.

Diethelm, R. 2012, *Inf. Bull. Var. Stars*, No. 6029, 1.

Gazeas, K., and Stępień, K. 2008, *Mon. Not. Roy. Astron. Soc.*, **390**, 1577.

Gettel, S. J., Geske, M. T., and McKay, T. A. 2006, *Astron. J.*, **131**, 621.

Henden, A. A., *et al.* 2014, AAVSO Photometric All-Sky Survey, data release 9 (http://www.aavso.org/apass).

Hoffman, D. I., Harrison, T. E., and McNamara, B. J. 2009, *Astron. J.*, **138**, 466.

Hoňková, K. *et al.* 2014, *Open Eur. J. Var. Stars*, No. 165, 1.

Hübscher, J. 2013b, *Inf. Bull. Var. Stars*, No. 6084, 1.

Hübscher, J. 2015b, *Inf. Bull. Var. Stars*, No. 6152, 1.

Hübscher, J. 2016, *Inf. Bull. Var. Stars*, No. 6157, 1.

Hübscher, J., and Lehmann, P. 2013a, *Inf. Bull. Var. Stars*, No. 6070, 1.

Hübscher, J., and Lehmann, P. 2015a, *Inf. Bull. Var. Stars*, No. 6149, 1.

Jester, S. *et al.*, 2005, *Astron. J.*, **130**, 873.

Jordi, K., Grebel, E. K., and Ammon, K. 2006, *Astron. Astrophys.*, **460**, 339.
Kafka, S. 2016, variable star observations from the AAVSO International Database (https://www.aavso.org/aavso-international-database
Lucy, L. B., 1968, *Astrophys. J.*, **151**, 1123.
Lucy, L. B., and Wilson, R. E. 1979, *Astrophys, J.*, **231**, 502.
Luo, A-Li, *et al.* 2015, *Res. Astron. Astrophys.*, **15**, 1095.
Mirametrics 2015, Image Processing, Visualization, Data Analysis (http://www.mirametrics.com).
Mochnacki, S. W. 1981, *Astrophys. J.*, **245**, 650.
Paschke, A. 2014, *Open Eur. J. Var. Stars*, No. 162, 1.
Pecaut, M. J., and Mamajek, E. E. 2013, *Astrophys. J., Suppl. Ser.*, **208**, 9 (http://www.pas.rochester.edu/~emamajek/EEM_dwarf_UBVIJHK_colors_Teff.txt).
Qian, S. 2003, *Mon. Not. Roy. Astron. Soc.*, **342**, 1260.
Reed, P. A. 2011, in *Mass Transfer Between Stars: Photometric Studies, Mass Transfer—Advanced Aspects*, ed. H. Nakajima, InTech DOI: 10.5772/19744. (http://www.intechopen.com/books/mass-transfer-advanced-aspects/mass-transfer-between-stars-photometric-studies).
Ruciński, S. M. 1969, *Acta Astron.*, **19**, 245.
Ruciński, S. M., and Duerbeck, H. W. 1997, *Publ. Astron. Soc. Pacific*, **109**, 1340.
Stępień, K., and Gazeas, K. 2012, *Acta Astron.*, **62**, 153.
Terrell, D., and Wilson, R. E. 2005, *Astrophys. Space Sci.*, **296**, 221.
Van Hamme, W. 1993, *Astron. J.*, **106**, 2096.
Van Hamme, W., and Wilson, R. E. 1998, *Bull. Amer. Astron. Soc.*, **30**, 1402.
Willingale, R., Starling, R. L. C., Beardmore, A. P., Tanvir, N. R., and O'Brien, P. T. 2013, *Mon. Not. Roy. Astron. Soc.*, **431**, 394, (http://www.swift.ac.uk/analysis/nhtot/).
Wilson, R. E. 1978, *Astrophys. J.*, **224**, 885.
Wilson, R. E., and Biermann, P. 1976, *Astron. Astrophys.*, **48**, 349.
Wilson, R. E., and Devinney, E. J. 1971, *Astrophys. J.*, **166**, 605.
Wozniak, P. R., *et al.* 2004, *Astron. J.*, **127**, 2436.

Two High-Latitude UXORs

Michael Poxon
AAVSO, 9 Rosebery Road, Great Plumstead, Norwich, UK, mike@starman.co.uk

Received September 1, 2015; revised September 8, 2016; accepted September 14, 2016

Abstract The active variables V1117 Her and RZ Psc are discussed with a proposition that star formation can occur far from the galactic plane and in relatively small, isolated environments, and that some YSOs may last longer in such places and help highlight the existence of high latitude star formation.

1. Introduction

YSOs are, almost by definition, to be found in the region of the parent gas clouds from which they condensed, and since these clouds lie overwhelmingly along the galactic equator or in starforming regions close to it, the notion of such variables being found at high galactic latitudes may be a puzzling one. The two objects examined here have galactic latitudes (b values) in excess of 30° and do not have starforming clouds or similar regions associated with them. Both stars show visual light curves punctuated by quasiperiodic Algol-type fadings characteristic of the class of star typified by UX Orionis (UXORs), although the spectral type of RZ Psc of K0 IV is highly atypical for these objects which are of much earlier spectral types as a rule.

Observed UXOR fades are believed to be be a combination of two basic factors: firstly, the presence of a circumstellar disc with a high axial inclination relative to the observer and so appearing edge-on or nearly so to our line of sight. Secondly, the presence in this disc of clumps of matter such as forming planetesimals which, because of the view we have of them, can occasionally "eclipse" the parent star and thus produce the observed dips in brightness. In fact some UXORs such as BO Cep and MQ Cas were originally thought to be Algol-type Eclipsing Binaries, and indeed one of the stars in this paper, V1117 Her, was once listed as a long period variable having an amplitude of 1.9 magnitudes, and period of 114 days, none of which parameters actually apply to it.

Assuming that the stars were originally formed at low galactic latitudes, we need to ask how they ended up where they are today; far away from any areas of star formation. While a high value for b does not alone confer such peculiarity (for example UX Orionis itself has b = –25° but it does lie close to a very extensive starforming region in the neighborhood of M42) most YSOs discovered so far inhabit regions with low galactic latitudes. Below is a quick list of random UXORs together with their distances from b = 0:

Table 1. Some UXOR-type variables together with their distances from the galactic equator.

Star	*abs (b)°*
VX Cas	00.8
GM Cep	03.8
DG Cir	04.2
GT Ori	15.0
RZ Psc	34.7
XX Sct	00.5
CQ Tau	04.0

With the exception of GT Ori (due to the fact that the Orion starforming region is so extensive that parts of it lie relatively quite far below the galactic equator; see the quoted example of UX Ori above) all the members of this admittedly small sample lie within 5 degrees of the galactic plane, and they are quite typical as regards this parameter.

2. The stars

RZ Psc (2MASS J01094205+2757020, ASAS J010942+2757.0) is catalogued as a bona fide UXOR variable, though it is hardly typical of the class. As regards galactic latitude Grinin *et al.* (2010) give an expression for the physical distance z from the galactic plane:

$$z = D \sin b - z_{\odot} \quad (1)$$

$z_{\odot}$ here is the distance of the Sun from the plane, taken as +25 parsecs, and D the distance to the star in parsecs. Inserting appropriate values for RZ Psc gives us a distance of –130 parsecs with reference to the galactic plane.

Determining a ballpark figure for the age of RZ Psc, which will relate to this distance, can yield a wide range of results, though none point to extreme youth as would be expected for an UXOR, and most methods are reliant on variables whose values are imprecise. For example, the value of D in equation (1) is arrived at indirectly here, using assumptions about its absolute magnitude M based on its spectral type and assumed age which are then used to derive a value for D. However, as we shall see next, the age of RZ Psc is the subject of debate.

One method that has been employed for some time is to determine the proportion of Lithium in the atmosphere. Lithium is a signature of youth since it is rapidly destroyed by nucleosynthesis as the star enters and then proceeds along the main sequence. Grinin *et al.* (2010) estimated an age for RZ Psc based on its Lithium abundance of between 10 to 70 Myr which was later refined to between 20–30 Myr—so, young but not as one might say "YSO-young" since this figure would lead us to expect that the circumstellar material should effectively have been used up to form a planetary system or dust features after such time, but studies have shown that there is IR excess present to an extent that suggests that there is still an active disc of some sort that interfaces with the parent star. Other estimates based on the star's proper motion when combined with gravitational mechanics of the Galaxy itself yield a slightly higher figure of about 50 Myr, and in this context another theory has emerged that relates to Gould's Belt.

Gould's Belt is a partial ring of relatively young, massive early-type stars in a plane spread around the sky, with a break in the direction of the galactic center and a diameter thought to be ~1 Kpc. The plane is inclined to that of the Galaxy by about 20° and the O- and B-type stars that define it are in the region of 50 Myr old. Also, including many well-known naked-eye stars such as Rigel, the belt also harbors active areas of massive star formation such as the Cep and Cas OB and Sco-Cen OB associations.

Although its cause—assuming that it is a real entity of course—has not been definitively established, one suggestion is that, since there is a break near the galactic centre, something extragalactic such as a huge gas cloud or even a region of dark matter ploughed into a spiral arm, generating a huge burst of star formation which resulted in those hot young stars of the belt and, in the same process, possibly ejecting some stars away from the arm. Some of those stars may have been in the process of forming independently at the time and, so to speak, are still carrying their youth with them. The proper motion of RZ Psc is reasonably high (25.4α, –11.9δ mas yr^{-1}), and in a direction away from the galactic plane, which has led some credence to this idea. However, if we look at a plot of proper motions of stars in the area of RZ Psc in Figure 1 we can see that there are several other stars with similar direction vectors comparable to that of RZ Psc or which actually exceed it, such as the star at about R.A. 01^h 11^m, Dec. 27° 50' ($\mu_{\alpha,\delta}$ = 36.9, –29.4 mas yr^{-1}) .

V1117 Her Although not catalogued as a UX Ori star, the second star in this paper, V1117 Her, shows UXOR-like dips in brightness and in fact at the time of writing (August 2016) has just emerged from one of these fades, as can be seen from examining the observations given in Table 2.

These fades are both deep and rapid as can be seen from the above observations, and the better-observed fade series in fact demonstrate that a typical minimum is around 15.0mv, an amplitude and duration similar to that of some active Herbig Ae stars such as V730 Cep. There appears to be some regularity to these major fades, which Kun *et al.* (2014) largely using AAVSO observations determine as 408 days, and suggest some form of eclipse of the parent star by a clump. Figure 2 shows the light curve of this star from 2002 to 2016 and it appears on a cursory examination that the fades are tending to become deeper. If this is indeed the case then it may point to evolution of the clump(s). The relative regularity of the fades could be indicative of a persistent clump, something that has been hypothesized in the case of another star on the AAVSO YSO program, GM Cep, a most definitely young star in the Cep OB2 association involved with the IC1396 starforming region and one that I urge observers to follow.

Spectral features such as the presence of Hα in emission and prominent Balmer-series absorption in the star indicate a spectral type of A for V1117 Her. But YSOs of such type are to be found closer to theatres of star formation and evolve so quickly that by the time they have reached the galactic latitude of 33° they would have lost any circumstellar material; and in any case there are no such star formation areas in the neighborhood of V1117 Her. Considering the proper motion of the star ($\mu_{\alpha,\delta}$ = –7.9, –5.9 mas yr^{-1}) we cannot even postulate a scenario like that hypothesized earlier for RZ Psc; tracing the space motion back over a time span similar to the expected age of the star encounters no suitable star formation areas. A plot of the proper motions of stars in the neighborhood of V1117 Her is shown in Figure 3, where positions are in galactic coordinates.

Assuming that the star is at, or near the ZAMS (Zero-Age Main Sequence) and its spectrum is indeed A-type then it should have M ~ +2. Comparing this M with its observed visual maximum of 12.1 whilst assuming minimal space reddening due to its observed distance above the galactic plane we can employ the formula for distance modulus:

$$m - M = 5 \log d - 5 \qquad (2)$$

and rearrange for d to give a value of about 870 pc, which

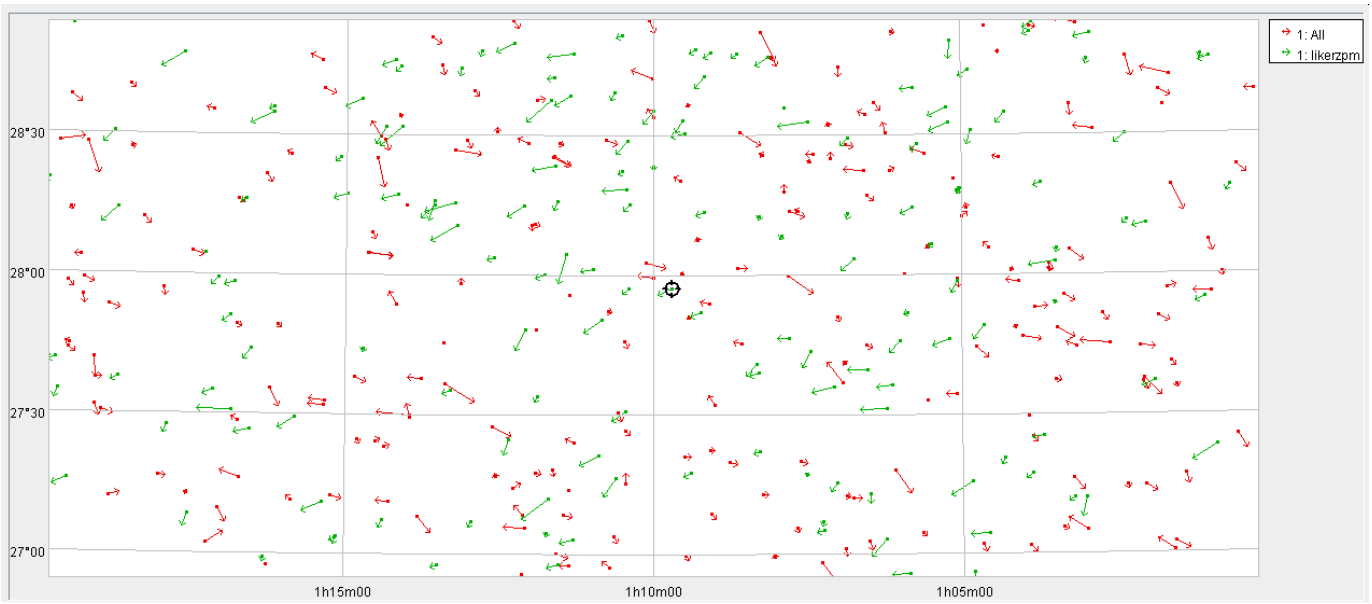

Figure 1. Proper motions of stars in the area of RZ Psc (circled). Position vectors similar to that of RZ (α +ve, δ –ve) in green. All vectors are to scale. Produced using the TOPCAT software tool.

Table 2. Visual observations of V1117 Her.

JD	UT	Magnitude	AAVSO Observer Initials
2457575.458	2016 Jul. 05.95800	12.9	PYG
2457587.440	2016 Jul. 17.94000	13.4	PYG
2457588.445	2016 Jul. 18.94500	13.5	PYG
2457594.435	2016 Jul. 24.93500	14.3	PYG
2457599.440	2016 Jul. 29.94000	14.0	PYG
2457600.43	2016 Jul. 30.93000	13.7	PYG
2457601.432	2016 Jul. 31.93200	13.5	PYG
2457605.427	2016 Aug. 04.92700	13.1	PYG
2457606.436	2016 Aug. 05.93600	12.5	PYG
2457607.4451	2016 Aug. 06.94510	12.5	POX

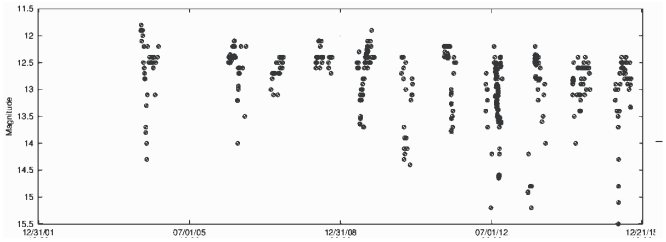

Figure 2. 15-year light curve of V1117 Her from the AAVSO light curve generator. Note the periodicity of the fades and their tendency to become deeper.

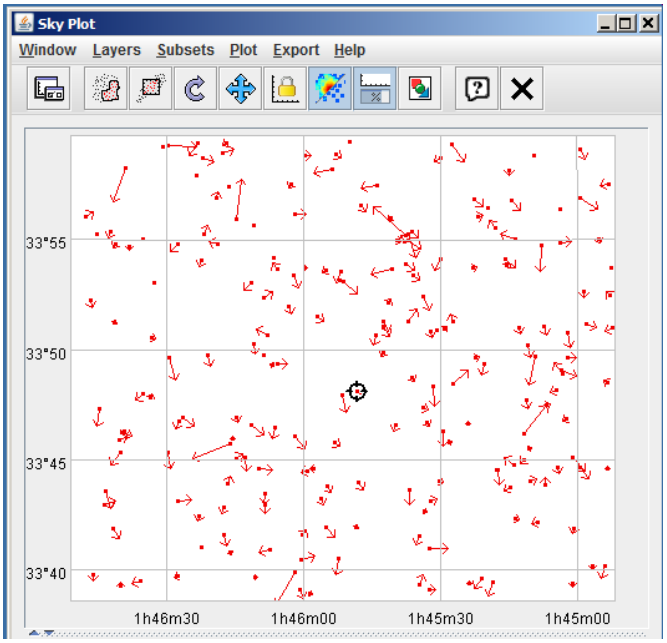

Figure 3. Proper motions of stars around V1117 Her (circled). Note its small vector when compared with many of the other objects in the plot. Coordinates are galactic. Plot prepared using TOPCAT software.

leads through trigonometry to a distance of ~400 pc above the plane, where ordinarily we would not expect to find starforming material, though there is a complex of dark nebulae near the star μ Serpentis of which the largest is LBN19. The proper motion of V1117 Her is, somewhat perversely toward, rather than away from, this area! However, the presence of nebular material at this position of b = 37.3° should demonstrate that nebulae are not only to be found at low galactic latitudes, and indeed in recent years several stellar associations known as T-associations (since they contain a high proportion of T Tauri stars) have been discovered well away from the galactic plane such as the nearby Tucana-Horologium association with b values at or greater than –50° and ages around 30 Myr, together with quite extensive molecular clouds in (for example) Octans, with an approximate b value of –30° and thus comparable to the values for the stars discussed here. Although most of the members of T-associations are of lower mass and later spectral types than a typical UXOR, early-type stars are typically found to be constituents of such groups, and this may be relevant to a suggestion to be made in the following conclusion.

3. Conclusion

We have seen that both stars show UXOR-like behavior in terms of the light variations and both have been shown to possess circumstellar discs. V1117 Her looks, from its spectrum, more like a typical UXOR than does RZ Psc. Similar variable types such as R Coronae Borealis stars also show deep fades, but these fades are random in depth, duration, and occurrence, and the variations of our two objects are more regular and show, at least in the case of V1117, some suggestions of dynamical processes such as clump evolution. RCB stars are also hydrogen-poor and this does not apply to the stars discussed here. However, the high galactic latitudes and distance from star-forming areas would seem to militate against their being stars comparable in age to a typical UXOR. So is it possible that RZ Psc and V1117 Her are members of a hitherto different variety of YSO that are actually formed away from the galactic plane? After all, as we saw in the previous paragraph above, there may be other places to look for starforming regions other than the immediate galactic equatorial area. If RZ Psc and V1117 Her were actually born at high latitudes out of such clouds then the gravitational influence of nearby stars in a stellar association (or indeed of the general mass of the immediate Galaxy) might not be so effective at disrupting the circumstellar environment, allowing the disc to persist for longer.

So—should we start looking for YSO's away from the galactic plane?

4. Acknowledgements

The author would like to thank John Murrell for an introduction to the TOPCAT software package and guidance on its use, along with its creators and administrators at Bristol University: http://www.star.bristol.ac.uk/~mbt/topcat/. For more information, see Taylor (2005).

References

Grinin, V. P., Potravnov, I. S., and Musaev, F. A. 2010, *Astron. Astrophys.*, **524**, 8 (arXiv:1109.2711v1 [astro-ph.SR] 13 Sep 2011).

Kun, M., Rácz, M., and Szabados, L. 2014, *Inf. Bull. Var. Stars*, No. 6089, 1.

Taylor, M. B. 2005, in *Astronomical Data Analysis Software and Systems XIV,* ASP Conf. Ser., 347, eds. P. Shopbell, M. Britton, and R. Ebert. Astronomical Society of the Pacific, San Francisco, 29.

Crowded Fields Photometry with DAOPHOT

Elisabetta Artusi
Circolo Astrofili "Galileo Galilei", viale G. Ferraris 1, 30036 S. Maria di Sala (Venezia), Italy; elisabetta.artusi@outlook.com

Giancarlo Conselvan
Circolo Astrofili "Guido Ruggieri", via padre E. Gelain 7, 30175 Marghera (Venezia), Italy; conselvan.giancarlo@gmail.com

Antonio Tegon
Circolo Astrofili "Guido Ruggieri", via padre E. Gelain 7, 30175 Marghera (Venezia), Italy; antonio.tegon@gmail.com

Danilo Zardin
Circolo Astrofili "Galileo Galilei", viale G. Ferraris 1 30036 S. Maria di Sala (Venezia), Italy; zardin.danilo@gmail.com

Abstract The DAOPHOT method provides an efficient solution to the problem of measuring stellar magnitudes in crowded fields. We present here a detailed description of the method as implemented in IRAF through a worked example on the emission-line star KW97 42-41. In the last chapter we also present, with the support of spectroscopic data, an analysis of the physical properties of the star.

Received March 2, 2016; revised May 19, 2016; accepted May 31, 2016

1. Introduction

The usual way of measuring stellar magnitudes is aperture photometry; this method generally gives good results providing that good photometric standard stars are available and that it is possible to define a region around the target star (the annulus) containing mostly sky background. This could be really difficult to define when the target star is located in a very crowded stellar field which is, generally, the case of stars lying on the galactic plane. Moreover, in crowded stellar fields it is easy to find overlapping stellar luminosity profiles. The method of the PSF fitting on stellar profiles implemented by DAOPHOT (Stetson 1987; for its implementation in IRAF see Davis 1994) bypasses these difficulties and allows astronomers (professional and amateur) to get good photometry even in crowded fields. In the following sections we will describe the main features of the DAOPHOT method and its implementation in IRAF by discussing its application to the measure of BVRI magnitudes of a variable star taken from the Kohoutek and Wehmeyer (1997, hereafter KW97) catalogue, a good source of emission-line stars containing more than 4000 stars with suspected emission-lines. (We have written a freely downloadable tutorial which describes in detail all the steps; see the post DAOPHOT on the AAVSO website data analysis forum https://www.aavso.org/daophot).

2. DAOPHOT: a description of the method

A three dimensional surface plot of a CCD frame of a stellar field may look like that represented in Figure 1, where stellar images are similar to mountains emerging from a plain, the plain being the sky background.

Since each point-like image produced by the optics of the telescope is spread mainly because of the atmospheric seeing, any stellar profile has the same shape with the same FWHM (Romanishin 2006). The luminosity profiles roughly follow a

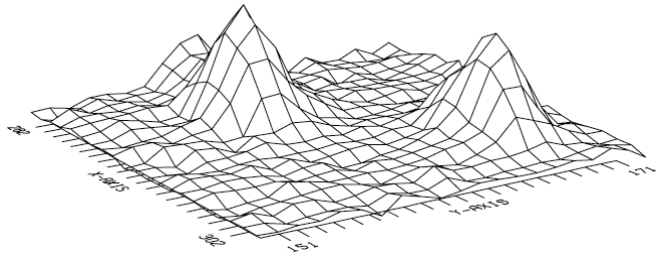

Figure 1. Example of a surface plot of a stellar field.

Gaussian curve centered on the peak and eventually fade into the sky background. As already stated in the introduction, it is generally impossible to use aperture photometry in crowded fields but we can bypass these difficulties by creating an articial stellar profile (the Point Spread Function, PSF) which can be used to identify any stellar feature on the frame. It is therefore possible to measure the instrumental magnitudes within one FWHM for any star. If the comparison stars are on the same frame as the target stars (differential photometry) it is possible to get the standard BVRI magnitudes. The standard BVRI magnitudes of the comparison stars have been probably measured within apertures larger than the value of our FWHM but, since we are comparing stellar profiles of the same shape and width, we can say that, for any filter, the following equation holds:

$$m_{target} - m_{comparison} = M_{target} - M_{comparison} \quad (1)$$

where m is the instrumental magnitude measured within one FWHM and M is the standard magnitude. On the other hand, if the comparison stars were not on the same frame as the target star (all-sky photometry) we should correct for atmospheric extinction. Moreover, we should measure the instrumental magnitudes within larger apertures because there could be differences in the stellar profiles of the frames. The problem,

now, is to calculate how many magnitudes we should subtract from those measured within one FWHM around the peak of the luminosity profile. Even in a very crowded field it is possible to find a few relatively isolated stars; if they are not isolated enough, we can clean their surroundings by subtracting the PSF from any unwanted stellar feature in order to get more free sky background. The basic idea is to measure the sky-subtracted instrumental magnitudes within regions of increasing radius. The absolute value of the instrumental magnitude to subtract will first show an abrupt growth and then will become constant. Since the outer regions are occupied only by sky background, after a certain distance from the central peak there is no further contribution to the magnitude of the star. This constant limit value is the aperture correction to use. It is crucial, for the method to work, to be able to build a reliable PSF which fits the true stellar profiles.

3. Using DAOPHOT inside IRAF: a worked example

Among the astronomical community, IRAF is a well-known software which, despite its old style interface, is still widely used, maintained, and updated. Among its strong points are a huge number of available algorithms and the possibility to adapt almost any task to the necessities of the user. IRAF tasks are organized into a tree structure, starting from a zero level root directory as in the following example, where any term refers to a collection of tasks or a collection of collections of tasks:

dataio	language	obsolete	softools	vo
dbms	lists	plot	system	
images	noao	proto	utilities	

DAOPHOT is the name of the method developed by Stetson while "daophot" is its implementation in IRAF and, like any other IRAF task, in this paper is written in lower case in quotes. We will use quotes also for keywords used as input by some IRAF tasks.

The task "daophot" is a collection of tasks inside "digiphot", which, in turn, is inside "noao". Here are the tasks inside a typical implementation of DAOPHOT in IRAF:

addstar	daotest	nstar	pexamine	psf
allstar	datapars@	pcalc	pfmerge	psort
centerpars@	findpars@	pconcat	phot	pstselect
daoedit	fitskypars@	pconvert	photpars@	seepsf
daofind	group	pdump	prenumber	setimpars
daopars@	grpselect	peak	pselect	substar

Packages whose name ends with an "@" like "centerpars@" are "wheels within wheels" (Massey and Davis 1992); they use one or more other tasks in order to get the appropriate values for a large variety of parameters.

3.1. Stellar profiles and sky background

The DAOPHOT method needs, first of all, some information about the stellar fields we are going to study. Basically, these are the FWHM of a typical stellar profile and the value of the mean sky background. It is therefore necessary to display the image and to interact with it; generally, IRAF uses DS9 for such a task (SAOImage DS9 at http://ds9.si.edu/site/Home.html; Figure 2)

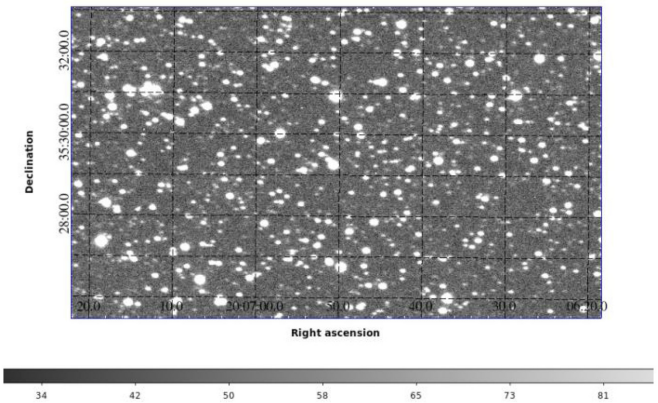

Figure 2. Stellar field around KW97 42-41 (TYC 2679-363-1). CCD R-band filter taken with the AAVSOnet telescope W28 on December 14, 2010. The emission-line star is close to the center of the field, R.A. $20^h\ 06^m\ 50.658^s$, Dec. +35 29' 14.89" (FK5 coordinates at J2000), on the upper-left.

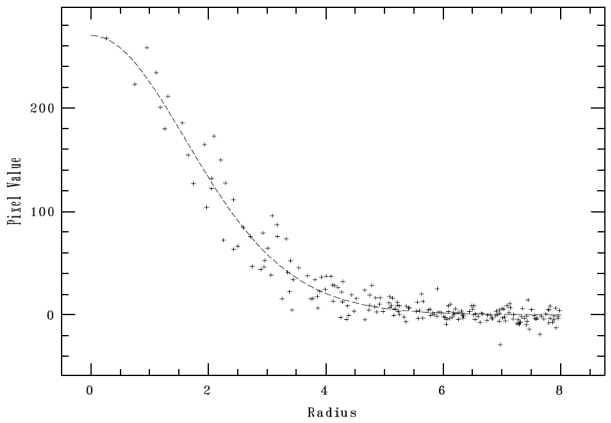

Figure 3. Stellar profile of a star in the field of KW97 39-30. Counts vs. distance from the central peak.

and, once an image is loaded into the DS9, we can interact with it. The task "imexamine" provides information on the FWHM of the stellar profiles and the sky background.

By placing the cursor on a star and clicking "r" we get a radial plot of the luminosity profile (Figure 3) fitted with a Gaussian curve.

The task "imexamine" calculates and displays some parameters of the stellar profile such as the FWHM (for further information see the help of "imexamine" inside IRAF). If the profile of the star is very weak, "imexamine" fails to draw a fit curve. The same task is used to measure the sky background by simply choosing a relatively clean area and pressing the key "m". All these operations should be repeated about ten times and the results should always be written into two text files for further analysis to get good values for the mean FWHM of the stellar profiles and of the mean sky background. (Our tutorial uses some Scilab (http://www.scilab.org/) scripts which ease and speed up some procedures. They are freely downloadable at http://ds9.si.edu/site/Home.html.)

3.2. Finding stars with "daofind"

The next step is to identify all the stellar profiles inside our images using "daofind". This task looks for profiles with the previously calculated parameters and identifies them as stars; it

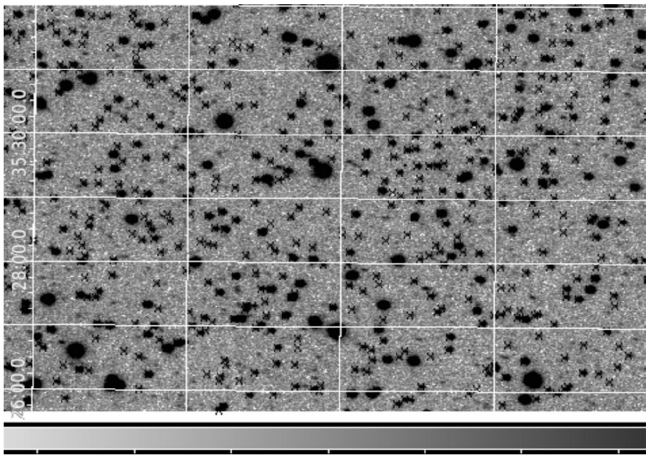

Figure 4. Enlargement of an area of Figure 2 with the stellar profiles identified by "daofind". The image is displayed in inverted grayscale to make the crosses stand out.

discards features too spiky (identified as cosmic rays or warm pixels) or too broadened (maybe some bad regions on the CCD or non-stellar objects like a nebula). Using "daofind", together with the tasks "tvmark" and "display", it is possible to identify any stellar feature by putting a mark (a colored point or a cross) upon it (Figure 4).

We can examine in detail each image with the magnifying glass of DS9 or with "imexamine" for a double check. The image displayed by DS9 immediately reveals whether the vast majority of all the stellar features have been identified.

3.3. First photometry

The following step is to get the instrumental magnitudes within one FWHM of all the stellar features found so far using "phot". This task does a simple aperture photometry within circular regions with a radius of 1 FWHM centered on the peak of each identified stellar profile. It is actually a composite photometry task as it uses other tasks as subroutines to which you can give many input parameters. Generally, the parameters "phot" requires are the radius and width of the annulus used for the photometry and the sky background to subtract. The output of "phot" is a long text file displaying data for any identified stars as in the example below:

Bea		493.791	5.436	1	Bea.coo.1	1	
493.791	5.436	0.000	0.000	*INDEF*	*INDEF*	0	NoError
25.7856		6.701344	4.857022	1464	289	0	NoError
240.	1.111398	*B*			02:46:00		
4.57	1959.753	66.01736	257.4565	24.924	0.239	0	NoError

A detailed description of the output of the task "phot" is available in the help of the "phot" task inside IRAF and in our tutorial. Anyway, the basic information hidden inside the preceding table are: i) the image name (Bea); ii) the XY coordinates of the identified star (493.791 and 5.436); iii) the mean sky background around the star (25.7856; iv) airmass, filter and time at the beginning of the exposure (1.111398, B, 02:46:00); v) data on the sky-subtracted countings (257.4565) inside 1 FWHM (4.57 pixels); vi) the measured instrumental magnitude with its uncertainty (24.924 and 0.239). "Bea" is a temporary name used in the data reduction process. It means that the image was taken using a B filter; it is a diminutive of the Italian name Beatrice.

An INDEF keyword is applied in every field where the task was not able to calculate a value. In order to be sure that "phot" worked correctly, it is possible to use the task "pdump" to make a list of the stars with no photometry (see the tutorial for a detailed explanation); generally, only a small percentage of stars had magnitudes set to INDEF.

3.4. Building the PSF image

The Point Spread Function (PSF) describes how the combination seeing+telescope+detector has spread out the point-like images of the stars. It is necessary to look, in every stellar field, for some (5–10) relatively isolated stars with very few or no neighbor stars and use the task "psf" together with "daopars". This last task is used to give "psf" the correct parameters to build the PSF function. The interaction with DS9 is done by placing the cursor on a chosen star and clicking "a"; Figure 5 is an example of the output.

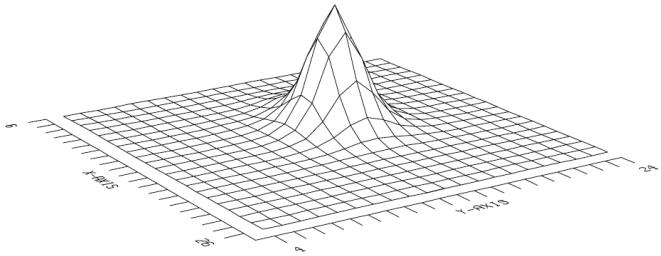

Figure 5. An example of a stellar PSF profile.

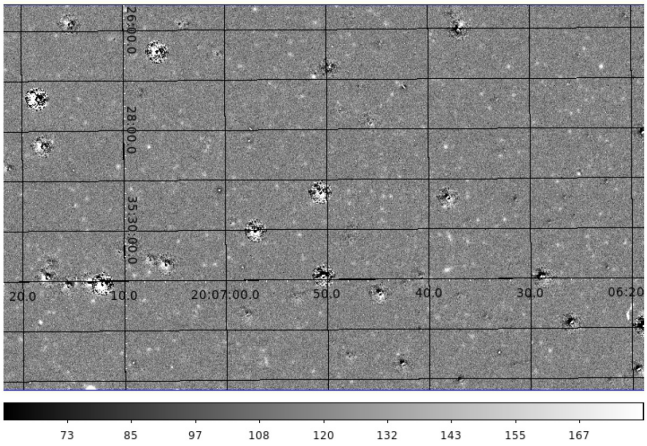

Figure 6. Stellar field with subtracted PSF profiles; holes are very bright stars not well subtracted.

By typing "a" you decide to use the star to build a stellar profile whereas, if the star is not suitable, you can discard it. After having collected a few acceptable profiles, you can tell the task to build the PSF image of that night and exit. At this point, you may want to check the PSF image built so far and see whether it is a good approximation of the stellar profiles. The task "nstar" is now used to fit the calculated profiles to each star in the field and then "substar" subtracts the calculated profiles from the real stars. The result is shown in Figure 6; the fit is still satisfying even though some very bright stars

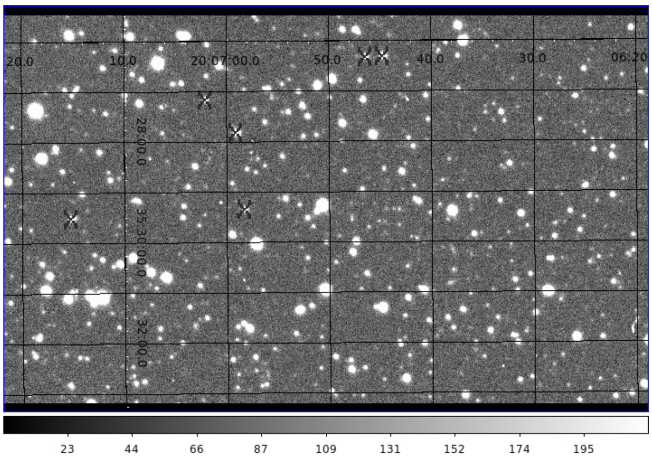

Figure 7. Crosses identify the stars used to build the PSF.

are not well subtracted. Anyway, if "substar" does not give a satisfactory result, there is the "imedit" task for a cosmetic smoothing process.

The test of the goodness of the cleaning process around the PSF stars can be done by using again "substar" and by creating two frames, one with both the PSF stars and their neighbors subtracted and another with only the neighbors subtracted. DS9 can show the two frames blinking; in order to point out where the PSF stars are, it is possible to previously mark them with "tvmark" (Figure 7).

The final and crucial test of the goodness of the fit is performed by the task "allstar", which subtracts from every single star the PSF profile just calculated. This task is the core of the DAOPHOT method because the fitted profile is used not only to subtract stars from the frames but also to give a better estimate of the stellar magnitudes (see section 3.6). These instrumental magnitudes are then used to get the standard BVRI magnitudes when dealing with differential photometry. We should see that, while bright stars are, generally, not completely erased from the field, PSF stars have disappeared; this means that the PSF profile is a good approximation of the star profiles, at least under a certain brightness. As an example of what IRAF can do, in the next paragraph we calculate the aperture correction even if it is superfluous in the case of differential photometry. If there are no good comparison stars in the same frame as they are too far from our target star, we have to correct for atmospheric extinction and do the aperture correction procedure; the results of the all-sky photometry will not be, generally, as accurate as those we get with differential photometry.

3.5. Measuring aperture correction

The (relatively) isolated stars used to build the PSF are also useful to calculate the aperture correction to apply to any star. Using the output from the task "psf" it is possible to build a file containing information (coordinates, magnitudes, and parameters on the shape of the candidate stars) to give as input to the task "phot". The aim is to perform photometry on PSF stars after having subtracted a certain number of neighbors from their surroundings. Using DS9 it is possible to define an annulus-shaped region centered on the aperture-correction stars that will contain, in addition to the central star, mostly sky

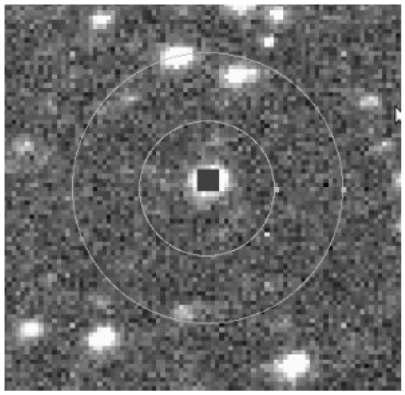

Figure 8. An example of a good choice for an annulus-shaped box.

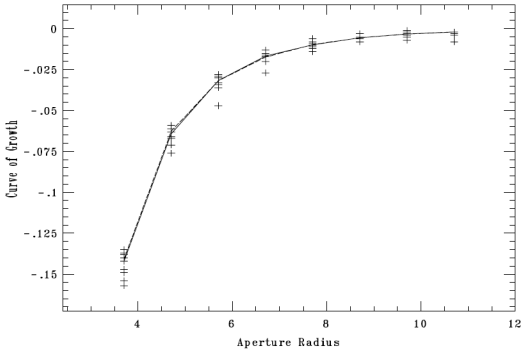

Figure 9. We can see that the fit is converging because the magnitudes measured inside growing regions tend to decrease with increasing apertures, meaning that we are adding less and less star light and more and more sky background; from a certain radius on what we get as starlight is compensated for by what we lose as background.

background inside the inner circle and very few or no stars at all in the annulus, as in Figure 8.

The dimension of the annulus is given to the sub-task "fitskypars" while a list of increasing values for the radius of the aperture is given to another sub-task, "photpars" (see again our tutorial for details on the exact syntax of the input parameters to give). The "phot" task evaluates the total amount of countings inside regions with growing radius. Finally, the task to use is "mkapfile". For every PSF star and aperture, "mkapfile" takes the total number of countings previously calculated by "phot", subtracts the sky background, and evaluates an instrumental magnitude. If the algorithm converges the growth curve (from now on GC) of the instrumental magnitudes calculated shows a steep increase at the beginning and tends to flatten as the aperture increases. This is because the increase in the total amount of light is balanced by a growing amount of subtracted sky background. The limit value of the horizontal branch of the CG is the aperture correction to use (Figure 9) and its value is found inside a text file produced by "mkapfile" as output.

3.6. Calculating instrumental magnitudes

The task "allstar" is used again to improve the instrumental magnitudes previously calculated with "phot". The PSF profile is fitted to any identified stellar feature, allowing the user to obtain a better estimate of the countings inside the same aperture (1 FWHM) used by "phot". Another photometry file (its default extension is .als), containing the aperture correction

value, is generated and will be used to give the final estimate of the instrumental magnitudes. This procedure has to be done for every filter. Before the final calculation it is important to correct the errors on the magnitudes by squaring and adding the uncertainties due to the aperture correction using the task "pcalc". All photometry files are to be sorted in ascending order of X coordinates with the task "psort" so that the task "mkobsfile" can create a file with all the useful data. Giving as inputs to "mkobsfile" the *.als* files it is possible to create an output file, called "photometry", where, for any identified star and for any filter used, there are the values of the instrumental magnitudes with their uncertainties. The final step is to extract from the photometry file only data referring to the target star and to the comparison stars.

3.7. Transforming to the standard system

The transformation from instrumental magnitudes to the standard BVRI, but, in the case of KW97 42-41, BV Johnson and RI Cousins, system is performed following the method outlined by Bruce L. Gary (2002–2006)in "CCD Transformation Equations for Use with Single Image (Differential) Photometry." The results are calculated using the weighted average of the magnitudes and the sigma of the weighted average. Here is an example of the results for KW97 42-41 on the night of 6/29/2011:

B	Ber	V	Ver	R_c	Rer	I_c	Ier
12.227	0.008	12.034	0.004	11.774	0.011	11.448	0.012

It is important to point out that in the field of KW97 42-41 we were able to find 12 comparison stars; as might be expected, with fewer reliable comparison stars the statistical uncertainties would have been higher.

Before giving the final results, we should check the reliability of the comparison stars by controlling whether we were able to reproduce their catalogue magnitudes. This can be done by treating each comparison star, in turn, as the target star and using the remaining comparison stars to calibrate its magnitude. This allows us, first, to discard comparison stars whose luminosities deviate too much from the catalogue and, second, to give a quantitative estimate of the reliability of our photometry by calculating the root mean square of the differences between the catalogue and the measured magnitudes. For instance, we found that in the photometry of 6/29/2011 the faintest comparison star has measured magnitudes which deviate considerably from the ones given in the catalogue; therefore we discarded it from our calculations. The new results are given below:

B	Ber	V	Ver	R_c	Rer	I_c	Ier
12.269	0.008	12.055	0.004	11.826	0.011	11.476	0.012

The root mean square on the differences between measured and catalogue magnitudes for each filter are:

B	V	R_c	I_c
0.030	0.050	0.045	0.083

The final results are calculated by using as uncertainties the combination of the two sigmas calculated above:

Table 1. Data for the light curve of KW97 42-41.

Date of Observation	*JD*	*B*	*V*	R_c	I_c
09/27/10	2455466.683	12.24	12.00	11.75	11.46
10/09/10	2455478.648	12.22	12.01	11.76	11.43
10/11/10	2455480.631	12.23	12.02	11.76	11.43
10/15/10	2455484.635	12.24	12.03	11.77	11.44
10/28/10	2455497.615	12.36	12.13	11.90	11.56
11/05/10	2455505.529	12.29	12.05	11.81	11.40
11/19/10	2455519.574	12.09	11.83	11.42	11.22
12/04/10	2455534.625	12.14	11.86	11.55	11.29
12/14/10	2455544.577	12.28	12.07	11.79	11.50
04/02/11	2455653.901	12.23	12.03	11.75	11.48
04/05/11	2455657.256	12.18	12.01	11.73	11.46
04/12/11	2455664.13	12.20	12.03	11.75	11.46
04/20/11	2455671.852	12.23	12.04	11.75	11.43
04/22/11	2455673.977	12.28	12.05	11.82	11.47
04/28/11	2455679.846	12.22	12.02	11.76	11.44
06/12/11	2455724.775	12.28	12.05	11.79	11.46
06/16/11	2455728.783	12.28	12.07	11.82	11.48
06/29/11	2455741.772	12.27	12.06	11.83	11.48
05/03/11	2455684.905	12.29	12.05	11.82	11.53
05/07/11	2455688.817	12.20	12.03	11.77	11.44
05/16/11	2455697.78	12.32	12.05	11.81	11.38
10/11/11	2455845.57	12.47	12.20	11.97	11.66
10/13/11	2455847.985	12.41	12.18	11.94	11.60
12/01/11	2455896.536	12.23	12.02	11.80	11.53
12/10/11	2455905.584	12.27	12.06	11.82	11.53
12/15/11	2455910.595	12.23	12.04	11.80	11.52
01/05/12	2455931.54	12.36	12.12	11.85	11.57
01/07/12	2455933.541	12.29	12.04	11.81	11.52

$B = 12.27 \pm 0.03$ $V = 12.06 \pm 0.05$ $R_c = 11.83 \pm 0.05$ $I_c = 11.48 \pm 0.08$

4. The emission-line star KW97 42-41

In 2010 we submifitted to AAVSO a list of variable star candidates taken from the H emission-line objective prism survey by Kohoutek and Wehmeyer (1997) to be observed by the AAVSOnet robotic telescopes. The data were collected by the AAVSOnet telescope W28 between September 2010 and January 2012 with a SBIG ST-7XME CCD and B and V Johnson and R and I Cousins filters. The emission-line star KW97 42-41 was the first to be analyzed with DAOPHOT. After having discarded poorly guided or out of focus frames, we measured instrumental magnitudes on every frame (see Table 1) and then transformed them into standard BVR_cI_c magnitudes. We present here a rough light curve, that is, raw data plotted without any kind of interpolation (Figure 10). There seem to be changes of about 0.2 magnitude that could take place on a time scale as short as a few weeks. In addition, there may also be a longer term variability on a time scale of several months. We tried a more quantitative analysis using the phase dispersion minimization algorithm (Stellingwerf 1978) as implemented by the IRAF task "pdm". This method

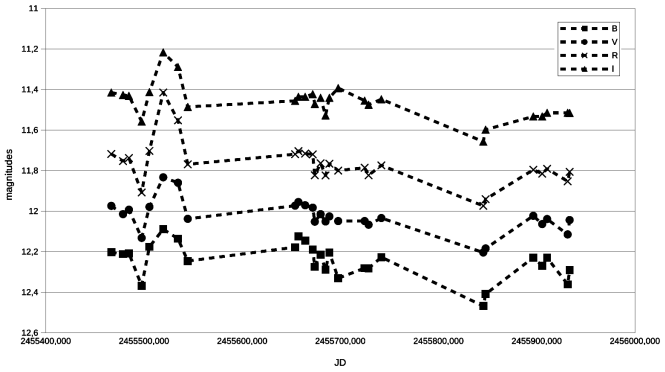

Figure 10. The light curve of KW97 42-41. Data: see Table 1.

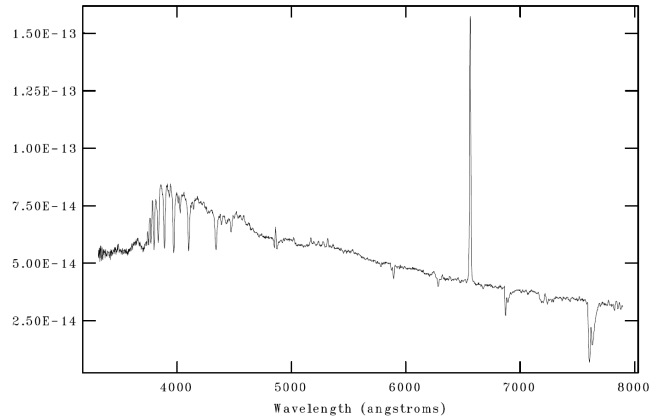

Figure 11. Optical spectrum of KW97 42-41. This is an average of two 1200-sec exposures, taken with a 300-lines mm^{-1} grating and a Boller and Chivens spectrometer attached to the Cassegrain focus of the 1.22-m "Galileo Galilei" telescope of the Asiago Astrophysical Observatory (Mount Pennar) of the Department of Physics and Astronomy of the University of Padova. Courtesy of Dr. Alessandro Siviero.

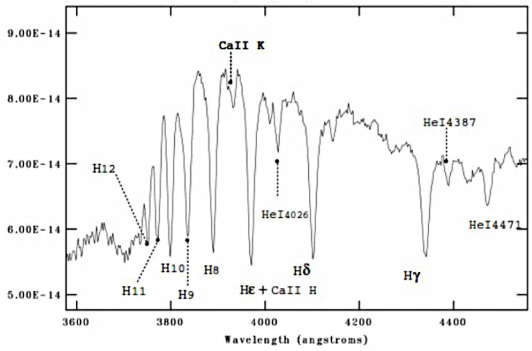

Figure 12. Blue side of the optical spectrum of KW97 42-41.

Table 2. Equivalent widths (in Å) of some absorption lines.

Star	*Hγ*	*HeI λ4026*	*HeI λ4471*
KW97 42-41	5.1	1.4	1.8
B2	5.1	1.5	1.4

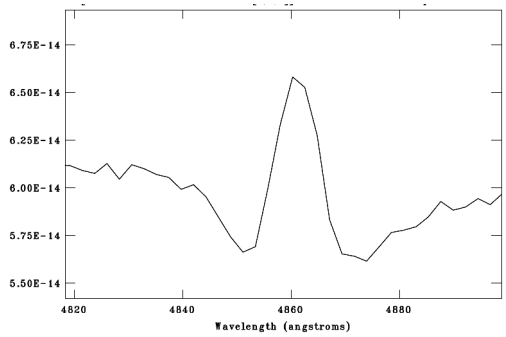

Figure 13: An enlargement around H showing its composite profile.

seems to confirm periodicities of about hundreds of days ($\simeq$ 225); however, it is important to take into consideration that the number of data available is just enough (28) to make a reliable estimate as specified in the help manual of the task. Moreover, to test the short term variability we would need much more data from close-up observations.

The mean color indexes (with a 3-sigma statistical uncertainty) are: B–V = 0.22 ± 0.09, V–R_c = 0.25 ± 0.06, and R_c–I_c = 0.32 ± 0.13. Since KW97 42-41 has a very low galactic latitude (l = 072.4949, b = +01.7511 J2000), these are not the true color indexes of the star as its light is heavily reddened by the interstellar medium. In order to have some more information on the physical nature of this star, we asked Dr. Alessandro Siviero of the Astrophysical Observatory of Asiago-Pennar to take a couple of medium-resolution spectra of this object (Figure 11). (Siviero 2016)

A strong Hα in emission and a remarkable Balmer series in absorption immediately stand out. Figure 12 shows an enlargement of the blue side of the optical spectrum of the star where it is possible to identify the Balmer series up to H12, the two H and K lines of the ionized calcium, and some remarkable neutral helium absorption lines. The following table shows the equivalent widths of the Hγ, HeI λ4026, and HeI λ4471 absorption lines of KW97 42-41 compared with the values given by Jaschek and Jaschek (1990; p.137). These values suggest that KW97 42-41 belongs to the B2 spectral type (Table 2).

The spectrum reveals not only Hα in emission but also a clear composite Hβ profile (Figure 13) where a strong emission is superimposed on a normal stellar absorption line. All this is consistent with the hypotheses that KW97 42-41 is a Be star seen pole-on (Kogure and Leung 2007).

Finally, we tried to estimate the absolute magnitude of the star. Green *et al.* (2016) implemented a three-dimensional map of the dust in the Milky Way on the website "3D Dust Mapping with Pan-STARRS 1" (http://argonaut.skymaps.info/). By giving the coordinates of an object, the website traces the interstellar reddening (E(B–V) vs. Distance Modulus) along that direction. We calculated a color excess value of 0.46 using the unreddened color index values given by Cox (2000, table 15.7, p. 388), which results in a distance modulus of 12. Knowing this and calculating a mean apparent visual magnitude of 12.1 from our data in Table 1, we obtained a visual absolute magnitude of 0.1 and a distance of 2.51 Kpc. Though fainter than a typical B2 main-sequence star (Cox 2000, Table 15.7, p. 388), the absolute magnitude is consistent with the classification of KW97 42-41 as an early-type emission line star.

References

Cox, A. N. (ed.), 2000, *Allens Astrophysical Quantities*, 4th ed., AIP Press, Springer, New York.

Davis, L. E. 1994, A Reference Guide to the IRAF/DAOPHOT Package (ftp://iraf.noao.edu/iraf/docs/daorefman.ps.Z).

Gary, B. L. 2002–2006, "CCD Transformation Equations for Use with Single Image (Differential) Photometry" (http://reductionism.net.seanic.net/CCD_TE/cte.html).

Green, G., Schlafly, E., and Finkbeiner, D. 2016, 3D Dust Mapping with Pan-STARRS 1 (argonaut.skymaps.info/).

Green, G. M., *et al.* 2015, *Astrophys. J.*, **810**, 25.

Jaschek, C., and Jaschek, M. 1990, *The Classication of Stars*, Cambridge Univ. Press, Cambridge.

Kogure, T., and Leung, K. 2007, *The Astrophysics of Emission-Line Stars*, Springer, Berlin.

Kohoutek, L., and Wehmeyer, R. 1997, *Abh. Hamburger Sternw.*, **11**, 2.

Massey, P., and Davis, L. E. 1992, A User's Guide to Stellar CCD photometry with IRAF (ftp://iraf.noao.edu/ftp/docs/daophot2.ps.Z).

Romanishin, W. 2006, An Introduction to Astronomical Photometry Using CCDs (http://www.physics.csbsju.edu/370/photometry/manuals/OU.edu_CCD_photometry_wrccd06.pdf).

Siviero, A. 2016, private communication.

Stellingwerf, R. F. 1978, *Astrophys. J.*, **224**, 953.

Stetson, P. B. 1987, *Publ. Astron. Soc. Pacific*, **99**, 191 (see also Stetson *et al.* 1990).

50 Forgotten Miras

Thomas Karlsson
Almers väg 19, 432 51 Varberg, Sweden, tkn@seaside.se

Hans Bengtsson
Sagogången 55, 422 45 Hisings Backa, hkibengtsson@gmail.com

Tomas Wikander
Bogservägen 8, 784 77 Borlänge, Sweden, wikander.tomas@gmail.com

Gustav Holmberg
Karl XI-gatan 8A, 222 20 Lund, Sweden, 5063.gustav.holmberg@gmail.com

Robert Wahlström
Klintens väg 6, 441 41 Alingsås, Sweden, robert.l.wahlstrom@gmail.com

Chris Allen
Jordgubbsgränd 3, 386 31 Färjestaden, Sweden, chris.allen@telia.com

Received August 10, 2016; revised August 25, 2015; accepted August 30, 2016

Abstract We report the results of 4 years observing of 50 poorly studied Mira stars. 247 maxima and 241 minima together with current period elements, ranges, and color indices for the stars are presented. "50 forgotten Miras" is an ongoing observing program run by the Variable star section of the Association of Swedish Amateur Astronomers (SAAF/V) that started in 2012.

1. Introduction

"50 forgotten Miras" is an observation program organized by the Variable star section of the Association of Swedish Amateur Astronomers (SAAF/V; Svensk AmatörAstronomisk Förening, Variabelsektionen) in which 50 poorly studied Mira stars have been observed since 2012-02-15.

During the 20th century, photographic patrol programs where run at several professional observatories (and also by many amateurs). Wide-angle photographic plates were analyzed with blink comparators in order to look for objects that moved or changed brightness. One of the results that came out of these large surveys was a large number of discoveries of new variable stars. They were entered into catalogues with some rudimentary data on periodicity, brightness, and so on, but in many cases they were then left behind. One gets the feeling that variables were discovered en masse in the photographic surveys but in many cases insufficiently followed after discovery. Many of the thousands of known Mira stars therefore have catalogue data that are derived from only old data.

The goal of this program is to revisit 50 of these Miras in order to provide modern data on their variations and update the data in the AAVSO International Variable Star Index (VSX, Watson *et al.* 2006–2016). The method is to observe the program stars regularly to establish light curves, and from the light curves to determine basic parameters such as period, range, and rise duration. V filter observations are most frequent, but some observations have been made in B and R, as well as a large number of visual observations.

The program stars were chosen by Hans Bengtsson following the criteria:

- Variable type is M or M: in GCVS4 (Kholopov 1985).
- Located in the northern hemisphere.
- No or only a few observations in AID (AAVSO International Database) in recent time.
- An estimated V magnitude of 11 to 12 or brighter at maximum.

After the observations began one of the stars had its type changed to SRA in VSX, the carbon star IV Peg.

We have also searched the literature for information on the discovery, history, and earlier observations of the stars. This information is published in a wiki (currently only in Swedish, at http://astronet.se/wiki/index.php/50_bortgl%C3%B6mda_Miror) together with the information in this article.

2. Observing

At the start of the program we contacted the AAVSO Chart and Sequence Team in order to get sequences of comparison stars. For the majority of the stars we swiftly got sequences. Four stars (GM Cam, CL Cyg, AM Dra, and IY Dra) lacked underlying data, at the start of the program, for generating charts. For these stars we used our own sequences with data from the Naval Observatory Merged Astrometric Dataset (NOMAD; Zacharias *et al.* 2011) or the fourth U.S. Naval Observatory CCD Astrograph Catalog (UCAC4; Zacharias *et al.* 2012) until AAVSO could generate sequences.

The program stars have then been observed by members of SAAF/V with different techniques and instruments. Some members used their own telescopes and observed the stars either visually or used photometrical filters and CCD imaging. Other members have used remote telescopes operated by iTelescope.net, the Bradford Robotic Telescope, Sierra Stars Observatory Network, and AAVSONet to take data.

AAVSO's online photometric tool VPHOT (Klingenberg and Henden 2013) was used to measure the stars on both the locally and remotely taken images. No transformation of the measured magnitudes was made. As several different persons, telescopes, filters, and cameras have been involved, one could expect some scatter in the derived magnitudes. By comparing V observations of the same star made within 2.5 days we estimate that the scatter on average are less than 0.1 magnitude with a maximum of 0.5 magnitude. As expected the scatter is lower when the stars are in their brightest phase. For the individual stars the average scatter is between 0.05 and 0.2 magnitude.

Up until 2016-07-01 12 persons have contributed a total of 8,690 observations; of these 98.7% were made by the authors. Of the observations 473 are visual, 1,027 are B, 5,710 are V, 1,471 are R, and 9 are I. From the light curves of the V observations maxima, minima, and range for the stars were recorded. We have also tried to do R and B observations evenly spread over the cycle of each star to see how the color indices B–V and V–R change with phase. Most stars have a good coverage in R over their whole phase, but due to the faintness we lack B observations of most stars at minimum.

In addition to the program stars, several other variables in the same fields were observed, many of them poorly studied in the past. We have made some analysis of these collateral catches. For example we discovered that V2331 Cyg is an eclipsing binary and not an L type variable, as the GCVS entry had (Bengtsson *et al.* 2013). We also found that the catalogue period for the RRAB star KR Lyr was wrong. A new period for the EA star GO Lac was calculated, and we were able to determine a new type and new elements for the stars AM Vul and DO Lac. These discoveries have been reported to VSX.

All observations are available in the Swedish variable observations database, SVO, at http://var.astronet.se. The vast majority are also reported to the AAVSO International Database.

3. Results

The results from our observations 2012–2016 of the 50 Miras are presented in the following tables and figures.

Table 1 shows date and magnitude for 247 maxima and 241 minima. These events were determined by manual examination of the light curves. Dates are JD – 2400000. Magnitudes are V. The O–C values (observed – calculated time of maximum) were calculated using the elements in Table 2. Dates followed by a colon are uncertain, and a double colon indicates very uncertain dates.

Table 2 shows period elements for the 50 stars. All stars have their recent elements listed; for most of the stars this means elements from all found maxima from 1996 forward. For some stars, those that have a fair amount of historical maxima obtained from the literature, elements from all their recorded maxima are also given. The elements were calculated from O–C diagrams so that a straight line fitted to the O–C values will be horizontal and cross the y-axis at zero.

The recent elements in Table 2 are based on all maxima from Table 1 together with maxima determined by us from the Northern Sky Variability Survey (NSVS, Woźniak *et al.* 2004) and the Third All Sky Automated Survey (ASAS-3, Pojmański *et al.* 2013). Also data from Association Française des Observateurs d'Étoiles Variables (AFOEV), Digital Access to a Sky Century @ Harvard (DASCH), the Kepler mission, and maxima published by some other sources were used, see notes under Table 2. A list of all maxima is published on the wiki. The first epoch for the recent elements is based on maxima from NSVS or ASAS-3 if available. For DU Aur, YZ Cam, V363 Cyg, WX Del, AU Gem, V393 Her, and V389 Lac no maximum was found in NSVS or ASAS-3; these stars have their first epoch based on maxima published by AFOEV or from other sources.

Miras are known to have random cycle-to-cycle variations of their period, some also show long-term modulations, and some, more rarely, have a steady decrease or increase in their periods (Willson and Marengo 2012). The size of the random variations is reflected in the O–C values in Table 1. To minimize the effects of the random variations when calculating the elements we chose to use maxima from the last 20 years for the recent elements. The differences in period between the recent elements and elements from all maxima are more likely due to long-term than random variations.

Rise% is the time from minimum to maximum in percentage of the period. This value is calculated only from the maxima in Table 1.

Table 3 shows spectral type from VSX together with V magnitude range and the color indices B–V and V–R from our observations 2012–2016. The color indices are calculated as follows. First, all B–V and V–R values were computed for all instances where there was a B and V or V and R observation from the same observer within one hour in time. All B–V and V–R were then grouped into ten bins of equal width after their period phase. For each bin the mean B–V and V–R was computed and then the mean of the means was determined as the value for the color indices.

The range of the bin means are listed within parentheses in Table 3. In general the variation in V–R is much stronger than the variation in B–V over the cycle. All stars have their lowest V–R value when they are at maximum in V, and their highest V–R value when at minimum. The variation patterns for B–V are more differentiated between the stars, although several stars seem to have the lowest B–V value just before maximum and the highest value after maximum. Figure 1 shows an example of how the color index varies during the cycle. Figure 2 shows color-color and period-color diagrams. The carbon star IV Peg is an outlier in both diagrams. For the rest there seems to be a positive correlation between period and color index, most pronounced for V–R.

We have also searched for humps in the light curves. The stars GS Cyg and V750 Cyg have a marked plateau on their rising branch, and hump events to a lesser degree are noticeable on V393 Her, V389 Lac, DT Ori, and IU Peg. Two other stars, EH Gem and V358 Lac, have a marked shoulder on their rising

Table 1. Maxima and minima of stars observed.

Star	*Magnitude*	*JD max. (2400000+)*	*O–C*	*Magnitude*	*JD min. (2400000+)*
YY Aur				<16.4	56150::
YY Aur	10.6	56290	–3	<16.6	56510::
YY Aur	11.3	56623	–7	<15.5	56825:
YY Aur	9.8	56962	–4	<16.7	57180:
YY Aur	11.0	57308	5		
DU Aur	>13.0	56080::	–18	16.7	56245
DU Aur	11.1	56365	–7	<16.4	56535::
DU Aur	11.8	56654	8	<16.3	56780:
DU Aur	10.8	56916	–5	17.0	57076
DU Aur	>13.0	57210::	15	17.5	57355
DU Aur	11.9	57470	1		
V483 Aur	12.3	56044	19	16.8	56190
V483 Aur	12.5	56337	9	16.2	56495:
V483 Aur	11.7	56626	–5	<16.6	56785:
V483 Aur	12.0	56931	–3	17.7	57080
V483 Aur	>12.7	57225::	–12	18.1	57400
TT Cam				17.0	56150::
TT Cam	10.8	56249	6	16.6	56390::
TT Cam	10.8	56505:	9	15.9	56642
TT Cam	10.3	56738	–11	15.8	56900:
TT Cam	10.8	57000	–1	15.6	57150:
TT Cam	10.0	57250:	–4	15.9	57405
UZ Cam				15.1	56090::
UZ Cam	10.7	56180:	–6	15.6	56300:
UZ Cam	10.9	56412	–6	<14.2	56540::
UZ Cam	>13.0	56640::	–10	15.4	56765
UZ Cam	10.5	56890	8	15.2	56985
UZ Cam	10.9	57120	6	15.5	57230:
UZ Cam	10.5	57350:	3	15.6	57468
YZ Cam				<14.5	56110::
YZ Cam	10.6	56303	4	<14.6	56480::
YZ Cam	10.3	56658	–1	16.2	56855:
YZ Cam	10.6	57011	–9	15.9	57215
YZ Cam	10.6	57375	–6		
GM Cam	>13.2	56040:	12	<17.0	56240::
GM Cam	>13.7	56410::	12	18.3	56585:
GM Cam	13.2	56775:	7	17.7	56940:
GM Cam	>13.0	57140:	2	18.1	57320
GM Cam	13.4	57485:	–24		
VZ CMi	11.3	56254	12	15.7	56386
VZ CMi	11.0	56525::	–1	16.0	56668
VZ CMi	>12.0	56810::	–1	16.0	56950:
VZ CMi	10.9	57090	–5	<14.2	57240:
VZ CMi	11.1	57375	–4		
TW Cep				<16.3	56050:
TW Cep	11.3	56161	3	<16.5	56335:
TW Cep	12.0	56437	–3	16.8	56580
TW Cep	11.2	56718	–4	16.9	56879
TW Cep	11.7	56992	–11	17.5	57171
TW Cep	11.7	57295	11	<16.2	57455:
AW Cep	10.9	56130	–4	15.6	56260
AW Cep	11.1	56373	–1	16.4	56505
AW Cep	11.5	56625	11	<15.8	56740
AW Cep	10.5	56850	–4	15.9	56988
AW Cep	11.1	57099	5	16.0	57221
AW Cep	10.9	57333	–2	<15.4	57460:
XY Cyg				15.3	56155
XY Cyg	10.7	56275	3	15.3	56459
XY Cyg	10.5	56581	9	14.9	56755
XY Cyg	10.4	56867	–4	14.7	57040
XY Cyg	10.5	57172	1	15.5	57355
XY Cyg	10.7	57474	4		
CL Cyg				<16.5	56250::
CL Cyg	11.5	56359	–11	<17.3	56580:
CL Cy	>13.0	56685::	11	18.0	56870
CL Cyg	12.5	56970	–8	17.6	57170
CL Cyg	13.0	57290	9	17.7	57485
GS Cyg	11.5	56221	–8	16.3	56435
GS Cyg	11.3	56632	–8	16.9	56864
GS Cyg	12.0	57060:	8	16.9	57280
GS Cyg	>12.1	57470:	7		
V363 Cyg				17.0	56230
V363 Cyg	11.7	56385	2	16.5	56576
V363 Cyg	10.3	56737	–7	16.7	56950
V363 Cyg	11.2	57100:	–5	16.8	57305
V363 Cyg	11.2	57470:	5		
V462 Cyg				13.6	56179
V462 Cyg	10.8	56380	–7	13.9	56555
V462 Cyg	10.0	56740	–10	13.7	56920
V462 Cyg	10.2	57115	2	14.1	57283
V462 Cyg	9.9	57475	–2		
V663 Cyg				16.3	56240
V663 Cyg	10.8	56370:	–5	16.4	56590
V663 Cyg	>11.9	56730:	–5	16.5	56965
V663 Cyg	>12.0	57100:	5	16.2	57320
V663 Cyg	11.0	57460:	4		
V673 Cyg	11.7	56030:	–17	17.0	56240
V673 Cyg	11.7	56374:	3	17.7	56570
V673 Cyg	11.8	56695:	–1	17.3	56880
V673 Cyg	11.7	57030	10	16.9	57215
V673 Cyg	11.6	57346	2		
V750 Cyg	11.4	56272	10	16.2	56494
V750 Cyg	11.2	56692:	–3	16.3	56910
V750 Cyg	11.6	57120	–7	16.2	57330:
V2072 Cyg	10.9	56143	–2	16.9	56310:
V2072 Cyg	10.4	56454	–8	17.9	56653:
V2072 Cyg	11.8	56779	0	17.5	56960
V2072 Cyg	11.5	57100:	4	17.6	57270
V2072 Cyg	10.9	57420:			
V2330 Cyg				17.0	56250
V2330 Cyg	11.4	56415	1	<17.3	56665:
V2330 Cyg	11.4	56795	–3	17.6	57050:
V2330 Cyg	11.6	57181	0	<17.5	57430:
WX Del				<16.5	56315:
WX Del	12.1	56505	0	17.3	56847
WX Del	10.5	57035:	1	<17.5	57380::
WZ Del	12.7	56144	–3	<17.0	56290:
WZ Del	12.4	56415	9	17.8	56560
WZ Del	12.6	56680::	14	17.9	56805:
WZ Del	12.4	56919	–7	<15.5	57065:

(Table 1 continued on following pages)

Table 1. Maxima and minima of stars observed, cont.

Star	*Magnitude*	*JD max. (2400000+)*	*O–C*	*Magnitude*	*JD min. (2400000+)*
WZ Del	12.7	57175	–10	<17.1	57320:
WZ Del	>14.0	57440::	–5		
AM Dra	9.9	56250	–7	16.5	56470
AM Dra	10.8	56581	–5	16.0	56805
AM Dra	10.0	56930	15	15.2	57111
AM Dra	9.3	57240	–5	15.5	57445
AN Dra	10.1	56060:	–1	15.2	56252:
AN Dra	10.3	56408	–5	14.9	56601
AN Dra	9.5	56767	2	14.9	56960
AN Dra	10.0	57115	–3	15.2	57320
AN Dra	9.8	57475	5		
IY Dra	11.4	56315:	–13	<17.5	56560:
IY Dra	12.0	56711	9	17.4	56920
IY Dra	11.2	57075	–1	18.4	57300
IY Dra	12.5	57453	3		
AU Gem				<15.6	56080::
AU Gem	11.0	56239	6	<15.5	56500::
AU Gem	12.0	56660	4	15.5	56900:
AU Gem	11.4	57085	6	15.1	57323
AU Gem	11.1	57485	–16		
EH Gem	12.3	56195:	12	15.9	56298
EH Gem	12.2	56430:	9	<15.6	56535::
EH Gem	12.1	56657	–1	<15.9	56780::
EH Gem	>12.4	56890::	–5	15.9	57000
EH Gem	12.4	57125	–7	<13.2	57240::
EH Gem	11.9	57364	–5	15.7	57480
VW Her				15.6	56295:
VW Her	11.2	56414	–1	16.2	56575
VW Her	10.8	56698	–3	16.6	56870
VW Her	11.8	56995:	9	16.4	57140
VW Her	11.0	57265	–7	17.2	57433
WX Her				15.0	56195
WX Her	11.8	56285:	15	15.3	56384
WX Her	11.9	56453	–3	15.3	56580:
WX Her	12.0	56650:	8	16.0	56735
WX Her	12.0	56833	5	16.2	56920
WX Her	11.9	57020:	6	15.7	57111
WX Her	12.0	57190	–10	15.5	57288:
WX Her	12.0	57370:	–16	15.2	57470
BI Her	12.1	56151	12	<15.5	56260:
BI Her	12.6	56348	0	17.4	56457
BI Her	12.4	56563	7	15.8	56678:
BI Her	12.6	56769	4	17.6	56875
BI Her	13.1	56973	–1	17.3	57090
BI Her	11.8	57173	–9	<17.2	57300:
BI Her	>13.0	57390:	–1	17.4	57493
CZ Her	11.2	56203	–7	16.3	56423
CZ Her	10.7	56519	–12	16.0	56737
CZ Her	11.1	56850	–3	16.2	57080
CZ Her	11.9	57194	19	<16.1	57390:
CZ Her	10.9	57500	3		
GP Her	11.3	56163	3	15.7	56290
GP Her	10.7	56420	3	16.0	56562
GP Her	11.0	56670	–4	15.8	56812
GP Her	10.5	56929	–1	15.7	57075
GP Her	11.0	57192	5	15.6	57322
GP Her	10.4	57450	7		
V393 Her				17.0	56180
V393 Her	12.2	56358	18	16.8	56615:
V393 Her	11.6	56760	–11	16.4	57025:
V393 Her	11.5	57190	–11	16.1	57450
TU Lac				16.1	56220
TU Lac	10.3	56354:	–6	17.0	56500:
TU Lac	10.7	56640	2	17.9	56780:
TU Lac	10.8	56924	7	16.9	57065:
TU Lac	10.5	57195:	–1	16.7	57340
TU Lac	>13.0	57470::	–4		
AS Lac	12.0	56176	5	16.5	56287
AS Lac	12.1	56375:	–15	16.9	56500
AS Lac	12.0	56609	1	<15.0	56710:
AS Lac	11.1	56815	–11	16.6	56950
AS Lac	12.2	57040	–4	17.5	57160:
AS Lac	12.7	57276	14	17.2	57374
AS Lac	>13.9	57490::	9		
V358 Lac				15.8	56185
V358 Lac	10.8	56340	–1	15.7	56516
V358 Lac	10.3	56671	3	15.7	56845
V358 Lac	10.4	56998	2	16.0	57160:
V358 Lac	10.4	57322	–2		
V389 Lac				13.6	56217
V389 Lac	11.1	56368	16	13.6	56470
V389 Lac	10.9	56616	1	<13.0	56725:
V389 Lac	11.3	56870	–9	13.5	56990
V389 Lac	11.0	57135:	–7	13.5	57260
V389 Lac	10.9	57397	–9	13.6	57520:
BI Lyr	11.8	56136	–16	<16.5	56295:
BI Lyr	12.1	56400	–6	16.9	56552
BI Lyr	12.1	56660:	0	17.5	56810
BI Lyr	11.6	56917	2	17.8	57060
BI Lyr	12.2	57174	5	17.7	57315
BI Lyr	12.2	57430:	6		
BK Lyr	11.9	55990:	10	16.3	56130
BK Lyr	11.7	56240	7	<16.2	56385:
BK Lyr	12.4	56494	8	16.6	56630
BK Lyr	11.7	56738	–1	16.1	56876
BK Lyr	12.0	56988	–4	16.3	57125
BK Lyr	11.4	57245	0	<16.3	57395:
BK Lyr	12.2	57487	–11		
EQ Lyr				17.0	56090
EQ Lyr	12.6	56225	–7	16.7	56382
EQ Lyr	11.8	56524	–7	<16.5	56690
EQ Lyr	12.5	56830	–1	17.3	56980:
EQ Lyr	12.6	57132	2	17.0	57285
EQ Lyr	12.2	57425	–5		
ER Lyr	10.5	56014	–3	14.4	56120
ER Lyr	10.6	56209	–6	15.4	56315:
ER Lyr	10.9	56415	2	15.0	56511
ER Lyr	10.3	56618	8	15.2	56710
ER Lyr	10.8	56813	5	15.5	56908
ER Lyr	10.6	57010	4	15.0	57105
ER Lyr	10.3	57200	–4	15.7	57303:
ER Lyr	>11.1	57395:	–6	15.1	57495

(Table 1 continued on next page)

Table 1. Maxima and minima of stars observed, cont.

Star	*Magnitude*	*JD max. (2400000+)*	*O–C*	*Magnitude*	*JD min. (2400000+)*
IX Lyr				17.6	56105
IX Lyr	12.2	56220	–2	17.3	56385
IX Lyr	11.2	56501	–7	17.3	56665:
IX Lyr	11.9	56790	–4	17.6	56955
IX Lyr	11.9	57085	5	17.2	57254
IX Lyr	12.1	57368	2		
KL Lyr				16.4	56040
KL Lyr	11.5	56154	–2	<16.0	56260:
KL Lyr	11.7	56365	–6	16.9	56480
KL Lyr	12.1	56587	0	17.1	56700:
KL Lyr	11.6	56820	18	16.7	56922
KL Lyr	>12.8	57030:	13	16.3	57139
KL Lyr	12.0	57225	–8	15.6	57350:
KL Lyr	11.5	57430:	–18		
OP Lyr	11.6	56150	8	<17.0	56335:
OP Lyr	12.6	56447	6	17.2	56630:
OP Lyr	11.5	56730	–9	17.3	56920
OP Lyr	12.1	57030:	–7	17.6	57220
OP Lyr	12.9	57335	–1		
AI Oph				<16.8	56215:
AI Oph	11.7	56427	11	16.2	56620:
AI Oph	11.9	56825	–5	16.0	57020:
AI Oph	11.2	57237	–7	16.8	57454
DT Ori	12.0	56247	–2	<15.6	56470::
DT Ori	11.0	56665	1	16.0	56880:
DT Ori	11.6	57085	6	16.1	57310:
DT Ori	11.0	57495	1		
IU Peg	11.2	56169	–17	<17.0	56475:
IU Peg	11.8	56640	10	17.1	56913
IU Peg	>12.8	57090::	16	16.7	57370
IU Peg	11.7	57520	2		
IV Peg	10.0	56244	6	11.6	56345:
IV Peg	9.7	56445	–7	11.4	56565
IV Peg	9.8	56665	–1	12.3	56770
IV Peg	10.1	56897	17	11.9	56985
IV Peg	>10.8	57100::	6	11.8	57200:
IV Peg	9.8	57305	–3	11.9	57410:
IV Peg	9.8	57520:	–2		
AC Vul				16.5	56244:
AC Vul	12.2	56365	1	17.0	56490
AC Vul	11.2	56607	9	<16.0	56730:
AC Vul	11.8	56843	11	16.2	56965
AC Vul	11.7	57065	–1	16.1	57205
AC Vul	11.2	57310	11	16.1	57430:
DX Vul				16.1	56165
DX Vul	11.4	56310:	1	16.0	56465
DX Vul	11.7	56604	–1	15.8	56760
DX Vul	11.1	56898	–4	<15.0	57050:
DX Vul	11.2	57201	3	16.0	57355
DX Vul	10.8	57500	6		

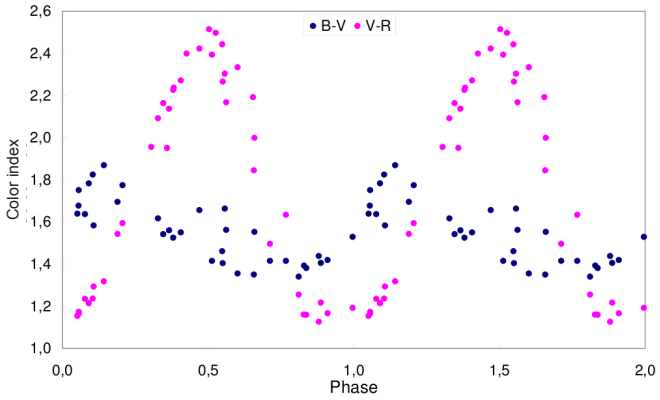

Figure 1. An example of a Phase-Color diagram for one star, UZ Cam.

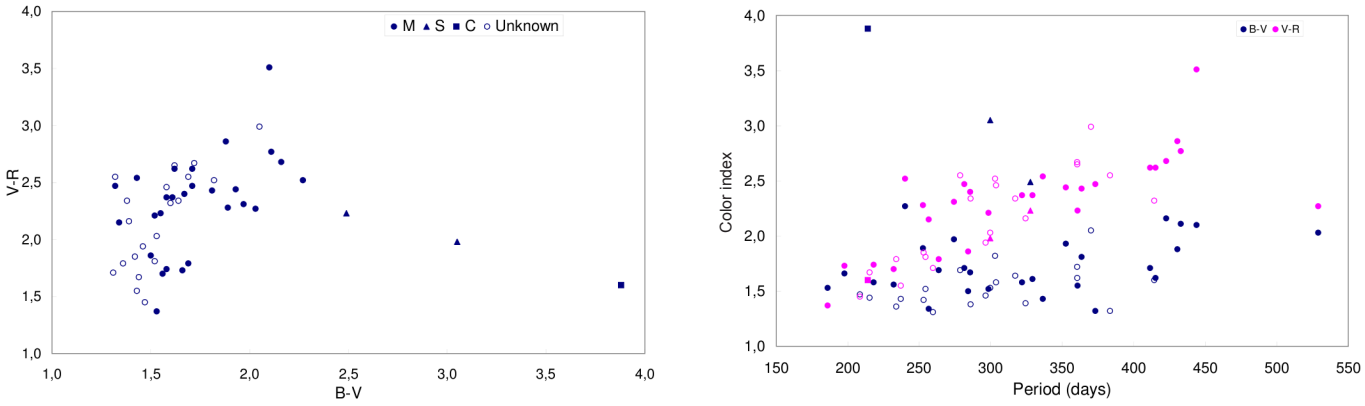

Figure 2. Color-Color and Period-Color diagrams. The shapes of the symbols in the right panel have the same meaning as in the left panel.

Table 2. Elements based on maxima from Table 1, NSVS, ASAS-3, and the other sources (see note at end of table).

		Recent elements			*Elements from all maxima*	
Star	*Source*	*Period*	*Epoch*	*Rise%*	*Period*	*Epoch*
YY Aur	1,7,8	336.4	2450911	38	337.3	2416494
DU Aur	1,7	274.3	2450886	45	275.5	2415054
V483 Aur		303.0	2451480	47		
TT Cam		252.6	2451444	40		
UZ Cam	9,10,11	232.1	2451312	49	232.3	2413630
YZ Cam	2	360.7	2431771	48		
GM Cam		370.1	2451587	49		
VZ CMi		284.2	2453116	49		
TW Cep		281.5	2451373	42		
AW Cep	3	240.1	2451332	47		
XY Cyg	1,2,9,12,13,14,15	299.6	2450280	40	300.0	2414879
CL Cyg		303.7	2451511	36		
GS Cyg	1	411.4	2451292	47		
V363 Cyg	1	360.5	2451697	44		
V462 Cyg	1,4,9,16	363.5	2450207	53	372.5	2412509
V663 Cyg		360.4	2451329	38		
V673 Cyg	17,18	324.3	2451507	42	327.0	2427916
V750 Cyg	1,19	432.9	2450201	47	433.4	2428093
V2072 Cyg		317.1	2451388	44		
V2330 Cyg		383.4	2451430	37		
WX Del	2	529.0	2430584	36		
WZ Del		259.6	2451474	45		
AM Dra		329.2	2451319	37		
AN Dra	3,9	352.5	2451478	45	354.7	2414206
IY Dra		373.8	2451469	41		
AU Gem	5,1	422.7	2435521	39	423.5	2416850
EH Gem		237.1	2452627	52		
VW Her		285.6	2451560	43		
WX Her		185.9	2451437	45		
BI Her		208.5	2451344	44		
CZ Her		321.9	2451381	34		
GP Her		256.6	2451285	47		
V393 Her	1	430.5	2450313	38		
TU Lac		278.6	2451345	49		
AS Lac		218.2	2451371	48		
V358 Lac	20	327.7	2451425	48	327.5	2437351
V389 Lac	1,6	263.6	2449498	55		
BI Lyr		254.4	2451318	43		
BK Lyr	1	253.0	2450667	43		
EQ Lyr	4	299.6	2451438	47		
ER Lyr	1,4,9	197.7	2450284	50	196.3	2414198
IX Lyr	1	285.9	2450504	42		
KL Lyr	1	215.3	2450343	48		
OP Lyr	1	298.4	2450771	37		
AI Oph		414.3	2451444	51		
DT Ori		415.2	2452927	47		
IU Peg		443.9	2451303	37		
IV Peg		214.0	2451530	51		
AC Vul		233.9	2451452	48		
DX Vul		296.4	2451270	48		

Note. Elements based on maxima from Table 1, NSVS, ASAS-3, and the following sources: 1) AFOEV; 2) Whitney 1960; 3) Rätz 2002; 4) Kepler; 5) Kukarkin 1957; 6) Dahlmark 1996; 7) Kurochkin 1951; 8) Splittgerber 1970; 9) DASCH; 10) Chernova 1951; 11) Fuhrmann 1981, 12) Wolf and Wolf 1905; 13) Graff 1921; 14) Beyer 1936; 15) Huth 1967; 16) Tramell 1987; 17) Rohlfs 1950; 18) Nikolaev 1988; 19) Wenzel 1953; 20) Romano and Perissinotto, 1975.

Table 3. Spectral type from VSX together with V magnitude range and the color indices B–V and V–R from our observations 2012–2016.

Star	*Sp.type*	*Maximum Magnitude*	*Minimum Magnitude*	*B–V*	*V–R*
YY Aur	M5e	9.8	<16.7	1.43 (1.4 – 1.5)	2.54 (1.5 – 3.5)
DU Aur	M6	10.8	17.5	1.97 (1.7 – 2.1)	2.31 (1.4 – 3.3)
V483 Aur		11.7	18.1	1.82 (1.6 – 2.0)	2.52 (1.6 – 3.5)
TT Cam	M0–M7	10.0	17.0	1.89 (1.8 – 2.0)	2.28 (1.4 – 3.0)
UZ Cam	M3	10.5	15.6	1.56 (1.4 – 1.8)	1.70 (1.2 – 2.4)
YZ Cam	M8	10.3	16.2	1.55 (1.3 – 1.8)	2.23 (1.5 – 2.9)
GM Cam		13.0	18.3	2.05 (2.0 – 2.1)	2.99 (2.1 – 3.3)
VZ CMi	M0	10.8	16.0	1.50 (1.3 – 1.7)	1.86 (1.3 – 2.3)
TW Cep	M6.5	11.2	17.5	1.71 (1.6 – 1.8)	2.47 (1.7 – 3.1)
AW Cep	M8	10.5	16.4	2.27 (2.1 – 2.5)	2.52 (1.8 – 3.2)
XY Cyg	S:e	10.4	15.5	3.05 (2.7 – 3.4)	1.98 (1.3 – 2.4)
CL Cyg		11.5	18.0	1.58 (1.5 – 1.7)	2.46 (1.9 – 3.2)
GS Cyg	M6e–M10e	11.3	16.9	1.71 (1.5 – 2.1)	2.62 (2.3 – 2.9)
V363 Cyg		10.3	17.0	1.62 (1.3 – 2.0)	2.65 (1.8 – 3.0)
V462 Cyg	M7e	9.9	14.1	1.81 (1.6 – 2.0)	2.43 (1.9 – 2.8)
V663 Cyg		10.8	16.5	1.72 (1.5 – 2.1)	2.67 (1.8 – 3.0)
V673 Cyg		11.6	17.7	1.39 (1.1 – 1.6)	2.16 (1.6 – 2.6)
V750 Cyg	M5ea	11.2	16.4	2.11 (1.9 – 2.4)	2.77 (2.1 – 3.2)
V2072 Cyg		10.4	17.9	1.64 (1.4 – 1.8)	2.34 (1.4 – 3.0)
V2330 Cyg		11.4	17.6	1.32 (1.2 – 1.5)	2.55 (1.7 – 3.0)
WX Del	M7	10.5	<17.5	2.03 (2.0 – 2.1)	2.27 (1.7 – 2.7)
WZ Del		12.4	17.9	1.31 (1.3 – 1.4)	1.71 (0.9 – 2.2)
AM Dra	M8	9.3	16.5	1.61 (1.4 – 1.8)	2.37 (1.6 – 3.0)
AN Dra	M5	9.5	15.2	1.93 (1.6 – 2.4)	2.44 (1.6 – 3.1)
IY Dra	M8.5	11.2	18.4	1.32 (1.1 – 1.7)	2.47 (1.5 – 3.2)
AU Gem	M10	11.0	<15.6	2.16 (1.7 – 2.9)	2.68 (2.2 – 3.0)
EH Gem		11.9	<15.9	1.43 (1.3 – 1.6)	1.55 (1.0 – 2.1)
VW Her	M3/4	10.2	17.2	1.67 (1.5 – 2.2)	2.40 (1.6 – 3.1)
WX Her	M1e	11.8	16.2	1.53 (1.2 – 1.9)	1.37 (0.9 – 1.8)
BI Her		11.8	17.6	1.47 (1.2 – 1.7)	1.45 (1.0 – 2.3)
CZ Her	M8/9	10.7	16.3	1.58 (1.4 – 2.0)	2.37 (1.6 – 3.0)
GP Her	M7/8	10.4	16.0	1.34 (1.2 – 1.5)	2.15 (1.4 – 2.8)
V393 Her	M8	11.5	17.0	1.88 (1.5 – 2.5)	2.86 (2.4 – 3.4)
TU Lac	M	10.3	17.9	1.69 (1.5 – 2.0)	2.55 (1.6 – 3.6)
AS Lac	M2	11.1	17.5	1.58 (1.4 – 1.7)	1.74 (1.1 – 2.6)
V358 Lac	S	10.3	16.0	2.49 (2.3 – 2.8)	2.23 (1.7 – 2.8)
V389 Lac	M7	10.9	13.6	1.69 (1.5 – 1.8)	1.79 (1.3 – 2.1)
BI Lyr		11.6	17.8	1.52 (1.4 – 1.6)	1.81 (1.0 – 2.7)
BK Lyr		11.4	16.6	1.42 (1.3 – 1.5)	1.85 (1.2 – 2.5)
EQ Lyr		11.8	17.3	1.53 (1.3 – 1.8)	2.03 (1.3 – 2.9)
ER Lyr	M5e	10.3	15.7	1.66 (1.5 – 1.9)	1.73 (1.1 – 2.4)
IX Lyr		11.2	17.6	1.38 (1.2 – 1.5)	2.34 (1.4 – 2.9)
KL Lyr		11.5	17.1	1.44 (1.3 – 1.6)	1.67 (1.1 – 2.4)
OP Lyr	M7:	11.5	17.6	1.52 (1.4 – 1.7)	2.21 (1.4 – 2.8)
AI Oph		11.2	<16.8	1.60 (1.5 – 1.8)	2.32 (1.6 – 3.1)
DT Ori	M10	11.0	16.1	1.62 (1.3 – 1.9)	2.62 (1.8 – 3.2)
IU Peg	M7	11.2	17.1	2.10 (1.9 – 2.2)	3.51 (3.1 – 3.7)
IV Peg	C5.2e	9.7	12.3	3.88 (3.3 – 4.2)	1.60 (1.3 – 1.9)
AC Vul		11.2	17.0	1.36 (1.1 – 1.6)	1.79 (1.1 – 2.6)
DX Vul		10.8	16.1	1.46 (1.2 – 1.6)	1.94 (1.4 – 2.7)

branch just before maximum. Thus, 8 out of 50 stars have humps, which is more or less the same proportion found in an earlier study, where 73 out of 450 miras (16 %) showed hump events (https://www.aavso.org/lpv-humps).

Two of the stars that have shown large variations in their period are UZ Cam and V462 Cyg (Karlsson 2013). The period for UZ Cam has varied from 240 days in 1948 to 224 days in 1975. For V462 Cyg the period has varied from 382 days in 1980 to 362 days in 2016.

4. Acknowledgements

We would thank the Chart and Sequence Team at AAVSO for their work on quickly developing charts and photometric sequences for the program stars; the organizations that run the remote telescopes at iTelescope.net, the Bradford Robotic Telescope, Sierra Stars Observatory Network, and AAVSONet; DC-3 Dreams and Bob Denny for ACP Expert that makes capturing lots of variable stars easy.

This research has made use of the AFOEV database, operated at CDS, France.

Some of the data presented in this paper were obtained from the Mikulski Archive for Space Telescopes (MAST). STScI is operated by the Association of Universities for Research in Astronomy, Inc., under NASA contract NAS5-26555. Support for MAST for non-HST data is provided by the NASA Office of Space Science via grant NNX09AF08G and by other grants and contracts.

This paper includes data collected by the Kepler mission. Funding for the Kepler mission is provided by the NASA Science Mission directorate.

We have also used data from DASCH, Digital Access to a Sky Century @ Harvard.

References

Bengtsson, H., Hallsten, P., Hemlin, A., Holmberg, G., Karlsson, T., Wahlström, R., and Wikander, T. 2013, *J. Amer. Assoc. Var. Star Obs.*, **41**, 264.

Beyer, M. 1936, *Astron. Nachr.*, **259**, 101.

Chernova, T. S. 1951, *Perem. Zvezdy*, **8**, 21.

Dahlmark, L. 1996, *Inf. Bull. Var. Stars*, No. 4329, 1.

Fuhrmann, B. 1981, *Mitt. Veränderl. Sterne*, **9**, 8.

Graff, K. 1921, *Astron. Nachr.*, **213**, 161.

Huth, H. 1967, *Mitt. Veränderl. Sterne*, **4**, 150.

Karlsson, T. 2013, *J. Amer. Assoc. Var. Star Obs.*, **41**, 348.

Kholopov, P. N., *et al.* 1985, *General Catalogue of Variable Stars*, 4th ed., Moscow.

Klingenberg, G., and Henden, A. A. 2013 VPHOT photometric analysis tool (http://www.aavso.org/vphot).

Kukarkin, B. V. 1957, *Perem. Zvezdy*, **12**, 33.

Kurochkin, N. E. 1951, *Perem. Zvezdy*, **8**, 351.

Nikolaev, S. E. 1988, *Perem. Zvezdy*, **22**, 781.

Pojmański, G., Szczygiel, D., and Pilecki, B. 2013, The All-Sky Automated Survey Catalogues (ASAS3; http://www.astrouw.edu.pl/asas/?page=catalogues).

Rätz, M. 2002, *BAV Mitt.*, **151**, 1.

Rohlfs, E. 1950, *Mitt. Veränderl. Sterne*, No. 121, 1.

Romano, G., and Perissinotto, M. 1975, *Mem. Soc. Astron. Italiana*, **46**, 259.

Splittgerber, E. 1970, *Mitt. Veränderl. Sterne*, **5**, 140.

Trammell, S. R. 1987, *J. Amer. Assoc. Var. Star Obs.*, **16**, 95.

Watson, C., Henden, A. A., and Price, C. A. 2014, AAVSO International Variable Star Index VSX (Watson+, 2006–2016; http://www.aavso.org/vsx).

Wenzel, W. 1953, *Astron. Nachr.*, **281**, 179.

Whitney, B. S. 1960, *Astron. J.*, **65**, 381.

Willson, L. A., and Marengo, M. 2012, *J. Amer. Assoc. Var. Star Obs.*, **40**, 516.

Wolf, M., and Wolf, G. 1905, *Astron. Nachr.*, **168**, 275.

Woźniak, P. R., *et al.* 2004, *Astron. J.*, **127**, 2436.

Zacharias, N., Finch, C., Girard, T., Henden, A., Bartlett, J., Monet, D., and Zacharias, M. 2012, The Fourth U.S. Naval Observatory CCD Astrograph Catalog (UCAC4; http://arxiv.org/abs/1212.6182).

Zacharias, N., Monet, D., Levine, S., Urban, S., Gaume, R., and Wycoff, G. 2011, The Naval Observatory Merged Astrometric Dataset (NOMAD, http://www.usno.navy.mil/USNO/astrometry/optical-IR-prod/nomad/the-nomad1-catalogue).

Recent Minima of 194 Eclipsing Binary Stars

Gerard Samolyk
P.O. Box 20677, Greenfield, WI 53220; gsamolyk@wi.rr.com

Received September 9, 2016; accepted September 9, 2016

Abstract This paper continues the publication of times of minima for eclipsing binary stars from observations reported to the AAVSO Eclipsing Binary section. Times of minima from CCD observations received by the author from February 2016 through July 2016 are presented.

1. Recent observations

The accompanying list contains times of minima calculated from recent CCD observations made by participants in the AAVSO's eclipsing binary program. This list will be web-archived and made available through the AAVSO ftp site at ftp://ftp.aavso.org/public/datasets/gsamoj442.txt. This list, along with the eclipsing binary data from earlier AAVSO publications, is also included in the Lichtenknecker database administrated by the Bundesdeutsche Arbeitsgemeinschaft für Veränderliche Sterne e. V. (BAV) at: http://www.bav-astro.de/LkDB/index.php?lang=en. These observations were reduced by the observers or the writer using the method of Kwee and Van Worden (1956). The standard error is included when available. Column F indicates the filter used. A "C" indicates a clear filter.

The linear elements in the *General Catalogue of Variable Star*s (GCVS; Kholopov *et al.* 1985) were used to compute the O–C values for most stars. For a few exceptions where the GCVS elements are missing or are in significant error, light elements from another source are used: AC CMi (Samolyk 2008), CW Cas (Samolyk 1992a), Z Dra (Danielkiewicz-Krosńiak amd Kurpińska-Winiarska 1996), DF Hya (Samolyk 1992b), DK Hya (Samolyk 1990), GU Ori (Samolyk 1985).

The light elements used for V471 Cas, MR Del, DE Lyn, HX UMa, KM UMa, and MS Vir are from Kreiner (2004).

The light elements used for LY And, V1713 Aql, V641 Aur, GW Boo, FV CVn, V2626 Cyg, PS Del, V1057 Her, V1097 Her, IZ Lac, AL Leo, VW LMi, FG Lyn, FI Lyn, V502 Oph, V2790 Ori, V1370 Tau, BX Tri, UY UMa, ES UMa, HN UMa, HV UMa, II UMa, and QT UMa are from Paschke (2014).

The light elements used for V560 Aur, V435 Gem, and V881 Per are from Nelson (2016).

The light elements used for V449 Aur, V610 Cyg, V2628 Cyg, V380 Gem, V383 Gem, V388 Gem, V485 Lac, V505 Lac, V740 Lyr, V736 Per, and V354 UMa are from the AAVSO VSX site (Watson *et al.* 2014). O–C values listed in this paper can be directly compared with values published in the AAVSO EB monographs.

References

Danielkiewicz-Krosńiak, E., and Kurpińska-Winiarska, M., eds. 1996, *Rocznik Astron.* (SAC 68), **68**, 1.

Kholopov, P. N., *et al.* 1985, *General Catalogue of Variable Stars*, 4th ed., Moscow.

Kreiner, J. M. 2004, "Up-to-date linear elements of eclipsing binaries," *Acta Astron.*, **54**, 207 (http://www.as.up.krakow.pl/ephem/).

Kwee, K. K., and van Woerden, H. 1956, *Bull. Astron. Inst. Netherlands*, **12**, 327.

Nelson, R. 2016, Eclipsing Binary O–C Files (http://www.aavso.org/bob-nelsons-o-c-files).

Paschke, A. 2014, "O–C Gateway" (http://var.astro.cz/ocgate/).

Samolyk, G. 1985, *J. Amer. Assoc. Var. Star Obs.*, **14**, 12.

Samolyk, G. 1990, *J. Amer. Assoc. Var. Star Obs.*, **19**, 5.

Samolyk, G. 1992, *J. Amer. Assoc. Var. Star Obs.*, **21**, 34.

Samolyk, G. 1992b, *J. Amer. Assoc. Var. Star Obs.*, **21**, 111.

Samolyk, G. 2008, *J. Amer. Assoc. Var. Star Obs.*, **36**, 171.

Watson, C., Henden, A. A., and Price, C. A. 2014, AAVSO International Variable Star Index VSX (Watson+, 2006–2016; http://www.aavso.org/vsx).

Table 1. Recent times of minima of stars in the AAVSO eclipsing binary program.

Star	*JD (min) Hel. 2400000 +*	*Cycle*	*O–C (day)*	*F*	*Observer*	*Error (day)*	*Star*	*JD (min) Hel. 2400000 +*	*Cycle*	*O–C (day)*	*F*	*Observer*	*Error (day)*
XZ And	57359.6236	24595	0.1797	V	S. Cook	0.0002	V346 Aql	57586.6837	14162	–0.0131	V	G. Samolyk	0.0002
AB And	57061.5627	63129	–0.0361	V	V. Petriew	0.0001	V1713 Aql	57233.7248	8937	–0.0210	V	B. Manske	0.0004
AB And	57581.7995	64696.5	–0.0403	V	K. Menzies	0.0001	SS Ari	57028.5967	44337	–0.3366	V	V. Petriew	0.0001
BD And	57573.8068	48847	0.0182	V	G. Samolyk	0.0002	AP Aur	57473.6161	26397.5	1.5804	V	G. Samolyk	0.0001
CN And	57046.5729	33426	–0.1399	V	V. Petriew	0.0003	EP Aur	57027.6271	51976	0.0133	V	V. Petriew	0.0001
LY And	57430.4926	34075	0.0263	V	K. Menzies	0.0002	IM Aur	57049.5826	13256	–0.1197	V	V. Petriew	0.0001
LY And	57437.5656	34095.5	0.0262	V	K. Menzies	0.0003	LY Aur	57088.7041	4504	0.0058	V	V. Petriew	0.0002
OO Aql	57542.8497	37352	0.0642	V	G. Samolyk	0.0001	V402 Aur	57066.6405	4890	0.0270	V	V. Petriew	0.0008
OO Aql	57585.4200	37436	0.0643	V	L. Corp	0.0001	V404 Aur	57064.6557	6050	0.0030	V	V. Petriew	0.0024
OO Aql	57586.6859	37438.5	0.0632	V	N. Simmons	0.0001	V449 Aur	57090.5817	12208.5	–0.1719	V	V. Petriew	0.0007

Table continued on following pages

Table 1. Recent times of minima of stars in the AAVSO eclipsing binary program, cont.

Star	*JD (min) Hel. 2400000 +*	*Cycle*	*O–C (day)*	*F*	*Observer*	*Error (day)*
V449 Aur	57357.9682	12588.5	–0.1716	V	V. Petriew	0.0002
V449 Aur	57360.7817	12592.5	–0.1728	V	V. Petriew	0.0004
V560 Aur	57027.7762	220	–0.0111	V	V. Petriew	0.0006
V585 Aur	57029.6175	10140	0.0399	V	V. Petriew	0.0003
V641 Aur	57430.6675	12193	–0.0010	V	K. Menzies	0.0001
SU Boo	57493.7774	23329	0.0258	V	B. Manske	0.0002
TU Boo	57511.8008	75382.5	–0.1529	V	G. Samolyk	0.0001
TU Boo	57559.6330	75530	–0.1530	V	G. Samolyk	0.0001
TY Boo	57526.6686	72667	0.0717	V	G. Samolyk	0.0001
TY Boo	57526.8290	72667.5	0.0735	V	G. Samolyk	0.0001
TY Boo	57559.6526	72771	0.0723	V	G. Samolyk	0.0001
TZ Boo	57473.7701	60037.5	0.0647	V	G. Samolyk	0.0002
TZ Boo	57527.7030	60219	0.0627	V	G. Samolyk	0.0002
TZ Boo	57527.8538	60219.5	0.0649	V	G. Samolyk	0.0003
TZ Boo	57549.6899	60293	0.0596	V	S. Cook	0.0007
TZ Boo	57559.6493	60326.5	0.0641	V	G. Samolyk	0.0001
UW Boo	57530.6352	15055	0.0011	V	G. Samolyk	0.0001
UW Boo	57542.6910	15067	0.0004	V	S. Cook	0.0004
VW Boo	57495.7435	76893.5	–0.2530	V	G. Samolyk	0.0001
VW Boo	57511.6614	76940	–0.2532	V	N. Simmons	0.0001
VW Boo	57524.6707	76978	–0.2522	V	G. Samolyk	0.0001
ZZ Boo	57494.6881	3792	0.0757	V	G. Samolyk	0.0001
AD Boo	57526.6652	15557	0.0346	V	G. Samolyk	0.0001
AD Boo	57557.6966	15587	0.0340	V	G. Samolyk	0.0001
EF Boo	57502.6881	11896	0.0183	V	B. Harris	0.0001
ET Boo	57088.8269	3265.5	–0.0112	V	V. Petriew	0.0003
GW Boo	57498.7097	8861.5	0.0000	V	K. Menzies	0.0002
i Boo	57552.7058	66090.5	0.1288	V	S. Cook	0.0013
WY Cnc	57470.3564	37520	–0.0413	V	L. Corp	0.0003
AC Cnc	57446.7095	43785	–0.0147	V	B. Harris	0.0001
FV CVn	57112.8928	12897.5	0.0007	V	V. Petriew	0.0003
R CMa	57468.6640	11602	0.1213	V	S. Cook	0.0030
R CMa	57476.6118	11609	0.1175	V	G. Samolyk	0.0001
RT CMa	57425.6086	23807	–0.7684	V	G. Samolyk	0.0001
SX CMa	57419.7785	18054	0.0177	V	G. Samolyk	0.0001
TZ CMa	57430.6267	15855	–0.2206	V	G. Samolyk	0.0001
UU CMa	57421.7480	5919	–0.0840	V	G. Samolyk	0.0001
XZ CMi	57090.5968	25304	–0.0005	B	G. Lubcke	0.0001
XZ CMi	57090.5968	25304	–0.0004	V	G. Lubcke	0.0001
XZ CMi	57090.5973	25304	0.0000	Ic	G. Lubcke	0.0001
XZ CMi	57428.6228	25888	0.0008	V	G. Samolyk	0.0001
XZ CMi	57458.7214	25940	0.0013	V	S. Cook	0.0004
AC CMi	57445.6882	6304	0.0038	V	G. Samolyk	0.0002
AM CMi	57476.6355	31625	0.2252	V	G. Samolyk	0.0002
CW Cas	57596.6548	50067	–0.0991	V	G. Samolyk	0.0001
CW Cas	57596.8143	50067.5	–0.0990	V	G. Samolyk	0.0002
IV Cas	57568.7786	16739	–0.1200	V	G. Samolyk	0.0001
V380 Cas	57595.6420	23540	–0.0694	V	G. Samolyk	0.0002
V471 Cas	57310.6561	11998	0.0048	V	G. Lubcke	0.0002
V471 Cas	57310.6563	11998	0.0050	Ic	G. Lubcke	0.0004
V471 Cas	57310.6572	11998	0.0058	B	G. Lubcke	0.0017
V471 Cas	57311.6578	12000.5	0.0041	V	G. Lubcke	0.0003
V471 Cas	57311.6578	12000.5	0.0041	Ic	G. Lubcke	0.0004
V471 Cas	57311.6583	12000.5	0.0046	B	G. Lubcke	0.0008
V471 Cas	57334.7125	12058	0.0050	B	G. Lubcke	0.0006
V471 Cas	57334.7126	12058	0.0050	V	G. Lubcke	0.0013
V471 Cas	57334.7127	12058	0.0051	Ic	G. Lubcke	0.0001
V471 Cas	57335.5143	12060	0.0049	V	G. Lubcke	0.0019
V471 Cas	57335.5143	12060	0.0049	B	G. Lubcke	0.0002
V471 Cas	57361.5751	12125	0.0048	V	G. Lubcke	0.0006
V471 Cas	57361.5755	12125	0.0052	Ic	G. Lubcke	0.0005
SU Cep	57560.8224	34652	0.0065	V	G. Samolyk	0.0001
WZ Cep	57542.8404	70673.5	–0.1632	V	G. Samolyk	0.0001
WZ Cep	57586.6690	70778.5	–0.1666	V	G. Samolyk	0.0002
ZZ Cep	57221.8340	13677	–0.0156	V	N. Simmons	0.0003
ZZ Cep	57538.8188	13825	–0.0172	V	N. Simmons	0.0002
ZZ Cep	57568.8047	13839	–0.0165	V	N. Simmons	0.0003
DK Cep	57569.8096	24322	0.0311	V	G. Samolyk	0.0001
DL Cep	57588.6475	14500	0.0650	V	G. Samolyk	0.0004
EG Cep	57538.8174	27440	0.0119	V	G. Samolyk	0.0001
EG Cep	57573.6735	27504	0.0122	V	N. Simmons	0.0001
RW Com	57124.7340	72056.5	0.0029	V	B. Manske	0.0001
RW Com	57445.8667	73409.5	0.0066	V	G. Samolyk	0.0002
RW Com	57524.6658	73741.5	0.0068	V	N. Simmons	0.0001
RW Com	57530.7175	73767	0.0062	V	R. Sabo	0.0001
RZ Com	57490.6333	66921	0.0508	V	N. Simmons	0.0001
RZ Com	57493.6801	66930	0.0510	V	G. Samolyk	0.0002
RZ Com	57493.8487	66930.5	0.0504	V	G. Samolyk	0.0001
RZ Com	57562.7331	67134	0.0488	V	S. Cook	0.0005
SS Com	57473.8100	78660.5	0.8828	V	G. Samolyk	0.0002
SS Com	57538.6233	78817.5	0.8877	V	G. Samolyk	0.0001
CC Com	57445.8907	81166.5	–0.0252	V	G. Samolyk	0.0002
CC Com	57494.6615	81387.5	–0.0261	V	N. Simmons	0.0001
U CrB	57511.6976	11808	0.1325	V	G. Samolyk	0.0001
TW CrB	57542.6470	33359	0.0555	V	G. Samolyk	0.0001
TW CrB	57575.6223	33415	0.0539	V	K. Menzies	0.0001
W Crv	57419.9457	45795	0.0181	V	G. Samolyk	0.0001
RV Crv	57513.6643	22060	–0.1010	V	G. Samolyk	0.0002
SX Crv	57513.6415	52100.5	–0.8435	V	G. Samolyk	0.0003
ZZ Cyg	57497.8109	19881	–0.0695	V	B. Harris	0.0001
BR Cyg	57596.8644	12050	0.0010	V	G. Samolyk	0.0001
CG Cyg	57564.8205	28741	0.0749	V	G. Samolyk	0.0001
CG Cyg	57573.6556	28755	0.0740	V	G. Samolyk	0.0001
DK Cyg	57541.8296	41518	0.1155	V	G. Samolyk	0.0001
DK Cyg	57600.6658	41643	0.1154	V	G. Samolyk	0.0001
KR Cyg	57573.6791	33683	0.0214	V	G. Samolyk	0.0001
KR Cyg	57589.7367	33702	0.0211	V	R. Sabo	0.0001
KV Cyg	57588.6818	9905	0.0612	V	G. Samolyk	0.0003
V387 Cyg	57543.8809	46142	0.0208	V	R. Sabo	0.0001
V401 Cyg	57246.6847	23015	0.0789	B	G. Lubcke	0.0004
V401 Cyg	57246.6853	23015	0.0794	V	G. Lubcke	0.0002
V401 Cyg	57246.6858	23015	0.0800	Ic	G. Lubcke	0.0002
V401 Cyg	57255.7179	23030.5	0.0798	V	G. Lubcke	0.0002
V401 Cyg	57255.7186	23030.5	0.0805	Ic	G. Lubcke	0.0002
V401 Cyg	57255.7190	23030.5	0.0810	B	G. Lubcke	0.0002
V401 Cyg	57265.6232	23047.5	0.0789	V	G. Lubcke	0.0011
V401 Cyg	57265.6258	23047.5	0.0815	Ic	G. Lubcke	0.0010
V401 Cyg	57265.6280	23047.5	0.0837	B	G. Lubcke	0.0009
V401 Cyg	57279.6107	23071.5	0.0811	V	G. Lubcke	0.0001
V401 Cyg	57279.6108	23071.5	0.0812	Ic	G. Lubcke	0.0001
V401 Cyg	57279.6110	23071.5	0.0813	B	G. Lubcke	0.0002
V401 Cyg	57557.8603	23549	0.0809	V	G. Samolyk	0.0002
V456 Cyg	57596.6333	14234	0.0505	V	G. Samolyk	0.0002
V466 Cyg	57568.6857	20692	0.0070	V	N. Simmons	0.0001
V488 Cyg	57573.6545	50629.5	–0.2494	V	G. Samolyk	0.0005
V548 Cyg	57531.8148	7243	0.0164	V	G. Samolyk	0.0002
V610 Cyg	57254.7327	0	–0.0013	V	V. Petriew	0.0005
V836 Cyg	57198.7553	18893.5	0.0216	V	V. Petriew	0.0007
V2551 Cyg	57559.8194	25164.5	–0.0509	V	K. Menzies	0.0001
V2626 Cyg	57194.8436	28652.5	–0.0292	V	V. Petriew	0.0005
V2628 Cyg	57194.8061	38354.5	0.0073	V	V. Petriew	0.0001
TY Del	57581.7866	12276	0.0679	V	K. Menzies	0.0001
YY Del	57573.8315	18427	0.0095	V	G. Samolyk	0.0001
MR Del	57598.5207	9772.5	–0.0074	V	L. Corp	0.0001
PS Del	57590.7989	6181	–0.0036	V	K. Menzies	0.0002
Z Dra	57140.6155	5375	–0.0024	Ic	G. Lubcke	0.0001
Z Dra	57140.6155	5375	–0.0024	B	G. Lubcke	0.0001
Z Dra	57140.6156	5375	–0.0023	V	G. Lubcke	0.0001
Z Dra	57573.6395	5694	–0.0004	V	G. Samolyk	0.0001
RZ Dra	57530.8023	24240	0.0659	V	G. Samolyk	0.0001
TW Dra	57586.6814	4792	–0.0244	V	G. Samolyk	0.0001
AI Dra	57588.7244	11926	0.0345	V	G. Samolyk	0.0002

Table continued on following pages

Table 1. Recent times of minima of stars in the AAVSO eclipsing binary program, cont.

Star	JD (min) Hel. 2400000 +	Cycle	O–C (day)	F	Observer	Error (day)	Star	JD (min) Hel. 2400000 +	Cycle	O–C (day)	F	Observer	Error (day)
YY Eri	57431.6025	49300.5	0.1561	V	G. Samolyk	0.0001	RY Lyn	57495.5972	10180	–0.0236	V	G. Samolyk	0.0001
WW Gem	57445.7339	25417	0.0347	V	G. Samolyk	0.0002	SW Lyn	57046.7274	20295	0.0707	V	V. Petriew	0.0001
V380 Gem	57454.6106	17352	0.0227	V	K. Menzies	0.0001	SW Lyn	57504.6639	21006	0.0781	V	B. Harris	0.0001
V383 Gem	57467.5963	5443	–0.0040	V	K. Menzies	0.0002	DE Lyn	57032.7707	11087	–0.0079	V	V. Petriew	0.0001
V388 Gem	57424.5734	9697	0.0065	V	K. Menzies	0.0001	DE Lyn	57436.6787	12075	–0.0125	V	K. Menzies	0.0002
V388 Gem	57484.5631	9796	0.0077	V	K. Menzies	0.0001	DE Lyn	57459.5720	12131	–0.0131	V	K. Menzies	0.0002
V435 Gem	57075.6819	1186	–0.0018	V	V. Petriew	0.0002	FG Lyn	57031.8084	3878	0.1224	V	V. Petriew	0.0005
V435 Gem	57075.8495	1186.5	–0.0025	V	V. Petriew	0.0002	FI Lyn	57026.9292	14596	–0.0004	V	V. Petriew	0.0001
RX Her	57586.6398	13728	–0.0001	V	G. Samolyk	0.0001	EW Lyr	57556.7701	15937	0.2746	V	G. Samolyk	0.0001
SZ Her	57526.7681	19145	–0.0286	V	N. Simmons	0.0001	FL Lyr	57493.8609	8848	–0.0017	V	G. Samolyk	0.0001
TT Her	57485.9135	19176	0.0465	V	R. Sabo	0.0002	FL Lyr	57530.8892	8865	–0.0021	V	R. Sabo	0.0001
TT Her	57560.7029	19258	0.0457	V	N. Simmons	0.0001	V740 Lyr	57214.8540	13267.5	0.0084	V	V. Petriew	0.0003
TT Her	57562.5274	19260	0.0460	V	L. Corp	0.0004	V740 Lyr	57223.7294	13294.5	0.0086	V	V. Petriew	0.0003
TT Her	57581.6811	19281	0.0462	V	K. Menzies	0.0001	V740 Lyr	57223.8932	13295	0.0080	V	V. Petriew	0.0003
TU Her	57531.7400	5942	–0.2390	V	G. Samolyk	0.0001	AT Mon	57446.5841	15199	0.0091	V	G. Samolyk	0.0001
UX Her	57575.6360	11559	0.1246	V	K. Menzies	0.0001	BB Mon	57422.6697	41956	–0.0040	V	G. Samolyk	0.0001
AK Her	57172.8492	35553	0.0172	V	V. Petriew	0.0002	BB Mon	57444.6516	41986	–0.0030	V	R. Sabo	0.0002
AK Her	57572.4521	36501	0.0172	V	L. Corp	0.0003	BO Mon	57419.6395	6252	–0.0286	V	G. Samolyk	0.0001
CC Her	57476.8677	10270	0.2861	V	G. Samolyk	0.0001	SX Oph	57527.8300	11694	–0.0016	V	G. Samolyk	0.0002
CT Her	57560.6480	8418	0.0129	V	G. Samolyk	0.0001	V501 Oph	57600.6820	27573	–0.0094	V	G. Samolyk	0.0001
LT Her	57537.7255	15481	–0.1469	V	R. Sabo	0.0003	V502 Oph	57596.4237	20063	0.0013	V	L. Corp	0.0003
V1057 Her	56810.7692	5845	0.0001	C	G. Frey	0.0003	V502 Oph	57598.4594	20067.5	–0.0032	V	L. Corp	0.0001
V1097 Her	57227.6847	13203	0.0016	V	B. Manske	0.0001	V508 Oph	57490.8965	35988	–0.0256	V	R. Sabo	0.0001
WY Hya	57430.8167	23547	0.0361	V	G. Samolyk	0.0001	V508 Oph	57523.6519	36083	–0.0255	V	B. Harris	0.0001
AV Hya	57431.7260	30375	–0.1133	V	G. Samolyk	0.0002	V508 Oph	57538.8219	36127	–0.0263	V	G. Samolyk	0.0001
DF Hya	57429.6222	44288	0.0016	V	G. Samolyk	0.0001	V508 Oph	57564.6817	36202	–0.0260	V	N. Simmons	0.0001
DI Hya	57425.7557	42673	–0.0317	V	G. Samolyk	0.0001	V508 Oph	57579.5088	36245	–0.0249	V	L. Corp	0.0001
DK Hya	57427.7508	27943	0.0027	V	G. Samolyk	0.0001	V839 Oph	57530.8153	41766	0.3039	V	G. Samolyk	0.0002
SW Lac	57262.8452	37377	–0.0876	V	V. Petriew	0.0001	V839 Oph	57596.6642	41927	0.3045	V	G. Samolyk	0.0001
SW Lac	57538.8286	38237.5	–0.0845	V	G. Samolyk	0.0001	V1010 Oph	57493.8992	28055	–0.1799	V	G. Samolyk	0.0001
CM Lac	57579.6399	19040	–0.0042	V	N. Simmons	0.0001	V1010 Oph	57560.7017	28156	–0.1814	V	G. Samolyk	0.0001
IZ Lac	57259.8594	30655.5	0.0103	V	V. Petriew	0.0010	EQ Ori	57428.7643	14885	–0.0371	V	G. Samolyk	0.0001
IZ Lac	57267.8461	30665.5	0.0078	V	V. Petriew	0.0009	GU Ori	57427.7299	30504.5	–0.0617	V	R. Sabo	0.0001
IZ Lac	57275.8346	30675.5	0.0072	V	V. Petriew	0.0031	GU Ori	57473.6221	30602	–0.0609	V	G. Samolyk	0.0002
IZ Lac	57278.6275	30679	0.0038	V	V. Petriew	0.0010	V2790 Ori	57459.5788	20629	0.0015	V	K. Menzies	0.0001
IZ Lac	57283.8247	30685.5	0.0080	V	V. Petriew	0.0008	BB Peg	57579.8358	38217	–0.0234	V	G. Samolyk	0.0001
V342 Lac	57259.6968	33398.5	–0.0496	V	V. Petriew	0.0004	BX Peg	56922.7233	45387	–0.1126	V	B. Manske	0.0001
V342 Lac	57260.7489	33400	–0.0484	V	V. Petriew	0.0005	BX Peg	57227.8163	46475	–0.1175	V	B. Manske	0.0001
V342 Lac	57267.7549	33410	–0.0481	V	V. Petriew	0.0005	BX Peg	57596.8471	47791	–0.1205	V	G. Samolyk	0.0002
V342 Lac	57272.6598	33417	–0.0473	V	V. Petriew	0.0022	XZ Per	57392.6574	12057	–0.0726	B	G. Lubcke	0.0001
V342 Lac	57275.8098	33421.5	–0.0499	V	V. Petriew	0.0004	XZ Per	57392.6574	12057	–0.0726	Ic	G. Lubcke	0.0001
V342 Lac	57276.8633	33423	–0.0473	V	V. Petriew	0.0004	XZ Per	57392.6574	12057	–0.0726	V	G. Lubcke	0.0001
V342 Lac	57283.8677	33433	–0.0487	V	V. Petriew	0.0004	IT Per	57365.7513	18245	–0.0216	V	S. Cook	0.0006
V485 Lac	57258.8790	0	0.0030	V	V. Petriew	0.0004	V736 Per	57421.5579	2321	0.0064	V	K. Menzies	0.0003
V485 Lac	57259.7587	1.5	0.0139	V	V. Petriew	0.0005	V873 Per	57301.8149	20111.5	–0.0199	V	V. Petriew	0.0001
V485 Lac	57267.8726	15.5	0.0185	V	V. Petriew	0.0006	V873 Per	57301.9611	20112	–0.0212	V	V. Petriew	0.0001
V485 Lac	57275.6781	29	0.0044	V	V. Petriew	0.0014	V881 Per	57031.6675	138	–0.0052	V	V. Petriew	0.0002
V485 Lac	57276.8337	31	0.0015	V	V. Petriew	0.0004	V881 Per	57310.7746	858.5	–0.0039	V	V. Petriew	0.0013
V485 Lac	57278.8734	34.5	0.0139	V	V. Petriew	0.0005	V881 Per	57310.9655	859	–0.0068	V	V. Petriew	0.0002
V485 Lac	57283.7879	43	0.0049	V	V. Petriew	0.0004	UZ Pup	57473.5854	16179	–0.0105	V	G. Samolyk	0.0001
V505 Lac	57284.6478	10150	–0.0798	V	V. Petriew	0.0003	V1968 Sgr	57225.7380	34452	–0.0166	V	G. Samolyk	0.0001
V505 Lac	57285.7923	10153.5	–0.0798	V	V. Petriew	0.0003	V1968 Sgr	57524.8241	34983	–0.0162	V	G. Samolyk	0.0002
V505 Lac	57285.9559	10154	–0.0798	V	V. Petriew	0.0003	RS Ser	57526.8089	37792	0.0501	V	G. Samolyk	0.0001
Y Leo	57476.8417	7141	–0.0637	V	G. Samolyk	0.0001	CC Ser	57430.9254	38659	1.0717	V	G. Samolyk	0.0002
UV Leo	57040.9949	30996	0.0407	V	V. Petriew	0.0001	CC Ser	57530.7795	38852.5	1.0786	V	N. Simmons	0.0002
UV Leo	57518.6626	31792	0.0409	V	S. Cook	0.0003	CC Ser	57597.6069	38982	1.0832	V	K. Menzies	0.0002
XY Leo	57512.6891	43781	0.1521	V	S. Cook	0.0007	V384 Ser	57225.6858	18086	–0.0044	V	B. Manske	0.0002
XZ Leo	57439.9934	25453.5	0.0700	V	R. Sabo	0.0003	EQ Tau	57034.6058	49279	–0.0309	V	V. Petriew	0.0001
AL Leo	57083.6309	5767	–0.0045	V	V. Petriew	0.0002	V1370 Tau	57032.5954	18830	–0.0007	V	V. Petriew	0.0002
AM Leo	57057.9915	39816	0.0132	V	V. Petriew	0.0001	V1370 Tau	57467.5970	20302	–0.0002	V	K. Menzies	0.0003
AM Leo	57460.5510	40916.5	0.0127	V	L. Corp	0.0002	BX Tri	57304.7911	30901.5	–0.0092	V	V. Petriew	0.0005
RT LMi	57037.8361	32101.5	–0.0088	V	V. Petriew	0.0001	W UMa	57032.9215	33771	–0.0887	V	V. Petriew	0.0001
VW LMi	57045.7340	17894.5	0.0150	V	V. Petriew	0.0002	W UMa	57092.6413	33950	–0.0899	V	G. Lubcke	0.0003
VW LMi	57045.9717	17895	0.0139	V	V. Petriew	0.0002	W UMa	57092.6414	33950	–0.0899	Ic	G. Lubcke	0.0001
VW LMi	57136.7080	18085	0.0156	V	V. Petriew	0.0003	W UMa	57092.6415	33950	–0.0897	B	G. Lubcke	0.0002
RR Lep	57421.6108	29543	–0.0406	V	G. Samolyk	0.0001	W UMa	57471.6480	35086	–0.0955	V	S. Cook	0.0004

Table continued on next page

Table 1. Recent times of minima of stars in the AAVSO eclipsing binary program, cont.

Star	*JD (min) Hel. 2400000 +*	*Cycle*	*O–C (day)*	*F*	*Observer*	*Error (day)*	*Star*	*JD (min) Hel. 2400000 +*	*Cycle*	*O–C (day)*	*F*	*Observer*	*Error (day)*
W UMa	57498.6714	35167	–0.0967	V	B. Harris	0.0001	QT UMa	57029.7681	11542	0.0017	V	V. Petriew	0.0002
TX UMa	57465.7467	4070	0.2197	V	S. Cook	0.0004	QT UMa	57030.0043	11542.5	0.0012	V	V. Petriew	0.0001
TY UMa	57445.7561	50524.5	0.3741	V	N. Simmons	0.0001	QT UMa	57498.5735	12532	0.0040	V	K. Menzies	0.0001
UX UMa	57074.7729	99872	–0.0016	V	V. Petriew	0.0000	V354 UMa	57089.8088	19294	0.0493	V	V. Petriew	0.0006
UX UMa	57494.6662	102007	–0.0015	V	G. Samolyk	0.0001	V354 UMa	57089.9538	19294.5	0.0473	V	V. Petriew	0.0006
UX UMa	57530.6573	102190	–0.0012	V	G. Samolyk	0.0001	W UMi	57564.6779	14039	–0.1966	V	G. Samolyk	0.0003
UX UMa	57568.6152	102383	–0.0009	V	G. Samolyk	0.0001	RU UMi	57513.6583	30323	–0.0148	V	G. Samolyk	0.0002
UX UMa	57569.7955	102389	–0.0006	V	N. Krumm	0.0001	RU UMi	57556.7027	30405	–0.0143	V	S. Cook	0.0004
UX UMa	57579.6287	102439	–0.0010	V	G. Samolyk	0.0001	VV Vir	57428.9706	58744	–0.0471	V	G. Samolyk	0.0001
UY UMa	57079.8009	78435	0.0025	V	V. Petriew	0.0002	AG Vir	57493.6718	18768	–0.0121	V	G. Samolyk	0.0001
UY UMa	57079.9896	78435.5	0.0032	V	V. Petriew	0.0002	AH Vir	57493.6044	28658.5	0.2788	V	G. Samolyk	0.0002
VV UMa	57089.6828	16402	–0.0605	Ic	G. Lubcke	0.0002	AH Vir	57513.3699	28707	0.2796	V	L. Corp	0.0002
VV UMa	57089.6832	16402	–0.0601	B	G. Lubcke	0.0004	AH Vir	57520.7056	28725	0.2799	V	S. Cook	0.0004
VV UMa	57089.6836	16402	–0.0597	V	G. Lubcke	0.0003	AK Vir	57425.9278	12441	–0.0342	V	G. Samolyk	0.0001
VV UMa	57476.6719	16965	–0.0663	V	G. Samolyk	0.0002	AW Vir	57424.9571	35035	0.0290	V	G. Samolyk	0.0001
XZ UMa	57446.6380	9227	–0.1346	V	G. Samolyk	0.0001	AW Vir	57573.6355	35455	0.0286	V	G. Samolyk	0.0001
XZ UMa	57446.6380	9227	–0.1346	V	N. Simmons	0.0001	AZ Vir	57427.9575	38469.5	–0.0244	V	G. Samolyk	0.0002
ZZ UMa	57511.6424	9377	–0.0026	V	G. Samolyk	0.0001	AZ Vir	57442.9936	38512.5	–0.0239	V	R. Sabo	0.0001
BM UMa	57505.6933	74320	0.0129	V	B. Harris	0.0001	AZ Vir	57542.6470	38797.5	–0.0251	V	G. Samolyk	0.0001
DN UMa	57087.7045	7600	0.0463	V	V. Petriew	0.0005	BH Vir	57431.9109	17385	–0.0110	V	G. Samolyk	0.0001
ES UMa	57070.7144	15063.5	0.0081	V	V. Petriew	0.0010	BH Vir	57521.7670	17495	–0.0108	V	S. Cook	0.0003
ES UMa	57070.9788	15064	0.0081	V	V. Petriew	0.0001	BH Vir	57476.8382	17440	–0.0117	V	G. Samolyk	0.0001
HN UMa	57086.8462	22442	0.0026	V	V. Petriew	0.0007	MS Vir	57531.6815	16104.5	0.0045	V	G. Samolyk	0.0002
HV UMa	57081.8609	8069	0.0178	V	V. Petriew	0.0003	MS Vir	57553.7098	16175	0.0059	V	S. Cook	0.0007
HX UMa	57045.0318	11987	–0.0225	V	V. Petriew	0.0008	Z Vul	57588.6910	5964	–0.0131	V	G. Samolyk	0.0001
II UMa	57066.7360	10381	0.0126	V	V. Petriew	0.0004	AW Vul	57579.7919	14005	–0.0251	V	N. Simmons	0.0001
KM UMa	57080.7182	13018	–0.0026	V	V. Petriew	0.0002	AX Vul	57595.6624	6293	–0.0369	V	G. Samolyk	0.0001
KM UMa	57080.9001	13018.5	0.0033	V	V. Petriew	0.0006	AY Vul	57579.6843	6174	–0.1392	V	G. Samolyk	0.0002
KM UMa	57098.8516	13069.5	0.0099	V	V. Petriew	0.0012	BE Vul	57579.7385	11255	0.1023	V	G. Samolyk	0.0001
KM UMa	57099.9069	13072.5	0.0097	V	V. Petriew	0.0013	BS Vul	57557.8294	30015	–0.0323	V	G. Samolyk	0.0001
KM UMa	57128.7501	13154.5	0.0003	V	V. Petriew	0.0007	BU Vul	57586.7383	42273	0.0142	V	G. Samolyk	0.0002
KM UMa	57128.9253	13155	–0.0004	V	V. Petriew	0.0001	CD Vul	57581.6646	16502	–0.0004	V	K. Menzies	0.0001
KM UMa	57502.5971	14217	–0.0042	V	B. Harris	0.0001	CD Vul	57596.7064	16524	–0.0010	V	G. Samolyk	0.0002

Variable Stars with the *Kepler* Space Telescope

László Molnár
Róbert Szabó
Emese Plachy
Konkoly Observatory, Research Centre for Astronomy and Earth Sciences, Konkoly Thege Miklós út 15-17, H-1121 Budapest, Hungary; address email correspondence to molnar.laszlo@csfk.mta.hu

Invited review paper, received September 21, 2016

Abstract The *Kepler* space telescope has revolutionized our knowledge about exoplanets and stars and is continuing to do so in the K2 mission. The exquisite photometric precision, together with the long, uninterrupted observations opened up a new way to investigate the structure and evolution of stars. Asteroseismology, the study of stellar oscillations, allowed us to investigate solar-like stars and to peer into the insides of red giants and massive stars. But many discoveries have been made about classical variable stars, too, ranging from pulsators like Cepheids and RR Lyraes to eclipsing binary stars and cataclysmic variables, and even supernovae. In this review, which is far from an exhaustive summary of all results obtained with *Kepler*, we collected some of the most interesting discoveries, and ponder on the role for amateur observers in this golden era of stellar astrophysics.

1. Introduction

The *Kepler* space telescope, as a Discovery-class space mission, was built to carry out a specific set of tasks to meet well-defined goals. It was conceived to do exoplanet statistics, and determine $\eta_{\rm Earth}$, the frequency of small, rocky planets within the habitable zone of their stars (Borucki 2016). However, it turned out to be, as many astronomers had hoped, much more than just an exoplanet-statistics mission. It is fair to say that during the last few years, *Kepler* has not only transformed our understanding of exoplanets but also revolutionized the field of stellar astrophysics.

But all good things come to an end, and the primary mission of *Kepler* ended in 2013, after collecting data from more than 160,000 stars in the same patch of sky for four years, quasi-continuously. This was not the end of the telescope itself though. With only two functioning reaction wheels remaining to point the spacecraft, an ingenious new mission called K2 was initiated (Howell *et al.* 2014). The telescope that was once built for a singular purpose was transformed into a community resource, open to any targets available within its new observing fields. It observes in 80-day campaigns along the Ecliptic, and at the time of writing finishes its 10th observing run with only minor technical problems.

The discoveries of the primary and extended missions of *Kepler* can already fill books. *Kepler*, along with the other space photometric missions, opened up a new window for us to explore what was considered utterly unreachable a century ago: the insides of stars. In this review we focus on the most important or interesting results about variable stars: stars that show light variations due to excited pulsation modes, turbulent convection, binarity, cataclysmic, or eruptive events. Some of these are out of reach of an amateur astronomer, but most of them are interesting to all variable star enthusiasts.

2. *Kepler* data

The success of the *Kepler* mission resulted from the combination of its unprecedented photometric accuracy (10^{-5}–10^{-6} relative precision), the length and the continuity of the observations, and the fast data sampling (1 and 30 minute cadence) that led to discoveries of light variation well below millimagnitude level and insight into the details of long-term behavior of a large number of stellar targets.

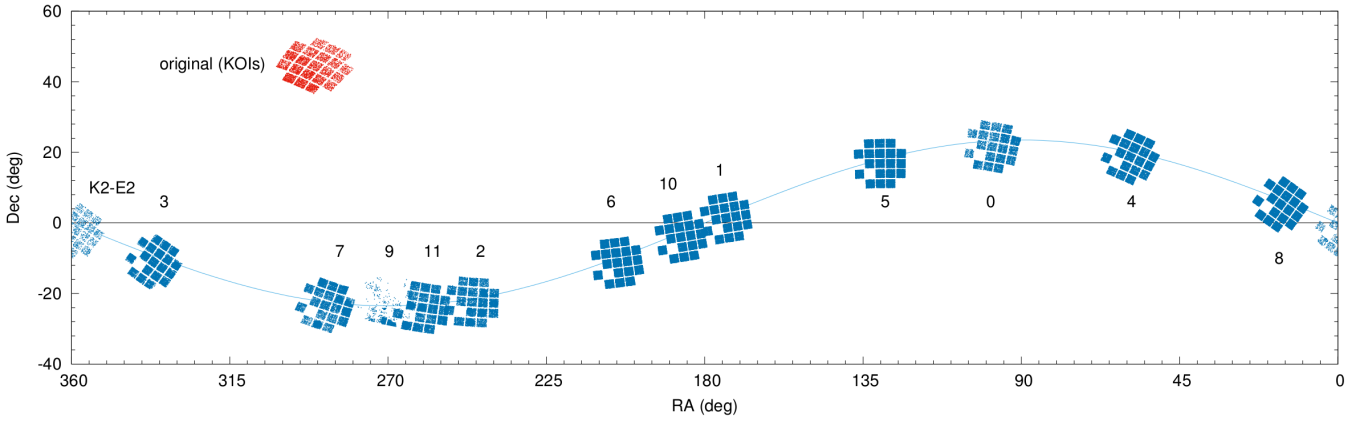

Figure 1. The observing fields of *Kepler* in the sky. For the original field (upper-left) we only plotted the KOIs (*Kepler* Object of Interest) instead of all targets. K2 fields include the positions of all observed targets and pixel mosaics. In Campaign 9 most of the pixels were assigned to a smaller, but continuous area to search for microlensing events, hence the sparse coverage for the other CCD modules.

However, like all instruments, *Kepler*, too, has unwanted artificial effects that contaminate the beautiful light curves. The most puzzling issue for which no perfect solution exists is stitching the individual data quarters to each other. In order to keep the solar panels pointed towards the Sun, the telescope had to roll 90 degrees after every three months, and as a consequence the targets ended up on different detectors for every quarter of a year, often causing significant differences in the measured flux. The correction of these differences requires scaling, shifting, and detrending of the observed flux, and are especially challenging for stars that show slow and irregular variability. *Kepler* light curves are also affected by a sinusoidal variability with the *Kepler*-year (372.5 days, the orbital period of the spacecraft around the Sun) due to the change of the thermal properties of the telescope elements. The amplitude and the phase of this effect are dependent on the position of the star within the field of view (Bányai and Kiss 2013).

Astronomers do not have to bother with these problems in the K2 mission any more—but other issues appeared instead. Due to the inherent instability of the positioning with only two functioning reaction wheels, the attitude of the telescope drifts (it rolls back and forth about the optical axis) and corrective maneuvers are required every 6 hours. The roll and correction causes stars to move across slightly differently sensitive pixels, causing distinctive 6-hour jumps to be present in the light curves. These effects are the strongest for stars that fall close to the edges of the field of view. Another source of noise is the zodiacal light, light scattered from the fine dust in the inner Solar System, that increases the background noise towards the end of each campaign.

Nevertheless, thanks to the Earth-trailing, i.e., heliocentric orbit of *Kepler* the data are devoid of other problems typical of space telescopes operating in low-Earth orbit. Instruments like CoRoT and the BRITE satellites are prone to scattered light from the Earth and the Moon, temperature changes when crossing the shadow of the Earth, and degradation or gaps in the data when they cross the swarm of charged particles called the South-Atlantic Anomaly. The patches of sky observed or targeted by *Kepler* are shown in Figure 1.

The core exoplanet science of the original mission was led by the *Kepler* Science Team. But in order to exploit the wealth of stellar oscillation data provided by *Kepler* optimally, a large collaboration (Kepler Asteroseismic Science Consortium) was also formed, which consists of some 600 scientists around the globe, and produced most of the results presented in this paper.

3. Solar-like oscillations

Probably the single greatest breakthrough that *Kepler* delivered for stellar astrophysics is the huge number of stars where solar-like oscillations have been detected. Detailed asteroseismic analysis is now routinely used to determine the physical parameters of stars, and, by extension, exoplanets. Asteroseismic modeling, e.g., fitting the spectrum of observed oscillation modes with values calculated from theoretical models, is extremely powerful, for multiple reasons. First, it requires photometric measurements instead of spectroscopic ones, so it can be done for a large number of stars simultaneously, with a relatively small telescope. (Although with the need of very high precision: oscillation signals are closer to the μmag level than the mmag level usually accessible with ground-based instruments.) Secondly, although resolved observations are not possible for distant stars, detailed seismic (i.e. intensity) observations allow for the determination of global parameters like mass, radius, and age much more precisely than with any other methods. The typical precision is 3–5% in mass and radius and 10% in age for main-sequence stars. The latter can be appreciated if we mention that the age of a typical (not so young) main sequence star can be determined with rather large (30–50%) uncertainties based on spectroscopic information alone. And any age or radius information about exoplanets is only as good as our knowledge on their host stars.

Before CoRoT and *Kepler*, seismic information was available only for a handful of stars, mainly through spectroscopic observations or small space telescopes, like WIRE. In contrast, *Kepler* delivered seismic information for hundreds of main-sequence stars (brightest ones), and over 15,000 red giants in the original *Kepler* field. Many more are expected from the ongoing K2 Mission. This amount of stars with accurate asteroseismic information already makes galactic archaeology and population studies possible. Thus, we can learn more about the history of our Galaxy, the stellar formation rate, initial mass function, etc., especially in conjunction with Gaia, the flagship mission of the European Space Agency, which provides accurate distances and proper motions for roughly one billion stars.

Kepler-16 A&B, the two solar-like components of a visual binary, allowed the execution of an exquisite proof-of-concept seismological study (Metcalfe *et al.* 2012). The masses of these stars are 1.10 ± 0.01 and 1.06 ± 0.01 solar masses and were resolvable even with *Kepler*'s not-so-good resolving power (it was optimized to gather as many photons as possible, hence the large pixels and relatively low spatial resolution). Thus, the oscillation spectra were derived for both stars, and their parameters could be determined independently and without any prior assumptions. Reassuringly, the age of the two objects (6.8 ± 0.4 billion years) and their bulk chemical compositions were found to be identical. That is what one would expect if the two objects were formed from the same blob of interstellar material at the same time. What's more, 16 Cyg A and B are close enough to us that their radii can be measured directly, and as such, they can help us validate the asteroseismic relations that are based on our knowledge of the Sun. Data from the CHARA (Center for High Angular Resolution Astronomy) Array revealed that the seismic and interferometric radii of solar-like stars agree within a few percent (White *et al.* 2013).

Not only individual stars can be scrutinized by applying asteroseismological methods. Models can be constrained even more if our object belongs to a stellar cluster, since in this case the cluster members were presumably formed from the same molecular cloud roughly at the same time (although recently evidence is accumulating for multi-epoch star formation in globular clusters). In the original *Kepler* field there were four open clusters (NGC 6811, NGC 6819, the very old NGC 6791, and NGC 6866, the youngest of the four). Their red giant population was investigated in great detail in a large number

of studies based on the *Kepler* data. For example, a new methodology was developed to determine cluster membership probability based on seismic constraints (Stello *et al.* 2011) and the very uncertain mass loss was studied along the red giant branch evolution (Miglio *et al.* 2012), again, based on *Kepler*'s seismic information.

The detection of seismic signals from the main sequence of an open cluster is a much harder task, since main-sequence stars are usually much fainter then their evolved fellow cluster members. Therefore this breakthrough was only recently reached: Lund *et al.* (2016) succeeded in detecting seismic signals from main-sequence stars in the Hyades cluster for the first time. Many more, already well studied, fiducial clusters will be observed during the K2 extension including the Pleiades, M44, M67, M35, etc., that will allow a stringent test for our knowledge of stellar evolution. Miglio *et al.* (2016) detected solar-like oscillation in the K giants belonging to the globular cluster M4 in the K2 Mission. This is also remarkable given the difficulty presented by the crowded nature of the target.

To close this section we briefly mention the synergies of stellar oscillations with exoplanetary science. The first one is the measurement of the radius of the previously discovered hot Jupiter, HAT-P-7b in the *Kepler* field. With the help of asteroseismology the radius of the host star was measured by more than an order of magnitude more precisely compared to traditional methods (Christensen-Dalsgaard *et al.* 2010). Similar improvement was achieved regarding the radius of the exoplanet, since the transit depth to the first order scales with the ratio of the planetary and stellar radii.

The second nice example for the complementary nature of exoplanetary and stellar astrophysics results is the Kepler-444 planetary system (Campante *et al.* 2015). The host star is a red dwarf with a mass of 0.758 ± 0.043 solar mass and can be found in the constellation Lyra at a distance of 117 light years from the Solar System. There are five rocky planets orbiting the host star as revealed from the *Kepler* photometry, since all of them show transits. The most important aspect of the system is its age. From seismology it was found to be 11.2 ± 0.4 Gyr. First, it is astonishing how accurate this age determination is. Secondly, this system is more than twice as old as our Solar System, and had to be formed right after the formation of the Milky Way galaxy. Another consequence is that the formation of planetary systems is not restricted to later, more metal-rich stars. Although the planets in the Kepler-444 system are too close to their star to be habitable, it seems that at least in some systems there has been ample time for undisturbed biological evolution—if other conditions are also right and conducive. Again, this result also relies on the investigation of stellar oscillations in the form of tiny intensity variations in the red dwarf.

4. From red giant variables to Miras

Oscillations in stars come in two distinct flavors. The *p*-modes, or sound waves, are governed by forces exerted by gas pressure, and are usually the strongest in the envelope, close to the surface. The other bunch is the *g*- or gravity modes. These are like waves on a pond, but in solar-like stars they are locked away in the core, and, as of yet, unobservable by us. But as stars leave the Main Sequence, their cores begin to contract, and their envelopes start to expand. Frequency regimes of the two types of modes, nicely separated on the Main Sequence, begin to shift towards each other, as they depend on the density of the core and envelope, respectively. Soon the frequencies of some *p*- and *g*-modes start to overlap, and so-called mixed modes appear: these travel in the core mostly as *g*-mode, but may traverse the steep core-envelope density boundary, and continue outwards more like a *p*-mode. It was soon realized that mixed modes may carry extremely valuable information about the insides of red giants, down to the very cores they come from. By an interesting twist of nature, we can now investigate the centers of these stars while that of the Sun remains unreachable for us.

For example it was possible to derive the rotation rate of the red giant envelope and the core independently—the rotation frequency was found to be at least ten times greater for the core (Beck *et al.* 2012). This is actually what one would expect if the core contracts and the envelope expands—it is enough to think about a ballerina or a skater performing a pirouette with stretched or pulled in arms. All these phenomena obey the same physical principle, namely the conservation of angular momentum. *Kepler* was able to probe the core rotation of many red giants, and suggested that as stars get older, their cores spin down (Mosser *et al.* 2012). This, too, was expected, as white dwarfs, the remnants of the cores of now gone stars, rotate slowly. However, the actual physical process(es) that transport angular momentum away from the core into the envelope are still hotly debated.

Another remarkable achievement was reached by the members of the *Kepler* Asteroseismic Science Consortium. Based on the investigation of period spacing between gravity modes it is possible to distinguish between H-shell burning and He-core burning stars (Bedding *et al.* 2011), i.e. different evolutionary states—information that is otherwise hidden deep inside these stars, and is not reflected in their surface or global parameters. Yet another major breakthrough in stellar astrophysics thanks to *Kepler* and its unbeatable photometric precision.

The concept that with seismology we can in fact map the stellar interior can be demonstrated with another recent result. *Kepler* observed over 15,000 red giants and almost all of them show solar-like oscillations. But 10–15% of them are peculiar: the amplitude of some of the nonradial (non-axysymmetric, namely $\ell = 2$ modes) are significantly suppressed, these can be hardly seen in the oscillation spectrum. What causes this dichotomy between the normal amplitude and suppressed amplitude red giants? Fuller *et al.* (2015) had an idea: *magnetic greenhouse effect*. It can be shown that if a strong magnetic field is present in the stellar interior then it can reflect and disperse certain incoming waves, that will be missing from the frequency spectrum. The critical magnetic field has a minimum in the H-burning shell that surrounds the He-core in these stars, therefore we can infer the minimum magnetic field at this specific point, which turns out to be 10^5–10^7 Gauss, much stronger than previously thought, but still too small to significantly alter the stellar structure. Voila: an ingenious way to see what is "hidden behind substantial barriers"—to quote Sir Arthur Eddington, the famous astrophysicist (Eddington 1926).

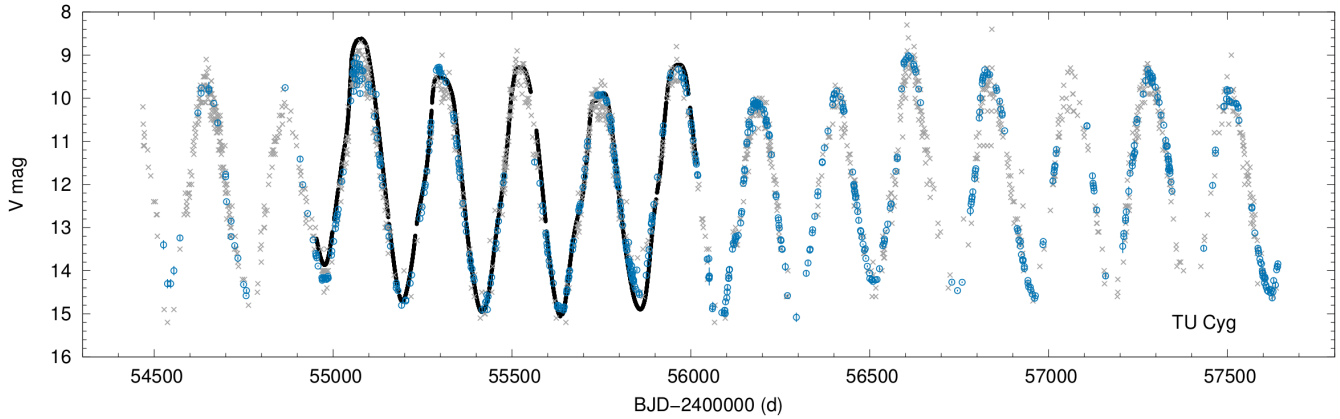

Figure 2. A comparison of the AAVSO visual (gray), digital *V*-band and green-filter (blue) observations, and the *Kepler* light curve (black) of the Mira star TU Cyg. Here we used the data from between 01/01/2009 and 16/09/2016. The corrected *Kepler* data, published by Bányai *et al.* (2013), are scaled to the amateur observations.

Still, although solar-like oscillations are now the Swiss Army knives for many professional astronomers, their observations are mostly out of reach for amateur astronomers. But as we go to larger and larger red giants, the nice and tidy relation between the dominant periods and amplitudes of the oscillations starts to break down. At periods above about 10 days, the observed amplitudes start to increase much faster than below (Bányai *et al.* 2013). This could be the transition from pure stochastic oscillations towards more coherent pulsations that lead to the more familiar landscape of semiregular and Mira stars above periods of 100 days. One Mira, TU Cyg, is shown in Figure 2, together with the more extended AAVSO observations.

5. Cepheids

One century ago, the analysis of Cepheid stars revealed that pulsating stars exist, and that we can measure extragalactic distances with them. Since then, they have been under intense scrutiny from all aspects. However, Cepheids are relatively rare stars in the Milky Way, and a thorough search for targets in the original *Kepler* field came up with a single classical Cepheid star, V1154 Cyg (Szabó *et al.* 2011). The first analysis and a later study based on 600 days of observations both showed that V1154 Cyg is a well-behaved Cepheid, e.g., it pulsates in the fundamental mode, without any signs of additional modes down to the sub-millimagnitude level. It was far from boring though: the quasi-continuous observations revealed that the variation of Cepheids may not be strictly periodic. Individual pulsation cycles of V1154 Cyg showed small changes in their respective shapes. Fluctuations up to 20–30 minutes occur in the O–C timings, but these average out on a time scale of ~15 cycles, and the 4.9-day pulsation period remains stable (Derekas *et al.* 2012). The physical cause behind this phenomenon is, so far, unclear: one hypothesis is that emerging convective hot spots can be responsible for the observed pulsation jitter (Neilson and Ignace 2014).

The latest analysis, based on the entire four-year data set, led to further discoveries. The star shows a 159-day-long modulation cycle, reminiscent of a very low-level Blazhko effect. The *Kepler* data were accurate enough to tease out the signals of granulation noise hiding under the large pulsation. This is the first firm detection of granulation in a Cepheid star: the effective timescale of the granulation cells is about 3.5 days and that agrees with the scaling relations derived for smaller red giants (Derekas *et al.* 2016). But there was one thing that *Kepler* would have been able to detect comfortably, but did not: solar-like oscillations. Apparently, coherent, large-scale pulsation inhibits the excitation of other, evanescent waves.

Kepler measured DF Cyg, a 24.9-day period type-II Cepheid, as well. This star belongs to the RVb subclass of RV Tau variables that exhibit slow, large-scale mean brightness variations on top of the pulsation. During the observations a sudden period change was detected that was accompanied with an increase of the pulsation amplitude and an interchange in the order of deep and shallow minima (Bódi *et al.* 2016). The origin of these changes is as of yet unclear, but we note that the change of the order in period-doubled light curves was observed elsewhere, for example in light curves of RR Lyr and RV Tau stars (Molnár *et al.* 2012a; Plachy *et al.* 2014) and hydrodynamic models of BL Her variables (Smolec and Moskalik 2012).

Cepheid stars also highlight one of the great advantages of the K2 mission over the primary one. Although the step-and-stare approach limits the baseline of individual observations, targeting multiple directions and different stellar populations can accumulate measurements of rare objects. *Kepler* is expected to observe dozens of Cepheids, from all subgroups, in the Galactic field, and potentially hundreds of stars during the campaigns that target the Galactic bulge. The first results from two W Vir-type stars (medium-period type II Cepheids) have already led to the detection of significant cycle-to-cycle variations that will be undoubtedly followed by other discoveries in the next few years (Plachy *et al.*, in prep).

6. RR Lyrae stars

Whereas the *Kepler* data of the Cepheid star were intriguing, the observations of RR Lyrae stars turned out to be downright revolutionary. The discovery of period doubling (alternating low- and high-amplitude cycles) and the new modeling efforts it sparked were already presented in the recent review of Kolenberg (2012). Our picture got much more complicated compared to the simple categorization of RRab (fundamental mode), RRc (first

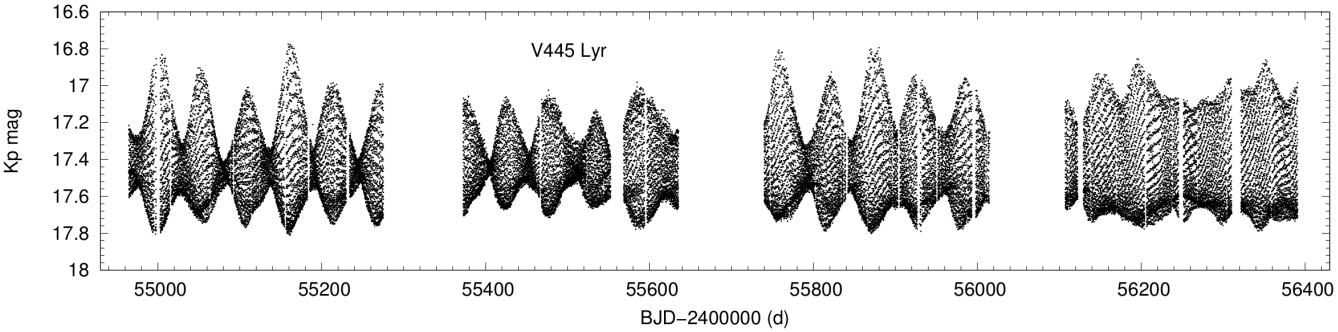

Figure 3. The complete *Kepler* light curve of the Blazhko RR Lyrae star V445 Lyr. Smaller gaps are caused by data download and safe mode periods, the three long ones by the failure of one of the CCD modules. Note the very strong modulation at the beginning that decreased to low levels towards the end.

overtone), and RRd (double mode) subtypes that we used less than a decade ago. The discovery of low-amplitude additional modes blurred the line between the three main groups, especially for the RRab class (Benkő *et al.* 2010, 2014). According to space-based photometry, fundamental-mode stars that do not show the Blazhko effect have no additional modes either, i.e., they are true single-mode pulsators. Blazhko stars, on the other hand, often (but not always) pulsate in a few additional modes as well. The prototype RR Lyrae is also a member of the latter group (Molnár *et al.* 2012a). Hydrodynamic modes managed to explain some, but not all of these discoveries: period doubling, for example, can destabilize the first overtone in stars that are otherwise away from the double-mode regime of RR Lyrae stars (Molnár *et al.* 2012b). What's more, the interplay of three different modes opens the possibility for intricate dynamical states, including low-dimensional chaos in the models (Plachy *et al.* 2013). Let's just think about that for a moment: the observations of *Kepler*, and the modeling work that it sparked, transformed these stars from "simple" radial pulsators into stars where even chaos may occur.

First-overtone and double-mode stars also held some surprises. As *Kepler* was busy collecting data, new results from the ground-based OGLE survey indicated that some first-overtone Cepheids and even a few RRc stars share similar additional modes in the f_1 / f ~ 0.60–0.64 frequency range (Moskalik and Kołaczkowski 2009; Soszyński *et al.* 2010). As more and more data poured in from OGLE, these modes started to form three distinct groups, and they were also found in double-mode stars, but still connected to the first overtone. But the precision of the OGLE data, even after a decade of observations, is limited compared to what *Kepler* was able to do, so it was still unclear just how frequent these weird modes are. And although the data from *Kepler* (and the first K2 observations) were limited to a handful of RRc and RRd stars, they suggested an intriguing answer: these modes are there in all RRc and RRd stars (Kurtz *et al.* 2016; Molnár *et al.* 2015b; Moskalik *et al.* 2015). This means that RRc and RRd stars are not single- and double-mode stars anymore, instead they pulsate at least in two and three modes, respectively (not counting any further modes seen in some of them). These additional periodicities most often do not fit the radial (axisymmetric) oscillation spectrum, so the most plausible explanation is the existence of nonradial (non-axisymmetric) modes in these objects.

The benefits of the continuous observations of *Kepler* are clearly illustrated when we look at the RR Lyrae light curves as a whole. Ground-based surveys suggested that some Blazhko stars have multiple or irregular modulation cycles, but the space-based data provided us with clear evidence (LaCluyzé *et al.* 2004; Sódor *et al.* 2011). In the original *Kepler* field, 80% of the modulated stars turned out to be "complicated," with changing or multiperiodic Blazhko cycles. V445 Lyr, for example, was heralded as one of the most extremely modulated stars observed, with pulsation amplitudes falling from 1.5 magnitudes to 0.15 magnitude, and the light curve getting completely distorted at minimum amplitude, based on the first few observing quarters (Guggenberger *et al.* 2012). Within a few years though, the modulation pattern barely resembled those extreme values, and the amplitude variation decreased from >1 magnitude to a meager 0.3 magnitude, as Figure 3 illustrates. These observations further highlight that a large portion of RR Lyrae stars are not just simple, repetitive pulsators, but are intricate physical laboratories that hold many more puzzles to solve.

Unfortunately, the K2 observations are limited to a maximum of 80 days per field that is often far too short to cover even a single modulation cycle. Nevertheless, K2 can be exploited for other purposes. For example, the very first engineering run already delivered us the first observations of two RRd and a modulated RRc stars that were lacking from the original field (Molnár *et al.* 2015b). The large aperture of *Kepler* (especially compared to other photometric missions) also allows us to reach faint stars down to 20–22 magnitudes. Given the intrinsic brightness of RR Lyrae stars (and Cepheids as well), we can thus reach the very edges of the halo of the Milky Way, and even the nearest galaxies in the Local Group. One such nearby object is the tiny, faint dwarf galaxy Leo IV, where only three RR Lyraes are known. *Kepler* observed all of them, and detected the Blazhko effect clearly in one, and possibly in another star out of the three (Molnár *et al.* 2015a). This represents the first unambiguous observation of the Blazhko effect beyond the Magellanic Clouds.

7. Main-sequence pulsators

Let us now turn back to the Main Sequence, to the young and large stars that populate the HRD above the Sun. Here, many types of variable stars can be found, from the largest O and B-type ones to the smaller δ Scuti- and γ Doradus-type

pulsators. O-type blue supergiants are very rare, and given their short life times of just a few tens of millions of years, they can be observed where they were formed. The original *Kepler* field lacked any star-forming regions, and thus O stars, but the K2 mission successfully covered a few of them. The initial results are puzzling. Many things seem to happen simultaneously in the light curve, including rotational modulation from chemical and/or temperature spots and various pulsation modes that are hard to disentangle (Buysschaert *et al.* 2015).

At slightly lower temperatures, B stars are well-known pulsators, hosting two groups: the β Cephei-type stars (not to be confused with the δ Cephei group), and the SPB, or Slowly Pulsating B stars, pulsating in *p*- and *g*-modes, respectively. However, many stars are *hybrids* that pulsate in both regimes simultaneously. From there, it is just a matter of observing enough modes to carry out an in-depth analysis and modeling of the structure of these stars, analogous to the study of solar-like oscillations (Moravveji *et al.* 2015; Pápics *et al.* 2015). And the analysis of the *Kepler* data revealed some intriguing insights into the inner workings of massive stars.

We instinctively assume, for example, that stars rotate in one direction, with some differences in the actual speed of the rotation. However, B stars tell a different story: it seems that in some stars the direction of rotation turns around at a given radius, and the upper envelope counter-rotates the core and the deeper layers (Triana *et al.* 2015). This also means that some layers of the star are essentially at standstill, and have no angular momentum. Our current stellar evolution models cannot explain these observations.

Moving downwards, the next large group is the δ Scuti-γ Doradus variables that have spectral types ranging from late A to early F stars. However, recent studies unearthed some variable stars that fall into the gap between the instability strips of classical SPB and A-type pulsators. These are currently called Maia-type and hot γ Dor stars, although their relation with the other groups and the excitation mechanisms behind their variation are both uncertain (Balona *et al.* 2015, 2016). We note that *Kepler* also observed Maia (20 Tau), a member of the Pleiades cluster, during Campaign 4, so the namesake of the group can also be studied.

Turning back to δ Scutis: these stars pulsate in radial and nonradial *p*-modes with somewhat shorter periods than γ Dor stars that exhibit *g*-modes. On the Hertzsprung-Russell diagram stars belonging to these classes overlap, therefore *hybrid stars* that would show both *p*- and *g*-modes are expected in these groups as well. Indeed, from ground-based observations a few such hybrid oscillators have been found. These are valued treasures, since more oscillation modes reveal more information about the stellar structure; in addition *p*- and *g*-modes probe different domains within the star. Enter *Kepler* which targeted hundreds of stars in this region of the parameter space. The result: too many (over 23% of) stars show periodic variations in these frequency regimes (Uytterhoeven *et al.* 2011). Maybe not all of these objects are genuine hybrids, since there are other possible explanations for the long-period variability: instrumental origin, stellar spots, binarity, or ellipsoidal variations. Confirming or refuting these alternative scenarios takes time and follow-up observations with many telescopes, but the hunt for genuine hybrid stars continues, in order to solve the mysteries they present.

Stellar pulsation can be exploited to investigate stars that themselves may not be variables, but are in a binary system with one (Murphy and Shibahashi 2015). The method is based on the idea that if a standard clock is placed in an orbit around a star, the signal from the clock will arrive sooner or later to the observer depending on the position of the clock along the orbit (Shibahashi and Kurtz 2012). In the studied systems the clocks are the independent pulsation frequencies of the variable star component. If periodic O–C modulation, or variations in period/frequency or phase can be detected in these stars, then one might conjecture that the star has a companion. It is important that simultaneous variation should be seen in all independent frequencies, and these variations should be in phase in order to exclude any spurious, intrinsic variations of the oscillation modes. And this is not a hypothetical issue: the same *Kepler* observations also revealed that a fraction of modes in δ Scuti stars indeed show intrinsic amplitude or phase variations, complicating such studies (Bowman *et al.* 2016).

But back to the O–C studies. In practice only the modes with the largest amplitudes can be studied, but this new method—allowed by the long, precise *Kepler* data—is a powerful technique to discover new binary systems. Its advantage is that no eclipses, e.g., lucky geometric configurations, are required; binary systems with arbitrary inclinations—excluding almost face-on configurations—can be found. The light-time effect, because its base is the finite speed of light, allows hundreds of binary systems to be discovered. And it has an unbeatable advantage: there is no need for time-consuming spectroscopy, since a radial velocity curve can be obtained from photometry alone! The astrophysical importance of the method lies in the fact that statistics of companions can be obtained for higher mass stars which are notoriously difficult to study with other techniques. With this method—which can be considered as a new planet-finding technique—even a high-mass planet (with 12 Jupiter masses) was discovered around an A-type star on a 840-day orbit (Murphy *et al.* 2016), demonstrating the potential and complementary nature of the new high-precision space photometry and the more conventional radial velocity methods.

8. Pulsating subdwarfs and white dwarfs

A number of variables called hot subdwarfs can be found in the region between the zero-age main sequence and the white dwarf cooling track, populating the so-called extended horizontal branch. These subdwarf stars are believed to be the exposed cores of stars that should be on the normal horizontal branch, but experienced extreme mass loss and basically shed their envelopes when they were red giants. These objects show non-radial pulsations in either *p*- or *g*-modes or in both of them. Asteroseismic analysis of these pulsation modes led to strong constraints on the surface properties and inner structures of these stars as well. Thanks to the *Kepler* data, mode identification techniques using the observed period spacings and frequency multiplets became a reality. One interesting discovery about sub-dwarfs is that their rotation periods are surprisingly long (10–100 days) even for short-period (~0.5 day), close binary

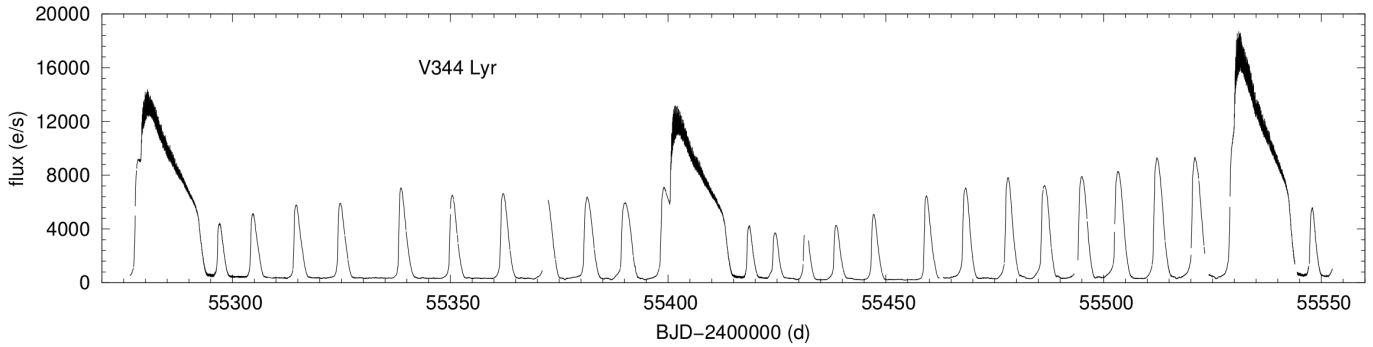

Figure 4. Light curve of V344 Lyr, an SU UMa-type dwarf nova from *Kepler* quarters 5, 6, and 7, spanning 276 days. Notice the normal and superoutbursts throughout observations. In the case of all superoutbursts a trigger (normal) outburst can be seen.

systems, where tidal forces are expected to synchronize the orbital and rotation periods (Reed *et al.* 2014).

White dwarfs are the remnant products of stellar evolution for the vast majority of stars. As the mission progressed, numerous white dwarfs were discovered in the original *Kepler* field of view. Unfortunately, however, only a few were actually selected for observation before the sudden end of the mission (Greiss *et al.* 2016). But these *Kepler* measurements led to a discovery of an entirely new phenomenon in pulsating white dwarfs: the occasional large-amplitude outbursts (Bell *et al.* 2015). The ~1.5-year-long data with one minute sampling of KIC 4552982, a pulsating white dwarf that belongs to the ZZ Cet subclass, shows 178 such events in which the flux of the star increased by several per cent, lasting from a few hours to a day. With the two-reaction-wheel mission the number of known outbursters has increased to four by now (Hermes *et al.* 2015; Bell *et al.* 2016). These discoveries suggest that such outbursts could be a common phenomenon that was either missed, by chance, during the past decades or was simply removed during the data processing. Ground-based observations are affected by atmospheric extinction that manifests as a slow brightening and fading as a star rises and sets, and it is seen through different amounts of air. These effects are easy to confuse with similar, but intrinsic variations.

Nevertheless, detailed theoretical explanation of this phenomenon is still needed. The four outbursters are among the longest pulsation period ones located at the red edge on the DAV instability strip, where mode coupling could be prevalent, therefore consideration of pulsation energy transfer via nonlinear resonances is plausible. Such discoveries show the power of space-based, continuous photometry that is free from the biases induced by the rotation period of our own planet.

9. Cataclysmic variables

Cataclysmic variable binary systems consist of low-mass main-sequence stars that transfer mass onto a white dwarf primary via an accretion disk. These variables (dwarf and recurrent novae, nova-like objects) are bona-fide amateur objects. Their erratic nature, the unpredictable, large-amplitude outbursts, and the involved timescales between consecutive outbursts (often decades or even centuries) make them ideal targets for a keen amateur observer. So what happens, if one is able to observe them continuously, with exquisite precision and with a large-aperture telescope? This sounds like a dream, and indeed one of the authors (RSz) was oftentimes dreaming about such a possibility while observing in his parents' garden some 25 years ago with a 10-inch Dobson-telescope (and submitted his observations to AAVSO, as well). *Kepler* offered just that and observed at least 16 cataclysmic variables in the original *Kepler* field continuously, with unprecedented precision, revealing subtle details and without missing a single outburst during the four-year mission in most of the cases. The sample contains six SU UMa-type variables, one of the WZ Sge type, two nova-like variable stars, three UG-type cataclysmic variables, two additional UG-types showing eclipses, and one AM Her variable. Even new cataclysmic variables were discovered, such as the nova-like, potentially SW Sex-type KIC 8751494 (Williams *et al.* 2010), or a background SU UMa-type variable in the photometric aperture of a G-type exoplanet target star (Barclay *et al.* 2012).

For example, early *Kepler* data revealed superhumps from V344 Lyr (Figure 4) during quiescence, normal outburst, and the longer and brighter superoutburst (Still *et al.* 2010), whereas so far these variations were detected only during superoutbursts. The orbital period of V344 Lyr is 2.11 hours, while the system displays both positive and negative superhumps with periods of 2.20 and 2.06 hours (longer and shorter than the orbital period), respectively. The quality of the *Kepler* data is such that it is possible to test the models for accretion disk dynamics quantitatively. The V344 Lyr data are consistent with the model that two physical sources yield positive superhumps: early in the superoutburst, the superhump signal is generated by viscous dissipation within the periodically flexing disk. But late in the superoutburst, the signal is generated as the accretion stream bright spot sweeps around the rim of the non-axisymmetric disk. The V344 Lyr data also reveal negative superhumps arising from accretion onto a tilted disk precessing in the retrograde direction. It is also found that at least some long superoutbursts appear to be triggered by short outbursts in some SU UMa stars (see, for example, Figure 4).

10. Supernovae

Supernova explosions are unexpected events, so it is very hard to catch the first hours of the explosion that may hold vital information about their progenitors. The continuous monitoring of external galaxies provide a great possibility to observe these

events from the very beginning and not only when the brightening is already in full swing. Type Ia supernovae are crucial objects in extragalactic distance measurements, therefore the importance of understanding the mechanisms driving the thermonuclear runaway reaction is unquestionable, so the targets of *Kepler* included some galaxies as well in its Guest Observer program, where all interested scientists could propose targets in *Kepler*'s field of view. Overall, three Type Ia supernovae were observed in the original *Kepler* mission. No signatures of interaction between the ejected material and potential companion stars were found, suggesting that the progenitor systems contained two compact stars and the explosion was caused by their merger (Olling *et al.* 2015). However, we cannot simply replace the classical, accretion-induced collapse theory with the double-degenerate scenario. Recent ground-based observations found evidence for a non-degenerate binary companion to a normal SN Ia (Marion *et al.* 2016). According to theoretical considerations both channels contribute to the observed SNIa events, but their relative importance is largely unknown. Early space-based photometric supernova observations in a significant number of cases may answer these questions in the future and inform us about the progenitors and their circumstellar environments in the other types of supernovae, too.

The K2 mission observed a few fields with large numbers of galaxies, but it has not yet discovered as many supernovae as was hoped. Nevertheless, it already measured two transient events that were identified as core-collapse supernovae (Garnavich *et al.* 2016). Thanks to *Kepler*, we were able to detect the shock breakout for the first time in the optical band. This short, sudden brightening precedes the actual explosion: it happens when the outwards shockwave from the collapsing core breaches the surface of the star. To give a sense of scale here: after the core starts to collapse, it takes about one day for the shockwave to travel to the surface of the star. The star then suddenly (within a few minutes) flares up, and then starts to fade back for a few hours, before the actual disruption begins. From there, it still takes about 10 days for the exploding star to reach peak brightness.

Interestingly, the shock breakout was only seen in the data of the larger supergiant, while the smaller one showed a slower excess brightening on the ascending branch instead. Both events had similar explosion energies, therefore the diversity of the two rising light curves is puzzling. A possible explanation is that the light from the breakout was absorbed by thicker circumstellar matter in the second case. The circumstellar matter reprocessed that light into heat, and that heating led to a slower but stronger excess brightening. Hopefully, the K2 campaigns aimed at nearby clusters will provide us with even more supernova light curves: Campaign 10, for example, includes nearly 5,000 selected galaxies in the direction of the Virgo galaxy cluster.

11. Eclipsing binaries

Currently there are 2878 known eclipsing binaries in the original *Kepler* field (Kirk *et al.* 2016). They come in all flavors (detached, semi-detached, contact, Algol-type, W UMa, binaries with third components (Borkovits *et al.* 2016)), all kinds of strange animals in the eclipsing binary zoo. It is important

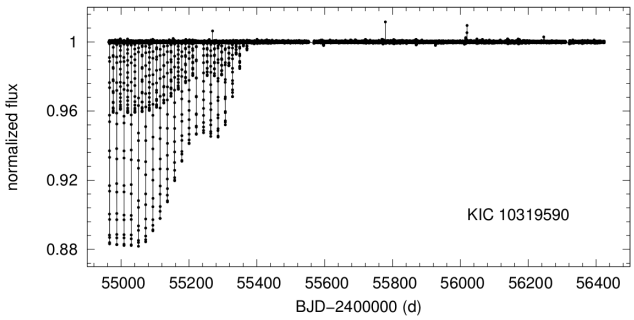

Figure 5. Four-year-long *Kepler* light curve of KIC 10319590. The object ceased to be an eclipsing binary.

to know the occurrence rates of different types to identify false positives in the transiting exoplanet search. Besides this practical usefulness, there have been a lot of interesting discoveries, where rare types of eclipsing binaries have been discovered. First of all, a long-awaited holy grail was found: a planet orbiting a binary star system. That was Kepler-16 (Doyle *et al.* 2011), which is a Saturn-size planet orbiting with a 289-day period around an eclipsing binary. The orbit of the planet is much wider than that of the binary, so it is much like Tatooine (also the unofficial name of the object), which was later found to be quite common in the Milky Way galaxy.

Another one is binaries that cease to show eclipses due to the precession of the plane of their orbit (Figure 5 shows an example from the *Kepler* original four-year mission). Although other cases were recorded, such as SS Lac (Zakirov and Azimov 1990) and HS Hya (Zasche and Paschke 2012), *Kepler* was the first where this process could be followed continuously, and the orbital evolution happened in front of our eyes (or in front of our detectors, to be more precise).

Yet another feat was the discovery of the triply-eclipsing hierarchical triple star, HD 181068 (dubbed as Trinity by the discoverers (Derekas *et al.* 2011)). Hierarchical triple systems comprise a close binary and a more distant component. They are important for testing theories of star formation and of stellar evolution in the presence of nearby companions. *Kepler* photometry of Trinity supplemented by ground-based spectroscopy and interferometry showed it to be a hierarchical triple with two types of mutual eclipses. The primary is a red giant that is in a 45-day orbit with a pair of red dwarfs in a close 0.9-day orbit. The red giant shows evidence for tidally induced oscillations that are driven by the orbital motion of the close pair. Thus, HD 181068 turned out to be an ideal target for studies of dynamical evolution and for testing tidal friction theories in hierarchical triple systems.

Besides stochastically excited solar-like oscillation and the good old κ-mechanism that drives the classical pulsators from RR Lyrae and Cepheid stars to δ Scutis and Miras, there is a third excitation mechanism, which is rarely mentioned. This is tidally-driven oscillations, a process that takes place in certain binary stars. In some cases the components of binary systems get close to each other during their orbital motion, where the gravitational interaction can excite modes that would be damped otherwise (one needs considerable eccentricity for a variable driving force). There is even an emerging new research field, called *tidal asteroseismology*, that benefits from the unusual

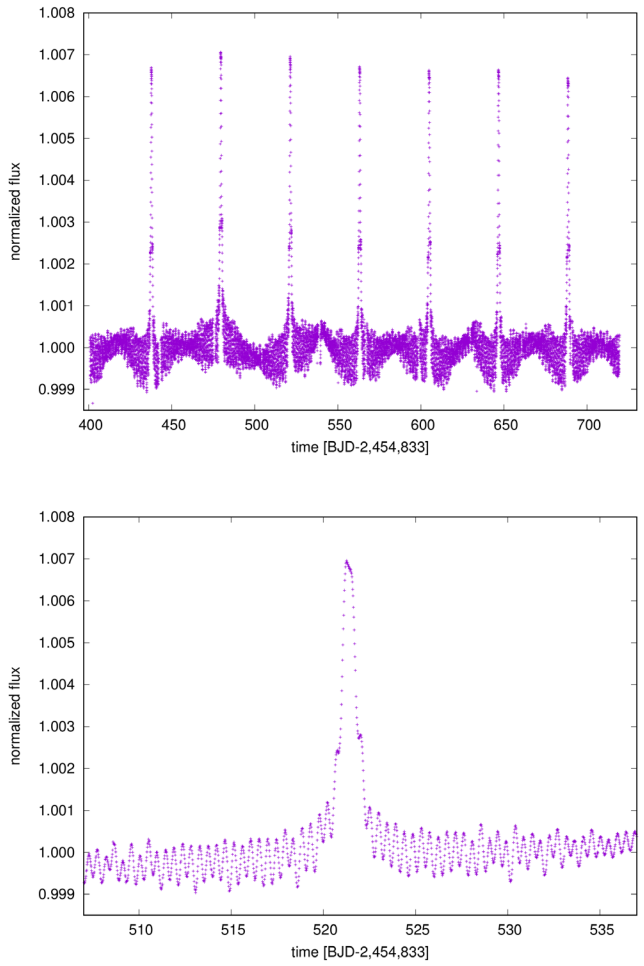

Figure 6. Top: The Kepler light curve of KOI-54, a heart-beat star. Bottom: A zoom-in on the light curve of KOI-54. In between the brightenings the system shows tidally induced oscillations.

geometrical configuration that does us the favor to sound out stars that otherwise would be too shy to oscillate.

A prime example is KOI-54 (aka KIC 8112039; Welsh *et al.* 2011) that made astronomers scratch their heads once it was found in the sea of unbelievable *Kepler* data. The light curve shows distinct, periodic brightenings of 0.7%, and ubiquitous oscillations in between (see the upper panel of Figure 6). First it was thought to be the manifestation of a very exotic binary system (maybe containing a black hole that causes gravitational lensing, hence brightening). Follow-up observations, however, showed something else: a highly eccentric pair of A-type stars dancing around each other in a 46-day orbit and approaching each other within a few stellar radii. The strong gravitational tug deforms the stars at the close encounter, and heats up the stellar hemispheres that face towards each other. This is the cause of the brightening (see the lower panel of Figure 6 for a zoom-in). In addition, the gravitational interaction excites oscillations in both components, allowing a detailed seismological investigation of otherwise non-oscillating main-sequence stars. The light curve reminded the astronomers of an electrocardiogram, so this type of object got an expressive name: *heart-beat stars*. It was soon found out that the system is not unique (in fact the existence of this configuration and the observable features were predicted two decades ago), and many other systems were unearthed from the *Kepler* data (Thompson *et al.* 2012).

12. What's left for amateurs?

With the influx of new discoveries based on ever more precise data, one could not help but to ask: is there still a place for amateur observations, or, indeed, smaller professional telescopes? Perhaps surprisingly, our answer is a wholehearted *yes*. The abrupt end of the primary mission of *Kepler* left astronomers with literally thousands (if not tens of thousands) of targets in need of follow-up observations. The best-known example is KIC 8462852, or Boyajian's star, the mysterious object that showed irregular, short and deep fadings, most of which occurred during the last 100 days of the 1,600-day-long mission (Boyajian *et al.* 2016). The star is being followed by various amateur and professional astronomers to catch another large "dip", and after a successful fundraising campaign, the authors also secured extended telescope time on the Las Cumbres Observatory Global Telescope Network (LCOGT) to search for smaller ones.

Turning back to the pulsating stars: one expectation of the *Kepler* mission was to see whether the modulation of the star RR Lyr indeed goes through four-year cycles, as suggested by Detre and Szeidl (1973). *Kepler* did not detect any signs of such a cycle or an associated shift in the phase of the Blazhko effect: instead the amplitude of the modulation was steadily decreasing towards the end of the primary mission. But where was it heading? Did the Blazhko effect turn off completely? Did it recover? The answer was provided by the observations of amateur astronomers from the AAVSO, compounded by an array of small telephoto lenses called the Very Tiny Telescopes (VTTs). These data allowed the researchers to follow the phase variations of RR Lyr, and revealed that the modulation effectively turned off by 2014, before restarting in 2015 (LeBorgne *et al.* 2014; Poretti *et al.* 2016). Several papers also used the AAVSO measurements to put the *Kepler* observations into broader temporal context. A few examples include works on Miras and semiregular stars (Bányai *et al.* 2013, see Figure 2), dwarf novae (Otulakowska-Hypka *et al.* 2016), and intermediate polar stars (Littlefield *et al.* 2016).

Despite the advent of large sky-surveys, like Pan-STARRS, Gaia, and LSST, long-term behavior of pulsating stars, for example, O–C variations, can be secured only through amateur observations (often extending to several decades or even centuries). Perhaps counterintuitively, the largest surveys will not replace the backyard astronomers at all. There is a simple reason for this: the large-aperture telescopes collecting data for Pan-STARRS or LSST are aimed at the billions of faint objects on the sky, but typically saturate in the 12 to 15 magnitude range, leaving the bright objects unchecked. There are some professional projects that aim to fill this gap, like the Fly's Eye, Evryscope, or MASCARA instruments (Pál *et al.* 2013; Law *et al.* 2015; Snellen *et al.* 2013), but unlike the observing network of the AAVSO, these depend on the funding flow instead of the supply of volunteer observers. The sky is still there to explore and to discover for everybody.

13. Acknowledgements

The authors have been supported by the Lendület 2009 and LP2014-17 Young Researchers Programs, the Hungarian National Research, Development and Innovation Office (NKFIH) grants K-115709, PD-116175, and PD-121203, the European Community's Seventh Framework Programme (FP7/2007-2013) under grant agreement no. 312844 (SPACEINN), and the ESA PECS Contract Nos. 4000110889/14/NL/NDe. L. M. was supported by the János Bolyai Research Scholarship. The authors wish to thank Dr. T. Borkovits for his useful comments on the precession of eclipsing binary systems. This paper includes data collected by the *Kepler* mission. Funding for the *Kepler* and K2 missions are provided by the NASA Science Mission Directorate. This research has made use of the NASA Exoplanet Archive, which is operated by the California Institute of Technology, under contract with NASA under the Exoplanet Exploration Program. The authors gratefully acknowledge Ball Aerospace, the Kepler Project, Science, and Guest Observer Offices, and all those who have contributed to the mission for their tireless efforts which have made these results possible.

References

Balona, L. A., Baran, A. S., Daszyńska-Daszkiewicz, J., and De Cat, P. 2015, *Mon. Not. Roy. Astron. Soc.*, **451**, 1445.

Balona, L. A., *et al.* 2016, *Mon. Not. Roy. Astron. Soc.*, **460**, 1318.

Bányai, E., and Kiss, L. L. 2013, *Proc. Int. Astron. Union*, **9**, 381.

Bányai, E., *et al.* 2013, *Mon. Not. Roy. Astron. Soc.*, 436, 1576.

Barclay, T., Still, M., Jenkins, J. M., Howell, S. B., and Roettenbacher, R. M. 2012, *Mon. Not. Roy. Astron. Soc.*, **422**, 1219.

Beck, P. G., *et al.* 2012, *Nature*, **481**, 55.

Bedding, T. R., *et al.* 2011, *Nature*, **471**, 608.

Bell, K. J., Hermes, J. J., Bischoff-Kim, A., Moorhead, S., Montgomery, M. H., Østensen, R., Castanheira, B. G., and Winget, D. E. 2015, *Astrophys. J.*, **809**, 14.

Bell, K. J., *et al.* 2016, *Astrophys. J.*, in press, arXiv:1607.01392.

Benkö, J. M., Plachy, E., Szabó, R., Molnár, L., and Kolláth, Z. 2014, *Astron. J., Suppl. Ser.*, **213**, 31.

Benkő, J. M., *et al.* 2010, *Mon. Not. Roy. Astron. Soc.*, **409**, 1585.

Bódi, A., Szatmáry, K., and Kiss, L. L. 2016, *Astron. Astrophys.*, in press, arXiv:1609.07944.

Borkovits, T., Hajdu, T., Sztakovics, J., Rappaport, S., Levine, A., Bíró, I. B., and Klagyivik, P. 2016, *Mon. Not. Roy. Astron. Soc.*, **455**, 4136.

Borucki, W. J. 2016, *Rep. Prog. Phys.*, **79**, 036901.

Bowman, D. M., Kurtz, D. W., Breger, M., Murphy, S. J., and Holdsworth, D. L. 2016, *Mon. Not. Roy. Astron. Soc.*, **460**, 1970.

Boyajian, T. S., *et al.* 2016, *Mon. Not. Roy. Astron. Soc.*, **457**, 3988.

Buysschaert, B., *et al.* 2015, *Mon. Not. Roy. Astron. Soc.*, **453**, 89.

Campante, T. L., *et al.* 2015, *Astrophys. J.*, **799**, 170.

Christensen-Dalsgaard, J., *et al.* 2010, *Astrophys. J., Lett.*, **713**, L164.

Derekas, A., *et al.* 2011, *Science*, **332**, 216.

Derekas, A., *et al.* 2012, *Mon. Not. Roy. Astron. Soc.*, **425**, 1312.

Derekas, A., *et al.* 2016, *Mon. Not. Roy. Astron. Soc.*, in press, arXiv:1609.05398.

Detre, L., and Szeidl, B. 1973, *Inf. Bull. Var. Stars*, **764**, 1.

Doyle, L. R., *et al.* 2011, *Science*, **333**, 1602.

Eddington, A. S. 1926, *The Internal Constitution of the Stars*, Cambridge University Press, Cambridge.

Fuller, J., Cantiello, M., Stello, D., Garcia, R. A., and Bildsten, L. 2015, *Science*, **350**, 423.

Garnavich, P. M., Tucker, B. E., Rest, A., Shaya, E. J., Olling, R. P., Kasen, D., and Villar, A. 2016, *Astrophys. J.*, **820**, 23.

Greiss, S., *et al.* 2016, *Mon. Not. Roy. Astron. Soc.*, **457**, 2855.

Guggenberger, E., *et al.* 2012, *Mon. Not. Roy. Astron. Soc.*, **424**, 649.

Hermes, J. J., *et al.* 2015, *Astrophys. J., Lett.*, **810**, L5.

Howell, S. B., *et al.* 2014, *Publ. Astron. Soc. Pacific*, **126**, 398.

Kirk, B., *et al.* 2016, *Astron. J.*, **151**, 68.

Kolenberg, K. 2012, *J. Amer. Assoc. Var. Star Obs.*, **40**, 481.

Kurtz, D. W., Bowman, D. M., Ebo, S. J., Moskalik, P., Handberg, R., and Lund, M. N. 2016, *Mon. Not. Roy. Astron. Soc.*, **455**, 1237.

LaCluyzé, A., *et al.* 2004, *Astron. J.*, **127**, 1653.

Law, N. M. *et al.* 2015, *Publ. Astron. Soc. Pacific*, **127**, 234.

Le Borgne, J. F., *et al.* 2014, *Mon. Not. Roy. Astron. Soc.*, **441**, 1435.

Littlefield, C., *et al.* 2016, *Astron. J.*, submitted, arXiv:1609.01026.

Lund, M. N., *et al.* 2016, *Mon. Not. Roy. Astron. Soc.*, in press, arXiv:1608.07290.

Marion, G. H., *et al.* 2016, *Astrophys. J.*, **820**, 92.

Metcalfe, T. S., *et al.* 2012, *Astrophys. J., Lett.*, 748, L10.

Miglio, A., *et al.* 2012, *Mon. Not. Roy. Astron. Soc.*, **419**, 2077.

Miglio, A., *et al.* 2016, *Mon. Not. Roy. Astron. Soc.*, **461**, 760.

Molnár, L., Kolláth, Z., Szabó, R., Bryson, S., Kolenberg, K., Mullally, F., and Thompson, S. E. 2012a, *Astrophys. J., Lett.*, **757**, L13.

Molnár, L., Kolláth, Z., Szabó, R., and Plachy, E. 2012b, *Astron. Nachr.*, **333**, 950.

Molnár, L., Pál, A., Plachy, E., Ripepi, V., Moretti, M. I., Szabó, R., Kiss, L. L. 2015a, *Astrophys. J.*, **812**, 2.

Molnár, L., *et al.* 2015b, *Mon. Not. Roy. Astron. Soc.*, **452**, 4283.

Moravveji, E., Aerts, C., Pápics, P. I., Triana, S. A., and Vandoren, B. 2015, *Astron. Astrophys.*, **580**, A27.

Moskalik, P., and Kołaczkowski, Z. 2009, *Mon. Not. Roy. Astron. Soc.*, **394**, 1649.

Moskalik, P., *et al.* 2015, *Mon. Not. Roy. Astron. Soc.*, **447**, 2348.

Mosser, B., *et al.* 2012, *Astron. Astrophys.*, **548**, A10.

Murphy, S. J., Bedding, T. R., and Shibahashi, H. 2016, *Astrophys. J., Lett.*, **827**, L17.

Murphy, S. J., and Shibahashi, H. 2015, *Mon. Not. Roy. Astron. Soc.*, **450**, 4475.

Neilson, H. R., and Ignace, R. 2014, *Astron. Astrophys.*, **563**, L4.

Olling, R. P., *et al.* 2015, *Nature*, **521**, 332.

Otulakowska-Hypka, M., Olech, A., and Patterson, J. 2016, *Mon. Not. Roy. Astron. Soc.*, **460**, 2526.

Pál, A., *et al.* 2013, *Astron. Nachr.*, **334**, 932.
Pápics, P. I., Tkachenko, A., Aerts, C., Van Reeth, T., De Smedt, K., Hillen, M., Østensen, R., and Moravveji, E. 2015, *Astrophys. J., Lett.*, **803**, L25.
Plachy, E., Kolláth, Z., and Molnár, L. 2013, *Mon. Not. Roy. Astron. Soc.*, **433**, 3590.
Plachy, E., Molnár, L., Kolláth, Z., Benkő, J. M., and Kolenberg, K. 2014, *Proc. Int. Astron. Union*, **301**, 473.
Poretti, E., Le Borgne, J.-F., Klotz, A., Audejean, M., and Hirosawa, K. 2016, *Commun. Konkoly Obs.*, **105**, 73.
Reed, M. D., Foster, H., Telting, J. H., Østensen, R. H., Farris, L. H., Oreiro, R., and Baran, A. S. 2014, *Mon. Not. Roy. Astron. Soc.*, **440**, 3809.
Shibahashi, H., and Kurtz, D. W. 2012, *Mon. Not. Roy. Astron. Soc.*, **422**, 738.
Smolec, R., and Moskalik, P. 2012, *Mon. Not. Roy. Astron. Soc.*, **426**, 108.
Snellen, I., *et al.* 2013, in *Hot Planets and Cool Stars*, EPJ Web of Conf., 47, 03008, EDP Sciences, London.
Sódor, Á, *et al.* 2011, *Mon. Not. Roy. Astron. Soc.*, **411**, 1585.
Soszyński, I., *et al.* 2010, *Acta Astron.*, **60**, 17.
Stello, D., *et al.* 2011, *Astrophys. J.*, **739**, 13.
Still, M., Howell, S. B., Wood, M. A., Cannizzo, J. K., and Smale, A. P. 2010, *Astrophys. J., Lett.*, **717**, L113.
Szabó, R., *et al.* 2011, *Mon. Not. Roy. Astron. Soc.*, **413**, 2709.
Thompson, S. E., *et al.* 2012, *Astrophys. J.*, **753**, 86.
Triana, S. A., Moravveji, E., Pápics, P. I., Aerts, C., Kawaler, S. D., and Christensen-Dalsgaard, J. 2015, *Astrophys. J.*, **810**, 16.
Uytterhoeven, K., *et al.* 2011, *Astron. Astrophys.*, **534**, A125.
Welsh, W. F., *et al.* 2011, *Astrophys. J., Suppl. Ser.*, **197**, 4.
White, T. R., *et al.* 2013, *Mon. Not. Roy. Astron. Soc.*, **433**, 1262.
Williams, K. A., *et al.* 2010, *Astron. J.*, **139**, 2587.
Zakirov, M. M., and Azimov, A. A. 1990, *Inf. Bull. Var. Stars*, No. 3487, 1.
Zasche, P., and Paschke, A. 2012, *Astron. Astrophys.*, **542**, L23.

Period Changes and Evolution in Pulsating Variable Stars

Hilding R. Neilson
John R. Percy
Department of Astronomy and Astrophysics, University of Toronto, Toronto, ON M5S 3H4, Canada; neilson@astro.utoronto.ca, john.percy@utoronto.ca

Horace A. Smith
Department of Physics and Astronomy, Michigan State University, East Lansing, MI 48824-2320; smith@pa.msu.edu

Invited review paper, received October 18, 2016

Abstract We review ways in which observations of the changing periods of pulsating variable stars can be used to detect and directly measure their evolution. We briefly describe the two main techniques of analysis—(O–C) analysis and wavelet analysis—and results for pulsating variable star types which are reasonably periodic: type I and II Cepheids, RR Lyrae stars, β Cephei stars, and Mira stars. We comment briefly on δ Scuti stars and pulsating white dwarfs. For some of these variable star types, observations agree approximately with the predictions of evolutionary models, but there still exist significant areas of disagreement that challenge future models of stellar evolution. There may be a need, for instance, to include processes such as rotation, mass loss, and magnetic fields. There may also be non-evolutionary processes which are contributing to the period changes.

1. Introduction

Star lives are measured in billions of years, millions of years for very rare massive stars. It might seem, therefore, that it would be impossible for astronomers to observe and measure changes, due to stellar evolution, during their short lives, or during the 400-year life of modern astronomy. But they can! If the star pulsates, then its pulsation period depends on its radius and mass; the period varies approximately as radius$^{1.5}$ and mass$^{-0.5}$, (or period x (mean density)$^{0.5}$ is a constant, called the pulsation constant). Evolutionary changes in one or both of these produce small changes in the pulsation period, which can have a *cumulative* effect on the observed time of the star's maximum (or minimum) brightness.

In this review, we explain how these period changes are measured in several types of pulsating stars, and how they are used, along with theoretical models of the stars, to confirm (or not) our understanding of stellar evolution. At a very basic level, the observations indicate whether the star is expanding or contracting due to evolution, and at what rate. They can also call attention to other processes which may cause period changes, but are not due to evolution. We will highlight ways in which AAVSO observers have contributed, or could contribute, to this area of research.

Note that stars in a more rapid phase of evolution would be rare, but would have larger and easier-to-measure period changes. Stars in a slower phase of evolution would be more common, but would have smaller period changes.

2. Methodology

The (O–C) method is the classical method for studying period changes in variable stars, because it is sensitive to the *cumulative* effect of the period changes. It is described in detail in some of the papers in Sterken (2005) and in less detail in the monograph by Percy (2007). It compares the observed time of maximum brightness O with the calculated time C, assuming a known constant period P. When (O–C) is plotted against time, it produces a straight line if the period is constant, a parabola opening upward if the period is increasing linearly, a parabola opening downward if the period is decreasing linearly, and a broken straight line if the period changes abruptly. As an analogy, consider a watch which is running one second more slowly every day. It will lose 1 second in day 1, 2 seconds in day 2, 3 seconds in day 3, 4 seconds on day 4, and so on. The *accumulated* error will be 1 second in day 1, 3 seconds in day 2, 6 seconds in day 3, 10 seconds in day 4, and so on. The accumulated error increases as the *square* of the elapsed time. As noted in section 4.2, there are potential problems if there are long gaps in the dataset. Note also that period changes are expressed in a variety of units, including days per day, days per million years, and seconds per year.

The observed times O can be determined from the observations of the light curve by Pogson's method of bisected chords, or by fitting a standard light curve or an appropriate mathematical function to the portion of the light curve around maximum. If the light curve is stable from cycle to cycle, each cycle of the observed light curve can be fitted to a template made from the average light curve. Since pulsating stars vary periodically in radial velocity, the (O–C) method can be applied to the observed velocity curve also.

The period, and its changes with time, can also be determined by *wavelet analysis*, which is described below.

3. Classical Cepheids

3.1. Introduction

The variability of Cepheids was first discovered more than two centuries ago thanks to the naked-eye observations of η Aquilae (Pigott 1785) and of δ Cephei (Goodricke and Bayer 1786). These stars were not the first found to vary, but have ignited centuries of observations of Cepheid variable stars. Along with these stars, Chandler (1893) produced one of the first catalogues of variable stars. That catalogue was soon

followed by another (Nijland 1903), which first suggested that the period of δ Cephei was changing with time. Chandler provided a measurement of how much the period was changing in his third catalogue (Chandler 1896, 1904), about –0.05 s yr^{-1}.

The discovery that the periods are changing was surprising, but its interpretation was lacking. At the turn of the twentieth century, astronomers argued that Cepheid variability is explained by eclipses in a binary star system (Belopolsky 1895; Campbell 1895). While the period was known to be changing, its meaning was elusive until two more discoveries occurred.

The first of these discoveries was the Leavitt Law (Leavitt and Pickering 1912). The Leavitt Law is the relation between a Cepheid's period and its absolute brightness and is one of the most important tools for measuring distances. Given the distances to the nearest Cepheids, Shapley (1914) showed that Cepheids cannot be eclipsing binary stars, building on the work of Ludendorff (1913), Plummer (1914), and others. If they were eclipsing binary stars, then the radii of the two components would have to be greater than their separation to explain their light curves. The binary hypothesis became absurd, but did persist for another decade (Jeans 1925). Shapley did not offer an alternative hypothesis.

The importance of measuring period change became clear when Eddington (1917) developed the mathematical framework of stellar pulsation. In that derivation, he showed that the pulsation period of a Cepheid depends on the average density within the star. This period-mean density relationship forms the basis for understanding stellar pulsation. Eddington (1918, 1919a) realized that this relationship means that if one measures a change in period then one also measures a change in density. That is, one can measure the evolution of a star from the change in period.

Eddington pointed out the importance of this measurement and implored observers to measure the period change for more Cepheids. He then applied the observations of Chandler, remeasured the period change of the prototype δ Cephei, and tested it against the evolution of stars (Eddington 1919b). Eddington showed that δ Cephei was evolving at too slow a rate for it to generate energy from gravitational contraction. Astronomers had theorized that stars might produce their energy by contraction, but this meant that stars would live for only a few million years. Eddington was able to prove that stars had to generate energy in other ways. This result built the foundation for theories of nuclear energy generation in stars, changing the course of stellar evolution theory.

This one result was crucial for developing ideas of hydrogen fusion in stars, and the groundwork for modern astrophysics. All it required was about one century of watching the variable star δ Cephei. More than 230 years have passed since the discovery of Cepheid variability, allowing for more and more observations. Furthermore, having a longer baseline of observations allows for more precise measurements of period change, hence of stellar evolution.

3.2. Period change in other Cepheids

Period changes have since been measured for other classical Cepheids and, in the next 80 years from 1920 to the new millennium, there are too many studies to cite them all. As such, we highlight some of the most significant developments in measuring Cepheid period change and using the measurements to understand the physics and evolution of these stars.

One of the first leaps ahead was reported by Kukarkin and Florja (1932) for eight Cepheids including the prototype δ Cephei. Even though their sample was small, they presented the first estimate of how rates of period change depend on the pulsation period. They showed that the rate of period change increases as a function of period. This result is striking since two stars in their sample, δ Cep and ζ Gem, have decreasing rates of period change, which means that their densities are increasing. But, it also suggests that the longest-period Cepheids are evolving the most rapidly.

Parenago (1957) measured rates of period change for 24 classical Cepheids plus ten Type II Cepheids. While much of his analysis was consistent with Kukarkin and Florja (1932), he did find evidence for abrupt changes in period that are inconsistent with stellar evolution. There is currently no physical explanation for these abrupt shifts, nor can we be sure that they are real.

While these observations broadened the view of Cepheid period change as function of period itself, it was not until the 1960s when theorists developed the first models of Cepheid evolution and of Cepheid pulsation. These models were another significant leap forward in the understanding of Cepheids (Baker and Kippenhahn 1965; Christy 1963), but they also raised a new set of challenges. For instance, if we can measure how hot and how luminous a Cepheid is, then we can use evolutionary models to measure the star's mass. Similarly, if we measure the period of the Cepheid, we can compute stellar pulsation models to also measure the star's mass. But, it quickly became apparent that stellar evolution models predicted Cepheid masses that were greater than the masses predicted by the pulsation models of the same star. This infamous problem, called the Cepheid mass discrepancy, persists today, though the difference is much less than it was fifty years ago (Cox 1980; Keller 2008; Neilson *et al.* 2011).

In a series of reports, (Hofmeister *et al.* 1964a, 1964b; Hofmeister 1967), Eddington's earlier advice to use Cepheid period change to test stellar evolution was first heeded. Hofmeister realized that having measurements of period change for a large number of Cepheids could be used to test the reliability of the stellar evolution models. This is because, on the Hertzsprung-Russell diagram, stars cross the Cepheid instability strip multiple times and in different directions. For instance, when the pulsation period of a Cepheid is decreasing, the density of the star must be increasing. The density increases when the star shrinks, that is the radius decreases. When the radius decreases the star becomes hotter, hence moves across the Hertzsprung-Russell diagram. In this illustration, the rate of period change tells us about how fast the star is evolving across the Hertzsprung-Russell diagram.

At the same time, the first modern stellar evolution models of Cepheids were produced that suggested Cepheids cross their instability strip at least three times in their lives. This evolution is shown for a star that is five times more massive than the Sun in Figure 1. The star first crosses the instability strip and pulsates relatively soon after the star ceases fusing hydrogen in the core. When this occurs, the star loses a source of energy and the star

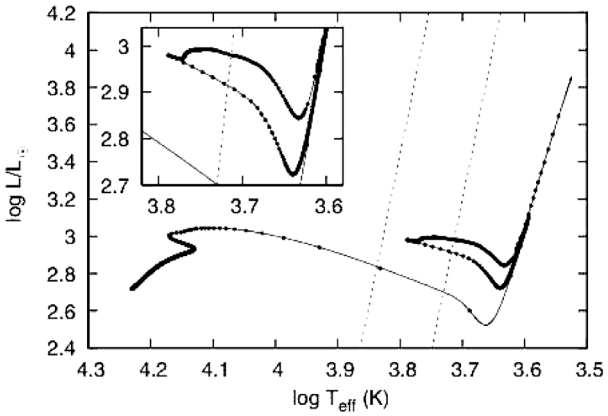

Figure 1. The evolution of a 5 $M_{\odot}$ star along the Cepheid instability strip on the Hertzsprung-Russell diagram. The dots represent changes in time of 100,000 years. From the number of points, the first crossing of the instability strip lasts less than 100,000 years, while the third crossing lasts about 10 million years. The boundaries of the instability strip were determined by Bono *et al.* (2000).

must expand rapidly to maintain the balance between gravity and pressure. This first crossing is short lasting, from about 100,000 years for the least massive Cepheids and decreasing to about 10,000 years for the most massive. Based on this relatively short time scale, we can expect that Cepheids at this stage of evolution will have rapidly changing periods.

The star then evolves into a red giant star, reaching its largest size. At the same time the core of the star is contracting and getting hotter. Eventually, nuclear fusion ignites again and the star changes direction in its evolution. The star travels in a blue loop, where the star loops through the Cepheid instability strip leading to the second and third crossings. During the second crossing the star is contracting, hence the mean density is increasing and the pulsation period is decreasing. On the third crossing the opposite occurs. These crossings last from about 10 million years to about 100,000 years for the least to most massive Cepheids, respectively.

These time scales suggest that we can test evolution models if we have measurements of period change for enough Cepheids. Thanks to the work of Hofmeister, a renewed and continuing effort was motivated to measure Cepheid period change. In the thirty to forty years since that work, rates of period change were reported for many more Cepheids, including many instances of measurements for individual Cepheids (for example, Winzer 1973; Erleksova 1978; Fernie 1979). But, of greater interest was the development of programs to gather rates of period change for populations of Cepheids.

One of the first such programs was led by the AAVSO (Cragg 1972). This program gathered observations of about twenty Cepheids as one of the first coordinated efforts to monitor Cepheids. Across the ocean, another program was gathering measurements of period change for about 70 Cepheids with a range of pulsation periods (Szabados 1983). These two analyses offered some of the first measurements of large populations of Cepheids and their period change.

Up to this time, all reports of Cepheid period change were for stars in our galaxy. But, the growth of surveys of Magellanic Cloud stars allowed for astronomers to measure rates of period change for Cepheids in other galaxies. Deasy and Wayman (1985) presented data for classical Cepheids in the Small and Large Magellanic Clouds based on observations spanning from almost 1910 (Payne-Gaposchkin and Gaposchkin 1966; Payne-Gaposchkin 1971) to 1978 (Martin 1981). Period changes were confirmed for about 50 Cepheids in their sample, adding a whole new dimension to understanding Cepheid evolution and pulsation. Because stars in the Magellanic Clouds have less iron, nickel, and elements other than hydrogen and helium in their interiors, their rates of period changes test different conditions for stellar evolution than those of Galactic Cepheids. From their measurements Deasy and Wayman (1985) showed that the evolutionary models developed by Hofmeister (1967) were mostly consistent with the observations. However, Deasy and Wayman (1985) did measure abrupt changes in period beyond the secular changes of period that could not be explained by models.

3.3. The current state of observations

Given the explosion of measurements and surveys since the 1980s, we can now consider the current state of Cepheid period change measurements. This is summarized for two cases: Cepheids in the Galaxy, and Cepheids in the Magellanic Clouds.

Measurements of period change of Cepheids in both the Small and Large Magellanic Clouds have been motivated by large time-series surveys originally designed to search for gravitational microlensing events caused by MACHOs. MACHOs, massive compact halo objects, are small, dim objects that exist in the outer halo of our galaxy. These hypothetical objects would exert gravitational forces on material in the Galactic disk and explain the observed rotation curve of the Galaxy. Hence, detecting MACHOs would solve the dark matter problem (Griest 1991). However, the two main surveys, OGLE (Paczyński *et al.* 1994) and the aptly named MACHO (Alcock *et al.* 1996), failed to detect MACHOs, but they did observe continuously thousands of Cepheids in the Magellanic Clouds. While the MACHO project has ended the OGLE survey is still ongoing, now in its fourth iteration. Poleski (2008) compiled period change measurements from both surveys for both first-overtone and fundamental mode pulsating Cepheids. He found that for observations spanning about 4,000 days, the period change was more pronounced for the first-overtone Cepheids and many of them displayed erratic changes in period that are inconsistent with evolution. These results are surprising and suggest that some other unknown physics is determining the period of Cepheids in these galaxies.

In our galaxy, Turner *et al.* (2006) compiled observations from the Harvard Plate collections and from the AAVSO to measure period changes in almost 200 Galactic Cepheids. These observations spanned about a century and required monumental effort, especially the evaluation of the observation plates. For example, we show a sample O–C diagram for Polaris spanning about 200 years in Figure 2 (Neilson *et al.* 2012a).

These measured rates of period change were found to, again, be broadly consistent with stellar evolution models. While that result might seem underwhelming, Turner *et al.* (2006) presented measurements for a large enough sample of Cepheids as suggested forty years previously by Hofmeister (1967). Neilson *et al.* (2012b) constructed state-of-the-art

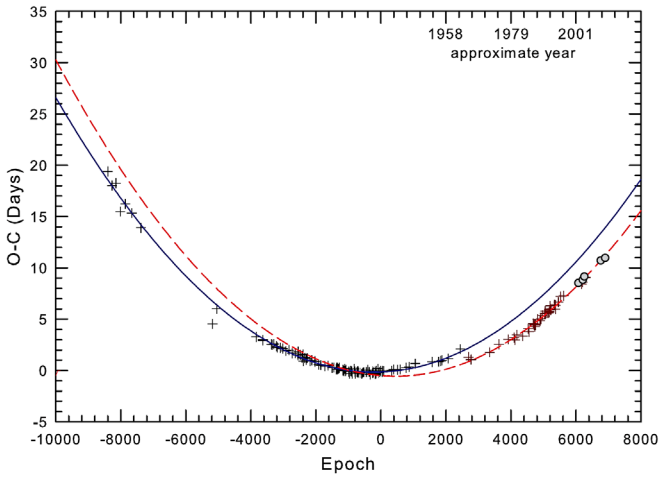

Figure 2. Timing measurements for the Cepheid Polaris over the past 200 years (Neilson *et al.* 2012a). There exists a notable glitch in 1963 that continues to be unexplained. The authors fit the O–C diagram separately over the time frames with lines to note the importance of the glitch. A fit of the period change over all the data yields a measurement of $\dot{P} = 4.47 \pm 1.46$ seconds per year.

stellar evolution models of Cepheids and predicted how many Cepheids would have increasing periods and how many would have decreasing periods. This is equivalent to comparing the evolutionary life times for Cepheids evolving on the first and third crossings to those evolving on the second crossing of the instability strip.

These life times are dependent on the physics of the models, such as the nuclear burning rates in the stellar core, rotation and even on their stellar winds. From the Turner *et al.* (2006) sample about two-thirds of Cepheids have positive rates of period change whereas the remaining one-third have negative rates of period change. Assuming so-called standard stellar evolution models, Neilson *et al.* (2012b) predicted that about 85% of Galactic Cepheids should have positive rates of period change. This prediction is much greater than suggested from observations—there appeared to be physics missing from the so-called standard models. The authors computed a new set of stellar evolution models, but this time assuming that during the Cepheid stage of evolution the star underwent enhanced mass loss. This enhanced mass loss has been hinted at by recent infrared and radio observations (Kervella *et al.* 2006; Neilson *et al.* 2010; Marengo *et al.* 2010; Matthews *et al.* 2012). From the new set of evolution models the predicted number of Cepheids with positive rates of period change decreased from 85% to about 70%, much more in line with the fraction suggested by observations. This is the first result to test populations of Galactic Cepheids and their corresponding rates of period change. In one century, Cepheid period changes have been used to disprove gravitational contraction by Eddington to now probing the precise details of their physics. Even more recently, Anderson *et al.* (2014, 2016) computed new stellar evolution models that include the physics of rotation. They showed that rotation impacts the future evolution of Cepheids and that including rotation in the models may be necessary to understand measured rates of period change as well.

While the results from Turner *et al.* (2006) demonstrated the power of period change for understanding stellar evolution, the emergence of new space-based telescopes designed for planet hunting adds yet another dimension. Derekas *et al.* (2012) presented continuous *Kepler* space telescope observations of the one Cepheid in its initial field, V1154 Oph. The time scale of observations was too short to definitively say anything about the evolution of the star but the period was seen to vary by about 30 minutes every pulsation cycle (4.9 days). This variation appeared random and unexplained, based on variations of light of the order of a millimagnitude. Poleski (2008) suggested previously that such variations might be caused by instabilities in the pulsation. Conversely, Neilson and Ignace (2014) showed that the variation might be due to convective granulation in Cepheids. Granules in the Sun are small bubbles of plasma that rise to surface and are both hotter and brighter than the surrounding material. In Cepheids if granules were somewhat bigger (which has been seen in red supergiant stars (Haubois *et al.* 2009)) then the brightness of the Cepheid would vary a small amount from cycle to cycle. Derekas *et al.* (2016) confirmed this hypothesis and quantified the convective granulation properties of the Cepheid. Evans *et al.* (2015) detected similar phenomena in two other Galactic Cepheids from MOST space telescope observations.

The Turner *et al.* (2006) and space-based measurements have allowed for a new path of Cepheid research, but a number of their measurements have since been revisited. Engle *et al.* (2014) and Anderson *et al.* (2015) presented new measurements of the rate of period change for δ Cep that are somewhat different. However, more significant is the revised rate of period change for the long-period Cepheid *l* Carinae. Turner *et al.* (2006) measured the period to be increasing by about 120 seconds every year, but Breitfelder *et al.* (2016) and Neilson *et al.* (2016) independently measured a rate of period change of about 25~seconds every year. Neilson *et al.* (2016) showed that this small rate of period change for such a long-period Cepheid could present significant challenges for understanding this star's evolution. These new results do not diminish the accomplishment of the Turner *et al.* (2006) work, but instead illustrate the need for continued observations of Galactic Cepheids with current precision via the work of the AAVSO.

3.4. The perplexing problem of Polaris

While we could finish the discussion of period change in Cepheids with the work of Turner *et al.* (2006) and the plea for continued monitoring of these stars to improve these measurements, our nearest Cepheid, Polaris, demands its own discussion. Polaris has been a subject of much discussion recently, not just because it is a key step in the cosmic distance ladder, or the celestial navigator, but because it is undergoing changes in its period and brightness that force us to question its evolution. Polaris has been measured to have not only a rapid and positive period change, but its amplitude has also been changing. For much of the past century, the amplitude of light variation in Polaris has been seen to decrease. By the early 1990's Fernie *et al.* (1993) argued that we were seeing Polaris transition from a Cepheid to a "normal" non-pulsating star. However, Polaris did not cease pulsating and its light amplitude appears to be increasing again (Bruntt *et al.* 2008). This variation of amplitude is not at all understood and is one of the open questions about this star.

Another simple and related, yet perplexing question is how far away is Polaris. Van Leeuwen *et al.* (2007) measured a distance of about 130 pc from its HIPPARCOS stellar parallax. However, from its spectrum, Turner *et al.* (2013) measured a smaller distance of about 100 pc. When combined with interferometric measurements of its angular diameter we measure the radius of Polaris. We can take the measured radius as a function of distance and calibrated period-radius relations (Gieren *et al.* 2005) to determine if Polaris is pulsating in the fundamental or first-overtone mode. If Polaris is at the closer distance then it is most likely pulsating in the first-overtone mode. If it is at the farther distance, then Polaris is a fundamental-mode Cepheid.

But, this distance problem is related to our understanding of Polaris from its rate of period change. Turner *et al.* (2005) measured a rate of about 4.5 s yr^{-1} from observations stretching as far back as 1844. This rate is perplexing; Turner *et al.* (2005) noted that this rate of period change challenges the likelihood that Polaris is a fundamental-mode Cepheid because it is too small for a fundamental-mode pulsator on the first crossing of the instability strip yet is too large for a Cepheid on the third crossing. Engle *et al.* (2004) presented independent measurements of the rate of period change of Polaris, yielding similar results to Turner *et al.* (2005). However, the interpretation that Polaris is a first-overtone Cepheid on the first crossing is true only if the HIPPARCOS distance is wrong.

These measurements left a tension between our understanding of the evolution of and distance to Polaris. Neilson *et al.* (2012a) remeasured the rate of period change and again found a similar rate of about 4.5 s yr^{-1}. They hypothesized that this tension could be resolved if Polaris were undergoing enhanced mass loss. This enhanced mass loss acts to increase the rate of period change, meaning that Polaris is evolving along the third crossing of the instability strip at the distance measured by van Leeuwen *et al.* (2007). While this idea is interesting it requires Polaris to lose almost one Earth mass of material every year, an amount about 1,000 times greater than understood from standard theory of stellar winds.

This hypothesis, while consistent with recent observations of Cepheid circumstellar environments (Mérand *et al.* 2006; Marengo *et al.* 2010; Matthews *et al.* 2012), is still contentious. As such, we still do not know whether the nearest Cepheid Polaris pulsates as a fundamental or first-overtone mode Cepheid, whether Polaris is about 100 pc away or 130 pc, or whether Polaris is actually undergoing enhanced mass loss in a wind or has a weak stellar wind.

On top of all of these challenges for understanding Polaris, continuous observations show that an unexplained glitch in the pulsation period occurred in 1963 (Turner *et al.* 2005; Neilson *et al.* 2012a). This is seen in the O–C diagram for Polaris, Figure 2 (Neilson *et al.* 2012a). This glitch may be an issue with the timing of observations in 1963 or there may have been some sort of spontaneous change in pulsation period. That type of glitch is still a mystery.

This glitch and the ongoing debate surrounding the period change of Polaris and its properties (Turner *et al.* 2013; van Leeuwen 2013; Neilson 2014; Anderson *et al.* 2016) requires new and continuous observations to help us test theories of pulsation and evolution and to understand the nearest Cepheid.

3.5. Outlook

We are entering an exciting time for probing the connections between pulsation and evolution in classical Cepheids. In the next decade, there will be new space-based telescopes, such as PLATO, TESS, and WFIRST that will take precise observations of Cepheids and measure the details of Cepheid light curves. There will be more continuous surveys from the Earth using facilities such as the Large Synoptic Survey Telescope, along with the continuous observations of OGLE. But, these facilities lack the ability to observe the nearest Cepheids in our galaxy and add to the century or more of time measurements to probe the physics of Cepheid evolution.

There is a continued need for observations of nearby Cepheids to explore the roles of rotation, winds, and other physics. As we learn more about these phenomena then we can also learn more about the evolution of massive stars and supernovae along with helping to precisely calibrate the Cepheid Leavitt Law for measuring the expansion of the Universe.

4. RR Lyrae stars and type II Cepheids

RR Lyrae stars and type II Cepheids are both believed to be varieties of old, low-mass stars in advanced but different stages of evolution. We begin with a look at the evolutionary state of RR Lyrae variables. RR Lyrae stars are modest giants, with radii about 4–6 solar radii, pulsation periods in the range 0.2 to 1.0 day, and masses of about 0.6 or 0.7 solar mass. RR Lyrae stars have already evolved off the main sequence, up the red giant branch, and initiated core helium burning at the tip of the red giant branch in a so-called helium flash. After igniting helium burning, they quickly move to the zero-age horizontal branch (ZAHB) where they spend about 10^8 years deriving energy from the fusion of helium into carbon and oxygen in the stellar core, supplemented by energy from fusing hydrogen to helium in a shell surrounding the helium core. Only those horizontal branch stars that find themselves within the instability strip will pulsate as RR Lyrae variables (Figure 3). A horizontal branch star may thus spend all, none, or only a portion of its core helium burning lifetime as an RR Lyrae. Once they exhaust their central helium, RR Lyrae variables will leave the horizontal branch, eventually exiting the instability strip and becoming red giant stars for a second time, so-called asymptotic branch red giants (Catelan and Smith 2015).

Like other low-mass horizontal branch stars, RR Lyrae stars are very old, older than about 10^{10} years. The Milky Way's globular clusters provide examples of such old stellar populations and many, but not all, globular clusters contain RR Lyrae variables. However, more RR Lyrae stars are now known to exist among the field stars of the Milky Way and other Local Group galaxies than are within globular clusters.

Type II Cepheids have periods that range from about 1 day to 25 days. They are sometimes called Population II Cepheids but, while all of the stars within this group appear to be very old, some are metal-rich, unlike true Population II stars. Thus, type II may be a better name. At the upper period limit, the distinction

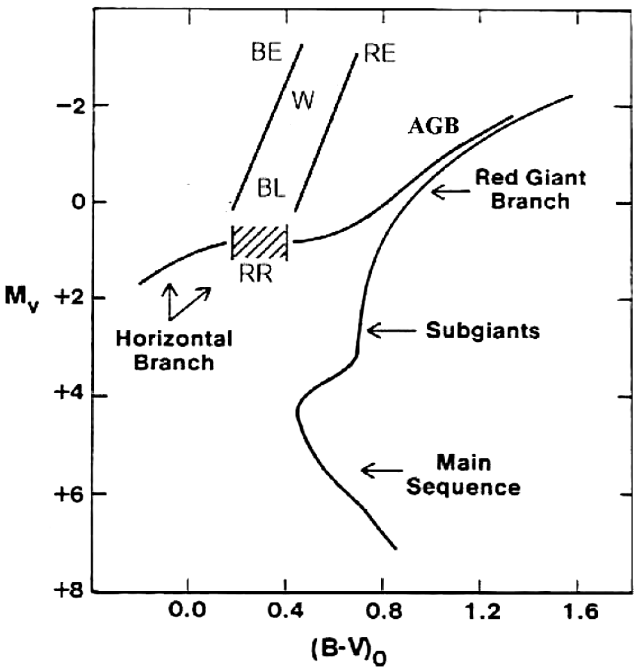

Figure 3. Representative color-magnitude diagram for a globular star cluster. The hatched area on the horizontal branch indicates the location of RR Lyrae variables. BL Her (BL) and W Virginis (W) variables are brighter than RR Lyrae stars and are found between the blue (hot) and red (cool) edges of the instability strip, the slanting lines marked by BE and RE, respectively. The second red giant sequence, labeled AGB, indicates the location of the asymptotic red giant branch.

is not always clear between W Vir and RV Tauri variables, and some stars with periods longer than 25 days might legitimately be called type II Cepheids.

Like the RR Lyrae stars, type II Cepheids are associated with very old stellar populations, such as globular clusters. They are found within the instability strip, but at luminosities brighter than the level of the horizontal branch (Figure 3). Their masses are smaller and their ages much older than those of the classical Cepheids.

A distinction has long been made between the shorter and longer period type II Cepheids, although different nomenclatures and dividing points have been adopted by different astronomers. Type II Cepheids with periods shorter than 4–8 days have been called BL Herculis stars or AHB1 stars (where the AHB stands for above the horizontal branch), whereas those of longer period are often called W Virginis variables. The *General Catalogue of Variable Stars* (GCVS; Kholopov *et al.* 1985) makes the dividing line 8 days, calling type II Cepheids with periods longer than 8 days CWA variables whereas those of shorter period are CWB stars.

When we consider the evolutionary states of type II Cepheids we find that things are not as well established as for the RR Lyrae variables. A clue to the evolutionary state of type II Cepheids comes from the circumstance that, when they are found within globular clusters, those globular clusters have horizontal branches with a strong component of stars on the blue (hot) side of the RR Lyrae instability strip. This has led to the idea that blue horizontal branch stars are in some fashion the progenitors of type II Cepheids, and that all type II Cepheids have already gone through core helium burning.

For BL Her variables, there is a plausible mechanism by which stars evolving from the blue horizontal branch might enter the instability strip. Blue horizontal branch stars with masses smaller than about 0.51 solar mass are thought to evolve directly to the white dwarf stage. However, theory tells us that blue horizontal branch stars with masses greater than about 0.52 solar mass will become brighter and cooler after the end of their horizontal branch lives, crossing the instability strip from blue to red at luminosities brighter than the level of the RR Lyrae variables. Such stars would occupy the lower portion of the Cepheid instability strip where BL Her variables are located. Eventually they would leave the instability strip to become red giant stars on the asymptotic red giant branch (Gingold 1976; Bono *et al*. 1997; Bono *et al.* 2016).

This evolutionary scenario may explain the occurrence of at least some BL Her variables, but such redward crossing post-horizontal branch stars would not be expected to become as bright as W Virginis variables. An additional crossing of the instability strip at the BL Her level, informally termed "Gingold's nose" after its discoverer, has not been seen in more recent theoretical calculations (Bono *et al.* 2016). In any case, some additional mechanism is necessary to put old stars within the instability strip at the brightness of the W Vir variables.

Unfortunately, the guidance of theory is not entirely clear as to what that mechanism might be. W Virginis variables have sometimes been thought to come from stars that have already reached the asymptotic red giant branch, well to the red of the Cepheid instability strip. It has been proposed that, under the right conditions, asymptotic red giants could undergo short duration loops that move them temporarily blueward into the instability strip while they are undergoing so-called thermal pulses caused by instabilities in their helium burning shells (Schwarzschild and Härm 1970). Thermal pulses are described in slightly more detail in the introduction to section 6. These loop stars would be bright enough to be W Vir stars when they were inside the instability strip. After undergoing such a loop, a W Vir star would, under this scenario, return once more to the asymptotic red giant branch. However, recent calculations have found that most stars with masses appropriate for blue horizontal branch stars may not undergo large thermal instability pulses when they reach the asymptotic red giant stage. Thus, the blueward loop mechanism may not work, or may not work for enough stars to explain the existence of W Vir variables (Bono *et al.* 2016).

Even without thermal pulses, asymptotic red giants would be expected to enter the instability strip at least one more time. At the end of their asymptotic red giant branch lives, they would move from from red to blue on their way to becoming white dwarf stars, crossing the instability strip in the process. This blueward crossing might happen at luminosities brighter than the W Vir level, and the stars might then appear as RV Tauri variables rather than W Vir stars, but it might also be a mechanism for creating W Vir variables. Moreover, blue horizontal branch stars with masses near 0.52 solar mass may not head directly for the asymptotic giant branch after core helium exhaustion, but could possibly briefly loop into the instability strip from the blue side at W Vir luminosities before they reverse course and head for the white dwarf cooling sequence (see Figure 2 in Bono *et al.* 2016).

If that is not confusing enough, there are even more possible sources of complication. The above evolutionary scenarios were modeled for single stars, whereas there is increasing evidence that some type II Cepheids might be members of binary stars (Welch 2012). Differences in photospheric chemical abundances for field type II Cepheids have also suggested that W Vir variables cannot have evolved from stars that were BL Her variables earlier in their existence (Maas *et al.* 2007).

4.1. Theoretical RR Lyrae period changes

The basic pulsation equation guides us in turning theoretical evolution through the Hertzsprung-Russell diagram into changes in period. If the density of a pulsating star decreases, we would expect its period to increase. If the density increases, the period should decrease. A horizontal branch star should slowly change its effective temperature and luminosity as it gradually converts its central helium into carbon and oxygen. However, the lifetime for helium burning by a horizontal branch star is about 10^8 years, and the resultant changes in density are thus expected to be small over the somewhat more than a century that RR Lyrae stars have been under observation.

Theoretical period changes due to stellar evolution are in almost all cases predicted to be less than about 0.1 day per million years and to occur at nearly constant rates over spans of a century or so (Sweigart and Renzini 1979; Koopmann *et al.* 1994; Kunder *et al.* 2011). Theoretical rates of period change are expected to be largest for RR Lyrae variables at the two extremes of horizontal branch life, the beginning and the end. Toward the end of the life of an RR Lyrae, as it begins to exhaust its central helium, its period might increase at rates of 0.2 or 0.3 day per million years. An RR Lyrae star in those end stages of horizontal branch life might also experience instabilities that could cause temporary period increases or decreases. However, the large majority of RR Lyrae stars would not be expected to be in these final stages of core helium burning.

Larger rates of period change, usually period decreases, might also occur for a small but perhaps non-negligible number of RR Lyrae stars that have not yet begun core helium burning on the horizontal branch but are just about to do so (Silva Aguirre *et al*. 2010). Most such pre-ZAHB RR Lyrae would have period changes between 0 and -1 days per million years, though a few might have even more extreme rates of period change.

4.2. RR Lyrae: observations confront theory

RR Lyrae stars were first established as a class of variable star through the efforts of Harvard astronomer Solon Bailey and his associates, who identified large numbers of them within certain globular clusters (for example, Bailey 1902). However, RR Lyrae itself, still the brightest known member of the class, is a field star that was discovered by another Harvard astronomer, Williamina Fleming (Pickering 1901). Most RR Lyrae stars can be placed into one of two groups: RRab type variables which are believed to be pulsating mainly in the fundamental radial mode, and RRc variables, which are believed to be pulsating in the first overtone radial mode. A smaller number of RR Lyrae variables pulsate in other radial modes or simultaneously in multiple modes (Percy 2007; Catelan and Smith 2015).

By the 1920s and 1930s, it became clear that at least some RR Lyrae variables experienced changes in period (Barnard 1919; Leavitt and Luyten 1924; Martin 1938; Prager 1939). Today, we have observational records for some RR Lyrae stars that extend for more than a century, about 100,000 pulsational cycles. Sometimes period changes of RR Lyrae stars have been discovered through the direct comparison of periods calculated for different years of observation, but more often through an application of some version of the O–C diagram. As noted in the Methodology section above, if the period of a star is increasing or decreasing at a small but constant rate, we expect the O–C diagram to look like a parabola. The rate of period change defined by a parabola can be parameterized by a single number, often called β, which is frequently given in units of days per million years. Note that there is a danger in applying the O–C method to determining the period changes for stars that have significant gaps in the observational record. If an RR Lyrae star is changing rapidly in period, it might not be possible to correctly count the number of cycles that have elapsed between two observed maxima of the star. If the cycle count is wrong, the period change deduced from the O–C diagram will be wrong.

Stellar evolution theory would lead us to expect that the O–C diagram for the large majority of RR Lyrae variables should appear to be either a straight line (no measurable period change) or a parabola corresponding to a value of β smaller than 0.1 day / Myr. A few RR Lyrae near the end of core helium burning might have somewhat larger values of β, up to about +0.3. A few pre-ZAHB RR Lyrae might have large negative values of β. Significant changes in the evolutionary rate of period change would not be expected to occur on a timescale as short as a century.

Observations in many cases contradict this theory. We see too many large and too many variable rates of period change. One example of this is shown by the O–C diagram of the RRab star AR Her. This O–C diagram, shown in Figure 4, is based upon observations obtained between 1926 and 2016 and is calculated assuming a constant period of 0.47000604 day. While the generally increasing O–C until the 1950s and the declining O–C beginning in the 1980s might remind one of rising and falling portions of a parabola, it is clear that something else is going on. Between the 1950s and the 1980s there are abrupt

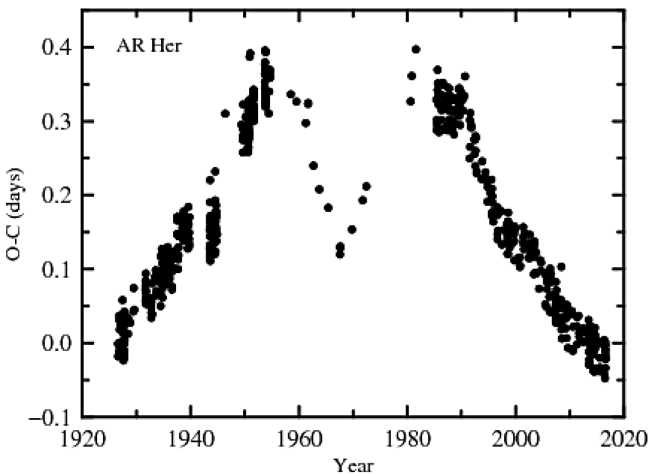

Figure 4. O–C diagram of the RRab star AR Her, courtesy of G. Samolyk and based in part upon AAVSO observations.

changes in period, both down and up. This diagram further illustrates the danger of gaps in the observational records of RR Lyrae stars. Had no observations of AR Her been obtained between 1960 and 1980 (and the observed maxima are few within that range), we would have no way of knowing how the period of the star fluctuated during those years.

O–C diagrams for many field RR Lyrae stars are available on the web through the GEOS project (LeBorgne *et al.* 2007, http://rr-lyr.irap.omp.eu/dbrr/). AR Her is not unique. The O–C diagrams of other RR Lyrae stars imply multiple, abrupt period changes, for example, those of XZ Cyg and RW Dra. By contrast, still others have O–C diagrams that imply small or negligible period changes, much more consistent with the predictions of stellar evolution theory. SU Dra and RR Cet would be examples of such variables. In fact, despite the clearly discrepant stars, for many stars the observed rates of period change are consistent with the predictions of stellar evolution theory (LeBorgne 2007; Percy and Tan 2013).

Poretti *et al.* (2016), analyzing 123 RRab stars in the GEOS database, found that 27 stars showed significant period increases, 21 showed signficant decreases, and 75 did not show a significant overall change in period. The median β value for the stars of increasing period was +0.14 day / Myr, while the median β for the stars of decreasing period was –0.20 day / Myr. A number of RR Lyrae stars had values of β more negative than –0.5 day / Myr or greater than +0.5 day / Myr. Most extreme was SV Eri, with a value of β near +2.1 (though O–C values for SV Eri show considerable departures from a perfect parabola).

Observed period changes thus suggest that there is some additional source or sources of period change, some sort of period change noise, superposed upon the smooth and generally small rates of period change caused by progressive nuclear burning. We have, then, two rather than one question to address using the observed period changes: (1) do observed rates of period change match those predicted by stellar evolution theory, and (2) what causes the period change noise?

Sweigart and Renzini (1979) suggested that the period change noise might be produced by discrete mixing events in the interiors of the stars that could produce both period increases and decreases. In the long run, these mixing events would average to the evolutionary rate of period change, but that would not necessarily be apparent over a timescale of a century or so. Mass loss on the horizontal branch, if large enough, might also produce additional period changes, but probably not ones as large as frequently observed (Koopmann *et al.* 1994; Catelan 2004). Cox (1998) proposed that period changes might result from the occasional dredging up of helium that had gravitationally settled beneath the convective zones of RR Lyrae variables. Stothers (1980) suggested that the period change noise might have a hydromagnetic origin, associated with changes in the radii of the stars. There are thus plausible mechanisms but no fully agreed upon answer as to which of them actually causes the period change noise.

Must we then give up all thought of testing the stellar evolution of RR Lyrae stars with observed period changes? Perhaps not. One might seek a solution by averaging out random period change noise to reveal the underlying evolutionary changes in period. For any individual RR Lyrae star, one can only be sure of doing this by keeping up observations for many, many years into the future. An alternative, more feasible now, is to average the rates of period change for many RR Lyrae stars. The mean value of β for the 123 RRab stars studied by Poretti *et al.* (2016) using the GEOS database is small, as might be expected from slow stellar evolution.

Globular cluster RR Lyrae stars can also help in this endeavor. Some globular clusters contain numerous RR Lyrae stars and have been under observation for a century or more. Perhaps the average behavior of RR Lyrae stars within globular clusters can allow a useful comparison between theory and observation. Again, however, the warning against gaps in the observational record must be given. As we have already noted, gaps can make the correct counting of cycles between points in an O–C diagram difficult, with consequent period change uncertainties.

Individual RR Lyrae variables within globular clusters show a range in period change behavior, as do individual RR Lyrae stars within the field of the Galaxy. However, the average RR Lyrae period changes in different globular clusters is usually close to zero, and in reasonable agreement with theory. Noteworthy is an expected rise in the mean rate of period change as we go to globular clusters with very blue horizontal branches. In these clusters, more RR Lyrae stars than usual would be expected to be evolving from blue to red toward the end of their horizontal branch lifetimes, producing an increase in average β. However, although this is observed, the higher rate of period increase for blue horizontal branch clusters depends strongly upon the period change results for only a few clusters, especially ω Centauri (Lee 1991; Catelan and Smith 2015).

As many as half of the RRab stars and perhaps 5–10% of RRc stars exhibit long secondary periods, a phenomenon called the Blazhko effect (Kolenberg 2012). Szeidl *et al.* (2011) and Jurcsik *et al.* (2012) found that RR Lyrae stars in the globular clusters M3 and M5 that exhibited the Blazhko effect were more likely to have erratic period changes. Arellano Ferro *et al.* (2016) note, however, that determining period changes can also be more difficult for such stars. AR Her, with the erratic O–C diagram shown in Figure 4, is also a star with the Blazhko effect. The 123 RRab GEOS stars for which Poretti *et al.* (2016) discussed period changes excluded stars known to show the Blazhko effect, thereby perhaps also excluding some stars with more erratic period behavior.

We note one final use of period change studies of RR Lyrae stars. An RR Lyrae star that is a member of a widely separated binary star can in principle exhibit periodic cycles in the O–C diagram because of differing light travel times when the star is in different portions of its orbit. The number of binary candidates found by this method is still small (Skarka *et al.* 2016), and the possible orbital periods tend to be long (23 years in the case of TU UMa, Wade *et al.* 1999). See also section 5.1 for a further discussion of binary star light-travel time.

4.3. RR Lyrae period changes: outlook for the future

AAVSO monitoring of selected field RR Lyrae variables was begun by Marvin Baldwin (1968) in the 1960s, with observations at first being obtained visually and more recently mainly with CCD cameras. That observing program now

continues under the aegis of the short period pulsating variables section of the AAVSO. One of the goals of this program is to provide continued observations of selected RR Lyrae stars, so that there are no gaps in the observational record and it is possible to understand period behavior even for those stars that undergo extreme or erratic variations of period. The AAVSO study of XZ Cygni (Baldwin and Samolyk 2003) shows how even the most extreme period changes can be followed, if there are no gaps in the observational record. Diligent work by AAVSO observers can ensure that the period changes of program stars will continue to be known. A major advantage of the AAVSO community is that, as a group, AAVSO members can target a star for periods of time greater than the observing careers of even the most dedicated individuals.

Long term observations of numerous RR Lyrae stars by programs such as the OGLE survey or the All Sky Automated Survey (Pojmański 1998) will undoubtedly become increasingly important to the study of period changes. An OGLE survey of almost 17,000 RR Lyrae stars in the Galactic bulge found period changes for only 4% of the RRab variables but for 38% of the RRc stars. 75% of the RRc stars with periods in the range 0.35 to 0.45 day showed detectable period changes (Soszyński *et al.* 2011). These results came from observations spanning only some 13 years, and the period change results will undoubtedly become increasingly valuable if the survey is continued for many more years.

4.4.Type II Cepheids: observations confront theory

We saw above that theory predicts that many if not all BL Her stars should show increasing periods, whereas the predicted period changes for W Vir stars are less certain. If blueward loops from the asymptotic red giant branch actually exist, they would generate both period decreases and increases. However, if W Vir stars are mainly evolving blueward in post-asymptotic branch evolution, we would expect period decreases.

Type II Cepheids are a relatively rare type of variable star, and we have available observed period changes for many fewer type II Cepheids than for RR Lyrae stars. In a catalog of variable stars in globular clusters, Clement *et al.* (2001) listed about 2,200 stars with known periods. Of these, about 1,800 were RR Lyrae stars but only about 54 were type II Cepheids (excluding so-called anomalous Cepheids and RV Tauri stars). In Figures 5 and 6 we show observed rates of period change for field and cluster type II Cepheids as a function of period, based upon the determinations in Wehlau and Bohlender (1982), Christianson (1983), Provencal (1986), Holroyd (1989), Wehlau and Froelich (1994), Diethelm (1996), Percy and Hoss (2000), Jurcsik *et al.* (2001), Templeton and Henden (2007), and Rabidoux *et al.* (2010). Period changes for BL Her variables were often determined in these papers by the O–C method, whereas for the W Vir stars a mixture of O–C diagrams and direct determinations of period at different epochs were employed. The timespans covered by the observations run from four decades to a little more than a century, depending upon the star. When more than one paper dealt with the same star, results from the most recent paper with the longest time coverage were adopted. While some researchers provided formal error bars for their period change results, others did not, and the actual errors might depend upon whether cycle counts between observed epochs of observations have been correctly calculated.

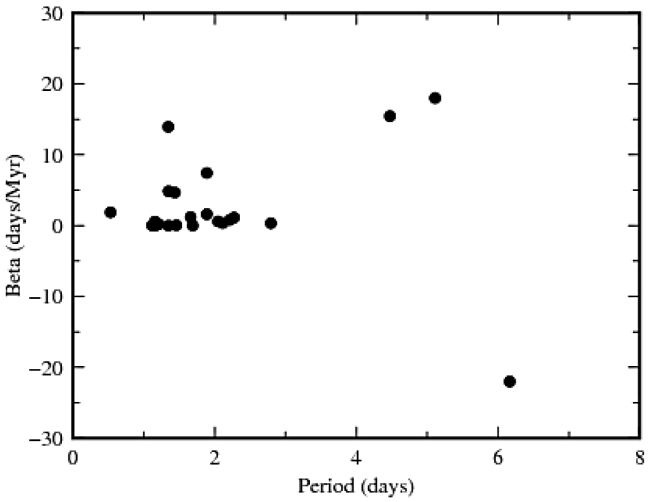

Figure 5. Rates of period change versus period for BL Her stars.

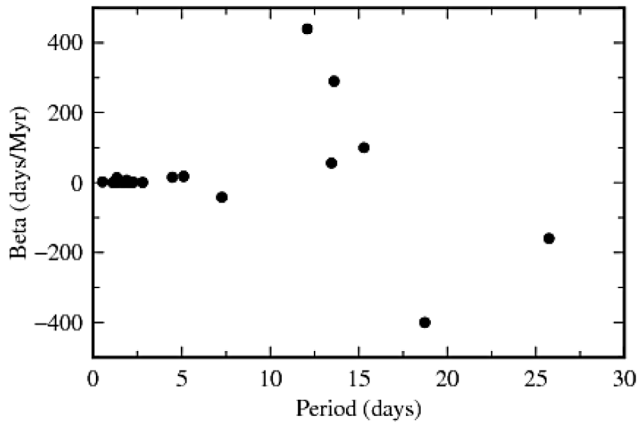

Figure 6. Rates of period change versus period for all type II Cepheids.

In Figure 5 we plot the observed rates of period change for type II Cepheids with periods smaller than 8 days, stars which might fall into the BL Her category. In that figure, almost all of the Cepheids show either small or positive rates of period change. The one star with a significant period decrease is TX Del, which, with a period of 6.165 days, falls at the long period end of the group (Percy and Hoss 2000). When the W Vir stars are added in Figure 6, a dramatically different picture appears. We find very large negative and positive rates of period change.

The observed period changes for type II Cepheids with periods shorter than about 6 days are in line with expectations from stellar evolution theory. Periods for these stars are increasing at rates generally consistent with those expected of post-blue horizontal branch stars evolving to the red. However, it is not clear that the W Vir period changes are consistent with theory. The large rates of period increase and decrease observed for some W Vir stars might be consistent with stars undergoing blue loops from the asymptotic giant branch, but we have seen that there may now be theoretical reasons to question the existence of blueward thermal instability loops. Period increases would not be consistent with the decreasing periods expected in the alternative in which W Vir stars are evolving rapidly to

the blue at the end of their asymptotic giant branch lives, but might be consistent with the redward loops into the instability strip predicted for stars with masses near 0.52 solar mass.

We must note, however, that there are complications in determining period changes for W Vir stars. The brighter W Vir stars seem to take on some of the erratic period and phase shift behavior seen among RV Tauri variables (for example, Rabidoux *et al.* 2010). This can introduce extra noise into the O–C diagram. Templeton and Henden (2007) also found that W Vir itself showed pulsation periods in addition to the dominant 17.27-day period. If multiple periods exist for other W Vir stars, that, too, could introduce scatter into an O–C diagram calculated for a constant, single period. As with the other types of variable in this review, there can be complications in interpreting O–C diagrams if there have been large gaps in the observational record.

The complex period behavior possible for W Vir stars can be illustrated by the extreme case of RU Cam (Percy and Hale 1998). In 1965–1966 this seeming type II Cepheid decreased in amplitude from about 1 magnitude to nearly zero. From 1966 until 1982, RU Cam varied with an amplitude of about 0.2 magnitude with a cycle length between 17.6 and 26.6 days, the mean period being about 21.75 days. AAVSO photoelectric observations of RU Cam in 1988–1998 showed a mean period of 22.20 days with variable amplitude. Once more the lesson is that stars sometimes reveal curious behavior when observers assiduously monitor them for long periods of time. The AAVSO should certainly have a role in such monitoring.

5. β Cephei stars

5.1. Introduction

The β Cephei stars (also once called β CMa stars), like classical Cepheids, are powerful probes of stellar evolution and structure. These stars, however, tend to be more massive than the classical Cepheids, ranging from about 6 $M_{\odot}$ to up to $\approx 20_{\odot}$ (Neilson and Ignace 2015). They are young stars that fuse hydrogen in their cores, similar to the Sun. But, they also exist at the boundary between main sequence blue stars and blue supergiant stars. They have small amplitudes, and require photometric observation.

Because of their evolutionary state, the β Cep stars are powerful laboratories for studying evolution of massive stars. But, even more interesting is the fact that these massive stars are laboratories for more exotic physical phenomena, such as magnetic fields, rotation, and interactions between binary companions. Measurements of period change for these stars allow astronomers to explore this physics.

The β Cep stars have been known to be variable for more than a century. Frost (1906) measured the pulsational veloocity variation of the prototype β Cep, and noted the unusually short period. However, it was not for a few decades that period changes were first detected (Struve 1950; Struve *et al.* 1953). Period changes were soon measured for a number of β Cep stars such as δ Cet, 12 Lac, and BW Vul (van Hoof 1965, 1968; Percy 1971).

Using those rates of period change along with other measurements, Eggleton and Percy (1973) conducted the first comparison of theoretical and observed rates of period change. The measured rates of period change ranged from about –1 second every century to about +3.5 seconds every century. Given that the pulsation periods of β Cep stars tend to be about a few hours then the pulsation period will change only a few seconds after almost 300,000 pulsation cycles. Eggleton and Percy (1973) computed stellar evolution models of these stars and predicted their rates of period change to compare to these measured rates. The model rates of period change ranged from about –15 seconds per century to about 100 seconds per century.

While the evolutionary models appeared to be broadly consistent with the measured rates of period change, there was no consensus regarding their state of evolution (Odgers 1965; Percy 1970) nor regarding the physical mechanism that was driving their pulsation. Eggleton and Percy (1973) suggested that β Cep stars pulsated during multiple stages of evolution. Pulsations would begin near the end of core hydrogen burning, a stage where the star is gravitationally contracting, and a third stage where the star burns hydrogen in a shell above the stellar core. The rates of period change reflect the stage of evolution. During the main sequence, rates of period change are small and positive, but during the contraction stage the rates are negative. Finally, during the shell hydrogen-burning stage the rates are greatest.

This analysis appeared to constrain the evolution stages of β Cep stars, but the question of the pulsation-driving mechanism persisted. It had been long-established that pulsations in the classical Cepheid and RR Lyrae stars were driven by ionization of helium in the outer layers of the star. However, Stellingwerf (1978) found that β Cephei pulsation could only be modelled by assuming "enhanced" helium opacities, although the nature of these opacities was unclear. This enhanced opacity mechanism was the leading theory until the study of stellar opacities was revisited (Iglesias *et al.* 1990; Iglesias and Rogers 1991). Moskalik and Dziembowski (1992) found that pulsation is driven by iron ionization in β Cep stars instead of by helium.

The changes in stellar models since the work of Eggleton and Percy (1973) motivated the need to revisit the comparison of theoretical and measured rates of period change. Furthermore, more detailed observations are leading to new measurements of period change. Pigulski and Boratyn (1992) and Pigulski (1992, 1993) revisited the O–C measurements for the prototype β Cep plus σ Sco and BW Vul. In their O–C diagrams, one can fit the standard parabola to measure the secular rate of period change, but when one delves into residual O–C measurements there is a periodic signal (Odell 1984; Jiang 1985). This periodic signal has been argued to be caused by orbital motions of the star in a binary system. In this system the pulsation period of the β Cep star appears longer when the star is moving away from the Earth and shorter when moving towards the Earth since the distance that light travels is changing. This effect is much more commonly observed for pulsar stars in binary systems, but can be seen in a few of these massive stars.

The analysis of Pigulski showed that the O–C and period change measurements can be influenced by binary motions if one is not careful. Along with that analysis, Jerzykiewicz (1999) presented rates of period change that were different from those presented by Eggleton and Percy (1973). The primary difference

is that the newer measurements were consistent with positive period change. The combination of new physics in the stellar evolution models and more precise observations motivate new calculations.

5.2. Current problems with β Cephei period change

Neilson and Ignace (2015) computed a new grid of stellar evolution models representing β Cephei stars that included physics for rotation and mass loss. It is important to include physical processes such as rapid rotation, magnetic fields, and stellar winds because these effects can help drive evolution in massive stars. Some β Cephei stars have been observed to rotate rapidly (Handler *et al.* 2012) and others slowly (Shultz *et al.* 2015). Some β Cephei stars have powerful magnetic fields (Silvester *et al.* 2009) while others have no detectable field (Fossati *et al.* 2015). All of these observations drive the need for better, more refined stellar evolution models for understanding the lives of massive stars and their deaths as supernovae.

The models computed by Neilson and Ignace (2015) are plotted on the Hertzsprung-Russell diagram in Figure 7 for stars with masses M = 7 to 20 $M_\odot$ that cross the β Cephei instability strip mapped by Pamyatnykh (2007). The models show the effect of different initial rotation rates on the evolution of the stars. Rotation acts to mix material from outer layers in the star into the core and can increase the main sequence lifetime.

When the different models were compared to a sample of period change measurements the results were surprising. The comparison can be summarized by three categories. Those β Cephei stars with measured period changes that were smallest and consistent with no detectable period change agreed with all stellar evolution models. That result simply means that for all stellar masses and physics there is a frame of time where the stars all change their radius and mass, hence period, very slowly. The second category is for the few β Cephei stars with the greatest rates of period change. None of the stellar evolution models and predicted rates of period change could match these measurements implying that there is some phenomenon that we are missing in the models or that the observed period change is not solely due to stellar evolution.

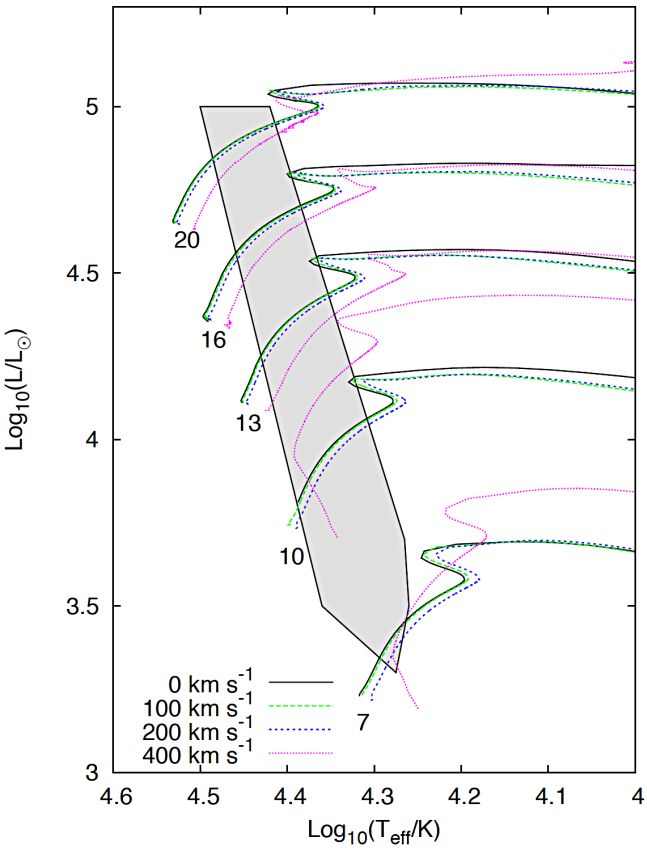

Figure 7. Evolutionary tracks of massive stars on the Hertzsprung-Russell diagram as a function of stellar rotation as the stars pass through the β Cephei instability strip mapped by Pamyatnykh (2007).

The third category includes measured rates of period change for which the stellar evolution models can be tested. For two β Cephei variable stars, δ Ceti and ξ^1 CMa, Neilson and Ignace (2015) used the observed rates of period change to measure the properties of the stars. They found that, thanks to the precision of the measured rates of period change, they could in turn measure both stars' masses and radii, helping to better understand these stars. However, that analysis raised other challenges. For instance, ξ^1 CMa is known to have a strong magnetic field (Shultz *et al.* 2015) and δ Ceti is suspected to have a strong magnetic field (Morel *et al.* 2006), whereas none of the β Cephei stars with the greatest rates of period change have strong magnetic fields. Why should the stellar evolution models that do not include magnetic field physics be able to match observations of stars that are strongly magnetic, but not the stars without magnetic fields? It is unclear if there is physics missing from all models or whether the magnetic fields in the β Cephei stars even impact their pulsation. Continued observations are necessary to even begin addressing this complex problem. If we can measure rates of period changes for more than the handful of stars in the Neilson and Ignace (2015) sample, we can start to learn about the impact of magnetic fields and rotation on pulsation and variability in these stars over their evolutionary time scales.

6. Period changes in pulsating red giants

When stars with masses of up to about 10 solar masses exhaust the hydrogen fuel in their core, they expand and cool and become *red giant stars*. When the helium in their core becomes hot and dense enough, a "helium flash" occurs; the stars contract somewhat, and begin using helium in their core as fuel. As the helium fuel source is exhausted, the star again expands and cools, and becomes an even more extreme *asymptotic giant branch (AGB) star*, with a radius of up to several hundred solar radii. This process of expansion lasts for hundreds of thousands of years.

Models of AGB star evolution (Wood and Zarro 1981; Iben and Renzini 1983; Boothroyd and Sackmann 1988; Vassiliadis and Wood 1993; Fadeyev 2016) indicate that these stars undergo *thermal pulses* that change their radius and temperature, and possibly their mass, on timescales of hundreds to thousands of years. Thermal pulses result from an instability in the thin shell where helium is being used as fuel. They last in total for a few percent of the AGB evolutionary lifetime, so a few percent of AGB stars should be undergoing such changes, and should therefore show more rapid period changes. AGB stars are highly convective, and convection is a complex and poorly-

understood process in cool stars, so the models are somewhat uncertain. Furthermore, the largest AGB stars lose mass at a significant rate, and this further complicates their evolution and the comparison between observation and theoretical models.

In principle, it should be possible to detect the cumulative effect of the slow pulsation period changes in pulsating red giants, due to their evolution up the AGB. This is complicated, first of all, by *random* period fluctuations, described below. Templeton *et al.* (2005) describe some other complications, including the limitations of the visual data on which such studies are usually based. Also, some Mira stars are found in binary systems, and the companion may well affect the structure and evolution of the Mira. Finally, there are other phenomena in pulsating red giants which are not well understood, such as the long secondary periods which are found in about one-third of such stars (Wood 2000), and the variable pulsation amplitudes found in almost all of them (Percy and Abachi 2013). Whatever causes these phenomena may also affect the observed period changes.

Smaller, warmer red giants initially pulsate in a complex mixture of low-amplitude non-radial modes, as the sun does. As the star expands and cools, it becomes unstable to radial pulsation. The period and amplitude are initially a few days and a few millimagnitudes, and the pulsation mode is often an overtone. Later, the period becomes hundreds of days, and the amplitude becomes many magnitudes, and the mode is most often the fundamental. When the visual amplitude exceeds 2.5 magnitudes, the star is by definition a Mira star. Pulsating red giants are classified as M (Mira), SR (semi-regular), and L (irregular). It is very difficult to measure period changes in SR and L stars because of their irregularity and smaller amplitude, but Mira stars, with their large amplitudes, are easy to observe, and reasonably periodic.

AAVSO observers have been systematically observing hundreds of Mira stars for over a century. Kowalsky *et al.* (1986) compiled a database of 75 years of times and magnitudes of maxima and minima of 391 Mira stars, which was used by Percy and others for studies of long-term changes in these stars. More recently, Karlsson (2013) has made public an on-line database on 489 Mira stars, which can be and has been (Karlsson 2014) used for studies of period changes. It includes times of maximum from the literature, and times determined by Karlsson and his colleagues, and other useful information about each star. Ivan Andronov (Kudashkina *et al.* 2014) and his colleagues at the Odessa Observatory, Ukraine, have used additional databases of visual observations to carry out statistical studies of Mira star behavior.

See Smith (2013) for a brief review of period changes in Mira stars up to 2013.

6.1. (O–C) Studies of period changes in pulsating red giants

It has been known for over a century that a few Mira stars show (O–C) diagrams which are parabolic, and which therefore indicate a significant linear change in period. Sterken *et al.* (1999), in elegantly analyzing the change in the period of χ Cyg since its discovery in 1686, have described some of the history of period-change studies of Mira stars. They find a linear increase in the period of χ Cyg, together with quasi-cyclic variations. Wood and Zarro (1981) mention R Aql, W Dra, and R Hya as other early examples ofi Miras with large period changes.

The (O–C) diagrams of most Miras are not parabolic, but exhibit a meandering or "random walk" appearance (Figure 8). (A random walk is a path which consists of a succession of random steps which may be positive or negative. A simple example is the succession of "heads" and "tails" which result from repeatedly tossing a coin. The steps do not necessarily have to be the same length.) Eddington and Plakidis (1929) showed, for a small number of stars, that this random-walk appearance could be explained by a combination of random, cycle-to-cycle period fluctuations, and random errors in determining the times of maximum. Percy and Colivas (1999) used the Kowalsky *et al.* (1986) database to show that this was true for almost all of the 391 stars, and they determined the size of the average fluctuation for each star. There was a tendency for larger fluctuations to occur in longer-period stars.

The presence of these random fluctuations makes it difficult to observe the slow period increases which should occur due to the slow evolution and expansion of the star. Nevertheless, the slow increases should be present, and might be observed by fitting parabolas to the (O–C) diagrams, determining the rates of period change β, in days per day, and averaging these over a very large number of stars observed over a very long period of time.

Percy and Au (1999) used the Kowalsky *et al.* (1986) database to create (O–C) diagrams for 391 Miras, fit parabolas to these, and average the values of β so obtained. They found that positive period changes outnumbered negative ones; the average value of β was $+16 \times 10^{-6}$ d/d, and the median value was $+14.5 \times 10^{-6}$ d/d. The average value for a model with one solar mass was $+28 \times 10^{-6}$ d/d if the star was pulsating in the fundamental mode and $+11 \times 10^{-6}$ d/d if it was pulsating in the first overtone (Vassiliadis and Wood 1993). The agreement between observation and theory was at about the 1.5σ level. Note that the masses of these stars are quite uncertain, so the predicted rates of period change are known only approximately.

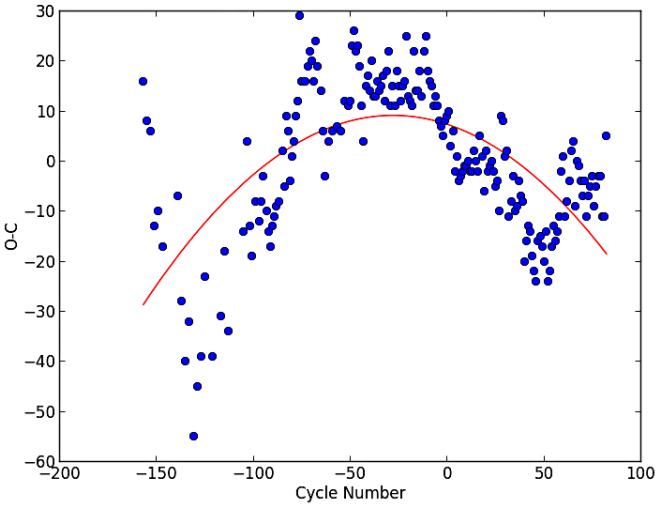

Figure 8. The (O–C) diagram of Z Cap, showing the random-walk pattern caused by the random cycle-to-cycle period fluctuations. The red line is the best-fit parabola, giving a value of β = −0.00455 d / d. Source: Karlsson (2014).

Karlsson (2014) used his database of times of maxima of 489 Mira stars (Karlsson 2013) to study long-term secular changes in period of Mira stars. Karlsson's database is about three decades longer than Kowalsky *et al.*'s. There were 362 stars which had sufficient data for analysis; he constructed (O–C) diagrams for these, and determined values of β. He then applied several tests to these values. (1) The mean period of all the stars increased by 0.15 day over 75 years. (2) Of the stars, 58 percent had increasing periods, and 42 percent had decreasing periods. (3) Almost 60 percent had longer periods in the second half of the dataset than in the first half. (4) The average value of β was $+6.8 \times 10^{-6}$ d / d with a standard error of 3.8×10^{-6} d / d. The data are consistent, at about the 2σ level, with the assumption of increasing periods, and with the predictions of models (e.g. Vassiliadis and Wood 1993).

6.2. Wavelet studies of period changes in pulsating red giants

Templeton *et al.* (2005) used a different technique—*wavelet analysis*—to study the period changes of 547 Mira stars in the AAVSO visual observing program. In wavelet analysis, a sine wave of a fixed frequency is fitted to the data using a Gaussian wavelet window function (Foster 1996). In this way, wavelet analysis produces a Fourier transform of each segment of the dataset, giving an estimate of the period(s) and amplitude(s) and how they change with time. A wavelet routine is available within the software package VSTAR (Benn 2013) on the AAVSO website. Unlike the (O–C) method, which is based on times of maximum, wavelet analysis uses all of the data in the light curve.

Templeton *et al.* (2005) found 57 stars which had period changes significant at the 2σ level, 21 at the 3σ level, and 8 at the 6σ level or higher. The larger period changes are almost equally divided between positive and negative values. As the authors note, the period changes in the 2–3σ range may simply be spurious results of the random fluctuations.

For the stars with the highest rate of period change, the period-versus-time graphs were reasonably linear. For those with lower rates, the graphs were clearly affected by the random fluctuations, and for those with no significant period change, the graphs were random walks. The stars with the largest period changes were: T UMi, LX Cyg, RR Aql, Z Tau, W Dra, R Cen, R Hya, and BH Cru; Templeton *et al.* (2005) discuss these stars individually in some detail; see also Zijlstra *et al.* (2002) for a detailed interpretation of R Hya. Gál and Szatmáry (1995a) have independently analyzed and discussed T UMi. T UMi has also decreased significantly in amplitude, LX Cyg has decreased in mean magnitude by about two magnitudes, and R Hya undergoes large, slow, cyclic variations in mean magnitude. These stars with the highest period changes are assumed to be undergoing thermal pulses. Figure 9 shows the time variation of the period of T UMi, determined by wavelet analysis.

It is alternately possible that T UMi is undergoing a pulsation mode switch from fundamental to first overtone. It is known that some red giants pulsate in the fundamental mode, some in the first overtone, and some in both, so occasional mode switching would not be unexpected. Gál and Szatmáry (1995b) reported possible mode switching in RY Dra, TX Dra, and AF Cyg.

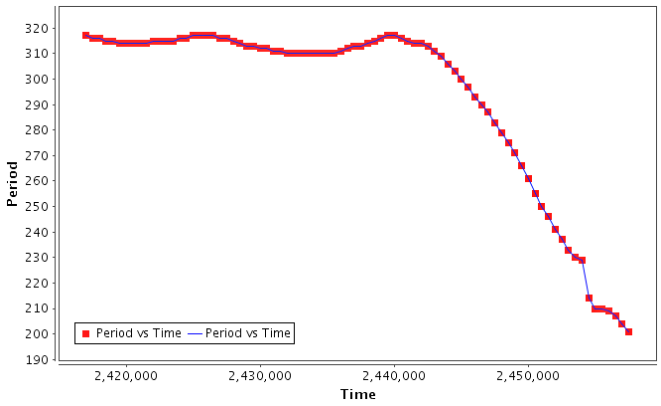

Figure 9. The period of T UMi versus time, determined by wavelet analysis using visual observations from the AAVSO International Database, and the AAVSO software package VSTAR (Benn 2013). T UMi has the largest rate of period change of any Mira studied by Templeton *et al.* (2005).

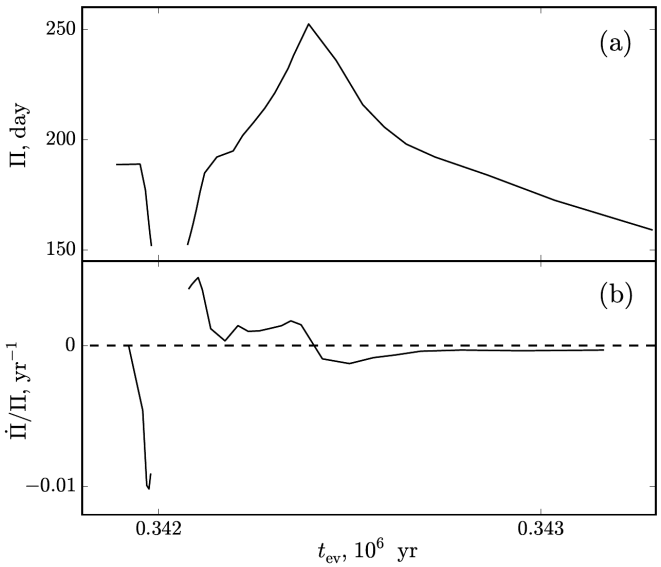

Figure 10. Time dependence of the period in days, and the rate of period change dP/dt/P in years^{-1} for a pulsating red giant model with an initial mass of three solar masses. Significant period changes occur for about a thousand years. From Fadeyev (2016).

Figure 10 shows the time dependence of the period, and rate of period change for a model undergoing a thermal pulse in a red giant with an initial mass of three solar masses (Fadeyev 2016) at a time when the "average" period is about 175 days. This period is somewhat lower than those of most of the stars found by Templeton *et al.* (2005) to have large period changes.

Sabin and Zijlstra (2006) carried out a study, similar to that of Templeton *et al.* (2005), but concentrating on stars with periods longer than 450 days.

Wood and Zarro (1981) call attention to stars, such as T Cep, with small, apparently "abrupt" period changes. Their Figure 4 suggests, however, that the change may simply be part of a random walk.

6.3. V725 Sgr: a unique case

Swope and Shapley (1937) called attention to this remarkable Population II Cepheid which, between 1926 and 1935, increased in period from 12 to 21 days. Percy *et al.* (2006) showed that the star had subsequently and apparently–smoothly changed

into a red semi-regular variable with a period of about 90 days. They pointed out that the star's behavior was consistent with a thermal pulse and blue loop in the H-R diagram, from the AGB to the Cepheid instability strip and back again.

6.4. Other observable effects of evolution in pulsating red giants

Since thermal pulses in AGB stars dredge up unstable technetium (Tc) isotopes, several studies have sought to relate the presence of Tc lines in the spectrum to the assumed evolutionary phase and presence of thermal pulses in the stars—Zijlstra *et al.* (2004), for example, who found no obvious correlation between large period changes and spectral features, and Uttenthaler *et al.* (2011), who found a small fraction of the Miras with rapid period changes to show Tc lines; see also the brief review by Whitelock (1999).

Thermal pulses also produce changes in the mean magnitude of the star, and these may be present in some of the hundreds of Miras in the AAVSO program. Since the changes are small and slow, it is essential, for detecting and interpreting them, that the observing procedure, including comparison star magnitudes, stays the same over many decades. Changes in mean magnitude could, however, be due to circumstellar dust formation, rather than to evolution.

Fadeyev (2016) has pointed out that there may also be changes in pulsation *amplitude*, due to the thermal pulses. Percy and Abachi (2013) have shown that semi-regular variables have large, systematic changes in amplitude on a time scale of a few tens of pulsation periods; Mira stars show a similar but smaller effect. These occur on timescales much shorter than the thermal pulse timescale, or the evolutionary one, so they presumably have some other cause. Several other studies have listed Miras which show long-term changes in period, mean magnitude, and/or amplitude—Lebzelter and Andronache (2011), for example, who listed 23 Miras which were candidates for pulsation period (or mode) change, and Percy *et al.* (1990) who used the Kowalsky *et al.* (1986) database, and listed 31 stars with possible changes.

6.5. Prospects for the future

• Red giant stars are highly convective, and convection in cool stars is complex and poorly understood, so evolutionary models could be improved by incorporating an improved theory of convection. This has been done for pulsation models (e.g. Xiong and Deng (2007)) but not yet for evolutionary models.

• The cause of the random cycle-to-cycle period fluctuations is not known, but could and should be investigated using either theory or observation or both. For instance: does the size of the fluctuation correlate with any physical property of the star? Could it be attributed to the effects of large convection cells? Does it reflect some process which occurs on time scales of cycles, or tens of cycles, such as thermal relaxation oscillations in the envelope (Templeton *et al.* 2005)?

• Observational measurements of the slow evolutionary period changes improve, in accuracy, as the square of the length of the dataset. Therefore it is desirable to sustain the systematic observations of as many Miras as possible, since the effects of the random fluctuations need to be averaged out. The present rate of observation seems about right; there is no need to increase the rate for any select group of stars. A perennial question is whether visual observations could be replaced by large-scale surveys with CCD cameras. The times of maximum brightness, determined by visual and CCD V observations, may not be the same, since the brightness of red stars is very sensitive to the wavelength band being used. Any such difference would have to be carefully taken into account.

• Given the present number of stars which have been observed, and the length of the dataset, it may be possible to look for differences in period-change rate and random period fluctuation between stars in different period ranges, and between M and C type red giant stars.

• One of the advantages of systematic observation of large numbers of variables by AAVSO observers is that they often discover stars with unusual behavior, such as significant changes in period, mean magnitude, amplitude, or extreme change as in V725 Sgr. An open question is whether there are any Mira stars which actually undergo *abrupt* period changes. If so, these would not be easy to explain, theoretically.

• Wood and Zarro (1981) proposed that, for R Aql, R Hya, and W Dra, there were changes in mean magnitude which could be explained by the luminosity changes which occur as a result of a thermal pulse. These may be detectable but, since they occur over several decades, it is very important for the observations to be made on the same magnitude system, relative to the same comparison stars, if such a claim is to be valid. This would be one advantage of accumulating sustained, systematic V data on Miras.

• The (O–C) method is a relatively simple one. Papers such as Sterken *et al.* (1999) illustrate the value of using more sophisticated statistical approaches to the problem.

7. Other types of pulsating stars

7.1. δ Scuti stars

δ Scuti stars are pulsating stars located in the Cepheid instability strip, on or near the main sequence in the H-R diagram. Most have small amplitudes, and many have two or more radial or non-radial pulsation modes, so they are difficult to observe, analyze, and interpret. A few have larger amplitudes and a single pulsation mode. If they are of Population II, they are usually called SX Phe stars. AAVSO observers frequently observe these larger-amplitude stars, usually using PEP or CCD techniques (see for example, Axelsen 2014).

Their period changes have been reviewed by Breger and Pamyatnykh (1998), and by Templeton (2005) in this *Journal*. They agree that, in most cases, the observed period changes are significantly larger than those predicted by evolutionary models. If the pulsating star is a member of a binary system, some of the apparent period changes may be caused by the light-time effect (Sterken 2005). More often, the large changes are caused

by nonlinear interactions between pulsation modes or secular changes in the chemical structure of the stars.

7.2. Degenerate stars

White dwarfs are the inert cores of low-mass stars, exposed at the end of their lives after the stars' outer layers have been cast off as planetary nebulas. White dwarfs have no nuclear energy supply; they shine by slow cooling. As they cool from temperatures of over 100,000 K, they pass through three regimes of pulsational instability, designated DOV, DBV, and DAV. See Kepler *et al.* (2005) for a brief review of white dwarfs and their period changes. Like the δ Scuti stars, they show numerous low-amplitude pulsation modes, so their period changes are also difficult to observe, analyze, and interpret.

In those DOV and DBV stars which have been studied, the observed period changes are greater than models predict, probably due to interaction between the modes. But in a few DAV stars (Kepler *et al.* 2005; Mukadam *et al.* 2013), several decades of high-precision photometry yield period changes in good agreement with evolutionary theory.

8. Concluding remarks

We have described how systematic, sustained observations of periodic pulsating variable stars can be used to measure rates of period change in these stars; these, in turn, can be used to detect and measure the slow evolution of the stars. These period changes can be compared with predictions from evolutionary models. Generally, the agreement is good, but there are many cases of disagreement. These disagreements can potentially be used to identify important physical processes, such as rotation, magnetic fields, or mass loss, which need to be incorporated into the evolutionary models.

We have also mentioned how AAVSO observations have helped in the past, and could help in the future. The AAVSO provides a mechanism for making and archiving systematic, sustained observations, which will continue to be useful to astronomers in the future.

9. Acknowledgements

We thank the observers who made the observations on which our results were based, including AAVSO observers, and the AAVSO staff who archived the observations. We are grateful to Yuri Fadeyev for permission to use Figure 10. HRN is grateful for instructive discussions with Scott Engle, Edward Guinan, Nancy R. Evans, David Turner, and Richard Ignace. JRP thanks the many students who have worked with him, over the years, on projects related to the subject of this review. HAS thanks Giuseppe Bono for helpful discussions on the theoretical period changes in type II Cepheids.

References

Alcock, C., *et al.* 1996, *Astrophys. J.*, **461**, 84.

Anderson, R. I., Ekström, S., Georgy, C., Meynet, G., Mowlavi, N., and Eyer, L. 2014, *Astron. Astrophys.*, **564**, A100.

Anderson, R. I., Sahlmann, J., Holl, B., Eyer, L., Palaversa, L., Mowlavi, N., Süveges, M., and Roelens, M. 2015, *Astrophys. J.*, **804**, 144.

Anderson, R. I., Saio, H., Ekström, S., Georgy, C., and Meynet, G. 2016, *Astron. Astrophys.*, **591**, A8.

Arellano Ferro, A., Ahumada, J. A., Kains, N., and Luna, A. 2016, *Mon. Not. Roy. Astron. Soc.*, **461**, 1032.

Axelsen, R. A. 2014, *J. Amer. Assoc. Var. Star Obs.*, **42**, 37.

Bailey, S. I. 1902, *Ann. Harvard Coll. Obs.*, **38**, 1.

Baker, N., and Kippenhahn, R. 1965, *Astrophys. J.*, **142**, 868.

Baldwin, M. E. 1968, *AAVSO Abstr.*, No. 36, 5.

Baldwin, M. E., and Samolyk, G. 2003, *Observed Maxima Timings of RR Lyrae Stars*, No. 1, AAVSO, Cambridge, MA.

Barnard, E. E. 1919, *Popular Astron.*, **27**, 522.

Belopolsky, A. 1895, *Astrophys. J.*, 1, 160.

Benn, D. 2013, VSTAR data analysis software (http://www.aavso.org/vstar-overview).

Bono, G., Caputo, F., and Santolamazza, P. 1997, *Astron. Astrophys.*, **317**, 171.

Bono, G., Castellani, V., and Marconi, M. 2000, *Astrophys. J.*, **529**, 293.

Bono, G., *et al.* 2016, *Commun. Konkoly Obs.*, **105**, 149.

Boothroyd, A. I., and Sackmann, I.-J. 1988, *Astrophys. J.*, **328**, 653.

Breger, M., and Pamyatnykh, A. A. 1998, *Astron. Astrophys.*, **332**, 958.

Breitfelder, J., Mérand, A., Kervella, P., Gallenne, A., Szabados, L., Anderson, R. I., and Le Bouquin, J.-B. 2016, *Astron. Astrophys.*, **587**, A117.

Bruntt, H., *et al.* 2008, *Astrophys. J.*, **683**, 433.

Campbell, W. W. 1895, *Publ. Astron. Soc. Pacific*, **7**, 68.

Catelan, M. 2004, *Astrophys. J.*, **600**, 409.

Catelan, M., and Smith, H. A. 2015, *Pulsating Stars*, Wiley-VCH, Weinheim, Germany.

Chandler, S. C. 1893, *Astron. J.*. **13**, 89.

Chandler, S. C. 1896, *Astron. J.*, **16**, 145.

Chandler, S. C. 1904, *Astron. J.*, **24**, 65.

Christianson, J. 1983, *J. Amer. Assoc. Var. Star Obs.*, **12**, 54.

Christy, R. F. 1963, *Astron. J.*, **68**, 275.

Clement, C. M., *et al.* 2001, *Astron. J.*, **122**, 2587.

Cox, A. N. 1980, *Ann. Rev. Astron. Astrophys.*, **18**, 15.

Cox, A. N. 1998, *Astrophys. J.*, **496**, 246.

Cragg, T. A. 1972, *J. Amer. Assoc. Var. Star Obs.*, **1**, 9.

Deasy, H. P., and Wayman, P. A. 1985, *Mon. Not. Roy. Astron. Soc.*, **212**, 395.

Derekas, A., *et al.* 2012, *Mon. Not. Roy. Astron. Soc.*, **425**, 1312.

Derekas, A., Plachy, E., Molnar, L., Sodor, A., Benko, J. M., Szabados, L., Bognar, Zs., Csak, B., Szabo, Gy., Szabo, R., and Pal, A. 2016, eprint arXiv:1609.05398.

Diethelm, R. 1996, *Astron. Astrophys.*, **307**, 803.

Eddington, A. S. 1917, *The Observatory*, **40**, 290.

Eddington, A. S. 1918, *Mon. Not. Roy. Astron. Soc.*, **79**, 2.

Eddington, A. S. 1919a, *The Observatory*, **42**, 338.

Eddington, A. S. 1919b, *Mon. Not. Roy. Astron. Soc.*, **79**, 177.

Eddington, A. S., and Plakidis, S. 1929, *Mon. Not. Roy. Astron. Soc.*, **90**. 65.

Eggleton, P. P., and Percy, J. R. 1973, *Mon. Not. Roy. Astron. Soc.*, **161**, 421.

Engle, S. G., Guinan, E. F., Harper, G. M., Neilson, H. R., and Remage Evans, N. 2014, *Astrophys. J.*, **794**, 80.

Engle, S. G., Guinan, E. F., and Kim, C.-W. 2004, *Bull. Amer. Astron. Soc.*, **37**, 378.
Erleksova, G. E. 1978, *Perem. Zvezdy*, **21**, 97.
Evans, N. R., *et al.* 2015, *Mon. Not. Roy. Astron. Soc.*, **446**, 4008.
Fadeyev, Y. A. 2016, arXiv:1605.03851v1.
Fernie, J. D. 1979, *Astrophys. J.*, **231**, 841.
Fernie, J. D., Kamper, K. W., and Seager, S. 1993, *Astrophys. J.*, **416**, 820.
Fossati, L., *et al.* 2015, *Astron. Astrophys.*, **582**, A45.
Foster, G. 1996, *Astron. J.*, **112**, 1209.
Frost, E. B. 1906, *Astrophys. J.*, **24**, 259.
Gál, J., and Szatmáry, K. 1995a, *Astron. Astrophys.*, **297**, 461.
Gál, J., and Szatmáry, K. 1995b, in *Astronomical Applications of Stellar Pulsation*, ed. R. S. Stobie, P. A. Whitelock, ASP Conf. Ser. 83, Astronomical Society of the Pacific, San Francisco, 405.
Gieren, W., Storm, J., Barnes, T. G. III, Fouqué, P., Pietrzyński, G., and Kienzle, F. 2005, *Astrophys. J.*, **627**, 224.
Gingold, R. A. 1976, *Astrophys. J.*, **204**, 116.
Goodricke, J., and Bayer, J. 1786, *Philos. Trans. Roy. Soc. London*, Ser. I, **76**, 48.
Griest, K. 1991, *Astrophys. J.*, **366**, 412.
Handler, G., *et al.* 2012, *Mon. Not. Roy. Astron. Soc.*, **424**, 2380.
Haubois, X., *et al.* 2009, *Astron. Astrophys.*, **508**, 923.
Hofmeister, E. 1967, *Astron. J.*, **72**, 304.
Hofmeister, E., Kippenhahn, R., and Weigert, A. 1964a, *Z. Astrophys.*, **59**, 242.
Hofmeister, E., Kippenhahn, R., and Weigert, A. 1964b, *Z. Astrophys.*, **60**, 57.
Holroyd, C. 1989, *J. Amer. Assoc. Var. Star Obs.*, **18**, 134.
Iben, I. Jr., and Renzini, A. 1983, *Ann. Rev. Astron. Astrophys.*, **21**, 271.
Iglesias, C. A., and Rogers, F. J. 1991, *Astrophys. J., Lett.*, **371**, L73.
Iglesias, C. A., Rogers, F. J., and Wilson, B. G. 1990, *Astrophys. J.*, **360**, 221.
Jeans, J. H. 1925, *Mon. Not. Roy. Astron. Soc.*, **85**, 797.
Jerzykiewicz, M. 1999, *New Astron. Rev.*, **43**, 455.
Jiang, S.-Y. 1985, *Chin. Astron. Astrophys.*, **9**, 191.
Jurcsik, J., Clement, C., Geyer, E. H., and Domsa, I. 2001, *Astrophys. J.*, **121**, 951.
Jurcsik, J., *et al.* 2012, *Mon. Not. Roy. Astron. Soc.*, **419**, 2173.
Karlsson, T. 2013, *J. Amer. Assoc. Var. Star Obs.*, **41**, 348.
Karlsson, T. 2014, *J. Amer. Assoc. Var. Star Obs.*, **42**, 280.
Keller, S. C. 2008, *Astrophys. J.*, **677**, 483.
Kepler, S. O., Costa, J. E. S., Mukadam, A., Mullally, F., Winget, D. E., Nather, R. E., and Sullivan, D. 2005, in *14th European Workshop on White Dwarfs*, eds. D. Koester, S. Moehler, ASP Conf. Ser. 334, Astronomical Society of the Pacific, San Francisco, 501.
Kervella, P., Mérand, A., Perrin, G., and Coudé du Foresto, V. 2006, *Astron. Astrophys.*, **448**, 623.
Kholopov, P. N., *et al.* 1985, *General Catalogue of Variable Stars*, 4th ed., Moscow.
Kolenberg, K. 2012, *J. Am. Assoc. Var. Star Obs.*, **40**, 481.
Koopmann, R. A., Lee, Y.-W., Demarque, P., and Howard, J. M. 1994, *Astrophys. J.*, **423**, 380.
Kowalsky, P. A., Percy, J. R., Mattei, J. A., and Waagen, E. O. 1986, *J. Amer. Assoc. Var. Star Obs.*, **15**, 236.
Kudashkina, L. S., Andronov, I. L., Marsakova, V. I., and Chinarova, L. L. 2014, arXiv:1411.1384.
Kukarkin, B. W., and Florja, N. 1932, *Z. Astrophys.*, **4**, 247.
Kunder, A., *et al.* 2011, *Astron. J.*, **141**, 15.
Leavitt, H. S., and Luyten, W. J. 1924, *Harvard Coll. Obs. Circ.*, No. 261, 1.
Leavitt, H. S., and Pickering, E. C. 1912, *Harvard Coll. Obs. Circ.*, No. 173, 1.
Le Borgne, J. F., *et al.* 2007, *Astron. Astrophys.*, **476**, 307.
Lebzelter, T., and Andronache, S. 2011, *Inf. Bull. Var. Stars*, No. 5981, 1.
Lee, Y.-W. 1991, *Astrophys. J.*, **367**, 524.
Ludendorff, H. 1913, *Astron. Nach.*, **193**, 301.
Maas, T., Giridhar, S., and Lambert, D. L. 2007, *Astrophys. J.*, **666**, 378.
Marengo, M., *et al.* 2010, *Astrophys. J.*, **725**, 2392.
Martin, W. C. 1938, *Ann. Sterrewacht Leiden*, **17**, B1.
Martin, W. L. 1981, *S. Afr. Astron. Obs. Circ.*, **6**, 96.
Matthews, L. D., Marengo, M., Evans, N. R., and Bono, G. 2012, *Astrophys. J.*, **744**, 53.
Mérand, A., *et al.* 2006, *Astron. Astrophys.*, **453**, 155.
Morel, T., Butler, K., Aerts, C., Neiner, C., and Briquet, M. 2006, *Astron. Astrophys.*, **457**, 651.
Moskalik, P., and Dziembowski, W. A. 1992, *Astron. Astrophys.*, **256**, L5.
Mukadam, A. S. *et al.* 2013, *Astrophys. J.*, **771**, 17.
Neilson, H. R. 2014, *Astron. Astrophys.*, **563**, A48.
Neilson, H. R., Cantiello, M., and Langer, N. 2011, *Astron. Astrophys.*, **529**, L9.
Neilson, H. R., Engle, S. G., Guinan, E. F., Bisol, A. C., and Butterworth, N. 2016, *Astrophys. J.*, **824**, 1.
Neilson, H. R., Engle, S. G., Guinan, E., Langer, N., Wasatonic, R. P., and Williams, D. B. 2012a, *Astrophys. J.*, **745**, L32.
Neilson, H. R., and Ignace, R. 2014, *Astron. Astrophys.*, **563**, L4.
Neilson, H. R. and Ignace, R. 2015, *Astron. Astrophys.*, **584**, A58.
Neilson, H. R., Langer, N., Engle, S. G., Guinan, E., and Izzard, R. 2012b, *Astrophys. J.*, **760**, L18.
Neilson, H. R., Ngeow, C.-C., Kanbur, S. M., and Lester, J. B. 2010, *Astrophys. J., Lett.*, **716**, 1136.
Nijland, A. A. 1903, *Astron. Nachr.*, **161**, 229.
Odell, A. P. 1984, *Publ. Astron. Soc. Pacific*, **96**, 657.
Odgers, G. J. 1965, *Veroff. Remeis-Sternw. Bamberg*, **27**, 145.
Paczyński, B., *et al.* 1994, arXiv e-print 94-11004.
Pamyatnykh, A. A. 2007, *Comm. Asteroseismology*, **150**, 207.
Parenago, P. P. 1957, *Commun. Konkoly Obs.*, **42**, 53.
Payne-Gaposchkin, C. H. 1971, *Smithsonian Contrib. Astrophys.*, **13**, 1.
Payne-Gaposchkin, C., and Gaposchkin, S. 1966, *Smithsonian Contrib. Astrophys.*, **9**, 1.
Percy, J. R. 1970, *Astrophys. J.*, **159**. 177.
Percy, J. R. 1971, *Astron. J.*, **76**, 1105.
Percy, J. R., 2007, *Understanding Variable Stars*, Cambridge Univ. Press, Cambridge.
Percy, J. R., and Abachi, R. 2013, *J. Amer. Assoc. Var. Star Obs.*, **41**, 193.

Percy, J. R., and Au, W. W.-Y. 1999, *Publ. Astron. Soc. Pacific*, **111**, 98.
Percy, J. R., and Colivas, T. 1999, *Publ. Astron. Soc. Pacific*, **111**, 94.
Percy, J. R., Colivas, T., Sloan, W. B., and Mattei, J. A. 1990, in *Confrontation between Stellar Pulsation and Evolution*, ASP Conf. Ser. 11, Astronomical Society of the Pacific, San Francisco, 446.
Percy, J. R., and Hale, J. 1998, *Publ. Astron. Soc. Pacific*, **110**, 1428.
Percy, J. R., and Hoss, J. X. 2000, *J. Amer. Assoc. Var. Star Obs.*, **29**, 14.
Percy, J. R., Molak, A., Lund, H., Overbeek, D., Wehlau, A. F., and Williams, P. F. 2006, *Publ. Astron. Soc. Pacific*, **118**, 805.
Percy, J. R., and Tan, P. J. 2013, *J. Amer. Assoc. Var. Star Obs.*, **41**, 75.
Pickering, E. C. 1901, *Astron. Nachr.*, **154**, 423.
Pigott, E. 1785, *Phil. Trans. Roy. Soc. London*, Series I, **75**, 127.
Pigulski, A. 1992, *Astron. Astrophys.*, **261**, 203.
Pigulski, A. 1993, *Astron. Astrophys.*, **274**, 269.
Pigulski, A., and Boratyn, D. A. 1992, *Astron. Astrophys.*, **253**, 178.
Plummer, H. G. 1914, *Mon. Not. Roy. Astron. Soc.*, **74**, 660.
Pojmański, G. 1998, *Acta Astron.*, **48**, 35.
Poleski, R. 2008, *Acta Astron.*, **58**, 313.
Poretti, E., Le Borgne, J. F., Klotz, A., Audejean, K., and Hirosawa, K. 2016, *Commun. Konkoly Obs.*, **105**, 73.
Prager, R. 1939, *Bull. Harvard Coll. Obs.*, No. 911, 1.
Provencal, J. 1986, *J. Amer. Assoc. Var. Star Obs.*, **15**, 36.
Rabidoux, K., *et al.* 2010 *Astron. J.*, **139**, 2300.
Sabin, L., and Zijlstra, A. A. 2006, *Mem. Soc. Astron. Italiana*, **77**, 933.
Schwarzschild, M., and Härm, R. 1970, *Astrophys. J.*, **160**, 341.
Shapley, H. 1914, *Astrophys. J.*, **40**, 448.
Shultz, M., Wade, G., Rivinius, T., Marcolino, W., Henrichs, H., and Grunhut, J. 2015, in *New Windows on Massive Stars*, ed. G. Meynet, Proc. IAU 307, Cambridge Univ. Press, Cambridge, 399.
Silva Aguirre, V., Catelan, M., Weiss, A., and Valcarce, A. A. R. 2010, *Astrophys. Space Sci.*, **328**, 123.
Silvester, J., *et al.* 2009, *Mon. Not. Roy. Astron. Soc.*, **398**, 1505.
Skarka, M., Liska, J., Zejda, M., and Mikulasek, Z. 2016, *Commun. Konkoly Obs.*, **105**, 141.
Smith, H. 2013, arXiv: 1310.0533v1.
Soszyński, I., *et al.* 2011, *Acta Astron.*, **61**, 1.
Stellingwerf, R. F. 1978, *Astron. J.*, **83**, 1184.
Sterken, C., ed. 2005, *The Light-Time Effect in Astrophysics: Causes and Cures of the O–C Diagram*, ASP Conf. Ser. 335, Astronomical Society of the Pacific, San Francisco.
Sterken, C., Broens, E., and Koen, C. 1999, *Astron. Astrophys.*, **342**, 167.
Stothers, R. 1980, *Publ. Astron. Soc. Pacific*, **92**, 475.
Struve, O. 1950, *Astrophys. J.*, **112**, 520.
Struve, O., McNamara, D. H., Kung, S. M., and Beymer, C. 1953, *Astrophys. J.*, **118**, 39.
Sweigart, A. V., and Renzini, A. 1979, *Astron. Astrophys.*, **71**, 66.
Swope, H. H., and Shapley, H. 1937, *Ann. Harvard Coll. Obs.*, **105**, 499.
Szabados, L. 1983, *Astrophys. Space Sci.*, **96**, 185.
Szeidl, B., Hurta, Zs., Jurcsik, J., Clement, C., and Lovas, M. 2011, *Mon. Not. Roy. Astron. Soc.*, **411**, 1744.
Templeton, M. R. 2005, *J. Amer. Assoc. Var. Star Obs.*, **34**, 1.
Templeton, M. R., and Henden, A. A. 2007, *Astron. J.*, **134**, 1999.
Templeton, M. R., Mattei, J. A., and Willson, L. A. 2005, *Astron. J.*, **130**, 776.
Turner, D. G., Abdel-Sabour, A., and Berdnikov, L. N. 2006, *Publ. Astron. Soc. Pacific*, **118**, 410.
Turner, D. G., Kovtyukh, V. V., Usenko, I. A., and Gorlova, N. I. 2013, *Astrophys. J., Lett.*, **762**, L8.
Turner, D. G., Savoy, J., Derrah, J., Abdel-Sabour Abdel-Latif, M., and Berdnikov, L. N. 2005, *Publ. Astron. Soc. Pacific*, **117**, 207.
Uttenthaler, S., *et al.* 2011, *Astron. Astrophys.*, **531**, A88.
van Hoof, A. 1965, *Veroff. Remeis-Sternw. Bamberg*, **27**, 149.
van Hoof, A. 1968, *Z. Astrophys.*, **68**, 156.
van Leeuwen, F. 2013, *Astron. Astrophys.*, **550**, L3.
van Leeuwen, F., Feast, M. W., Whitelock, P. A., and Laney, C. D. 2007, *Mon. Not. Roy. Astron. Soc.*, **379**, 723.
Vassiliadis, E., and Wood, P. R. 1993, *Astrophys. J.*, **413**, 641.
Wade, R. A., Donley, J., Fried, R., White, R. E., and Saha, A. 1999, *Astronom. J.*, **118**, 2442.
Wehlau, A., and Bohlender, D. 1982, *Astron. J.*, **87**, 780.
Wehlau, A., and Froelich, N. 1994, *Astron. J.*, **108**, 134.
Welch, D. L. 2012, *J. Amer. Assoc. Var. Star Obs.*, **40**, 492.
Whitelock, P. A . 1999, *New Astron. Rev.*, **43**, 437.
Winzer, J. E. 1973, *Astron. J.*, **78**, 618.
Wood, P. R. 2000, *Publ. Astron. Soc. Australia*, **17**, 18.
Wood, P. R., and Zarro, D. M. 1981, *Astrophys. J.*, **247**, 247.
Xiong, D. R., and Deng, L. 2007, *Mon. Not. Roy. Astron. Soc.*, **378**, 1270.
Zijlstra, A. A., Bedding, T. R., and Mattei, J. A. 2002, *Mon. Not. Roy. Astron. Soc.*, **334**, 498.
Zijlstra, A. A., *et al.* 2004, *Mon. Not. Roy. Astron. Soc.*, **352**, 325.

Abstracts of Papers and Posters Presented at the 105th Spring Meeting of the AAVSO, Held in St. Louis, Missouri, May 5–7, 2016

Invited Talk

Learning from Pulsating Stars: Progress over the Last Century

Horace Smith
Michigan State University, Department of Physics and Astronomy, Bio-Physical Sciences Building, 567 Wilson Road, East Lansing, MI 48824; smith@pa.msu.edu

Abstract Scarcely more than a century has elapsed since it began to be widely accepted that pulsation plays an important role in the variability of stars. During that century pulsating stars have been used as tools to explore a variety of astrophysical questions, including the determination of distances to other galaxies, the testing of timescales of evolution through the HR diagram, and the identification of the ages and star formation histories of stellar populations. Among the significant early milestones along this investigative path are Henrietta Leavitt's discovery of a relation between the periods and luminosities of Cepheids, Harlow Shapley's proposal that all Cepheids are pulsating stars, and Arthur Stanley Eddington's use of the observed period change of δ Cephei to constrain its power source. Today our explorations of pulsating stars are bolstered by long observational histories of brighter variables, surveys involving unprecedentedly large numbers of stars, and improved theoretical analyses. This talk will review aspects of the history and our current understanding of pulsating stars, paying particular attention to RR Lyrae, δ Scuti, and Cepheid variables. Observations by AAVSO members have provided insight into several questions regarding the behavior of these stars.

Paper Session: Pulsating Variable Stars I

Invited Talk

Miras, Mass Loss, and the Ultimate Fate of the Earth

Lee Anne Willson
Department of Physics and Astronomy, Iowa State University, Ames, IA 50011; lwillson@iastate.edu

Abstract The broad category of pulsating red giants includes semiregular variables and Mira variables. The Miras are distinguished by their large amplitude variation in visible light, late spectral types (cool atmospheres), and the presence of emission lines during part of the cycle. The emission lines result from shock waves generated by pulsation that traverse their atmospheres. These stars' atmosphere are often dusty, an indication of mass loss. Based on decades of detailed modeling we can recognize that the Mira stage corresponds to the onset of devastating mass loss, a process that removes most of the remaining envelope and reveals the degenerate core, a new white dwarf star. I'll review the evidence for this claim, and then examine the effects of Mira stage mass loss on the future solar system. Finally, I shall draw some very general conclusions about the ultimate fate of the Earth.

Paper Session: Pulsating Variable Stars II

A Detailed Survey of Pulsating Variables in Five Globular Clusters

Brian W. Murphy
Butler University, Department of Physics and Astronomy, 46oo Sunset Avenue, Indianapolis, IN 46208; bmurphy@butler.edu

Abstract Globular clusters are ideal laboratories for conducting a stellar census. Of particular interest are pulsating variables, which provide astronomers with a tool to probe the properties of the stars and the cluster. We observed each of five globular clusters hundreds to thousands of times over a time span ranging from 2 to 4 years in B, V, and I filters using the SARA 0.6-meter telescope located at Cerro Tololo Interamerican Observatory and the 0.9-meter telescope located at Kitt Peak, Arizona. The images were analyzed using difference image analysis to identify and produce light curves of all variables found in each cluster. In total we identified 377 variables, with 140 of these being newly discovered, increasing the number of known variables stars in these clusters by 60%. Of the total we have identified 319 RR Lyrae variables (193 RR0, 18 RR01, 101 RR1, 7 RR2), 9 SX Phe stars, 5 Cepheid variables, 11 eclipsing variables, and 33 long period variables. For IC 4499 we identified 64 RR0, 18 RR01, 14 RR1, 4 RR2, 1 SX Phe, 1 eclipsing binary, and 2 long period variables. For NGC 4833 we identified 10 RR0, 7 RR1, 3 RR2, 6 SX Phe, 5 eclipsing binaries, and 9 long period variables. For NGC 6171 (M107) we identified 14 RR0, 7 RR1, and 1 SX Phe. For NGC 6402 (M14) we identified 55 RR0, 57 RR1, 1 RR2, 1 SX Phe, 6 Cepheids, 1 eclipsing binary, and 15 long period variables. For NGC 6584 we identified 50 RR0, 16 RR1, 4 eclipsing binaries, and 7 long period variables. From our extensive data set we were able to obtain sufficient temporal and complete phase coverage of the RR Lyrae variables. This has allowed us not only to properly classify each of the RR Lyrae variables but also to use Fourier decomposition of the B, V, and I light curves to further analyze the properties of the variable stars and hence the physical properties of each globular cluster.

Establishing a CCD Light Curve For BW Vul

David Cowall
20361 Nanticoke Drive, Nanticoke, MD 21840; cowall@comcast.net

Abstract BW Vul is a pulsating variable star of the class BCEP. Review of the AID over the last 20 years reveals only scattered visual observations. Since 2011, a few CCD observations have been obtained with the BSMs, but not enough to obtain any knowledge of the light curve other than a mean color. Rapid cadence time series of BW Vul are currently underway using the AAVSOnet. The data generated should allow for modeling of the light curve and an updated ephemeris of Tmin values with O–C analysis.

Studying RR Lyrae Stars with Kepler/K2

Charles Kuehn
University of Northern Colorado, Campus Box 127, 0232 Ross Hall, Greeley, CO 80639; charles.kuehn@unco.edu

Abstract While RR Lyrae stars have long been studied from the ground, the high photometric precision, high cadence, and long observing times offered by the Kepler Space Telescope have yielded exciting discoveries that are revolutionizing our understanding of these stars. In its new K2 mission, Kepler is observing an even larger sample of RR Lyrae stars, promising to provide new insights into them and our Milky Way. In this talk I will present some of the most exciting new discoveries about RR Lyrae stars from the K2 mission with a special focus on what we are learning about the RR Lyrae in the globular cluster M4, our first chance to observe a single population of RR Lyrae with Kepler.

Paper Session: Pulsating Variable Stars III

Unsolved Problems for Main-Sequence Variable Stars Revealed by the NASA Kepler Data

Joyce Ann Guzik
432 Pruitt Avenue, White Rock, NM 87544; jguzik@mindspring.com

Abstract The NASA Kepler spacecraft's long time-series photometric data have enabled interesting studies of γ Doradus, δ Scuti, slowly-pulsating B, and β Cephei variable stars by revealing many new variables and characterizing frequencies and amplitudes to high precision. These stars pulsate in multiple nonradial modes, with periods of hours to days.We will discuss some questions that the Kepler data have raised and are helping to solve, including: Why have so many "hybrid" γ Dor/δ Sct variables been discovered? Why are there apparently "constant" non-pulsating stars within the pulsation instability regions? What are the causes of amplitude variations that occur over relatively short timescales? Can we find patterns in the frequencies and amplitude spectra that will help with mode identification and facilitate asteroseismology? Are large increases in the opacities used for stellar models needed to explain the B-type pulsators and to solve the 'solar abundance problem'?

Type C Semiregulars and Irregulars: the Forgotten Pulsating Luminous Stars

David G. Turner
St. Mary's University, Department of Astronomy and Physics, 56 Shalimar Crescent, Dartmouth, NS B2W 4L8, Canada; turner@ap.smu.ca

Abstract Variable M supergiants, comprising the SRC and LC classes of semiregular and irregular variables, represent late stages of evolution for stars of about 20–25 solar masses, and the likely progenitors for many core collapse supernovae. Most have escaped dedicated study, either long-term photometry or detailed spectroscopy, primarily because of lengthy pulsation periods of 100–1000 days. Yet they appear to share many of the characteristics of classical Cepheids, and their high luminosities make them just as valuable, if not more so, for calibrating the extragalactic distance scale. Many are double-mode, and possibly triple-mode, pulsators, much like Cepheids, which complicates estimates for their periods of variability. Demonstrated here are some of the techniques used for studying such stars, and what has been learned so far about their characteristics. AAVSO observers have a wonderful opportunity to contribute to the field through observations of the forthcoming 2016 maximum of μ Cephei.

Identification of ASAS Ellipsoidal Variables Misclassified as Miscellaneous in VSX (Poster)

Kristine Larsen
Corwin Hoover
Department of Physics and Earth Sciences, Central Connecticut State University, 1615 Stanley Street, New Britain, CT 06053; Larsen@ccsu.edu

Abstract Over 25,000 variable stars found in VSX were classified as miscellaneous by the automated analysis program for ASAS (All Sky Automated Survey) light curve data. As has been demonstrated by other authors, many of these stars can be classified as one of a number of standard variable classes through human analysis. Among the types of variable stars mislabeled as miscellaneous are ellipsoidal variable stars (ELL's). These are close binary systems in which the stars do not eclipse; the changes in brightness are due to the nonspherical shape of the stars. This project identified and then analyzed ELL candidates in the spreadsheet of ASAS "miscellaneous stars," specifically concentrating on early spectral class variables with periods of less than 15 days. ASAS data of the candidates were analyzed using VSTAR in order to generate phase plots and determine periods. The goal of this project has been to identify ELL's from this sample in order to update the VSX (Variable Star Index). This poster will describe the process used to identify and analyze 540 candidates as well as preliminary results.

Utilizing the AAVSO's Variable Star Index (VSX) in Undergraduate Research Projects (Poster)

Kristine Larsen
Department of Physics and Earth Sciences, Central Connecticut State University, 1615 Stanley Street, New Britain, CT 06053; Larsen@ccsu.edu

Abstract Among the many important services that the American Association of Variable Star Observers (AAVSO) provides to the astronomical community is the Variable Star Index (VSX; https://www.aavso.org/vsx/). This online catalog of variable stars is the repository of data on over 334,000 variable stars, including information on spectral type, range of magnitude, period, and type of variable, among other properties. A number of these stars were identified as being variable through automated telescope surveys, such as ASAS (All Sky Automated Survey). The computer code of this survey classified newly discovered variables as best it could, but a significant number of false classifications have been noted. The reclassification of ASAS variables in the VSX data, as well as a closer look at variables identified as miscellaneous type in VSX, are two of many projects that can be undertaken by interested undergraduates. In doing so, students learn about the physical properties of various types of variable stars as well as statistical analysis and computer software, especially the VSTAR variable star data visualization and analysis tool that is available to the astronomical community free of charge on the AAVSO website (https://www.aavso.org/vstar-overview). Three such projects are described in this presentation: to identify in ASAS data and VSX BY Draconis variables misidentified as Cepheids or "miscellaneous", and SRD semiregular variables and ELL (rotating ellipsoidal) variables misidentified as "miscellaneous."

RR Lyrae in Sagittarius Dwarf Globular Clusters (Poster)

Barton J. Pritzl
Thomas J. Gehrman
Ellyn Bell
Ricardo Salinas
Horace A. Smith
Maircio Catelan
University of Wisconsin Oshkosh, Department of Physics and Astronomy, 800 Algoma Boulevard, Oshkosh, WI 54901; pritzlb@uwosh.edu

Abstract The Milky Way Galaxy was built up in part by the cannibalization of smaller dwarf galaxies. Some of them likely contained globular clusters. The Sagittarius dwarf galaxy provides a unique opportunity to study a system of globular clusters that originated outside the Milky Way. We have investigated the RR Lyrae populations in two Sagittarius globular clusters, Arp 2 and Terzan 8. The RR Lyrae are used to study the properties of the clusters and to compare this system to Milky Way globular clusters. We will discuss whether or not dwarf galaxies similar to the Sagittarius dwarf galaxy could have played a role in the formation of the Milky Way Galaxy.

A Photometric Study of Three Eclipsing Binary Stars (Poster)

Austin Ryan
University of Nebraska Kearney, Department of Physics, Bruner Hall of Science, 2401 11th Avenue, Kearney, NE 68849

Abstract As part of a program to study eclipsing binary stars that exhibit the O'Connell Effect (OCE) we are observing a selection of binary stars in a long term study. The OCE is a difference in maximum light across the ligthcurve possibly cause by starspots. We observed for 7 nights at McDonald Observatory using the 30-inch telescope in July 2015, and used the same telescope remotely for a total of 20 additional nights in August, October, December, and January. We will present light curves for three stars from this study, characterize the OCE for these stars, and present our model results for the physical parameters of the star making up each of these systems.

First Look at Photometric Reduction via Mixed-Model Regression (Poster)

Eric Dose
4021 SW 10th Avenue #412, Topeka, KS 66604; astro@ericdose.com

Abstract Mixed-model regression is proposed as a new approach to photometric reduction, especially for variable star photometry in several filters. Mixed-model regression adds to normal multivariate regression certain "random effects": categorical-variable terms that model and extract specific systematic errors such as image-to-image zero-point fluctuations (cirrus effect) or even errors in comp-star catalog magnitudes. In some contrast to the traditional approach of applying formulas to instrumental magnitudes in order to obtain estimated star magnitudes, the presented approach models measured data, then uses the same model to predict the best estimated magnitudes of all check and target stars in the same large image set, typically all a night's images. In the ideal case where no data are missing (e.g., no stars saturated or too faint), the approach is very similar to ensemble (multi-comp-star) photometry. However, the new workflow: (1) is robust to missing data points; (2) delivers plots that expose numerous types of systematic errors; and (3) is readily extensible to new terms, including isolating and removing the effects of imperfect image flat-fielding. Remaining challenges include (1) modeling hourly extinction-coefficient changes, and (2) target-star magnitude uncertainty estimates that can be contaminated by large magnitude errors of comp stars from other sequences.

Paper Session: Pulsating Variable Stars IV

Studying Variable Stars with Undergraduate Students at the University of Nebraska Kearney

William Lee Powell Jr.
University of Nebraska at Kearney, Department of Physics, Bruner Hall of Science, 2401 11th Avenue, Kearney, NE 68849; powellwl@unk.edu

Abstract Over the past several years I have involved undergraduate students in studies of intrinsic variable stars and, more recently, binary stars. In this talk I will address the challenges that come when working exclusively with undergraduate students, as well as detail recent results from this work. In particular I will cover the results of a study of three RR Lyrae (RRL) stars that were identified from the SDSS using a novel technique, and a follow-up study on a previously unknown W UMa contact binary star that exhibits the O'Connell Effect (OCE) that we found in the field of one of the RRL we studied. Finally, I will describe our current work on binary stars and the OCE. Our current work will also be presented in more detail in my student's poster at this meeting.

Photometry and Spectroscopy of V2455 Cygni

Michael D. Joner
Brigham Young University, Department of Physics and Astronomy, N488 ESC, Provo, UT 84602; xxcygni@gmail.com

Abstract We present photometry and spectroscopy of the high amplitude δ Scuti variable star V2455 Cygni. Analysis is presented of the BVRI light curves secured over several years on the 0.9-meter and 0.3-meter telescopes at the Brigham Young University West Mountain Observatory as well as the Orson Pratt Observatory located on the BYU Provo campus. In addition, we present radial velocity measurements and spectrophotometric H-alpha and H-beta measurements secured at the 1.2-meter telescope of the Dominion Astrophysical Observatory in Saanich, British Columbia. These data are used to determine the fundamental properties of this pulsating variable star. We acknowledge the Department of Physics and Astronomy at BYU for continued support of the research work being done at the West Mountain Observatory.

Invited Talk

Exoplanets and Multiverses

Virginia Trimble
University of California, Irvine, Department of Physics and Astronomy, 4129 Physical Sciences 2, Irvine, CA 92697-4575; vtrimble@astro.umd.edu

Abstract To the ancients, the Earth was the Universe, of a size to be crossed by a god in a day, by boat or chariot, and by humans in a lifetime. Thus an exoplanet would have been a multiverse. The ideas gradually separated over centuries, with gradual acceptance of a sun-centered solar system, the stars as suns likely to have their own planets, other galaxies beyond the Milky Way, and so forth. And whenever the community divided between "just one" of anything versus "many," the "manies" have won. Discoveries beginning in 1991 and 1995 have gradually led to a battalion or two of planets orbiting other stars, very few like our own little family, and to moderately serious consideration of even larger numbers of other universes, again very few like our own. I'm betting, however, on habitable (though not necessarily inhabited) exoplanets to be found, and habitable (though again not necessarily inhabited) universes. Only the former will yield pretty pictures.

General Paper Session I

SLAS Library Telescope Program

James Small
St. Louis Astronomical Society, 13128 Cozyhill Drive, St. Louis, MO 63122; president@slasonline.org

Abstract In the fall of 2014, I submitted to the members of the St. Louis Astronomical Society to take the $1,000 profit we had from a convention we had hosted and use it to purchase three telescopes to modify for a Library Telescope program that was invented by Mark Stowbridge and promoted by the New Hampshire Astronomical Society. I had met Mark at NEAF in 2012 when he was walking the floor demonstrating the telescope. We held meetings with three libraries, the St. Louis County Library system, the St. Louis Public Library system and an independent library in Kirkwood, Missouri. The response was overwhelming! SLCL responded with a request for ten telescopes and SLPL asked for five. We did our first build in October, 2014 and placed a total of eighteen telescopes. Since that time, SLAS has placed a total of eighty-eight telescopes in library systems around the St. Louis Metro area, expanding into neighboring counties and across the river in Illinois. In this talk, I will discuss how to approach this project and put it in place in your libraries!

Three New Z Cam Stars

Mike Simonsen
AAVSO Headquarters, 49 Bay State Road, Cambridge, MA 02138; msimonsen@aavso.org

Abstract I will present the evidence and discovery stories of three cataclysmic variables who appear to be members of the Z Cam class of dwarf novae. One was discovered by a lone visual observer and his unwavering patience and persistence, one through the directed effort of the ongoing Z CamPaign, and one via survey data from the Gaia satellite.

General Paper Session II

Converting Differential Photometry Results to the Standard System using Transform Generator and Transform Applier

Marco Ciocca
212 Eastway Drive, Richmond, KY 40475; marco.ciocca@eku.edu

Abstract Since October 2014, the AAVSO has made available two very useful software tools: TRANSFORM GENERATOR (TG) and TRANSFORM APPLIER (TA). TG, authored by Gordon Myers (gordonmyers@hotmail.com), is a program running under PYTHON that allows the user to obtain the transformation coefficients of their imaging train. TA, authored by George Silvis (SGEO@gasilvis.net), allows users to apply the transformation coefficients obtained previously to their photometric observation. The data so processed become then directly comparable to those of other observers. I will show how to obtain transform coefficients using two Standard Fields (M67 and NGC 7790), how consistent the results are, and, as an application, I will present transformed data for two AAVSO target stars, AE UMa and RR Cet.

V571 Lyrae is a Multiple System

Gary Billings
P.O. Box 263, Rockyford, Alberta T0J 2R0, Canada; obs681@gmail.com

Abstract V571 Lyr (GSC 3116-1047) was discovered by the ROTSE survey to be an EA-type eclipsing binary with 1.25-day period. Primary and secondary eclipses are very similar, with depth V = 0.58 magnitude. In 2000, the then-active AAVSO "EB Team" started observing it, to refine the period estimate. A few eclipses were readily found, and a revised period computed. Subsequent eclipses diverged from the revised linear ephemeris by more than the expected amount of error, so observations were continued. Now, more than 100 time-of-minimum observations, over 15 years, clearly show that V571 Lyr is a triple system, with a third-body orbital period of 5.013 ± 0.008 years, and eccentricity of 0.74 ± 0.03. Our orbit fit also yields a period for the close pair, of 1.252 596 66(6) days. After removing the third-body light-time effect, the eclipse-time residuals still show larger than expected scatter, and possibly non-randomness, perhaps due to significant starspots and/or additional bodies in the system. The color of the system is B–V = 0.52 ± 0.01, corresponding to spectral type F7V, and we obtained a spectrum that we classify as F7V ± 2. The mass function computed from the fitted third-body orbit yields a minimum mass of 1.0 ± 0.1 $M_{\odot}$, corresponding to a spectral range of F9V to G5V for the third star. We assume the two stars of the close pair are very similar, so the remaining light in eclipses (59%) is consistent with total eclipses and 3rd light from a star slightly dimmer than each of the pair.

The Mystery of V523 Lyrae

Mike Simonsen
AAVSO Headquarters, 49 Bay State Road, Cambridge, MA 02138; msimonsen@aavso.org

Abstract In the course of vetting submissions to VSX, it was suggested by a user that V523 Lyrae might be a Z Cam star. Investigations led to quite a bit of confusion initially because V523 Lyr was addressed in two separate papers on Kepler observations of cataclysmic variables, with two different light curves and conclusions as to its nature and classification. Adding to the confusion was the fact that the principal author of one paper was also a co-author on the other paper.

Eggen Card Project: Progress and Plans

George Silvis
194 Clipper Road, Bourne, MA 02532; gasilvis@gmail.com

Jack Crast
1784 Lisle Road, Owego, NY 13827; jackcrast@gmail.com

Abstract The Eggen Card Project has been running since 2009 and has involved 30+ AAVSO staff and volunteers. Let me offer a short review of the project, our progress this year, and our plans for the future. Phase 1 of the project has been to index the 108,000 card images, identifying the stars they belong to. We've passed the 75% point on this phase. The next phase is how to use these data. Jack Crast has identified the photometric schemes used by Olin Eggen and developed a spreadsheet tool to prepare these data for inclusion in the AAVSO International Database (AID). Anyone want good photometry from 1970? We got it!

Erratum. Current Light Elements of the δ Scuti Star V393 Carinae

Roy Andrew Axelsen
P. O. Box 706, Kenmore, Queensland 4069, Australia; reaxelsen@gmail.com

In the article "Current Light Elements of the δ Scuti Star V393 Carinae" (*JAAVSO*, 2014, **42**, 292–297), the light elements in Equation (2) on page 296 were given incorrectly.

T_{max} = HJD 2456734.0484 (6) + 0.14129328 (1) E (2)

should be:

T_{max} = HJD 2456732.0484 (6) + 0.14129328 (1) E (2)

as it is stated in the abstract.

Index to Volume 44

Author

Subject